A GENERIC RIGOROUS MODEL FOR ALONG TRACK STEREO SATELLITE SENSORS

By

Pantelis Michalis

A Thesis Submitted for the Degree of

Doctor of Philosophy

of the University of London

Department of Geomatic Engineering

University College London

February 2005

ProQuest LLC
789 East Eisenhower Parkway
P.O. Box 1346
Ann Arbor, MI 48106-1346

Abstract

The aim of this thesis is to develop a generic rigorous sensor model for high resolution optical satellite sensors, with along track stereoscopic capabilities, in order to orientate directly and simultaneously all the along track stereo images. In other words, the idea is to determine the orbit of the satellite platform covering the time acquisition of all images, using satellite photogrammetry in combination with astrodynamics, thus finding common exterior orientation parameters for all images directly or indirectly. As a result, the number of unknown parameters is reduced and also the correlation between them, thus giving a more stable solution. Moreover, the simultaneous solution extends the narrow field of view of each satellite image because all along track images are treated as one iconic image, with the field of view equal to the angle between the first and the last image. Great effort is made in order to define the essential forces which are involved in the acquisition of the pushbroom images, according to the needed accuracy and the data provided.

The fundamental assumptions is that Kepler motion is maintained along the acquisition time of all the along track images. Various versions of the model are developed, based on different orbit determination-propagation methods. The first one, based on the Kepler problem (orbit propagation), can be used for more than two along track images. The second one is based on Gauss-Lambert method which can be used only for two along track images like SPOT-HRS and TERRA-ASTER. The final one is based on Herrick-Gibbs method which is combined with the Gauss-Lambert method in order to be used in the case of more than two along track images. An accuracy assessment is made of the above different orbit determination-propagation methods.

It is possible to extract the exterior orientation of all images together directly, without Ground Control Points using the metadata information, with accepted accuracy. The model is evaluated using TERRA-ASTER and SPOT5-HRS imagery with precision close to pixel size. Finally the accuracy of the along track model is compared with the accuracy of single image sensor model and of a commercial sensor model (Leica Photogrammetry Suite).

To my lovely wife Vaso
and to my sons
Nicholas and Chris

CONTENTS

LIST OF TABLES

LIST OF FIGURES

ACKNOWLEDGMENTS

The name list of acknowledgements followed is definitely incomplete, and I apologize if any people or organization has been missed on the list.

Firstly, I am grateful to the following individuals and organizations that helped me directly in the production of the thesis:

Professor Ian Dowman for supervising this PhD project along with his understanding and support when many difficulties were occurred at home.
Dr. Marek Ziebart for his help in understanding the theory of the satellite orbits.
Mr. Ant Sibthorpe for his help in geodetic transformations.
All the staff and PhD students of UCL Geomatics Engineering Department for their help and friendship.
Hellenic (Greek) Military Geographic Service for providing the reference data of the model evaluation.
Greek Government for this PhD grant.

Secondly, many thanks to the following individuals:
Professor Dimitrios Argialas (National Technical University of Athens) who advised me to take the PhD program in UCL
Mr. Lambros Liakopoulos who helped me to start and finish this PhD program.

I am in debt to my family. Especially, my wife is the main supporter behind this thesis. Although, she had great problems with her pregnancy in the first year of my PhD she was encouraging me to continue with all her heart. Finally, I would to ask an apology from my sons because I was away from them for a long period of time during this PhD project.

CHAPTER 1.

INTRODUCTION

The aim of this thesis is to develop a generic rigorous sensor model for high resolution optical satellite sensors, with along track stereoscopic capabilities, in order to orientate simultaneously all the along track stereo images. In other words, the idea is to determine the orbit of the satellite platform covering the time of acquisition of all images, using satellite photogrammetry in combination with astrodynamics, thus finding common exterior orientation parameters for all images directly or indirectly. A more stable solution is achieved as, the number of unknown parameters is reduced along with the correlation between them. Moreover, the simultaneous solution extends the narrow field of view of each satellite image because all along track images are treated as one iconic image, with the field of view equal to the angle between the first and the last image.

Along track stereo images are acquired on the same orbit by satellites which usually have on board more than one sensor looking at the earth with different angles, or satellites that can rotate their sensor in the along track direction. The advantages of along track stereo images compared with images that are taken from adjacent orbits (across track) are that they are acquired in almost the same ground and atmospheric conditions.

The German MOMS and the Japanese JERS-OPS were the first satellite instruments with along track stereo capability, allowing stereoscopic coverage in all cases and with only a small difference in time. Obviously the same seasonal conditions can improve the image matching results. For this reason, more and more sensors are following this principle, like TERRA-ASTER with a nadir and 27.7° backward view. Also SPOT 5 is built with a High Resolution Stereo (HRS) instrument with 20° forward and 20° backward view. The Japanese ALOS, which will be launched in September 2005, has on board the PRISM sensor, with a nadir and two tilted 23.8° telescopes looking backward and forward. IKONOS and QuickBird high resolution sensors have the ability

of rotating their sensor in both along and across track directions. The EROS satellite has the ability of rotating its sensor, too, but is working in non-synchronous mode, where ground scanning velocity is different than the satellite's ground velocity.

1.1. Research background

In frame camera photogrammetry the geometry model of each image is based on the collinearity equations. Having in mind that a frame camera image is acquired instantaneously, it is assumed that the frame camera model is a static model. On the other hand, the satellite images which are produced by digital sensors are time dependent, and thus it represents a kinematic sensor model. Therefore, a rigorous sensor model based on the collinearity equations should be reformed, in order to describe the satellite motion during the acquisition time of the image.

In the first stage of this research, general and along track sensor models which were developed during the past seventeen years are examined. The rigorous model which developed in UCL, in 1987, by Dowman and Gugan (1987) is set as the most complicated model in this development, and the exterior orientation parameters are reduced accordingly.

The main and fundamental point during the development of along track model is to benefit, from the same orbit acquisition. The collinearity equations are modified, taking into account this specific characteristic using orbit determination-propagation methods. Although, different versions of this model are introduced, depending mainly on orbit determination-propagation method used, the initial and fundamental research assumptions are common for all model versions.

1.2. Research guideline

As it is already mentioned, the main research objective of this thesis is to develop a generic rigorous model for along track stereo pushbroom satellite sensors in order to orientate them simultaneously.

At this stage the way that the sensor modelling is reached in this research should be presented. Generally, there are two ways to describe a phenomenon. The first one is to define and formulate the forces that cause it. The second one is to describe the phenomenon itself without trying (or not interested) to find the reason (force) why this phenomenon is happen. In pushbroom sensor modelling the second way of solving the problem is represented by models based on affine, polynomial or rational function methods (Dowman and Dolloff, 2000; Fraser, 2000). Moreover, models which are based in the interpolation of the navigation data provided with the images in order to simulate the orbit of the satellite are also belong to this second category. A critical disadvantage of this approach is as the forces that act on the satellite are not known is impossible to predict the behaviour of the model in parts of the image where no observations are presented.

In this research the first way of reaching the sensor modelling issue is adopted. Great effort is made in order to define the essential forces which are involved in the acquisition of the pushbroom images, according to the needed accuracy and the data provided.

Moreover, as it is very important to understand how the image acquisition process is described by the developed model tie points are not used in any phase of model solution. The use of tie points could change (improve) the relative orientation between the images which is unwanted in this phase as it is needed to be established by the model itself only. Exactly for the same reason (to understand the behaviour of the model) estimators with constraints are not used. **In this stage, it is most important to understand how good the image acquisition process is described by the developed model instead of trying to find the best available solution.**

1.3. Thesis Outline

The structure of this thesis follows a number of themes which have been explored in order to arrive at the developed along track model.

At the beginning of chapter 2 the following along track sensors are described:

- The JERS1-OPS, only for historical reasons.
- The MOMS-2P which was used in the evaluation process of along track models.
- The TERRA-ASTER and SPOT-HRS sensors which are used in the evaluation of this thesis. Also the SPOT HRV sensor, although it is not along track sensor, is described as it is the main sensor which is evaluated in the literature general sensor modelling
- Finally, the ALOS-PRISM sensor as the most promising forthcoming along track stereo sensor with its triplet of images of 2.5m pixel size.

Then, the sensor modelling issue is introduced based on the modified collinearity equations, along with the necessary theoretical background of astrodynamics covering mainly the orbit determination with analytical methods. Finally, the adjustment of the computations is discussed using the least squares estimator and the general ridge estimator which is proposed in this thesis as more appropriate estimator than the least squares estimator for pushbroom images.

Chapter 3 is a literature review. In this chapter all the important rigorous general and specific along track sensor models which have been developed since 1987 are examined. The French SPOT mission, with a 10m pixel size, guided all the researchers to propose more accurate models based on photogrammetry in order to reach the expected accuracy. As the time passed, new more detailed sensors were produced raising the need of better accuracy of the sensor model. However, in all models the satellite images are treated as independent images with their own exterior orientation parameters. A direct physical relation between the orientation parameters of the along track satellite images has never been established. Even during the bundle block adjustment procedure where tie points are used only a relative relation between the images themselves is achieved, while the exterior orientation parameters of the images are still unrelated.

Chapter 4 is a very important transitional stage to chapter 5. In this chapter the acquisition geometry of the pushbroom scanner is examined in depth and a generic

rigorous sensor model for a single image is developed. The generic along track stereo model is based on this. At the beginning of this chapter the general considerations of this thesis and the assumptions that are adopted from the literature are introduced. The development of the modified general sensor model for a single pushbroom image is carried out step by step starting from the frame camera model which, although inappropriate for satellite images, is tested trying to have an idea of the imprecision caused, when this model is used with pushbroom images. Also, starting from this model, it is known how much the precision of the pushbroom models should be improved. A model, with the assumption that the motion of the satellite during the acquisition time of the image is a Keplerian motion, is established as the most appropriate rigorous model for the representation of single satellite image geometry, in two different versions. In the first one the exterior orientation parameters are the state vector while in the second one the orbital elements. Extensive tests are done in order to understand the behaviour of each version and from the results the conclusion is that the orbital elements model is not stable. Mainly, for this reason, the state vector sensor model is adopted. Finally, the general ridge estimator value is defined along with an important incompatibility that is found to the results when this estimator is used in the single image solution.

In Chapter 5 a generic model for along track stereo images are introduced in various versions, in depth. The fundamental assumption is that Kepler motion is maintained along the acquisition time of all the along track images. For each version different orbit determination-propagation methods are used. The first one based on the Kepler problem (orbit propagation) which can be used in more than two along track images. The second one is based on Gauss-Lambert method which can be used only for two along track images like SPOT-HRS and TERRA-ASTER. The final one is based on Herrick-Gibbs method which is combined with the Gauss-Lambert method in order to be used in case of more than two along track images. In the second part of this chapter an accuracy assessment is presented of the different orbit determination-propagation methods used in along track model. Finally, a step forward is done in order to find if the time interval where the assumption that the motion of the satellite is a Keplerian motion is larger than

the acquisition time interval of 90 sec(HRS images) using the metadata information of SPOT5- HRS data.

In Chapter 6 the along track stereo sensor model is evaluated. The data sets which are used for testing are two TERRA-ASTER along track stereo images obtained under the NERC COMET project in Northern Greece and SPOT5-HRS stereo images in France under the SPOT Assessment Project (SAP) set up by CNES and ISPRS. Just from the results, it seems that the idea of solving the along track images simultaneously using a proper sensor model where a direct physical relation between the exterior orientation parameters is achieved is very promising, giving a stable and accurate solution. An attempt is made in order to solve the model without GCPs. As it is shown in §6.4 the metadata which is provided with SPOT5-HRS does not give all the information needed to solve the model directly. A modified model for this purpose is proposed where the missing information should be calculated once using GCPs as this information is constant and refers to satellite geometry.

Conclusion and further work that arise from all the previous chapters are discussed and summarized in Chapter 7.

1.4. Research achievements

The main achievement of this thesis is to introduce a new generic rigorous sensor model for along track stereo satellite sensors where a direct physical relation between the exterior orientation parameters of the images is established. Hence, it is possible to extract the exterior orientation of all images together, with or without Ground Control Points, with accepted accuracy. In such a case all the along track images are like one iconic image.

The satellite motion during the acquisition of the along track images are examined, in depth. It is assumed that the satellite motion during the acquisition period of the along track images is a Keplerian motion.

It is the first time when the rigorous along stereo sensor model is developed in this way where the collinearity equations are corporate directly with orbit determination-propagation methods. It is proven that using this combination the accuracy, precision and stability of the solution is improved compared to the single image model which is adopted in chapter 4.

CHAPTER2.

THEORETICAL BACKGROUND

2.1. Overview

This chapter is divided into three major parts. The first part covers the satellite photogrammetry issues while the second one deals with the astrodynamics which are integrated into the developed along track stereo model, improving the rigorousness and the stability of the solution. The final part refers to the adjustment of the observations.

General characteristics of the orbit and the optical sensors of remote sensing satellites are described in this first part. The optical remote sensing satellites which, their data are involved in the evaluation processes or in literature review are introduced. Modified collinearity equations for time-dependent sensors as the optical remote sensing sensors are, along with a reference to the essential coordinate systems that are used in satellite photogrammetry, are established.

The second part deals with the fundamental principles of artificial satellite motion. The inertial coordinate system and the time reference are set. Also, the necessary coordinate transformations for geodetic or geocentric coordinate system to an inertial coordinate are briefly presented. The orbit determination and propagation are described next, which are carried out using analytical methods. The new along track stereo model, although the fundamental assumptions are the same, is developed in different versions depending mainly on the used orbit determination method and the available navigation information.

The final part deals with the adjustment of the solution. Generally, the Least Squares Estimator (LSE) is used in photogrammetry as the most appropriate estimator. In the satellite photogrammetry it seems that this estimator is not enough. The high correlation of the exterior orientation parameters between adjacent scanned lines should not only force the improvement of the model in order to find the most uncorrelated of the

parameters model but also to improve the method of the adjustment. In this part the General Ridge Estimator (GRE) is described. It is evaluated in this thesis and it is proposed as a more appropriate estimator for solving the pushbroom geometry than the Least Squares Estimator. After the adjustment of the observations it is quite important to analyze the results and provide a statement regarding the quality of the estimates. This operation is referred to as post-adjustment analysis, and applies various well-known statistical techniques.

2.2. Remote sensing satellites

2.2.1. Orbit and types of sensors

Remote sensing satellites are designed to acquire images of Earth in such a way as the images taken on different dates can be compared between each other (SPOT, 2002). This can only be achieved if the orbit has the following characteristics:

- The orbit is **phased**, which means that the satellite passes repeatedly over a ground point after a whole number of days.
- The orbit is **sun-synchronous**, where the angle between the orbital plane and the Earth-Sun direction is constant (Figure 1). As a result, constant local solar time for passage through a given location is achieved, thereby guaranteeing an almost constant illumination, varying only with the seasons.
- The orbit is near-**polar**. This characteristic is a consequence of the previous two properties. This characteristic enables a full coverage of the Earth
- The orbit is near-**circular**, with a perigee close to the Earth North Pole. This means that a constant altitude may be maintained over a given point on the ground.

The two major types of optical satellite sensors are:

Pushbroom sensors which are the simplest, in the sense that there is no active sensor scanning, consist usually of single strip of pixel oriented perpendicular to the direction of platform motion. The scanning effect on the ground which is passive is due to the motion of the sensor platform (Figure 2). All the along track stereo sensors that are

involved in this thesis are pushbroom scanners, thus a detailed description of the pushbroom scanner geometry is introduced in §2.3.1.

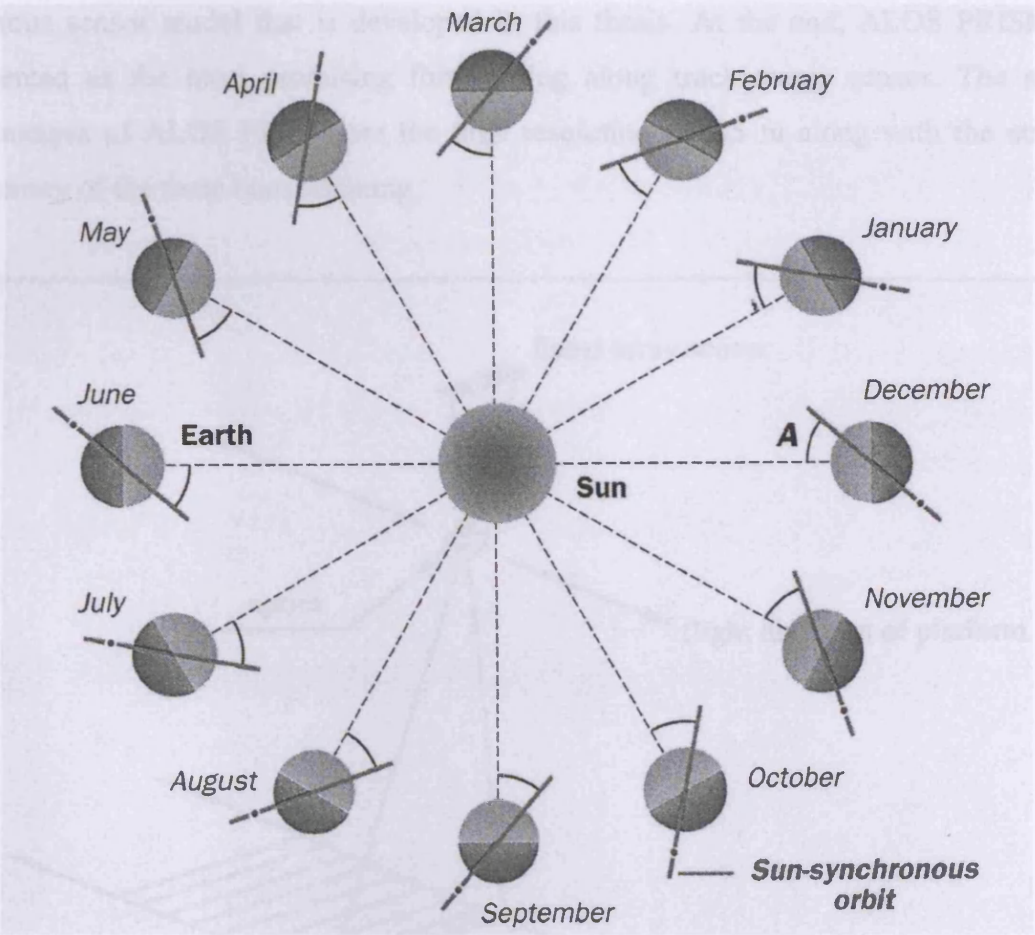

Figure 1. Sun-synchronous orbit. (Verger F. et al., 2003)

Whiskbroom sensors are more complicated than the pushbroom scanners which are usually consisted of a very short strip of pixels that rapidly scans in direction perpendicular to the platform motion, while the motion of the satellite provides the notion needed between images scans similar to pushbroom scanners. Typical examples are Landsat MMS and TM sensors.

In the following sections the remote sensing satellites that are involved in this thesis are introduced, starting from JERS-OPS for historical reasons, only, as the first along track stereo sensor. The MOMS sensor is next which is tested in the along track models in the

literature. SPOT HRV follows, which although it is not along track sensor, is described because it is the main sensor which is evaluated in the literature. TERRA-ASTER and SPOT5-HRS are introduced in depth, as they are used in the evaluation processes of the rigorous sensor model that is developed in this thesis. At the end, ALOS PRISM is presented as the most promising forthcoming along track stereo sensor. The main advantages of ALOS PRISM are the high resolution of 2.5 m along with the strong geometry of the three lines scanning.

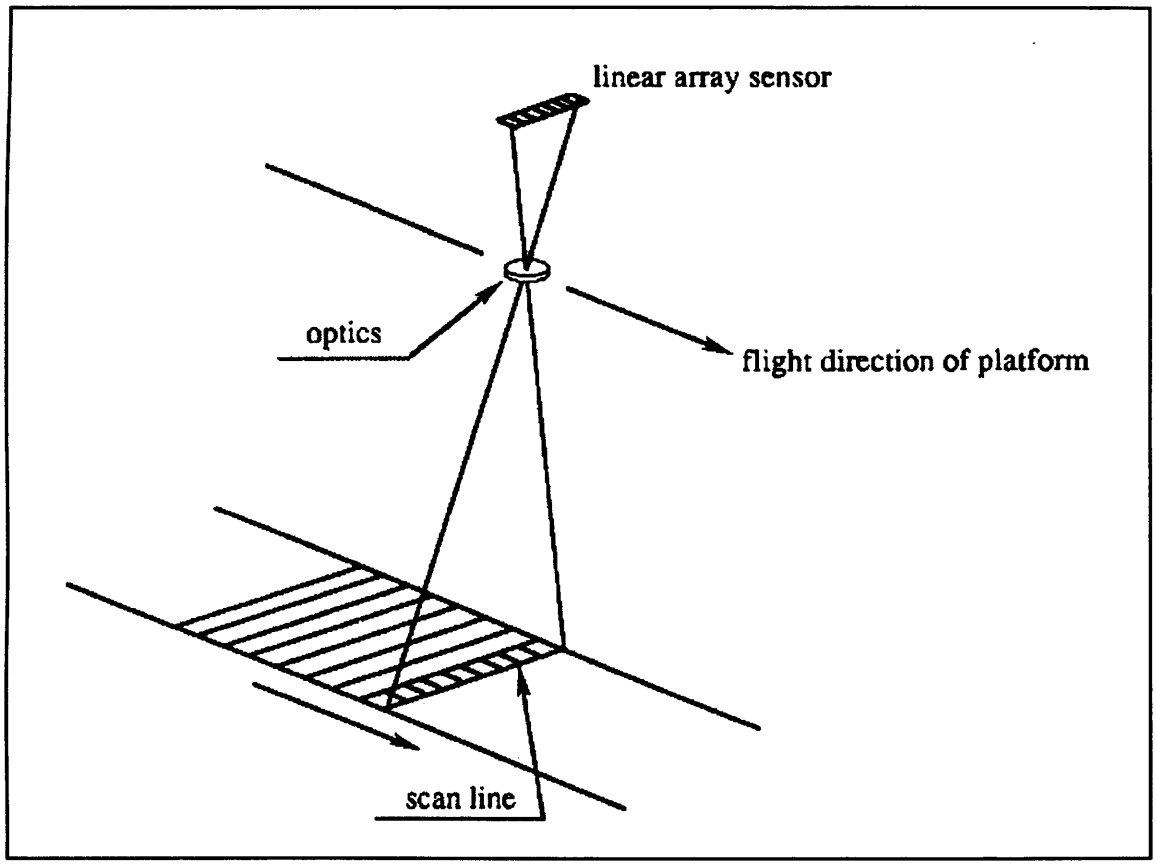

Figure 2. Passive acquisition of pushbroom scanner

2.2.2. JERS1-OPS

JERS 1 (Japanese Earth Resources Satellite) that was development by the National Space Development Agency of Japan (NASDA) and Ministry of International Trade and Industry (MITI) carried a Synthetic Aperture Radar (SAR) and an Optical Sensor

(OPS). JERS 1 (Figure 3) was launched in February 1992, operated at an attitude of 568km. This relatively low altitude implied a need for weekly orbit adjustments in order to keep to a regular 44-day cycle. JERS 1 operation was terminated in autumn 1998. (Tokunaga et al., 1994)

The OPS is a passive linear array sensor that measures in the visible, near infrared, and short wave infrared. Each spectral band has a 4096 elements linear CCD. The Near Infrared Radiometer (VNIR) can produce stereoscopic images using Band3 and Band4 which looks at nadir and 15.3 degrees forward in the orbit plane, respectively. This means that the base to height ratio (B/H) is 0.3. The swath width is about 75km and the ground resolution is about 18.3m on the cross track and about 24.2m on the along track. The relative accuracy of the produced DEM was 30-40m (Tokunaga et al., 1994) having the potentiality of drawing 1:200,000 scale topographic map.

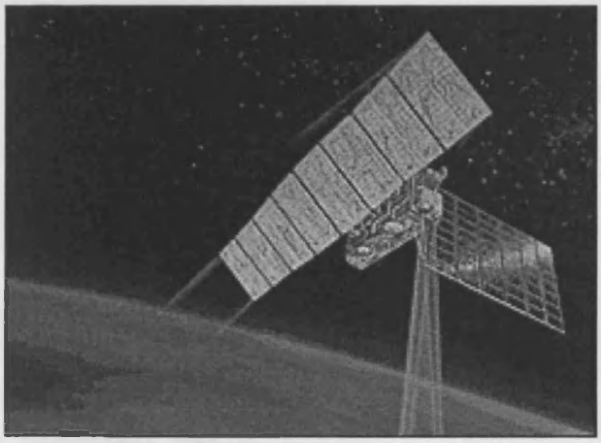

Figure 3. JERS1 in orbit (NASDA)

It is obvious that the accuracy of the produced DEM is poor. For a comparison the produced DEM from ASTER data which has slightly better pixel size (15m) is between 7-15m (Hirano et al., 2003). It seems that, the main reason for the lack of accuracy is the small base to height ratio which is only 0.3 for OPS sensor. (ASTER base to height ratio is 0.6).

This is the only reference to JERS1-OPS as it has already mentioned this sensor is described only for historical reasons as the first sensor with along track stereo capabilities.

2.2.3. MOMS (Modular Optoelectronic Multispectral Stereoscanner)

MOMS (Modular Optoelectronic Multispectral Stereoscanner) is a German spaceborne pushbroom scanner for high resolution (HR), multispectral (MS) and threefold along-track stereoscopic imaging (Figure 4). In fact, MOMS does not meet the orbit characteristics of remote sensing satellites as they are introduced in § 2.2.1., because MOMS was not constantly on board at a specific spacecraft. MOMS was involved in two missions; in German Spacelab mission D2 in spring 1993 and in the PRIRODA module of the Russian space station MIR from 1996 to 1999 (Seige P. et al., 1999).

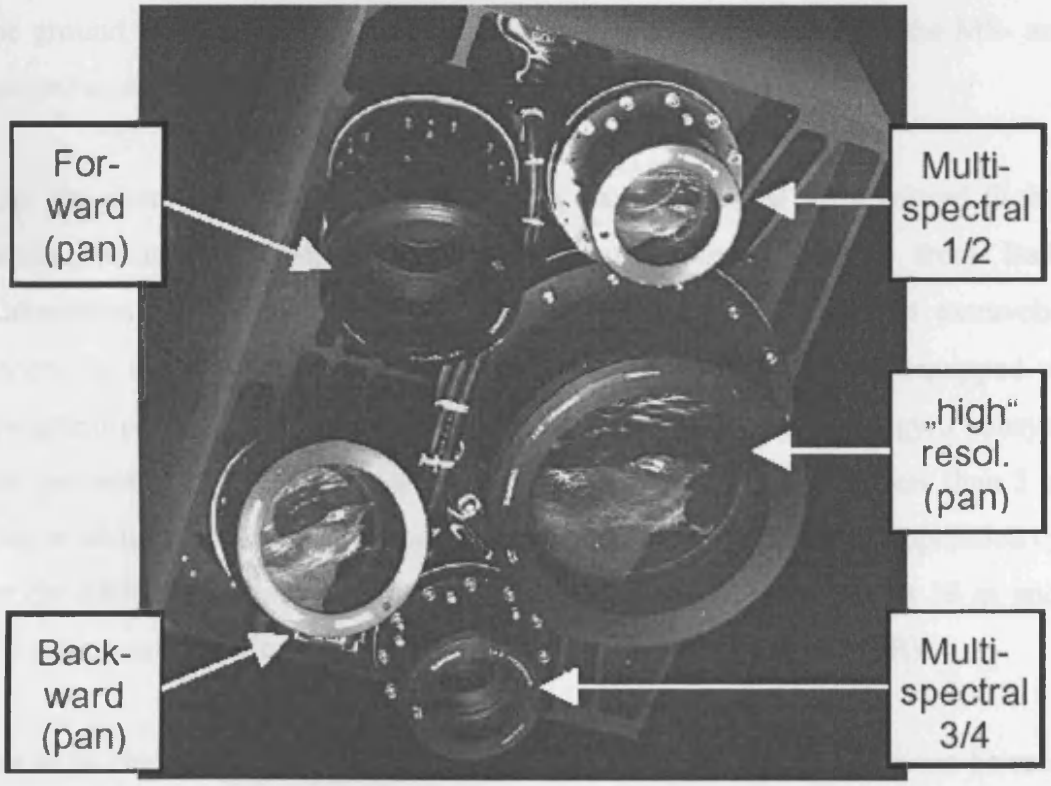

Figure 4. Optical module of MOMS-02 (DLR)

The **stereo-module** consists of the High-Resolution (HR) nadir looking lens with a focal length of 660 mm and two inclined lenses with 237 mm focal length (Figure 5). Thus, the Earth's surface is imaged three times from three different directions within approximately 40 seconds only, corresponding to an orbit altitude of approximately 300 km. The stereo angle of 21.4° results in a base to height ratio of approximately 0.8. The spectral bandwidth of all three channels is 520-760 nm.

The **multispectral-module** consists of two lenses with 220 mm focal length. Both focal planes contain two linear CCD-arrays each with different spectral filter glasses for imaging in the following four bands: 440-505 nm (blue), 530-575 nm (green), 645-680 nm (red), 770-810 nm (NIR).

The MOMS camera was onboard in a German Spacelab mission D2 in spring 1993. Within 11 days 48 image strips were taken from a 300 km orbit with 28.5° inclination. The ground pixel size was 4.5 m for the HR-channel and 13.5 m for the MS- and the inclined stereo-channels.

After the shuttle mission the camera system was refurbished for a second flight. The camera, renamed MOMS-2P, was launched on May 5th, 1996 from Baikonur (Kazakhstan) and mounted to the outside wall of PRIRODA in an extravehicular activity by the crew on May 30th, 1996. MOMS-2P is additionally equipped with a navigation package consisting of a GPS receiver and two redundant gyro subsystems. Post processing of these data delivers an absolute orbit accuracy of less than 5 m and relative attitude accuracy of approximately 10'' for typically 5 minutes operation cycles. For the MIR orbit altitude of approx. 400 km the ground pixel size is 18 m and 6 m (HR); the corresponding swath width is 100 km respectively 50 km (HR).

Due to its limited data rate in MIR, only subsets of all seven channels can be recorded simultaneously. For MOMS-2P four operation modes were defined:

- Mode A: HR nadir and the two inclined stereo channels for DEM generation
- Mode B: Four MS channels for thematic analysis and classification

- Mode C: Three MS channels and HR channel for thematic analysis and classification
- Mode D: Two MS channels and the two inclined stereo channels for DEM generation and thematic analysis.

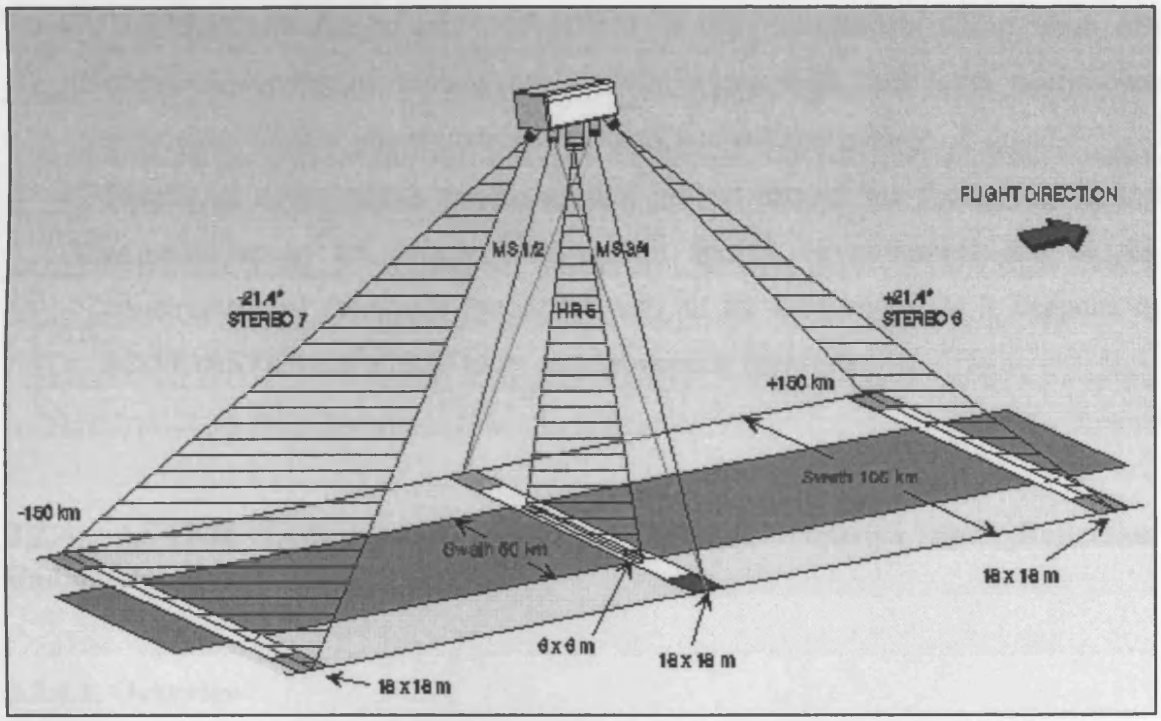

Figure 5. MOMS three lines scanning capability (DLR)

In March 1997 the image quality of the HR channel was adversely affected by strong defocusing effects probably caused by a malfunction of the temperature control mechanism. Since that time only operation modes B and D were used. The main breaks in operation were caused 1997 by the collision accident of MIR with a Progress spacecraft and by the failure of the MOMS-power box. The power box was replaced by a new one. The operation started again in January 1998. The operation of the camera was terminated 16 August 1999.

Although detailed accuracy results for MOMS data are introduced in §3.2 a few general comments could be done here:

- The MOMS concept was based on a very promising idea, the along track acquisition using more than two images which is generally, provides better

DEM accuracy from the two along stereo images and even better from the across track stereo images geometry.

- The implementation of this idea was not so successive. The complexity of the camera, where all sensors were all together in the same module, brought some functionality problems.
- Together with the necessity of carried on two spacecrafts which were not designed for remote sensing applications, along with their own operational problems, the data sets are not in the expect amount and quality.
- Finally, it seems that a remote sensing project should not focus only in the construction of the sensor itself, but it should be continued and in the construction of the whole spacecraft with all its subsystems, as it happens in SPOT, ASTER and a lot of other remote sensing missions.

2.2.4. ASTER (Advanced Spaceborne Thermal Emission and Reflection Radiometer)

2.2.4.1. Overview

The Advanced Spaceborne Thermal Emission and Reflection Radiometer (ASTER) is an advanced multispectral imager that was launched on board NASA's Terra spacecraft in December, 1999. It is a cooperative effort between NASA and Japan's Ministry of Economy Trade and Industry (METI) formerly known as Ministry of International Trade and Industry (MITI), with the collaboration of scientific and industry organizations in both countries (Abrams et al., 2002).

Terra is the first of a series of multi-instrument spacecraft forming NASA's Earth Observing System (EOS). The Terra spacecraft flies in a circular, near-polar orbit at an altitude of 705 km. The orbit is sun-synchronous with equatorial crossing at local time of 10:30 a.m., returning to the same orbit every 16 days. Orbital and physical characteristics of TERRA are shown in table 1 (ERSDAC, 2001).

In addition to ASTER, the other instruments on Terra are:

- Moderate-Resolution Imaging Spectroradiometer (MODIS),
- Multi-angle Imaging Spectro-Radiometer (MISR),
- Clouds and the Earth's Radiant Energy System (CERES), and
- Measurements of Pollution in the Troposphere (MOPITT).

As the only high spatial resolution instrument on Terra, ASTER is the "telephoto lens" for the other instruments.

Mission period	6 years
Orbit	Sun synchronous
Semi-major axis (Mean)	7078 km
Eccentricity	0.0012
Time of day	10:30 ± 15 min. am
Altitude range	700-737km (705 km at equator)
Inclination	98.2deg±0.15deg
Repeat cycle	16 days (233 revolutions/16days)
Distance between adjacent orbits	172 km
Orbit period	98.88 min
Orbit position knowledge	±150 m/3 axes, 3σ
Repetition accuracy	±20 km, 3σ
Dimensions (Stowed)	Approximately 6.8 m long x 3.2m diameter
Satellite Weight	Maximum 5,040 kg

Table 1. TERRA satellite orbital and physical characteristics

ASTER consists of three different subsystems; the Visible and Near-infrared (VNIR) which has three bands with a spatial resolution of 15 m and an additional backward telescope for stereo coverage; the Shortwave Infrared (SWIR) that has 6 bands with a spatial resolution of 30 m; and the Thermal Infrared (TIR) that has 5 bands with a spatial resolution of 90 m. Each subsystem operates in a different spectral region, with its own telescopes(s).

2.2.4.2. The VNIR subsystem

The VNIR subsystem consists of two independent telescope assemblies that minimize image distortion in the backward- and nadir-looking telescopes (Figure 6). The focal plane of the nadir telescope contains three silicon-charge-coupled detector line arrays (Bands 1, 2, 3N), while the focal plane of the backward telescope has only one (3B). The backward- and nadir-looking telescope pair is used for same-orbit stereo imaging (along-track stereo). The two near-infrared spectral bands, 3N and 3B, generate along-track stereo image pair with a base to height ratio (B/H) of about 0.6, and an intersection angle of about 27.7 degrees.

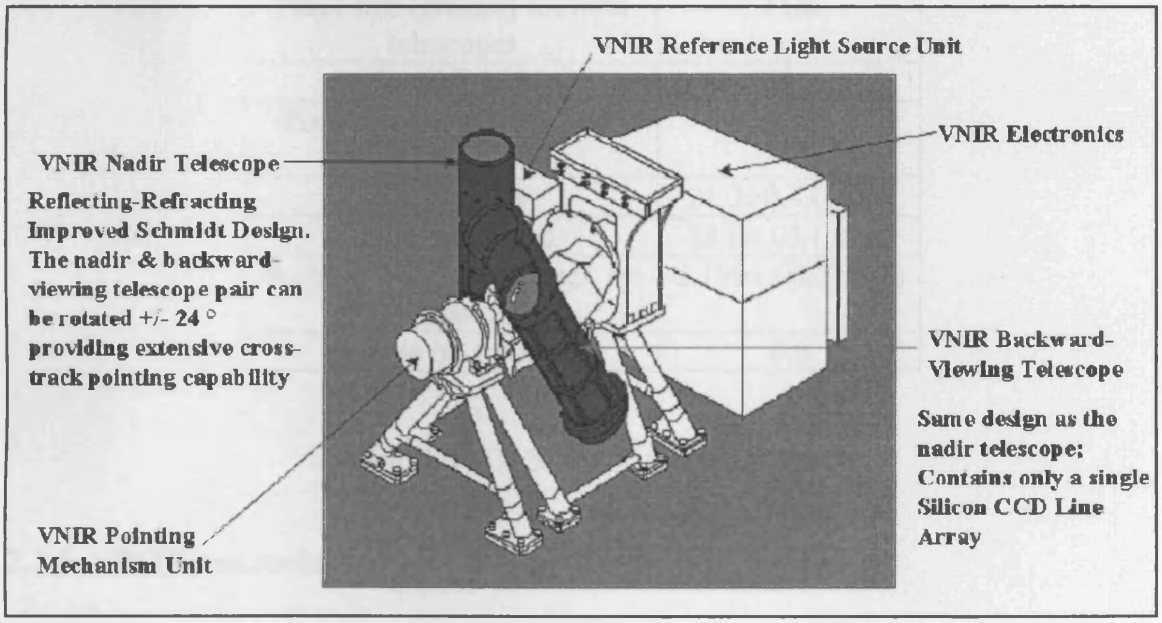

Figure 6. ASTER NVIR subsystem with its main modules (Abrams, 2002)

The two telescopes can be rotated plus-or-minus 24 degrees to provide extensive cross-track pointing capability and five-day revisit capability. Across-track stereo imaging with a better B/H ratio is theoretically possible. However, due to the high data rate of the three ASTER imaging subsystems, only eight minutes of data are acquired per orbit, and the along-track stereo imaging is then favored. The NVIR characteristics are shown in table 2 (ERSDAC, 2001). The focal length (c) of the backward telescope is not published and calculated from the equation 1:

$$c = \frac{d}{2 \cdot \tan\left(\frac{IFOV}{2}\right)} = \frac{0.007mm}{2 \cdot \tan\left(\frac{18.6\mu rad}{2}\right)} = 376.3mm \qquad \text{Eq. 1}$$

where

IFOV is cross-track instantaneous field of view for aft telescope

d is detector pixel size

Focal length of nadir telescope	329mm
Focal length of backward telescope	376.3mm
Pixel size (ground) for both telescopes	15m
Swath width	60km
Pixel size (sensor) for both telescopes	7μm
IFOV nadir	21.3±0.4 (μrad)
IFOV backward	18.6±.03 (μrad)
Scan period in along track for both telescopes	2.199±.002(μsec)
Base to height ratio	0.6

Table 2. ASTER NVIR technical data

2.2.5. SPOT constellation

2.2.5.1. Overview

Since 1986, SPOT satellites have been acquiring images of the Earth. Except SPOT3 that stopped acquisition on November 1996, SPOT 1, 2 and 4 formed a constellation where it reinforced with the launching of SPOT 5 in 2002. The first three SPOT missions belong to the first generation satellite, while the fourth satellite (SPOT4) represents the second generation including improvements in term of payload and positioning capabilities. SPOT 5 belongs to the latest generation of SPOT missions with significant improvements in terms of on-board instruments and autonomous system of

positioning and attitude control that is enable a high absolute location accuracy (SPOT,2002).

SPOT satellites are in the same orbit with different orbital phases with respect to each other along the orbit. The latter was put into orbit with a precise phasing in relation to SPOT 2 and SPOT 4. Thus, SPOT5 is placed at 97° ahead of SPOT 4 (Figure 7) while SPOT 4 is 97° of SPOT 2.

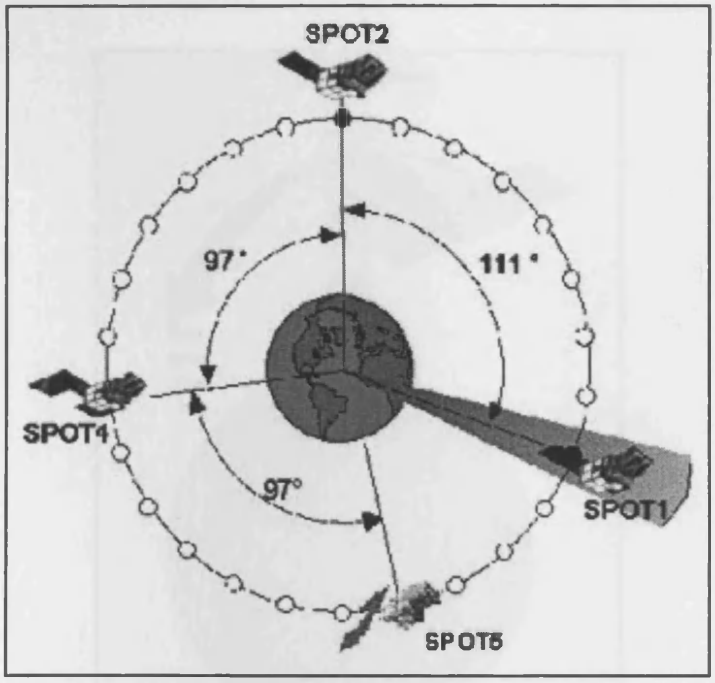

Figure 7. SPOT constellation (CNES)

2.2.5.2. SPOT-HRV

From SPOT1 to SPOT4, the main optical imaging instrument used, is the HRV (High Resolution Visible). Each satellite carries two HRVs (Figure 8) with the capability of scanning in either a multispectral mode or a panchromatic mode. The multispectral mode captures data in three spectral bands: 0.50-0.59, 0.61-0.68 and 0.79-0.89 micrometers. The three bands are co-registered and have a ground resolution of 20 meters. **The panchromatic mode images data in the spectral range 0.51-0.73 micrometers at a 10 meter ground resolution**. The HRV sensor consists of a mirror that can rotate up to 27 degrees right or left of the nadir position (earth curvature effects

produce a 31 degree angle). This cross-track pointing capability allows the same point on the earth to be viewed from several different orbits and enables the acquisition of stereoscopic imagery. An area is covered up to every three or four days depending upon the latitude of the area. The ground imaging swath is 60 km per HRV sensor. With both HRVs scanning in the twin vertical viewing mode the cross-track swath is 117 km. Each nominal scene covers a 60 by 60 km area. An improved version of HRV, called HRVIS, is carried by SPOT-4. It has a supplementary band in the multispectral mode at 1.5 - 1.7 micrometers.

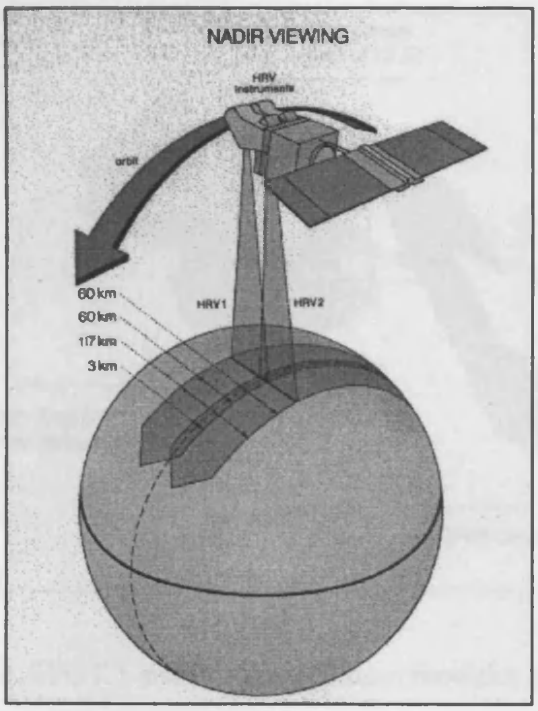

Figure 8. SPOT HRV (CNES)

2.2.5.3. SPOT5

2.2.5.3.1. Overview

SPOT 5 belongs to the third generation of SPOT constellation and is the latest satellite of SPOT family (Figure 9). It was launched during the night of the 3rd to the 4th of May 2002 from the European Spaceport in Kourou (French Guyana) with one of the last Ariane 4.

SPOT 5 gains significant improvements in terms of on-board instruments and autonomous system of positioning and attitude control, which enables high absolute

location accuracy. The two new HRG (High Resolution Geometry) instruments have derived from the HRV instruments on SPOT 4. They offer higher resolution: 2.5 meters to 5 meters in panchromatic mode and 10 meters in multispectral mode. Imagery at a resolution of 2.5 meters is generated using a new sampling concept dubbed "Supermode".

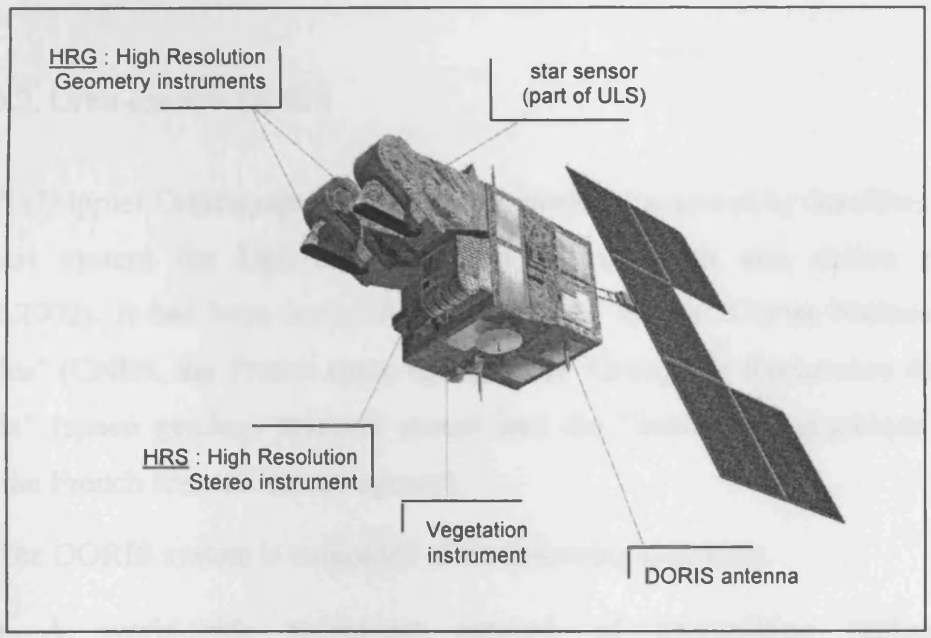

Figure 9. SPOT 5 satellite and its main modules (CNES)

SPOT 5 features a new HRS (High Resolution Stereo) imaging instrument operating in panchromatic mode (§2.2.5.3.4.). HRS points forwards and afterwards of the satellite position, giving the ability to acquire stereopair images almost simultaneously.

SPOT 5 also carries the recurrent VEGETATION 2 instrument. The SPOT 5 bus has also been derived from SPOT 4. A new star tracker will improve image location accuracy from 350 meters on previous satellites to just 50 meters. Orbital and physical characteristics of SPOT 5 are shown in table 3.

Mission period	5 years
Orbit	Sun synchronous
Attitude at equator	822 km
Time of day	10:30 am
Repeat cycle	26 days
Dimensions	3.1x3.1x5.7m
Satellite Weight	3000kg
Orbit determination	Doris in real time, 5m rms
Location accuracy	50m

Table 3. Orbital and physical characteristics of SPOT5

2.2.5.3.2. Orbit control- DORIS

DORIS (Doppler Orbitography and Radiopositioning Integrated by Satellite) is a radio-electrical system for high accuracy orbit determination and station positioning (SPOT,2002). It has been designed and developed by the "Centre National d'Études Spatiales" (CNES, the French space agency), the "Groupe de Recherches de Géodésie Spatiale" (space geodesy research group) and the "Institut Géographique National" (IGN, the French national survey agency).

The DORIS system is composed of the following elements:

- A world-wide permanent network of transmitting stations, called "orbitography network",
- Receivers on-board several satellites (currently SPOT2, SPOT4, SPOT5,Jason and Envisat),
- So-called "ground location stations", whose position is unknown a priori,
- A control center that performs system monitoring, instrument programming, and data processing / archiving.

DORIS can determine accurately the orbit of the satellites. For SPOT5, the DORIS-DIODE (Détermination Immédiate d'Orbite par DORIS Embarqué) system, which was used in SPOT4 for real-time determination has been coupled with an orbit propagator software called TRIODE, which is able to compute position and velocity with sub-meter accuracy. These ephemeris are dated every 30 seconds in UTC referential and ITRF terrestrial referential and transmitted to the ground along with the image telemetry.

2.2.5.3.3. Attitude control

Attitude control (angular orientation) is needed so that the optical system covers the programmed ground area at all times (SPOT, 2002). However, the satellite tends to change its orientation due to torque produced by the environment (drag of the residual atmosphere on the solar array, solar radiation pressure, etc.) or by itself (due to movement of mechanical parts such as on-board recorders or solar panel rotation). Therefore, the angular orientation has to be actively controlled. Another reason is the need to prevent "blurring" of the scenes acquired.

SPOT 5 has an inertial platform on board consisting of four rate gyros. Two-axis rate gyros are enough to provide angular rate measurements along the three axes of the satellite. The other two are used as backups. Gyros measure angular velocities along each one of the three axes, a star tracking unit computes absolute angles along the three attitude axis identifying constellations on the celestial vault. These measurements combined with the AOCS (Attitude and Orbit Control System) values provide high accuracy attitude measures to the ground (ULS).

2.2.5.3.4. SPOT-HRS

The High Resolution Stereoscopic instrument (HRS) has two telescopes and acquires nearly simultaneous stereopairs (at about 90-second interval) of 120-km swath, along the track of the satellite, with a base to height ratio of about 0.8 (Figure 10).

Forward and backward acquisitions cannot be performed at the same time. As a consequence, the maximum stereo segment that can be acquired is a little bit more than 600 km ($\approx$ 832 km altitude x 2 x tan (20°)).

Forward and backward images are obtained on the same panchromatic spectral band as for HRG. The size of the pixels on ground is 10m x 10m (SPOT, 2002). However, the HRS instrument has been designed for a ground sampling distance of 5 meters along the track. In a direction close to the epipolar planes, this along-track over-sampling allows

higher altimetric accuracy of the DEM to be obtained (absolute planimetric resolution from 10 to 15 meters). Detailed specifications of HRS sensor are shown in table 4.

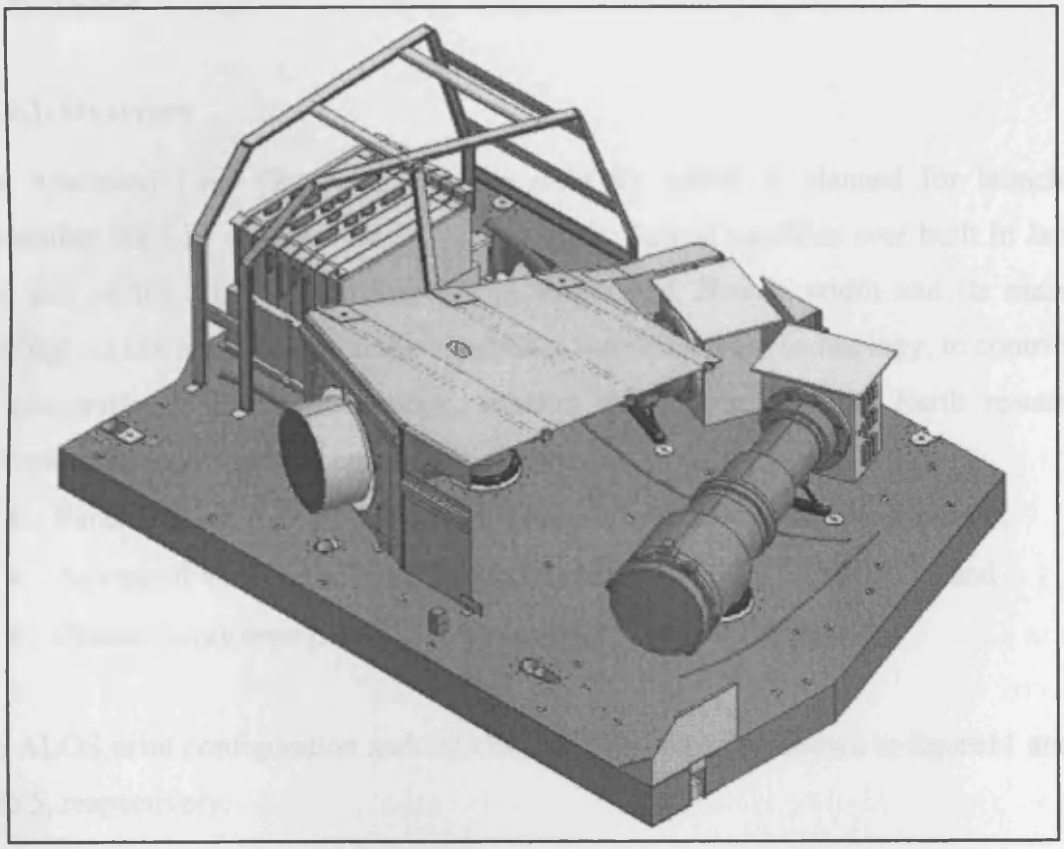

Figure 10. Detail figure of HRS camera (CNES)

Spectral range(panchromatic)	0.48μm-0.70μm
Focal length	580mm
Forward/after viewing angle	±20°
Detector per line	12000
Field of view	±4°
Pixel size (ground) across track	10m
Pixel size (ground) along track	5m
Swath width	120km
Detector pitch	6.5 μm
Integration time per line	0.752ms
Base to height ratio	0.8

Table 4.SPOT5-HRS specifications

2.2.6. ALOS

2.2.6.1. Overview

The Advanced Land Observing Satellite (ALOS), which is planned for launch in September 2005 by Japanese H-IIA vehicle, is the largest satellites ever built in Japan. The size of the ALOS is roughly 9m in length and 28m in width and its mass is 4,000kg. ALOS has five objectives: to advance land-observing technology, to contribute to cartography, regional observation, disaster monitoring, and the Earth resources surveying. Its major sensors are (Osawa, 2004):

- Panchromatic Remote-sensing Instruments for Stereo Mapping (PRISM),
- Advanced Visible and Near Infrared Radiometer type 2 (AVNIR-2), and
- Phased Array type L-band Synthetic Aperture Radar (PALSAR).

The ALOS orbit configuration and ALOS's specifications are shown in figure11 and in table 5, respectively.

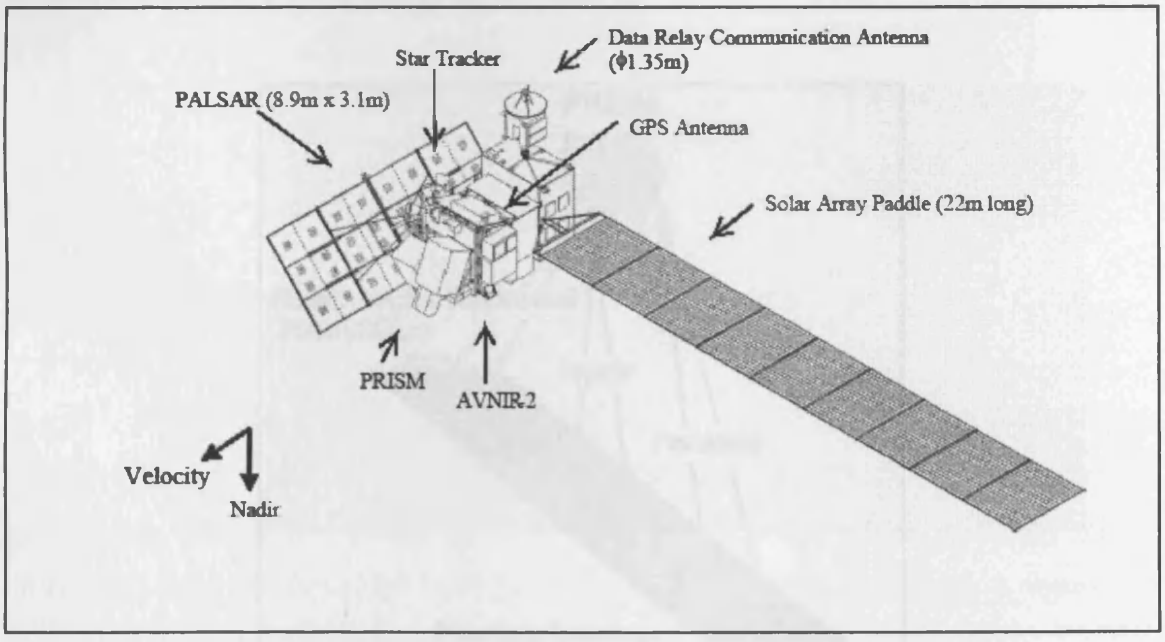

Figure 11. ALOS satellite and its main modules (Osawa, 2004)

Mission period	3-5 years
Orbit	Sun synchronous
Attitude at equator	691.65 km
Time of day	10:30 am
Repeat cycle	46 days
Inclination	98.16°
Satellite Weight	4000kg
Attitude determination accuracy	2.0×10^{-4} deg(with GCP)
Position determination accuracy	1m (off line)

Table 5.ALOS orbital characteristics

2.2.6.2. PRISM

The Panchromatic Remote-sensing Instrument for Stereo Mapping (PRISM) is a sensor mainly for mapping (Figure 12). It consists of three independent telescopes for forward, nadir and backward view and each telescope provides 2.5m spatial resolution. These specifications are given to generate precise Digital Elevation Model (DEM), and to achieve the accuracy for 1/25,000 scale maps.

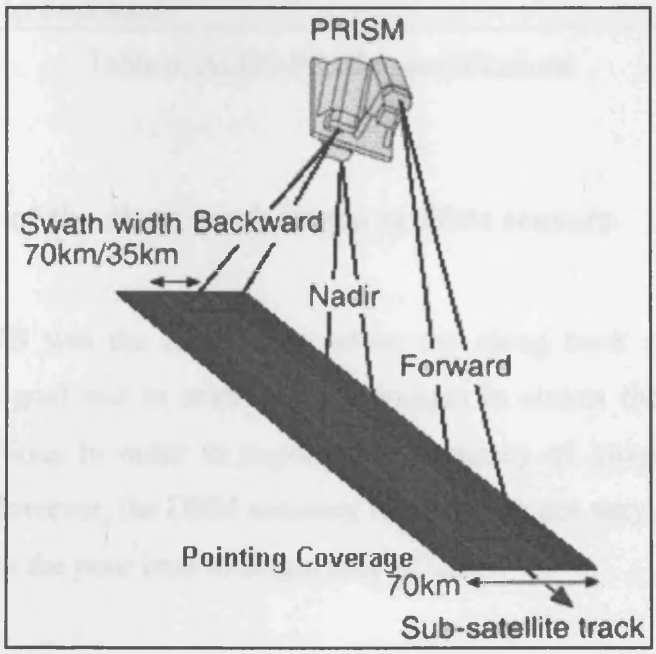

Figure 12. ALOS-PRISM three line acquisition (Tadono, 2004)

Each telescope consists of three mirrors and several CCD detectors for pushbroom scanning. The nadir-looking telescope provides 70 km width coverage; forward and backward telescopes provide 35 km width coverage each. Detailed specifications of ALOS-PRISM sensor are shown in table 6 (Chen et al., 2004; Tadono, 2004).

The telescopes are installed on both side of its optical bench with precise temperature control. Forward and backward telescopes are inclined + and - 24 degrees from nadir to realize a base to height ratio of 1.0. PRISM's wide field of view (FOV) provides fully overlapped three-stereo (triplet) images (35 km width) without mechanical scanning or yaw steering of the satellite. Without this wide FOV, forward, nadir, and backward looking images would not overlap each other due to the Earth's rotation.

Number of optics	3(Nadir; Forward; Backward)
Spectral range(panchromatic)	0.52μm-0.77μm
Focal length	1939mm
Angle from nadir	±23.8°
IFOV	3.61μrad
Swath width	70km(nadir)/35km(triplet mode)
Pixel size (ground)	2.5m
Number of detectors	14000(in triplet mode)
Pointing Angle	±1.5° (in triplet mode, cross track)
Integration time per line	0.37ms
Base to height ratio (forward to backward)	1

Table 6. ALOS-PRISM specifications

2.2.7. Summary of the along track stereo satellite sensors

In 1992, JERS-OPS was the first sensor where the along track stereo concept was applied. The main goal was to acquire stereo images in almost the same ground and atmospheric conditions in order to improve the accuracy of image matching during DEM procedure. However, the DEM accuracy results were not very good. It seems that the main reason was the poor base to height ratio of 0.3.

The MOMS concept in 1993 was based on a very promising idea of acquiring three along track images which is generally, provides better DEM accuracy from the two along stereo images. However, the implementation of this idea was not so successful due to the complexity of the camera which brought some functionality problems, along with the necessity of carrying the sensor on two spacecrafts (Space Shuttle and MIR), which were not designed for remote sensing applications.

TERRA-ASTER, SPOT5-HRS and ALOS-PRISM specifications are compared in table 7. TERRA-ASTER is one of the five instruments of TERRA satellite. In NVIR, it is preferred the nadir and the backward view instead of two oblique views because the deformation of the nadir images is minimum. However, this configuration of the optics leads to small base to height ratio of 0.6 as the angle (only 27.6°) between the two images is small.

On the other hand the configuration of the SPOT5-HRS is different. Forward and backward images are acquired providing an improved base to height ratio of 0.8. The deformation of the images are bigger than a nadir image and became critical in cases where the ground slope in along track direction is bigger than 30° (Dowman and Michalis, 2004). HRS images have a very large swath width and high navigation data accuracy. The onboard DORIS system in combination with the attitude control systems provides a very high accuracy of heights of about 5m without any use of GCPs in most cases (Airault et al., 2003; Valorge, 2003).

Finally, in ALOS-PRISM is used the most promising along track stereo configuration. The triple image acquisition has the advantages of both previous sensors. These advantages are the best base to height ratio of 1 (from forward to backward images) and the small deformation of the nadir image. Also from the geometry point of view the combination of the three rays give more accurate solution (§5.6) and in DEM generation process the accuracy is better since the heights are extracted from three images instead of two. The pixel size is better (2.5m) than the previous sensors and it is expected to produce detailed DEM of 10m.

	ASTER-NVIR	SPOT5-HRS	ALOS-PRISM
Orbit Altitude at equator	705km	822km	691.65km
Inclination	98.2°	98.7°	98.16°
Number of optics	2	2	3
Configuration of optics	nadir/back	for/back	for/nadir/back
Viewing angles	0°/-27.6°	+20°/-20°	+23.8°/0°/-23.8°
Base to height ratio	0.6	0.8	1(forward to backward)
Focal length (mm)	329mm(nadir) 376.3mm(back)	580mm	1939mm
Pixel size on the ground	15m	5m(along) 10m(across)	2.5m
Swath width	60km	120km	70km(nadir) 35km(triplet mode)

Table 7. TERRA-ASTER, SPOT5-HRS and ALOS-PRISM specifications comparison

In this thesis, two contiguous ASTER and an HRS data sets are used in the evaluation process of the sensor models which are described in §5.3.

2.3. Satellite Photogrammetry

2.3.1 Geometry of Pushbroom sensor

It has already been mentioned (§ 2.2.1.) in pushbroom scanner configuration that the scanning effect on the ground is due to the motion of the satellite, thus the image is not acquired instantaneously. **A pushbroom sensor model is a kinematic model trying to simulate the satellite motion during the acquisition time of the image.**

This is a popular configuration for solid-state sensors, since linear arrays are easier to build than area arrays and no mechanical scanning is required. (Mikhail et al., 2001). The perspective geometry in this case is interesting, since a pushbroom image has a perspective projection only in a perpendicular direction along the flight path. In the flight path generally the satellite holds a curvilinear motion.

The orientation of a pushbroom sensor on a satellite platform can be constructed in the following way: **Each line of the imagery, corresponding to one integration period of the sensor, can be considered to be a separate perspective image, with only a single dimension in the y-direction**. Each of these lines would therefore have its own perspective centre and orientation parameters. Thus, what may appear from the casual inspection to be a state image frame is, in fact a mosaic of many tiny **framelets** (Mikhail et al., 2001). The near functional dependency among this multitude of orientation parameters makes it impossible to attempt to estimate all. The usual strategy is to select a few independent parameters, estimate them, and express all the others in terms of this few. The most common approach in the literature is to model the kinematic orientation parameters with low order polynomials as a function of the sampling time (§2.3.4.).

The geometric strength of pushbroom images is poor, since each line is an independent image and has its own position and orientation due to platform motion. This can be ameliorated somewhat by the use of GPS and INS and also using a combination of linear sensors. The use of three line sensors, one pointing vertically and two others pointing forward and backward, yield much more stronger geometry for point determination (Mikhail et al., 2001).

2.3.2. Along track geometry

The basic principle of along track stereo imaging is to photograph ground objects by two or more pushbroom sensors from different view angles during in the same orbit. As an example the two line HRS pushbroom scanner (Figure 13) produces two stereo strips, each for the corresponding sensor.

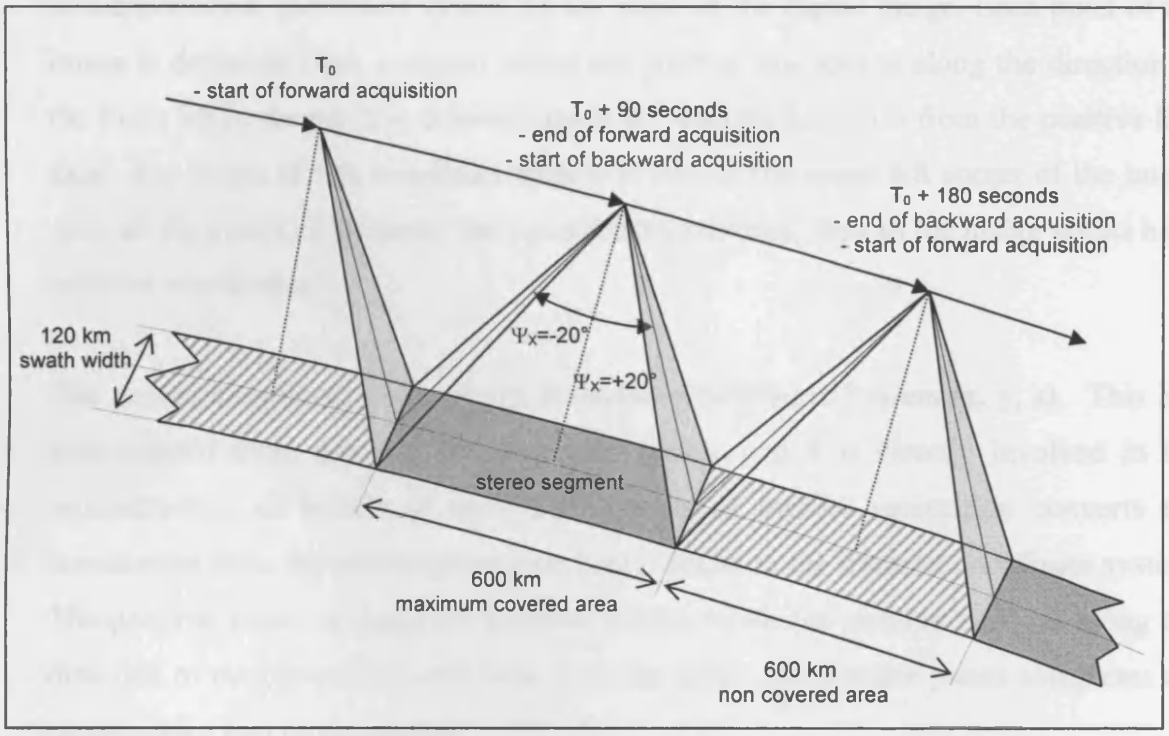

Figure 13. Along track geometry of SPOT5- HRS (SPOT, 2002)

In a few words the way of collecting the images is as follows: When the satellite approaches the mapping area, it collects data first by the fore-looking angle sensor and when it leaves the mapping area it collects data by the after-looking sensor at the same angle as the fore-looking imaging. The two image strips collected provide the simplest along-track stereo model. The three line sensor has also a nadir sensor giving a better geometric stability and image matching accuracy.

2.3.3. Reference coordinate systems in satellite photogrammetry

The essential reference coordinate systems for pushbroom sensor modeling are defined in this section.

The first coordinate system is **the measurement coordinate system (l,c)** which is a two-dimensional coordinate system on the plane of the digital image. Each pixel of the image is define as (line, column) where the positive line axis is along the direction of the flight while the positive column axis is 90° counterclockwise from the positive line axis. The origin of this coordinate system is usually the upper left corner of the image such all the pixels of the image have positive coordinates, thus all the image points have positive coordinates.

The second coordinate system is the **Framelet Coordinate System (x, y, z)**. This is a right-handed three dimensional coordinate system and it is directly involved in the reconstruction of bundle of rays. The process of interior orientation converts the coordinates from the measurement coordinate system to the framelet coordinate system. The positive x-axis is along the platform motion while the positive z-axis is along the direction of the optical axis and away from the earth. The positive y-axis completes the right-handed coordinate system.

The third coordinate system is the **Navigation Reference Coordinate System (O_1, X_1, Y_1, Z_1)** (Figure 14). The Navigation Reference Coordinate System (SPOT, 2002) is the body-fixed system used for spacecraft attitude determination and control. The coordinate axes are defined by the spacecraft attitude control system (ACS) which attempts to keep the navigation reference frame aligned with the Orbital Coordinate System so that the optical axis of instrument without mirror deviation is always pointing towards the center of the Earth.

As illustrated in (Fig 14), Y_1 axis is not necessarily strictly aligned with the satellite velocity vector. This misalignment may be due to small drift of yaw and pitch values in nominal case.

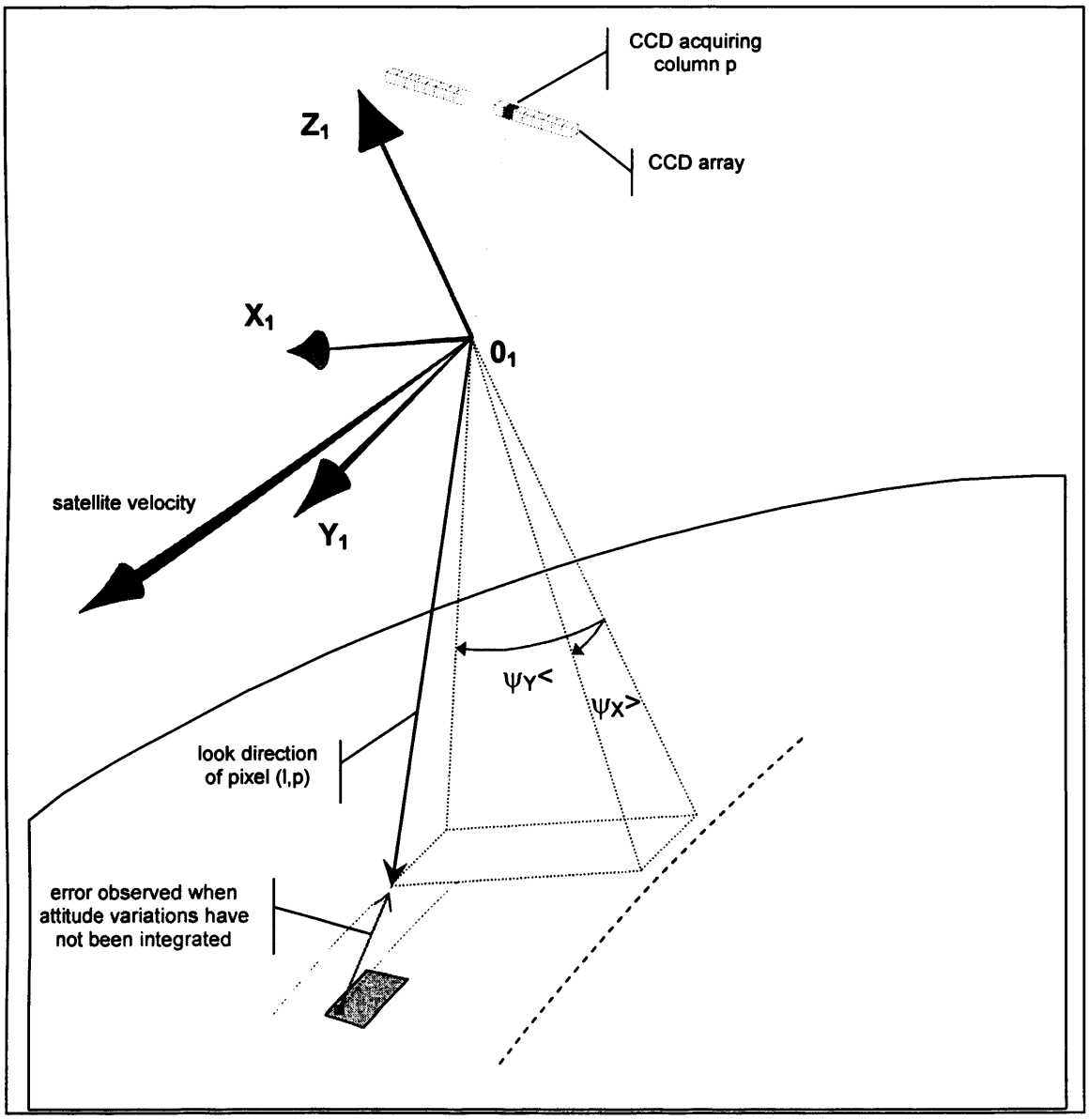

Figure 14. Navigation Reference Coordinate System (SPOT,2002)

The forth coordinate system **is the Orbital Coordinate System (O_2, X_2, Y_2, Z_2)** which is centered on the satellite (Figure 15), and its orientation is based on the spacecraft position in space (SPOT5, 2002). The origin is the spacecraft center of mass O_2, with the Z_2 axis pointing from the Earth center of mass to the spacecraft center of mass. The X_2 axis is the normalized cross product of the instantaneous velocity vector with Z_2 axis. Y_2 is the third unitary vector of the system (Eq. 2).

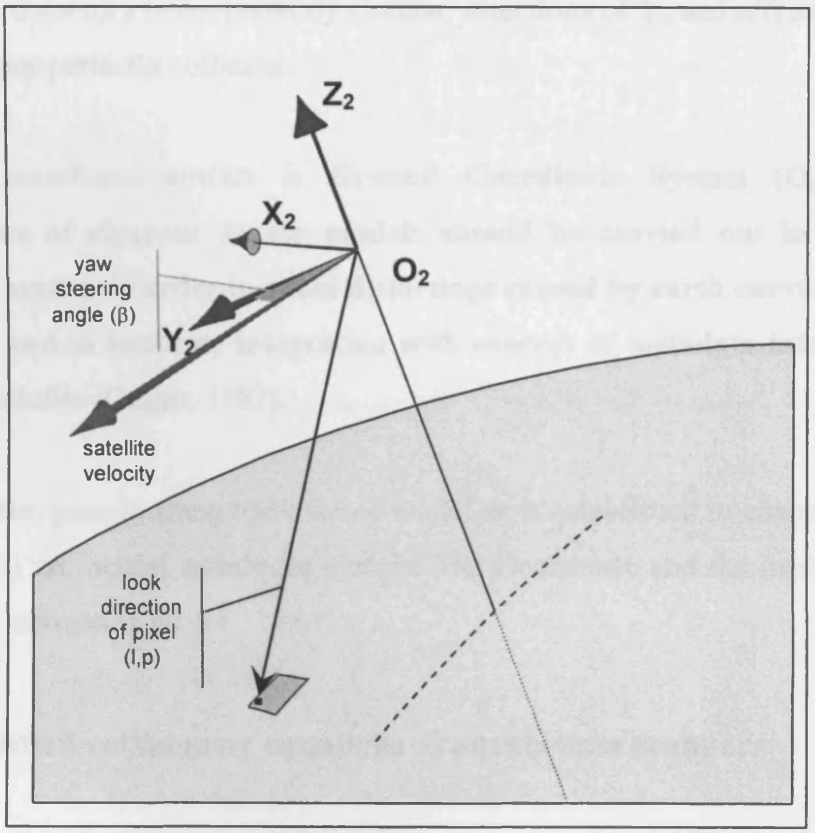

Figure 15. Orbital Reference Coordinate System (SPOT,2002)

$$\vec{Z}_2 = \frac{\vec{P}(t)}{\left\|\vec{P}(t)\right\|}$$

$$\vec{X}_2 = \frac{\vec{u}(t) \times \vec{Z}_2}{\left\|\vec{u}(t) \times \vec{Z}_2\right\|} \qquad \text{Eq. 2}$$

$$\vec{Y}_2 = \vec{Z}_2 \times \vec{X}_2$$

Where

$\vec{P}(t)$ is the position vector

$\vec{u}(t)$ is the velocity vector of the satellite at time t

Because the trajectory is not perfectly circular, directions of Y_2 and u(t) are close but the vectors are not perfectly collinear.

The fifth coordinate system is **Ground Coordinate System (O,X,Y,Z). The development of rigorous sensor models should be carried out in a geocentric coordinate system in order to avoid distortions caused by earth curvature and map projection and to facilitate integration with sources of metadata information that may be available** (Gugan, 1987).

Moreover, the generic along track stereo model as is established in chapter 5 should be developed in an inertial coordinate system. The Geocentric and the inertial coordinate systems are defined in §2.4.1.

2.3.4. Modified collinearity equations of pushbroom scanners

The well-known frame camera collinearity equations need modification before they are applied to pushbroom images. The principal point is mathematically defined as the intersection of the perpendicular line through the perspective center to the framelet. The length from the principal point to the perspective center is called the focal length or principal distance.

As it has already been mentioned (§2.3.1) a pushbroom image consists of a number of consecutive framelets which are one-dimensional scan lines. The relationship among framelets is modelled with low order polynomials as a function of the sampling time. Thus, the collinearity equations are modified as follows:

- x coordinate is always zero
- the z coordinate fixed at the negative of the principal distance (c)
- The ground coordinates and the rotations of the perspective sensor are modelled as a function of time.

$$\begin{bmatrix} 0 \\ y - y_0 \\ -c \end{bmatrix} = \lambda M(t) \begin{bmatrix} X - X_c(t) \\ Y - Y_c(t) \\ Z - Z_c(t) \end{bmatrix} \qquad \text{Eq. 3}$$

where

t is the acquisition time of a framelet which is defined in terms of image coordinates and it is calculated from equation 8

X, Y, Z are the ground coordinates of a point

$X_c(t)$, $Y_c(t)$, $Z_c(t)$ are the ground coordinates of the framelet perspective center as a function of time

λ is a scale factor which varies from point to point

$M(t)$ is a 3x3 rotation matrix which brings the ground coordinate system parallel to the framelet coordinate system as a function of time, as follows (rotation matrix components are shown in equation 7):

$$M(t) = \begin{bmatrix} m_{11}(t) & m_{12}(t) & m_{13}(t) \\ m_{21}(t) & m_{22}(t) & m_{23}(t) \\ m_{31}(t) & m_{32}(t) & m_{33}(t) \end{bmatrix} \qquad \text{Eq. 4}$$

y is the y-framelet coordinates of the corresponding point

y_0 is a small offset from the perspective center origin.

Multiplying the matrix and the vector on the right-hand side of the equation, three scalar equations are obtained instead of matrix equation:

$$\begin{aligned} 0 &= \lambda[m_{11}(t)(X - X_c(t)) + m_{12}(t)(Y - Y_c(t)) + m_{13}(t)(Z - Z_c(t))] \\ y - y_0 &= \lambda[m_{21}(t)(X - X_c(t)) + m_{22}(t)(Y - Y_c(t)) + m_{23}(t)(Z - Z_c(t))] \\ -c &= \lambda[m_{31}(t)(X - X_c(t)) + m_{32}(t)(Y - Y_c(t)) + m_{33}(t)(Z - Z_c(t))] \end{aligned} \qquad \text{Eq. 5}$$

By dividing the first two equations by the third the modified collinearity equations in classical form:

$$0 = -c\frac{m_{11}(t)(X - X_c(t)) + m_{12}(t)(Y - Y_c(t)) + m_{13}(t)(Z - Z_c(t))}{m_{31}(t)(X - X_c(t)) + m_{32}(t)(Y - Y_c(t)) + m_{33}(t)(Z - Z_c(t))}$$

Eq. 6

$$y - y_0 = -c\frac{m_{21}(t)(X - X_c(t)) + m_{22}(t)(Y - Y_c(t)) + m_{23}(t)(Z - Z_c(t))}{m_{31}(t)(X - X_c(t)) + m_{32}(t)(Y - Y_c(t)) + m_{33}(t)(Z - Z_c(t)))}$$

where the rotation matrix components are constructed as follows:

$$m_{11}(t) = \cos\phi_c(t)\cos k_c(t)$$

$$m_{12}(t) = \cos\omega_c(t)sink_c(t) + \sin\omega_c(t)\sin\phi_c(t)\cos k_c(t)$$

$$m_{13}(t) = \sin\omega_c(t)\sin k_c(t) - \cos\omega_c(t)\sin\phi_c(t)\cos k_c(t)$$

$$m_{21}(t) = -\cos\phi_c(t)\sin k_c(t)$$

$$m_{22}(t) = \cos\omega_c(t)\cos k_c(t) - \sin\omega_c(t)\sin\phi_c(t)\sin k_c(t)$$ Eq. 7

$$m_{23}(t) = \sin\omega_c(t)\cos k_c(t) + \cos\omega_c(t)\sin\phi_c(t)\sin k_c(t)$$

$$m_{31}(t) = \sin\phi_c(t)$$

$$m_{32}(t) = -\sin\omega_c(t)\cos\phi_c(t)$$

$$m_{33}(t) = \cos\omega_c(t)\cos\phi_c(t)$$

2.3.5. Time of acquisition

The time of acquisition is proportional to the coordinate of the point in the along scan direction. The main assumption that should be done at this point is that the scanning time interval is constant during the acquisition time of the image (McGlone, 2004).

$$t = t_o + (line - line_o)dt_{line}$$ Eq. 8

where

t is the corresponded time of the framelet containing a point on the image

line is the line coordinate of the point, parallel to the scanning direction

$line_o$ is the line coordinate of the reference time t_o

dt_{line} is the acquisition time for one line.

The reference point is not strictly defined, in advance. Having in mind that generally in photogrammetry, the origin of the image space coordinate system is the center of the image it is obvious to think even in the case of time dependent images that the center point of the central framelet should act as the origin. However for the satellite images this statement is not compulsory. As it has already been accepted (§2.3.1) a pushbroom image consists of a number of consecutive one-dimensional scan lines with their own exterior orientation parameters. This means, that every framelet could act as a base line. The appropriate reference framelet should be chosen according to which one in the image is time related. This means every framelet center could be the principal point of the pushbroom image if there is a strictly time relation with the framelet, itself.

2.4. Astrodynamics

In this thesis, astrodynamics provides the essential tools in the development of the along track stereo sensor model. Astrodynamics is defined as **the study of the motion of man-made object in space, subject to both natural and artificially induced forces (Vallado, 2001).** From a historical perspective, true astrodynamics has only existed since 1950's. However, the basic principals of Astrodynamics are based on the Kepler and Newton laws, which were discovered in 16th century.

2.4.1. Reference Coordinate Systems

One of the first requirements for describing an orbit is to define a suitable inertial reference frame, along with appropriate coordinate systems for observation measurements. In this thesis three Earth based reference coordinate systems are used:

- The space-fixed, inertial reference system (CIS)
- The earth-fixed terrestrial reference system (CTS)
- The Perifocal coordinate system

2.4.1.1. The space-fixed, inertial reference system (CIS)

It is a geocentric system where the fundamental plane is the Earth's equator (Figure 16). The positive X axis points towards the vernal equinox; the positive Z-axis is oriented towards the North Pole and the Y-axis completes a right-handed coordinate system. It is the most common system in astrodynamics, but it is also the most confusing (Vallado, 2001). This system is also named, **Conventional Inertial System (CIS)**. The equinox and plane of the equator moves slightly over time, so the term 'inertial' can cause confusion. It is achieved a 'pseudo' Newtonian inertial system if there is a reference to the equator and equinox at a particular epoch. For the time being this system is defined from the FK5. The FK5 system is based on the Fundamental Katalog, FK5 star catalogue and J2000 is a quasi-inertial frame realized in the FK5 system. The equator and equinox's motion is precisely modelled, so inertial frames of other times can be transformed to the J2000 frame. It is important to mention that the geocentric equatorial frame is nonrotating with respect to the stars (except for precession of the equinoxes) and the earth turns relative to it.

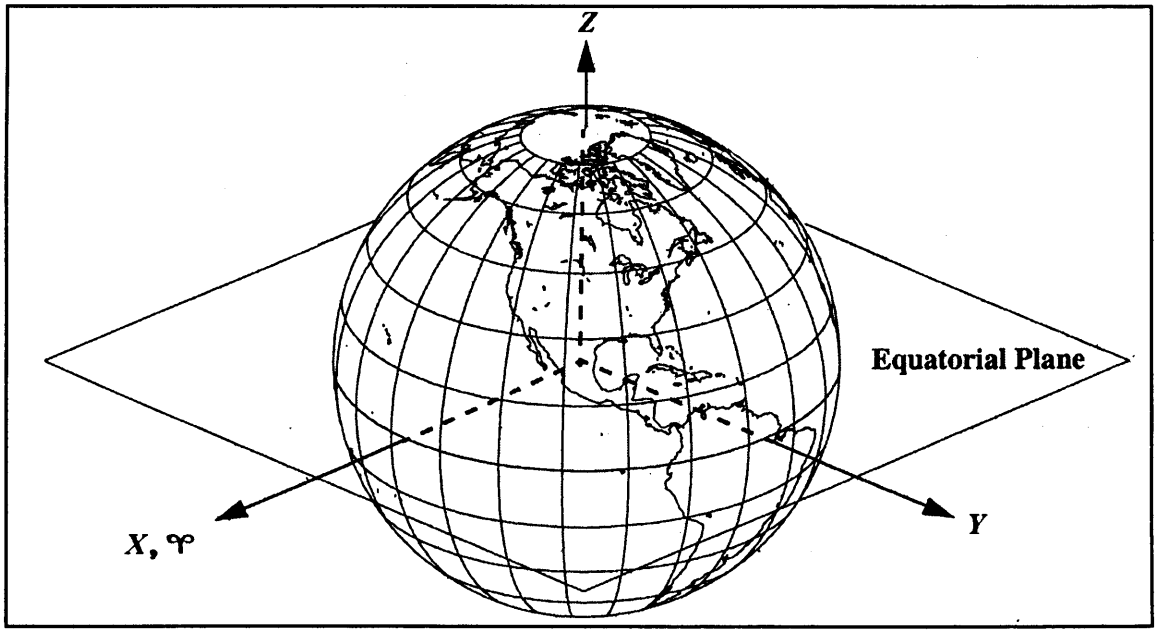

Figure 16. Conventional Inertial System (CIS)

2.4.1.2. The earth-fixed terrestrial reference system (CTS)

A suitable earth-fixed reference system must be connected in a well defined way with the earth's centre. A Conventional Terrestrial system is the International Terrestrial Reference Frame (ITRF) which is realized through a set of Cartesian coordinates of the fundamental stations within a global network. Another conventional Terrestrial system is the WGS84 system which is realized through GPS observations, although the fundamental WGS-84 stations are usually constrained by their adopted ITRF coordinates during solution. Thus, the WGS-84 and ITRF terrestrial frames agree at the centimetre level, so within the uncertainty of the WGS-84 frame, they are practically identical. Typically, the CTS is used to process actual observations and acceleration calculations during orbit determination.

2.4.1.3. The Perifocal Coordinate System (PQW)

A convenient system for processing satellite observations is the perifocal coordinate system, PQW (Vallado, 2001). In this system the fundamental plane is the satellite orbit, and the origin is at the centre of the Earth (Figure 17).

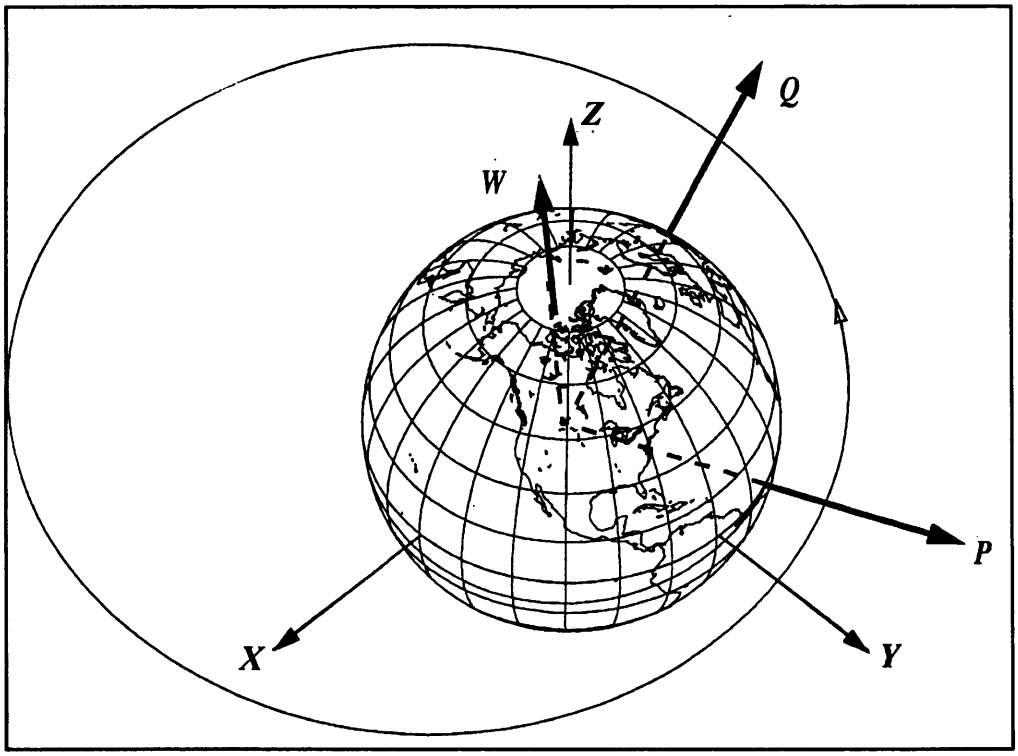

Figure 17. Perifocal Coordinate System

The *P* axis points towards perigee and the *Q* axis is 90° from the P axis in the direction of satellite motion. The W axis is perpendicular to the orbit.

2.4.1.4. Transition from CIS to CTS

The transition from the CIS to CTS is realized through a sequence of rotations that account for (Seeber, 1993):

- Precession
- Nutation
- Earth rotation including polar motion

2.4.1.4.1. Precession and Nutation

The earth's axis of rotation and its equatorial plane are not fixed in space, but rotate with respect to an inertial system. This is due to the gravitational attraction of the moon and the sun on the equatorial bulge of the earth. The total motion is composed of the mean secular component (precession) and the periodic component (nutation). The position and orientation of the equatorial plane and the first point of Aries is called mean equator and mean equinox, respectively, when only the influence of precession is considered. When nutation is taken into account, they are called true equator and true equinox. The respective star coordinates are termed mean positions or true positions.

Precession and nutation can be transformed from the reference epoch J 2000 to the required observation epoch through known formulation.

2.4.1.4.2. Earth rotation and polar motion

For a transition from an instantaneous space-fixed equatorial system to a conventional terrestrial reference system three further parameters are needed. They are called Earth Rotation Parameters (ERP), namely:

Apparent Greenwich sidereal time (GAST)
Pole coordinates.

Unlike precession and nutation, the earth rotation parameters can not be described through theory but must be determined through actual observations by an international time and latitude service. For the last 80 years, this service was based mainly on astronomical observations. On January 1, 1998 the International Earth Rotation Service (IERS) took over this task. The principle observation techniques now used are Laser ranging to satellites and to the moon and Very Long Baseline Interferometry (VLBI).

2.4.1.5. Ellipsoidal Reference Coordinate Systems

For practical applications ellipsoidal coordinate systems are preferred because they closely approximate the earth's surface, and they facilitate a separation of the horizontal position and height. A rotational ellipsoid is selected and created by rotating the meridian about the minor axis b. The geometric parameters are

a	Semi-major axis
f	Flattening
e	First numerical eccentricity

The best possible approximation to the figure of the whole earth is a global ellipsoidal system. The ellipsoidal geographical coordinates are:

φ	ellipsoidal latitude
λ	ellipsoidal longitude
h	ellipsoidal height

The earth-fixed terrestrial coordinate system X,Y,Z (Cartesian coordinates) can be defined within the ellipsoid where the origin is the earth centre; the Z- Axis directed to the northern ellipsoid pole; the X- Axis directed to the ellipsoid zero meridians and the

Y-axis completing a right-hand system. The transformation equation between the geographical ellipsoidal coordinates and the Cartesian coordinates is Eq. 9.

$$\begin{aligned} X &= (N+h)\cos\phi\cos\lambda \\ Y &= (N+h)\cos\phi\sin\lambda \\ Z &= ((1-e^2)N+h)\sin\phi \end{aligned} \qquad \text{Eq. 9}$$

Where N is the radius of curvature in the prime vertical

$$N = \frac{a}{\sqrt{1-e^2\sin^2\phi}} \qquad \text{Eq. 10}$$

One solution of the inverse problem is

$$\begin{aligned} h &= \frac{\sqrt{X^2+Y^2}}{\cos\phi} - N \\ \phi &= \arctan\frac{Z}{\sqrt{X^2+Y^2}}\left(1-e^2\frac{N}{N+h}\right)^{-1} \\ \lambda &= \arctan\frac{Y}{X} \end{aligned} \qquad \text{Eq. 11}$$

The equation can only be solved by iterations, because φ and h are also present on the right-hand side of the equations. The convergence is fast since h<<N

2.4.1.6. Ellipsoid, Geoid and Geodetic Datum

The physical shape of the real earth is closely approximated by the mathematical surface of the rotational ellipsoid. The ellipsoidal surface is smooth and convenient for

the mathematical operations. This is why the ellipsoid is widely used as the reference surface for the horizontal coordinates in geodetic networks (Seeber, 1993).

On the other hand the ellipsoid is much less suitable as a reference surface for the vertical coordinates. Instead the geoid is used. It is defined as the level surface of the gravity field which best fits the mean sea level, and may extend inside the solid body of the earth.

The vertical separation between the geoid and a particular reference ellipsoid is called the geoid undulation. The numerical values of the undulation for a global reference ellipsoid can reach up to 100m. The geometrical relation between the geoid undulation N, the ellipsoid height h and the orthometric height H (obtained from the spirit level) is approximately:

$$h = N + H \qquad \text{Eq. 12}$$

It is evident that the geoid undulation N must be known when observations from the satellite geodesy (leading to ellipsoidal heights) and from terrestrial geodesy (leading to heights defined in the gravity field) are used in a combined adjustment.

A global ellipsoidal system is related to a reference ellipsoid that best fits the figure of the earth as a whole. The origin of the ellipsoid is supposed to coincide with the earth's centre of masses. Furthermore the directions of the ellipsoidal axes are defined so as to be parallel to the conventional terrestrial reference system. The set of parameters that describe the relationship between a particular local ellipsoid and a global geodetic reference system is called a geodetic datum.

A geodetic datum where the coordinates of Ground Control Points are measured is defined by a set of at least five parameters:

a	semi-major axis of the reference ellipsoid
f	flattening
$\Delta X, \Delta Y, \Delta Z$	coordinates of the ellipsoid origin with respect to the Earth centre.

In practice the establishment of a local geodetic datum does not always achieve the objective of axes parallel to the conventional terrestrial reference system. This is in particular the case of many existing national datums. Out of this reason, a transition from one ellipsoidal reference coordinate system to another also includes rotations. Usually such a datum transformations are established between Cartesian systems.

A complete datum transformation equation between Cartesian systems requires seven parameters:

3 translations ΔX, ΔY, ΔZ
3 rotations ε_x, ε_y, ε_z
1 scale factor m

2.4.2. Time

According to Newcomb (1960), 'the main purpose of time is to define with precision the moment of a phenomenon'. In this thesis **time** is assumed as **a unique one-dimensional coordinate system which is defined universally and associates individual phenomenon together.** Having the previous state in mind, time should be defined as a coordinate system. Time origin should be established along the unity vector which is simply the time interval. The Christian era, although others exist, is the fundamental epochs (origin) from which intervals are counted. The moment of a phenomenon is referred to as the **epoch** of the event. In order to determine the epoch of an event, the time interval should be precisely defined.

However, it is difficult to find precise repeatable time interval. Four time scales now provide accurate timekeeping: sidereal time, solar (universal time), dynamical time, and atomic time. Sidereal time and solar time are based on the Earth's rotation and are related through mathematical relationship. Atomic and dynamical times are independent from earth rotation.

Solar time is based on the interval between successive transits of the Sun over a local meridian, which establishes the solar day. The most common time used is the **Coordinated Universal Time, UTC**, which is derived from atomic time. UTC is the basic of the time systems and is on ordinary clocks. UTC and TAI (later in this section) always differ by an integer numbers of seconds.

Sidereal time is a direct measure of the Earth's rotation and it is measured positively in the counter-clockwise direction when viewed from the North Pole. Sidereal time is defined as the hour angle of the vernal equinox relative to the local meridian. Because the vernal equinox is the reference point, the sidereal time associated with the Greenwich meridian is termed **Greenwich Mean Sidereal Time,** θ_{GMST} or GMST. The sidereal time at a particular longitude is called Local Sidereal Time, θ_{LST} or LST. However the mean sidereal time refers to a mean equinox that moves slowly with the secular motion (precession). **Apparent sidereal time** is measured from the true vernal equinox which includes secular and periodic contributions to the motion of the vernal equinox. The apparent sidereal time associated with the Greenwich meridian is termed **Greenwich Apparent Sidereal Time,** θ_{GAST} or GAST.

Dynamical time is measured by the equation of motion where time is an independent value. The motion which used is the moon's motion about the Earth.

Atomic time is the most precise time standard. It is based on the specific quantum transition of electrons in the cesium-133 atom. The transition causes the emission of photons of a known frequency, which can be counted. The atomic second is defined by a fixed number of cycles. **International Atomic Time (TAI)** is a product of the Bureau International des Poids in Serves, France and is based on the analysis of individual standards for commercial frequencies plus the primary frequency standards maintain by several countries (Vallado, 2001). TAI achieves a precision that permits the observation of relativistic effect for clocks in motion or accelerated by a local gravitational field.

Julian Date (JD) is the number of days since noon January 1, 4713 BC including the fraction of day. It thus provides a continuous time scale which, for all practical

purposes, is always positive. Presently, the Julian Day numbers are already quite large (over two millions) and it is also desirable to start counting at midnight. Therefore, a **Modified Julian Date (MJD)** is defined as:

$$MJD=JD-2400000.5 \qquad \text{Eq. 13}$$

2.4.3. Historical background and basic laws

In 1609, **Johann Kepler** (1571-1630) published his first two laws of the planetary motion. The third law followed in 1619. From 1601 until 1606 he tried fitting various geometrical curves to Tycho Brahe (1456-1601) accurate observations of planets motion.

These laws which mark the beginning of a new epoch in the history of mathematical science are as follows:

1. **The orbit of each planet is an ellipse with the sun at one focus.**
2. **The line joining the planet to the sun sweeps out equal areas in equal times.**
3. **The square of the period of a planet is proportional to the cube of its mean distance from the sun.**

Still, Kepler's laws only describe the planetary motion without giving any explanation. It remained for the **Isaac Newton** (1642-1727) to unravel the mystery. **The laws of planetary motion can also be applied to a satellite's orbit around the Earth. This is due to the fact that the force resulting from the Earth's central mass dominates all other forces acting on the satellite by several orders of magnitude (§ 2.4.9), in much the same way as the attraction of the Sun governs the motion of the planets (Montenbruck et al.,2001).**

In 1687, Isaac Newton published one of the supreme achievements of the human mind, 'The Mathematical Principles of Natural Philosophy', or, more simply, 'the Principia'.

In Principia were included all the work that Newton did twenty years earlier when he was a student at the University of Cambridge.

In Book I of the Principia, Newton introduced his three laws of motion:

1. **Every body continues in its state of rest or of the uniform motion in a straight line unless it is compelled to change that state by forces impressed upon it.**
2. **The rate of change of momentum is proportional to the force impressed and is in the same direction as that force acts.**
3. **To every action there is always an equal and opposite reaction**

Beside his three laws of motion Newton formulated **the law of universal gravity by stating that any two bodies attracts one another with a force proportional to the product of their masses and inversely proportional to the square of the distance between them.**

The mathematical expression of the law of the universal gravity in vector notation is:

$$\vec{F} = -\frac{GMm}{r^2}\frac{\vec{r}}{r} \qquad \text{Eq. 14}$$

where

$\vec{F}$ is the force of the mass m due to the mass M

$\vec{r}$ is the vector from M to m and finally

G is the universal gravitational constant with a value of $6.673 \cdot 10^{-20} km^3/(kg \cdot s^2)$

Before Newton's second law is applied in two body problem to determine their relative motion, an inertial reference frame should be established. Newton described this inertial reference frame by saying that it was fixed in absolute in its own nature, without

relation to anything external, remained always similar and immovable. However, he failed to establish this frame which is absolute at rest.

2.4.4. Two body problem

In astrodynamics the motion of celestial bodies is concerned with the influence of mutual mass attraction. The simplest form is the motion of the two bodies (two-body motion). For the artificial satellites the mass of the smaller body (the satellite) can be neglected compared with the mass of the central body (the Earth). It is considered a system of only two bodies which are the Earth with mass M and a satellite in an orbit around earth with mass m_{sat} (Figure 18).

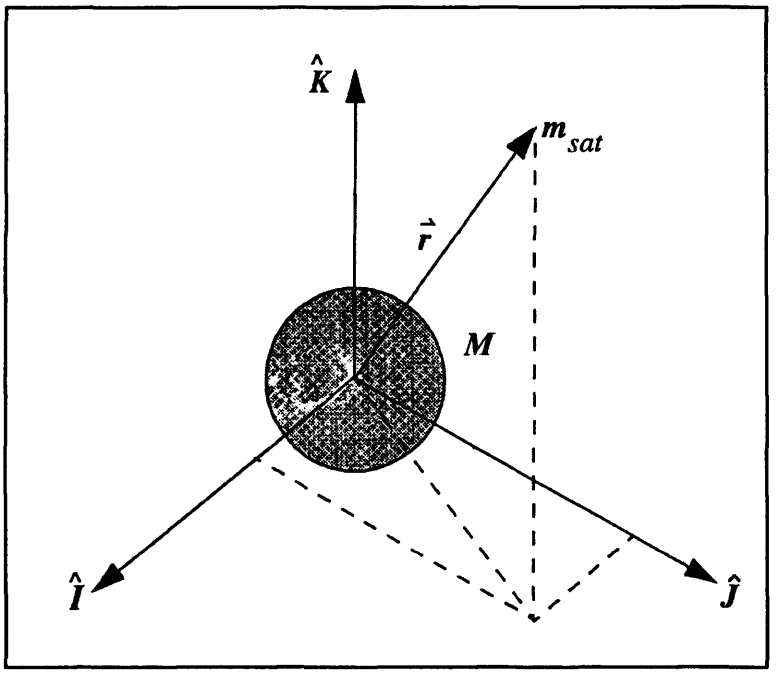

Figure 18.Two body motion (Vallado, 2001)

To develop the two-body equations, it is assumed (Vallado, 2001):

- The mass of the satellite is negligible compared to that of the attracting body. This is reasonable for the artificial satellites in the foreseeable future.
- The coordinate system chosen for the particular problem is inertial. The importance of this assumption becomes apparent in the derivations which

follow; in essence, it removes derivatives of the coordinate system itself when differentiating vectors.

- The bodies of the satellite and the attracting body are spherically symmetrical, with uniform density. This allows us to treat each as a point mass.
- No other forces act on the system except for gravitational forces that act along a line joining the centres of the two bodies.

The fundamental differential equation for two-body problem can be formulated in the following way:

$$\ddot{\vec{r}} + \frac{GM}{r^3}\vec{r} = 0 \qquad \text{Eq. 15}$$

where

the $\ddot{\vec{r}}$ is the relative acceleration due to the mass M in the neglected m

$\vec{r}$ is the vector from M to m and

the Earth gravitational parameter, GM, has the value of $398600{,}4415 km^3/s^2$.

$$\text{or } \frac{d\vec{u}}{dt} = -\frac{GM}{r^3}\vec{r} \qquad \text{Eq. 16}$$

where $\vec{u}$ represents the velocity vector.

It is worth emphasizing that equation 16 is actually the vector form of three simultaneous second-order, nonlinear, scalar differential equation in the components of vector $\vec{r}$ as (Battin, 1999):

$$\vec{r} = X \cdot \vec{i} + Y \cdot \vec{j} + Z \cdot \vec{k} \qquad \text{Eq. 17}$$

Specifically,

$$\frac{du_x}{dt} = -\frac{GM}{r^3}X \qquad \frac{du_y}{dt} = -\frac{GM}{r^3}Y \qquad \frac{du_z}{dt} = -\frac{GM}{r^3}Z \qquad \text{Eq. 18}$$

where

$$r = \sqrt{X^2 + Y^2 + Z^2} \qquad \text{Eq. 19}$$

and (u_x, u_y, u_z) represent the velocity vector of the corresponding position (X,Y,Z).

Even though the second-order vector differential equation is nonlinear, it is capable of a completely general analytical solution (Battin, 1999). In order to solve this equation, initial values of the velocity and the position vector are needed at a specific time stamp (epoch). The position and the velocity vectors at a specific epoch represent the **state vector of the satellite**. It is obvious that from equation 18 it is possible to calculate the state vector of the satellite at a future epoch. The initial quantities can take on many equivalent forms. A classical alternative of the state vector is the **orbital elements**. Orbital elements are typically used for the scalar magnitude and the angular representation of the orbit. Either set of quantities completely specify the two-body orbit and provide a complete set of initial conditions for solving the differential equation of two-body problem. **Time is always associated with a state vector and is often considered the seventh component.**

2.4.5. Orbital Elements

2.4.5.1. Classical orbital elements

The second-order differential equation which describes the relative motion of two bodies is immediately integrable. **The constants of integration are the orbital elements (Battin, 1999).** Therefore, as it has already been mentioned, the unknowns in equation 14 are six. Therefore six integration constants of the two-body orbit are referred to as the elements of the orbit. Various combinations of elements are found in the literature. In this thesis, classical elements are used in sensor modelling.

Five independent quantities are sufficient to completely describe the size, shape and the orientation of the orbit. A sixth element is required to pinpoint the position of the satellite along the orbit at a particular time.

The classical six orbital elements are defined with the help of figure 19 and 20 as follows:

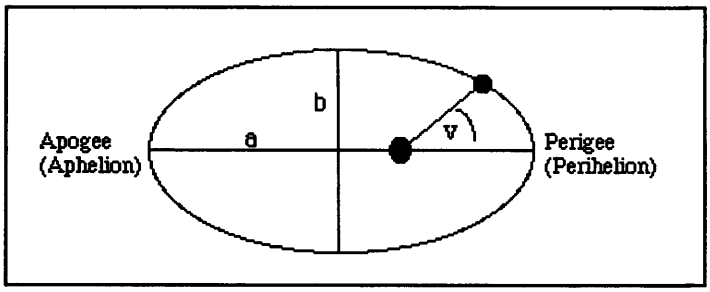

Figure 19. Orbital elements (1)

a Semi-major Axis (meters) defining the size of the orbit

e Eccentricity defining the shape of the orbit

v True Anomaly (degrees) defining the angle between perigee and the satellite (in the orbit plane)

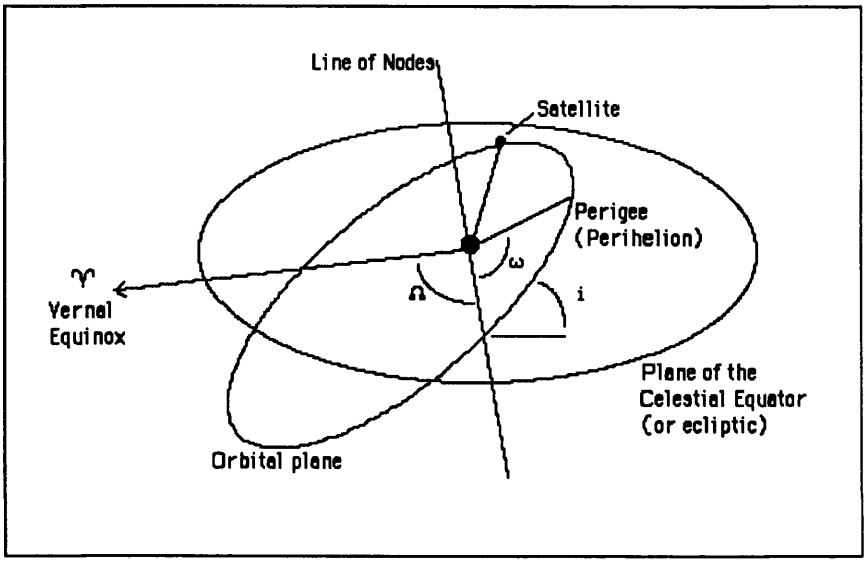

Figure 20.Orbital elements (2)

i Inclination (degrees) defining the angle between the equator and the orbit plane

Ω Right Ascension of the Ascending Node (degrees) defining the angle between vernal equinox and the point where the orbit crosses the equatorial plan (going north)

ω Argument of Perigee (degrees) defining the angle between the ascending node and the orbit's point of closest approach to the earth (perigee) .

Also same important terminology is introduced:

Apogee The furthest a satellite gets from the Earth in its orbit.

Perigee The closest a satellite gets to the Earth in its orbit.

Line of Nodes The point where the satellite crosses the equator.

Ascending Node The node where the satellite crosses the equator from below to above.

2.4.5.2. Nonsingular orbital elements

The orbit of remote sensing satellites are chosen to be near-circular, to provide a constant distance from the surface of the Earth. While there is no inherent difficulty in calculating position and velocity from known orbital elements with eccentricity close to zero, the reverse task caused practical and numerical problems (Montenbruck et al., 2001). These problems are due to the singularities arising from the definition of some of the classical orbital elements. The argument of perigee is not a meaningful orbital element for small eccentricities, since the perigee itself is not well defined for an almost circular orbit. Small changes of the orbit may change the perigee location by a large amount. Several attempts have therefore been made to substitute other parameters for the classical orbital elements. These elements are usually referred as non-singular elements. A possible set of regular elements that may be used for low eccentricities is defined as follows:

a	$h= e \sin(\Omega+\omega)$	$p=\sin(i/2)\sin\Omega$	
$l=\Omega+\omega+M$	$\kappa=e\cos(\Omega+\omega)$	$q=\sin(i/2)\cos\Omega$	Eq. 20

In this thesis, a model based on classical orbital elements is evaluated where the above statements are approved. However, **the instability of this model seems that it is not only because of the singularities of the classical orbital elements but also because of the attempt of describing the orbit (shape and orientation) which has a period of almost 101 minutes using information (image) covering only 10 seconds of this orbit (§ 4.8.2).**

2.4.6. State vector from orbital elements

Converting between state vectors to orbital elements is one of the most common problems in astrodynamics (Bate et al., 1971). In this thesis a transformation from the orbital elements to the state vector is used (§ 4.9). The formulation is the following:

$$X = \frac{p}{1+e\cos\theta}\{[\cos(\Omega)\cos(\omega)-\sin(\Omega)\cos(i)\sin(\omega)]\cos(\theta)+[-\cos(\Omega)\sin(\omega)-\sin(\Omega)\cos(i)\cos(\omega)]\sin(\theta)\}$$
$$Y = \frac{p}{1+e\cos\theta}\{[\sin(\Omega)\cos(\omega)+\cos(\Omega)\cos(i)\sin(\omega)]\cos(\theta)+[-\sin(\Omega)\sin(\omega)+\cos(\Omega)\cos(i)\cos(\omega)]\sin(\theta)\}$$
$$Z = \frac{p}{1+e\cos\theta}[\sin(i)\sin(\omega)\cos(\theta)+\sin(i)\cos(\omega)\sin(\theta)]$$

$$u_x = n\{-[\cos(\Omega)\cos(\omega)-\sin(\Omega)\cos(i)\sin(\omega)]\sin(\theta)+[-\cos(\Omega)\sin(\omega)-\sin(\Omega)\cos(i)\cos(\omega)](e+\cos(\theta)\}$$
$$u_y = n\{-[\sin(\Omega)\cos(\omega)+\cos(\Omega)\cos(i)\sin(\omega)]\sin(\theta)+[-\sin(\Omega)\sin(\omega)+\cos(\Omega)\cos(i)\cos(\omega)](e+\cos(\theta)\}$$
$$u_z = n[-\sin(i)\sin(\omega)\sin(\theta)+\sin(i)\cos(\omega)(e+\cos(\theta)]$$

Eq. 21

Where

$$n = \sqrt{\frac{GM}{p}} \qquad \text{Eq. 22}$$

and

$$p = a(1-e^2) \qquad \text{Eq. 23}$$

is the semiparameter of the orbit.

2.4.7. Specific Angular Momentum and Mechanical Energy

The specific angular momentum ($\vec{h}$) that is independent of mass; begin by cross-multiplying the two-body equation with the position vector, $\vec{r}$.

$$\vec{h} = \vec{r} \times \vec{u} = const \qquad \text{Eq. 24}$$

An alternative equation of the specific angular momentum is:

$$h = r^2 \cdot \dot{u} \qquad \text{Eq. 25}$$

Thus any position and velocity vector pair taken at the same point in time will uniquely determine the specific angular momentum. With the following equations the magnitude of this specific angular momentum is determine in case where the position and velocity vectors are unknown.

$$p = \frac{h^2}{GM} = a \cdot (1-e^2) \quad \text{and} \quad h = \sqrt{GM \cdot p} \qquad \text{Eq. 26}$$

To derive the energy constant of motion that is also independent of mass which is the specific mechanical energy (ξ) is extracted by dot multiplying the two-body equation with the velocity vector. The formulation of ξ in terms of semi-major axis, a, where the position and velocity vectors are not known is the following:

$$\xi = -\frac{GM}{2 \cdot a} = \frac{u^2}{2} - \frac{GM}{r} \qquad \text{Eq. 27}$$

where u, r are the magnitudes of the velocity and position.

2.4.8. Propagation and orbit determination

2.4.8.1. Introduction

As it is mentioned in the beginning of this thesis the developed along track stereo sensor model is based on the idea of finding common exterior orientation parameters for all images directly or indirectly. A very convenient approach is to determine the orbit of the satellite platform covering the time of acquisition of all images, using satellite photogrammetry in combination with astrodynamics. The astrodynamics methods that are involved in sensor modelling are derived from propagation and orbit determination theory.

Propagation is to find a satellite's future location given the last known position and velocity vectors (state vector) at a particular time. It is also known as Kepler's problem.

Orbit determination is to estimate the state of a satellite at one epoch, from observations, using a specific mathematical model.

Generally in this thesis, observations are the coordinates of the GCPs in the framelet coordinate system. The specific mathematical model is the collinearity equations as they are modified using the astrodynamics methods. The methods that are used in this thesis are following, along with the way that they are involved in the model development.

2.4.8.2. Kepler problem

2.4.8.2.1. Method description

The Kepler's problem is based on the equation 14. Using this equation the future state $(\vec{r},\vec{u})$ of a satellite can be found given the last known position and velocity vectors $(\vec{r}_o,\vec{u}_o)$ at a particular time (Figure 21).

In the sensor modeling this equation can be used as follows: Assuming that, the state vector of the principal point of the base framelet of the first image of the along track images sequence is known. Then, **using this equation the state vector of the base**

framelet of the first image is related to the state vectors of principal point of the base framelet of each along track images and even more to the state vectors of all the other framelets in every image. Thus, the number of unknown parameters is reduced, as only the state vector of the first along track image should be defined.

The model which is based in Kepler's problem is described in detail in § 4.7.5 (for single image) and in § 5.3.1. However, an important comment should be made here. In the formulation of this model, the equation 14 could be used in order to simulate the keplerian motion during the acquisition time of the images without solving this equation, itself. In other words the equation 14 contribution in the model is only with its physical effect, because only the state vectors of base framelet of the first image is computed (not the state vectors of the base framelets of the rest images). This approach is adopted because the model is simplest than the one where the exterior orientation parameters and the state vector of the base framelets of all image are found (§2.4.8.2.4.).

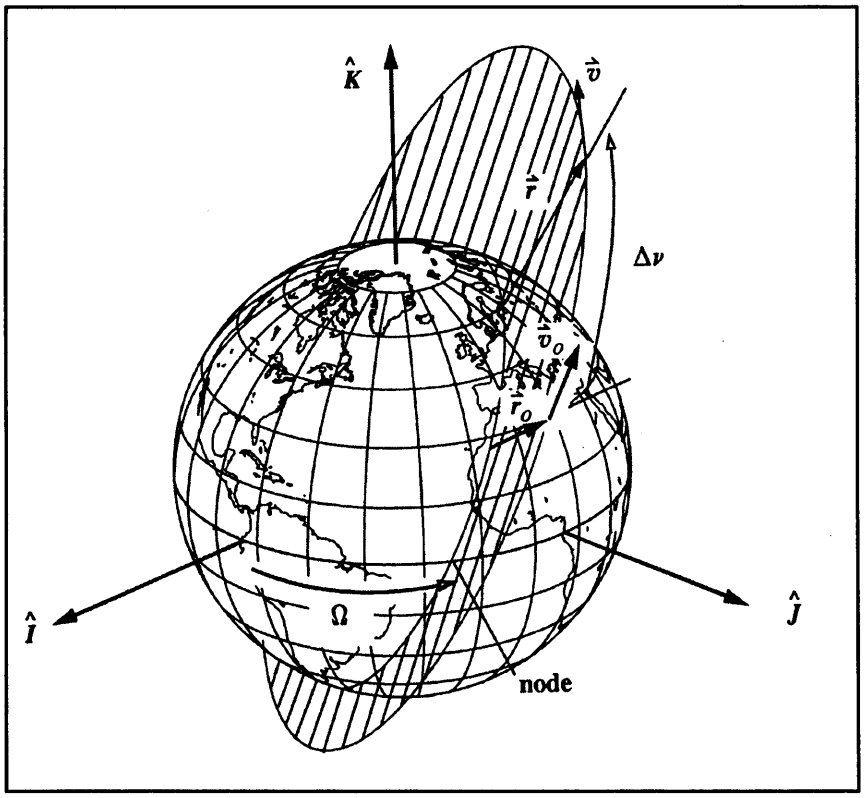

Figure 21. Kepler problem (Vallado, 2001)

It is efficient, especially for the accuracy tests which are introduced in § 5.4, although it is not really used in the specific sensor model, to introduce a solution process of the Kepler's problem. Also, it is possible to develop the sensor model where the solution technique of this equation is used instead of the equation 14, itself, if the state vectors of all along track images should be extracted.

For this problem there are rigorous and complete solutions using different techniques: an orbital elements technique, the board series technique and the universal-variable technique (Vallado, 2001).

In this thesis, it is decided to use state vectors instead of orbital elements during the model (§ 4.9). In order to have compatibility in model formulation, the universal-variable technique which is the only one technique that state vectors can use directly is adopted. In the others techniques the state vectors should be transform to orbital elements and visa versa. The formulation of this technique is following along with the description of two important topics, which provide an efficient and more convenient way of solving, generally propagation and orbit determination problems. These topics are the ***f, g* functions and the universal formulation**.

2.4.8.2.2. Introduce *f, g* functions

It is worth finding an expression to establish the relation between state vectors in the same orbit. In determining this relationship, a fundamental theorem concerning coplanar vectors will be used: *If* $\vec{A}, \vec{B}$ *and* $\vec{C}$ *are coplanar vectors, and* $\vec{A}$ *and* $\vec{B}$ *are not collinear, it is possible to express* $\vec{C}$ *as a linear combination of* $\vec{A}$ *and* $\vec{B}$ (Bate at al, 1971).

Since the Keplerian motion is confined to a plane, it is obvious that the position and velocity vectors of the same orbit are coplanar. Assuming, that the position vectors $\vec{r}_o$, $\vec{r}$ and the velocity vectors $\vec{u}_o$, $\vec{u}$ represent the state of the satellite in two epochs in the same orbit, the relation of $\vec{r}$, $\vec{u}$ is calculated in terms of $\vec{r}_o$, $\vec{u}_o$.

Thus, having in mind the above theorem:

$$\vec{r} = f \cdot \vec{r}_o + g \cdot \vec{u}_o \qquad \text{Eq. 28}$$

Differentiating this expression gives:

$$\vec{u} = \dot{f} \cdot \vec{r}_o + \dot{g} \cdot \vec{u}_o \qquad \text{Eq. 29}$$

where f, g, $\dot{f}$, $\dot{g}$ are time dependent scalar quantities.

It is also possible to adopt a matrix notation and write equations 28, 29 as a state vector of position and velocity vectors, and Φ as a matrix containing scalar 3x3 matrices of the f and g values.

$$\overline{X}_{k+1} = \begin{bmatrix} f & g \\ \dot{f} & \dot{g} \end{bmatrix} \cdot \overline{X}_k = \Phi \cdot \overline{X}_k \qquad \text{Eq. 30}$$

The Φ matrix is called the **state-transition matrix** because it moves the state through time. The advantage of using Φ is the case where the position and velocity vector are calculated through time, once the f and g functions are calculated (Vallado, 2001).

The solution of equations 28, 29 are beyond of the scope of this thesis (detailed computations is in Bate et al., 1971). Solving the equations 28, 29 the expressions for $f, g, \dot{f}, \dot{g}$ are :

$$f = \frac{x \cdot \dot{y}_o - \dot{x}_o \cdot y}{h}$$

$$\dot{f} = \frac{\dot{x} \cdot \dot{y}_o - \dot{x}_o \cdot \dot{y}}{h}$$

$$g = \frac{x_o \cdot y - x \cdot y_o}{h} \qquad \text{Eq. 31}$$

$$\dot{g} = \frac{x_o \cdot \dot{y} - \dot{x} \cdot y_o}{h}$$

$$1 = f \cdot \dot{g} - \dot{f} \cdot g$$

where

x,y are coordinates of the position of the satellite in perifocal PQW coordinate system

$\dot{x},\dot{y}$ are coordinates of the velocity of the satellite in perifocal PQW coordinate system

and h is the angular momentum.

The f and g expression could be used in various solutions depending on what information is available for the problem. To determine the f and g functions for various sets of initial data, the x and y should be found first.

2.4.8.2.3. Universal formulation

The classical formulation for time of flight involves the eccentric anomalies. For near circular orbits where it is difficult to define the perigee an alternative variable could be used. This is the universal variable χ which also can be used for all conic orbits. Actually this is the main reason of universal value development.

Begin with the specific mechanical energy Eq.25. Resolve the velocity into radial and transverse components, the energy equation can be written:

$$\xi = \frac{\dot{r}^2}{2} + \frac{(r \cdot \dot{u})^2}{2} - \frac{GM}{r} \qquad \text{Eq. 32}$$

Recalling, angular momentum ($h = \sqrt{GM \cdot p} = r^2 \cdot \dot{u}$) the above equation is solved for $\dot{r}^2$:

$$\dot{r}^2 = -\frac{GM \cdot p}{r^2} + \frac{2 \cdot GM}{r} - \frac{GM}{a} \qquad \text{Eq. 33}$$

The solution is not immediately apparent; it requires the definition of an independent, *universal value* χ to replace time as the independent variable. Define the derivative of the universal variable χ as:

$$\dot{\chi} = \frac{\sqrt{GM}}{r} \qquad \text{Eq. 34}$$

where GM is the gravitational constant and r is the magnitude of the position vector. Equation 34 is called Sundman transformation, where χ is the new independent variable- a kind of general anomaly. It is remarkable that χ is used as an independent variable instead of time t. Thus, the nonlinear equation of motion can be converted into linear constant-coefficient differential equation (Vallado, 2001).

It is needed to develop a general equation for position, r, in terms of the universal variable, position and velocity. Detailed computations from equation 31 to final equation are cut out as they are beyond of the scope of this thesis (detailed computations is in Vallado, 2001)

$$r = \chi^2 \cdot c_2 + \frac{\vec{r}_o \cdot \vec{u}_o}{\sqrt{GM}} \cdot \chi \cdot (1 - \psi \cdot c_3) + r_o \cdot (1 - \psi \cdot c_2) \qquad \text{Eq. 35}$$

where

$(\vec{r}_o, \vec{u}_o)$ are the position and velocity vectors in initial time, χ = t = 0,

r is a magnitude of the position vector at the epoch t

$$\psi = \frac{\chi^2}{\alpha} \qquad \text{Eq. 36}$$

$$c_2 = \frac{1-\cos(\sqrt{\psi})}{\psi} \quad \text{and} \quad c_3 = \frac{\sqrt{\psi}-\sin(\sqrt{\psi})}{\sqrt{\psi^3}} \qquad \text{Eq. 37}$$

The above values are referred to the elliptical orbit as the remote sensing satellites orbits are. Equation 34 relates the change of time to the universal variable. Thus, **it constitutes the universal variable form of Kepler's equation**. The ultimate goal is to find χ when the time interval (Δt) between the epochs is known. Unfortunately, it is not possible to isolate χ in the equation 34. From this reason a numerical method is used to reach to a solution (§ 2.4.8.2.4).

2.4.8.2.4. Kepler problem-Universal value solution

After the introduction of the f, g functions and the universal formulation topics it is possible to describe the solution of Kepler's problem which is based on these topics. As a remainder the Kepler's problem is to find the future state $(\vec{r},\vec{u})$ with time interval Δt from the last known position and velocity vectors $(\vec{r}_o,\vec{u}_o)$ at a particular time (Figure 21).

From the equation 27

$$\frac{1}{a} = \frac{-u_o^2}{GM} + \frac{2}{r_o} \qquad \text{Eq. 38}$$

As it is mentioned in § 2.4.8.2.3 it is not possible to isolate the universal value χ in the equation 34. The following iteration process is used base on the Newton-Rapson numerical method (Vallado, 2001):

The initial value of the loop is $\chi_o \approx \sqrt{GM}\cdot\Delta t\cdot\frac{1}{a}$ Eq. 39

and

$$\psi = \chi_n^2 \frac{1}{a} \qquad \text{Eq. 40}$$

then

$$r = \chi_n{}^2 \cdot c_2 + \frac{\vec{r}_o \cdot \vec{u}_o}{\sqrt{GM}} \cdot \chi_n \cdot (1 - \psi \cdot c_3) + r_o \cdot (1 - \psi \cdot c_2)$$

$$\chi_{n+1} = \chi_n + \frac{\sqrt{GM} \cdot \Delta t - \chi_n{}^3 \cdot c_3 - \frac{\vec{r}_o \cdot \vec{u}_o}{\sqrt{GM}} \cdot \chi^2{}_n \cdot c_2 - r_o \cdot \chi_n \cdot (1 - \psi \cdot c_3)}{r} \qquad \text{Eq. 41}$$

$$\chi_n \Leftarrow \chi_{n+1} \text{ until } |\chi_n - \chi_{n+1}| < 10^{-6}$$

After the iteration process the *f, g* functions are used in order to moves the state through time (Δt):

$$f = 1 - \frac{\chi_n^2}{r_o} \cdot c_2$$

$$g = \Delta t - \frac{\chi_n^3}{\sqrt{GM}} \cdot c_3 \qquad \text{Eq. 42}$$

$$\dot{g} = 1 - \frac{\chi_n^2}{r} \cdot c_2$$

$$\dot{f} = \frac{\sqrt{GM}}{r_o \cdot r} \cdot \chi_n \cdot (\psi \cdot c_3 - 1)$$

and finally the position and velocity vectors $(\vec{r}, \vec{u})$ are found using the equation 28, 29.

This is the solution of Kepler's problem using the *f,g* functions and the universal variables. As it was mentioned this formulations is not used in Kepler sensor model. However, it is used in the accuracy test of § 5.4. Finally, it could be used in sensor model development if the state vectors of all along track images should be extracted.

2.4.8.3. Two Position vectors and time-Lambert's problem

2.4.8.3.1. Description

The problem of two position vectors and the time of flight between them is known as Lambert's problem because Lambert first formed the solution (Vallado, 2001). It is referred as orbit determination technique. Although similar to the Kepler problem it is considered a technique for determining the initial orbit because the orbit is not yet fully known. Two position vector and the time of flight between each position is known, but the orbit between the endpoints is unknown.

In the sensor modeling the Lambert's problem can be used as follows: Assuming that, the position vectors of the principal points of the base framelet of the two images of the along track images sequence are known along with the time of flight between them. Then, **using this technique the velocity vectors of principal point of the base framelet of both along track images are calculated.** It is obvious that the number of unknown parameters is reduced, as only the position vectors of the two images should be defined. The along track model which is based in Lambert's problem is introduced in detail in § 5.3.2.

2.4.8.3.2. Lambert's problem-Gauss solution

The Lambert-Gauss problem is defined as follows: Given the position vectors and the time of flight between these to vectors, find the velocities. Also generally the direction of the flight should be known. In case of along track geometry the direction of fight is supposed to be short-way (Figure 22). It is an orbit determination technique because the orbit is not yet fully known, although it is very similar to Kepler problem discussed in § 2.4.8.2.

It is obvious then that the two vectors can uniquely defined the orbital plane. The relationship between the four vectors (position and velocity vectors in both epochs) is contained in the *f* and *g* functions which are introduced in § 2.4.8.2.2.

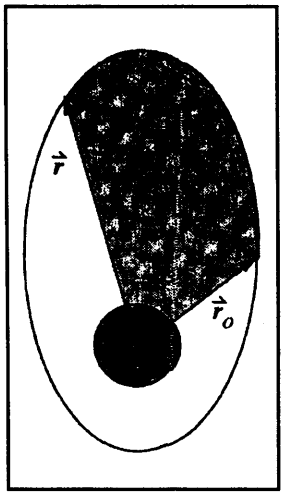

Figure 22. Short-way flight direction for along track images (Vallado, 2001)

In this thesis the original Gauss solution, relied on geometric considerations and is limited to elliptic orbits, is used along with the use of *f* and *g* functions. The original method of Gauss proposed to solve the Lambert's problem relied on geometric considerations and was limited to elliptical transfers. This method relied on the area the satellite sweeps out during the transfer. Figure 23 shows the geometry.

From Kepler's second law, it is known that the area is swept out at a constant rate,

$$dt = \frac{2}{h} dA \qquad \text{Eq. 43}$$

which make a total area

$$A = \frac{1}{2}\sqrt{GM \cdot p} \cdot \Delta t \qquad \text{Eq. 44}$$

where Δt represents the time of flight between the two position vectors. The area of the triangle formed by the two position vectors and the connecting chord is defined:

$$A_{\Delta} = \frac{1}{2} r_o \cdot r \cdot \sin(\Delta v) \qquad \text{Eq. 45}$$

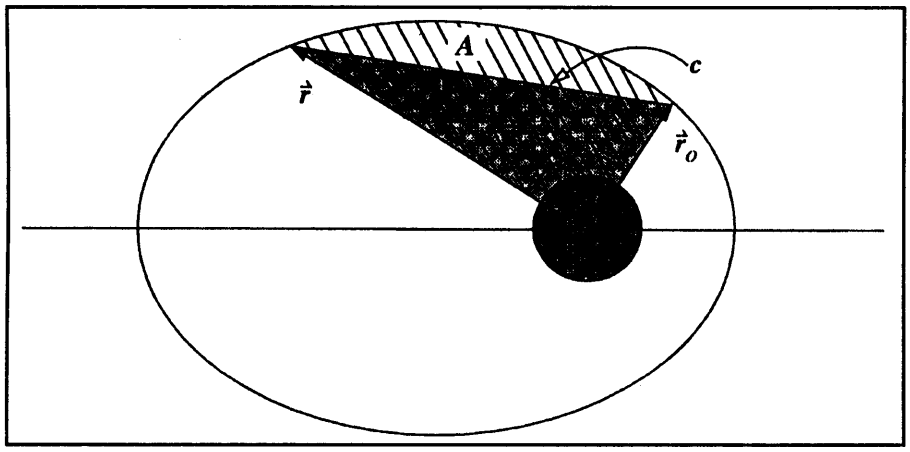

Figure 23. Area swept out by a satellite during transfer (Vallado, 2001)

The ratio y, of the area the satellite sweeps out the triangular area are bounded by the two position vectors is:

$$y = \frac{\sqrt{GM \cdot p} \cdot \Delta t}{r_o \cdot r \cdot \sin(\Delta v)} \qquad \text{Eq. 46}$$

Gauss's method is based on obtaining two independent equations relating y and the change in eccentric anomaly (ΔE). Typically, a trail value of y=1 in the first equation is used and then it is solved for ΔE. This approach works well when the angles between the two position vectors are relatively small, as they are in the case of along track acquisition geometry.

Using an alternative expression of the semiparameter:

$$p = \frac{2 \cdot r_o \cdot r \cdot \sin^2\left(\frac{\Delta v}{2}\right)}{r_o + r - 2 \cdot \sqrt{r_o \cdot r} \cdot \cos\left(\frac{\Delta v}{2}\right) \cdot \cos\left(\frac{\Delta E}{2}\right)} \qquad \text{Eq. 47}$$

Substitute this expression into the sector relation and square the result:

$$y^2 = \frac{GM \cdot \Delta t^2 \cdot \sec^2\left(\frac{\Delta v}{2}\right)}{2 \cdot r_o \cdot r \cdot \left(r_o + r - 2 \cdot \sqrt{r_o \cdot r} \cdot \cos\left(\frac{\Delta v}{2}\right) \cdot \cos\left(\frac{\Delta E}{2}\right)\right)} \qquad \text{Eq. 48}$$

which is known as first Gauss equation. Using several temporary variables simplifies the notation:

$$l \equiv \frac{r_o + r}{4 \cdot \sqrt{r_o \cdot r} \cdot \cos\left(\frac{\Delta v}{2}\right)} - \frac{1}{2} \qquad \text{Eq. 49}$$

$$m \equiv \frac{GM \cdot \Delta t^2}{\left(2 \cdot \sqrt{r_o \cdot r} \cdot \cos\left(\frac{\Delta v}{2}\right)\right)^3} \qquad \text{Eq. 50}$$

and

$$x_1 \equiv \sin^2\left(\frac{\Delta E}{4}\right) \qquad \text{Eq. 51}$$

The final result is the common form of the first equation of Gauss

$$y^2 = \frac{m}{l + x_1} \qquad \text{Eq. 52}$$

The next goal is to arrive at an independent equation relating the change in eccentric anomaly and y. With a temporary variable,

$$x_2 = \frac{\Delta E - \sin(\Delta E)}{\sin^3\left(\frac{\Delta E}{2}\right)} \qquad \text{Eq. 53}$$

and the second equation of Gauss is developed as follows:

$$y^3 - y^2 = m \cdot x_2 = y^2 \cdot (y-1) \qquad \text{Eq. 54}$$

if equation 50 is substituted to equation 52 and solve for the sector ratio then

$$y = (l + x_1) \cdot x_2 + 1 \qquad \text{Eq. 55}$$

Once the y is found, ΔE could be found by solving Gauss's first equation (eq. 48) and finally the semiparameter from equation 47.

It is possible to calculate the f, g function using the following formulation:

$$f = 1 - \frac{r}{p} \cdot (1 - \cos(\Delta\nu))$$

$$g = \frac{r \cdot r_o \cdot \sin(\Delta\nu)}{\sqrt{GM \cdot p}}$$

Eq. 56

$$\dot{f} = \sqrt{\frac{GM}{p}} \cdot \tan\left(\frac{\Delta\nu}{2}\right) \cdot \left(\frac{1 - \cos(\Delta\nu)}{p} - \frac{1}{r} - \frac{1}{r_o}\right)$$

$$\dot{g} = 1 - \frac{r_o}{p}(1 - \cos(\Delta\nu))$$

The velocities vectors of both positions are calculated using f, g functions as follows:

$$\vec{u}_o = \frac{\vec{r} - f \cdot \vec{r}_o}{g} \quad \text{and} \quad \vec{u} = \frac{\dot{g} \cdot \vec{r} - \vec{r}_o}{g} \qquad \text{Eq. 57}$$

2.4.8.4. Three position vectors. Herrick-Gibbs method

This method is used to determine the orbit when three nonzero, coplanar position vectors, which represent three time-sequential vectors of the satellite in its orbits (Figure 24).

In the sensor modeling the Herrick-Gibbs method could be used in combination with Lambert-Gauss model in more than two along track stereo images, as follows. Assuming that there is a triplet of along track images where the position vectors of the principal points of the base framelet of the three images of the along track images sequence are known along with the time of flight between them. Then, **using this technique the velocity vector of principal point of the base framelet of the middle along track image is calculated. On the other hand using the Lambert-Gauss model the velocities vectors of the other two images are calculated.** This combined method could be extended in the case of more than three along track images where the velocities of the intermediate images are calculated using the Herrick-Gibbs method while the velocities of the first and last images are calculated using Lambert-Gauss method. It is obvious that the number of unknown parameters is reduced, as only the position vectors of the images should be defined. The model which is based in Herrick-Gibbs model is introduced in detail in § 5.3.3.

It is the simplest problem of the three and is based in Taylor series expansion and works best when the vectors are relatively close together, as they are the position vectors of along track satellite sensors.

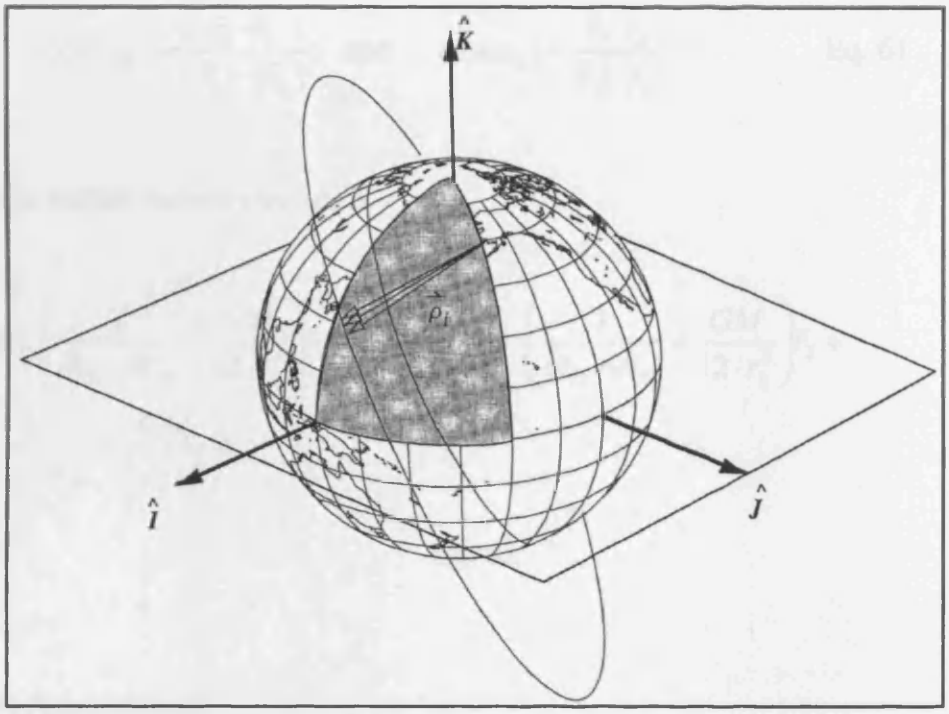

Figure 24. Orbit Geometry of Herrick-Gibbs method (Vallado, 2001)

Assuming that, the position vectors $\vec{r}_1, \vec{r}_2, \vec{r}_3$ are known in epochs MJD_1, MJD_2, MJD_3 respectively, the velocity vector $\vec{u}_2$ is found in position 2 using the following formulation:

$$dt_{31}=MJD_3-MJD_1$$
$$dt_{32}=MJD_3-MJD_2 \qquad \text{Eq. 58}$$
$$dt_{21}=MJD_2-MJD_1$$

$$\vec{Z}_{23} = \vec{r}_2 \times \vec{r}_3 \qquad \text{Eq. 59}$$

$$a_{cop} = 90° - \cos^{-1}\left(\frac{Z_{23} \cdot r_1}{|Z_{23}| \cdot |\vec{r}_1|}\right) \qquad \text{Eq. 60}$$

$$\cos(a_{12}) = \frac{\vec{r}_1 \cdot \vec{r}_2}{|\vec{r}_1| \cdot |\vec{r}_2|} \quad \text{and} \quad \cos(\alpha_{23}) = \frac{\vec{r}_2 \cdot \vec{r}_3}{|\vec{r}_2| \cdot |\vec{r}_3|} \qquad \text{Eq. 61}$$

Finally the middle velocity vector is

$$\vec{u}_2 = -dt_{32}\left(\frac{1}{dt_{21} \cdot dt_{31}} + \frac{GM}{12 \cdot r_1^3}\right)\vec{r}_1 + (dt_{32} - dt_{21}) \cdot \left(\frac{1}{dt_{21} \cdot dt_{32}} + \frac{GM}{12 \cdot r_2^3}\right)\vec{r}_2 + dt_{21}\left(\frac{1}{dt_{32} \cdot dt_{31}} + \frac{GM}{12 \cdot r_3^3}\right)\vec{r}_3$$

Eq. 62

2.4.9. Perturbations

In the framework of Newtonian physics the motion of the satellite is described with the second order differential equation 14. This is a basic model establishing, in an inertial coordinate system, the gravitational attraction of the satellite from a point mass Earth. In this thesis, this model based on the Keplerian motion is evaluated as appropriate enough to describe the satellite motion during the acquisition time of along track stereo of about 90 seconds. The accuracy of this model is described in chapter 5. If a better accuracy is needed or the time interval is larger (e.g. trying to solve simultaneously more than one data set) the effect of various perturbations should be examined (Figure 25).

For the satellites with a flight height of about 800km above the earth the greater effect is the central attraction of the earth (GM) which is described in equation 15.

Due to the daily rotation, the Earth is not a perfect sphere, but has a form of an oblate spheroid with an equatorial diameter that exceeds the polar diameter by about 20km (Montenbruck, et al., 2001). The resulting equator bulge exerts a force that pulls the satellite back to the equatorial plane whenever it is above or below this plane and thus tries to align the orbital plane with the equator. This perturbation ($J_{2,0}$, $J_{2,2}$, $J_{6,6}$, $J_{18,18}$ in Figure 25) is three orders of magnitude smaller than the central attraction (GM).

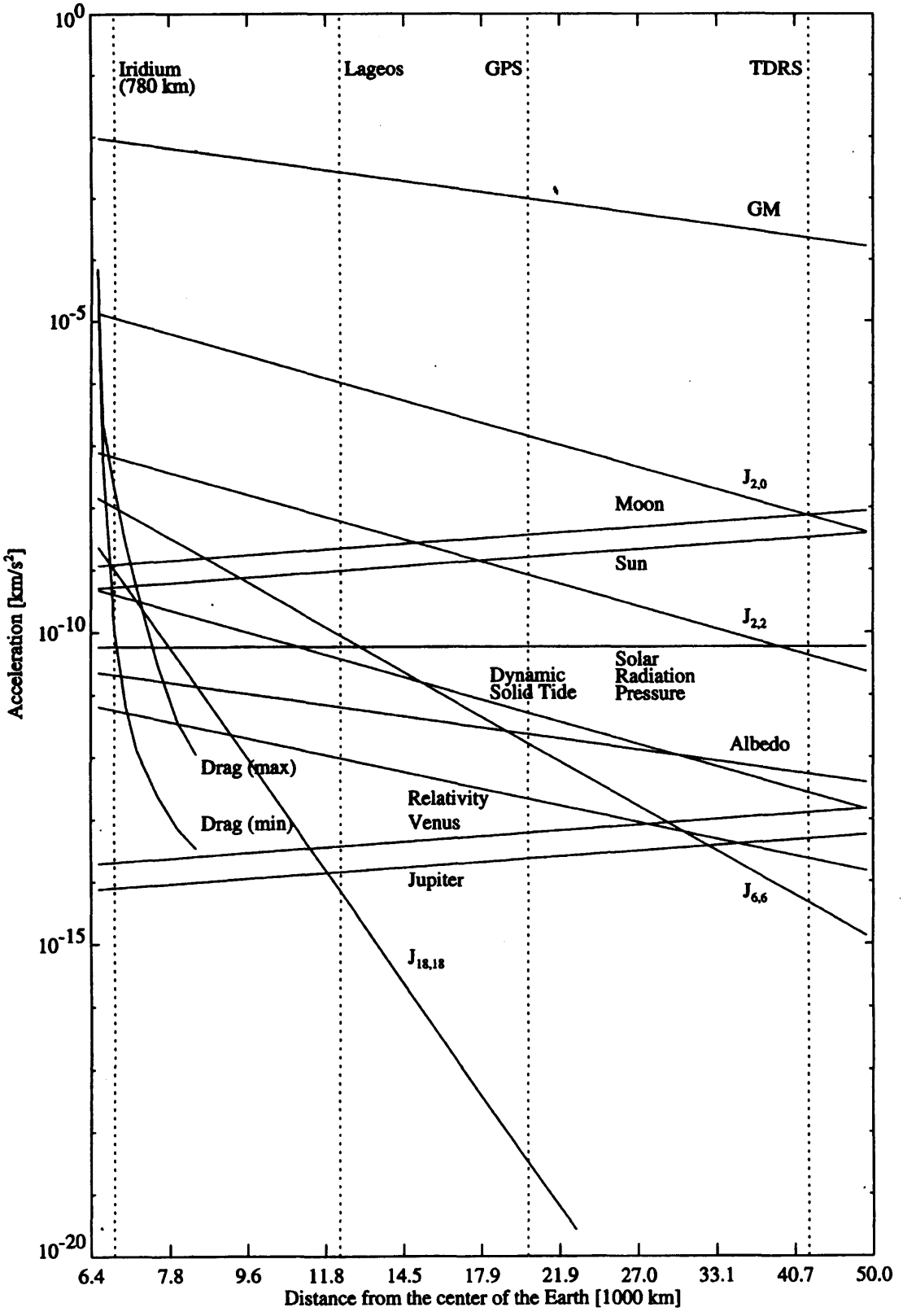

Figure 25. Order of magnitude of various perturbations of a satellite orbit (Montenbruck, et al., 2001)

A different behavior is observed for the perturbations that arise from the gravitational attraction of the Sun and the Moon. Also the lunar and the solar forces on both the Earth and the satellite should be taken into consideration. Moreover the remote sensing satellites as low orbit satellites affected from the atmospheric drag, which is strongest close to perigee of an orbit.

While the acceleration due the gravitational forces is independent of the satellite's mass and area, this is not true for drag and other surface forces. Among these the solar radiation pressure is most notable especially if the solar panels are large.

All the above perturbations have a magnitude smaller that 10^{-5} km/sec^2 for the remote sensing satellites flight height (Figure 25). Thus, during the development of the along track stereo model these forces are not taken into consideration. However, the effect of the perturbations could be involved in the model development if it required.

2.5. Adjustment of the observations-Estimation

2.5.1. Introduction

In reality in §2.4.8.2-4 the orbit of the remote sensing satellite is determined, where image measurements are used as observations. In pushbroom modeling, modified collinearity equations are used simulating the satellite motion which is assumed as a Keplerian motion. Generally, the observations are more than they are needed for the determination of the unknowns. In this case, redundancy (or number of degrees of freedom) is said to exist among the measurements or observations (Mikhail et al., 2001). If the total number of the measurements is n, and it takes a minimum of n_o measurements to uniquely determine the model underlying the problem, then the redundancy is given by

$$r = n - n_o \qquad \text{Eq. 63}$$

When redundancy exists, subsets of n_o measurements from the given n measurements will yield a solution. The solution using one subset is generally different from the

solution obtain using any other subset. This means that the total observations are inconsistent with respect to the model and that **an adjustment** must be performed in order to eliminate the inconsistency. After the adjustment, no matter which subset of the measurements is used, the solution is always the same. This is possible only if the original measurements l are replaced by another set of estimate $\hat{l}$, often called adjusted observations, by adding a set of residuals or corrections v to the measurements.

$$\hat{l} = l + v \qquad \text{Eq. 64}$$

Then an additional criterion, **estimator**, must be imposed on the residuals so that their selection is not arbitrary. In the literature, in satellite photogrammetry and in orbit determination **Least Square Estimator (LSE)** is used, universally. However, as it is shown in chapter 4, it seems that an alternative estimator, the **General Ridge Estimator (GRE)**, can be used which provides better internal accuracy of the adjustment than **LSE**.

2.5.2. Mathematical model and quality of the adjustment

The mathematical model is composed of two parts (Mikhail et al., 2001). **The first one is the functional model which describes the geometry or the physical characteristics of the problem.** Thus the functional (sensor) model in our case involves the exterior orientation parameters estimation (orbit and rotations determination) in an inertial space through measurements on framelet coordinate system on at least one pushbroom satellite image. On the other hand **the stochastic model is the part of the mathematical model that deals with the statistical properties of all the elements involved in the functional model.** Generally the orbit determination procedure is non linear which is undertaken using an iterative linear processing solution that is called differential correction.

An important part of the stochastic model is the quality modification of the measurements. For this purpose, the accuracy and precision criterions are used. **Precision** represent the degree of consistency between measurements and is based on

the sizes of the discrepancies in a data set. Thus the precision expresses the degree of closeness of the observations to their mean. **Accuracy (or Bias)** is a measure of the absolute nearness of the measured quantity to its true value. Accuracy refers to the degree of closeness of an estimate to its parameter. (Figure 26). **Noise** is a statistical indication (actually the standard deviation) of the random variation about the measured mean. Thus noise indicates the precision of the estimation. **Drift** represent a slow and unpredictable variation over time of the observed mean value over the interval of time.

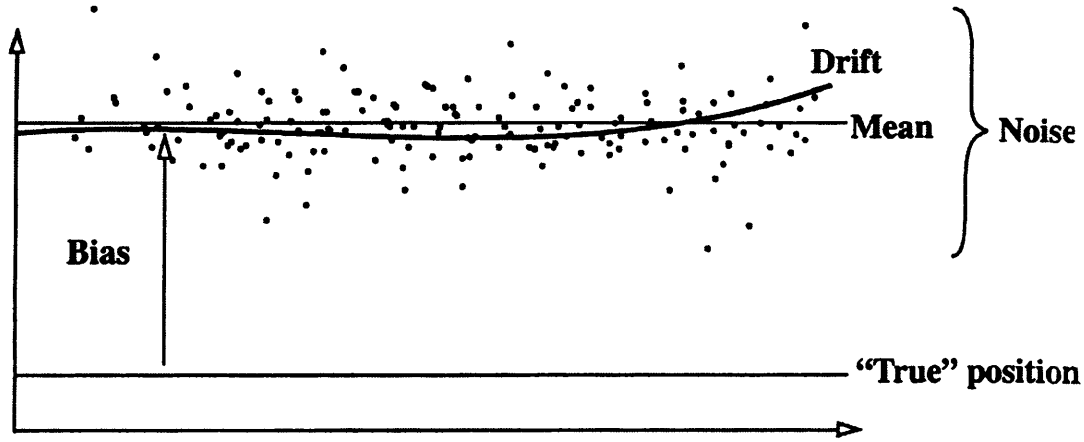

Figure 26. Representation of Noise (Precision), Bias (Accuracy) and Drift. (Vallado, 2001)

2.5.3. Least square estimator (LSE)

2.5.3.1. Least squares criterion

In the elementary treatment of adjustment, it is assumed that all measurements are independently made and no correlation exists between them. One measurement does not influence another measurement. Under this assumption, one of the two conditions could exist:

- All the measurements have equal quality.
- Each measurement can have different quality.

The quality of the measurement is given in terms of its weights, **W**.

Under the condition of equal weights, the least squares criterion states that the sum of the squares of the n residuals to a set of n measurements must be a minimum. That is in matrix notation:

$$\phi = \mathbf{v}^T\mathbf{v} = minimum \qquad \text{Eq. 65}$$

If the observations have different weights, the least squares criterion became:

$$\phi = \mathbf{v}^T\mathbf{W}\mathbf{v} = minimum \qquad \text{Eq. 66}$$

in which **W** is the weight matrix:

$$\mathbf{W} = \begin{bmatrix} w_1 & 0 & \cdots & 0 & 0 \\ 0 & w_2 & \cdots & 0 & 0 \\ \vdots & \vdots & \vdots & \vdots & \vdots \\ 0 & 0 & \cdots & 0 & w_n \end{bmatrix} \qquad \text{Eq. 67}$$

2.5.3.2. Adjustment of indirect observations

In this thesis the technique of adjustment of indirect observations is used where each equation contains just one observation. Moreover, all the developed sensor models are based in non-linear functions. For these reasons, the non-linear least square adjustment of indirect observations is introduced.

Because of nonlinearity of the functions, first-order Taylor series approximations are used. Modified collinearity equations (equations 6) can reorganize, slightly, in the following form:

$$F_1 = f\frac{m_{11}(t)(X - X_c(t)) + m_{12}(t)(Y - Y_c(t)) + m_{13}(t)(Z - Z_c(t))}{m_{31}(t)(X - X_c(t)) + m_{32}(t)(Y - Y_c(t)) + m_{33}(t)(Z - Z_c(t))} = 0$$

Eq. 68

$$F_2 = y - y_0 + f\frac{m_{21}(t)(X - X_c(t)) + m_{22}(t)(Y - Y_c(t)) + m_{23}(t)(Z - Z_c(t))}{m_{31}(t)(X - X_c(t)) + m_{32}(t)(Y - Y_c(t)) + m_{33}(t)(Z - Z_c(t))} = 0$$

The initial values of the unknown parameters are required, and the results are the adjustments of the initial parameters. This is repeated until the results converge (the adjustments become very close to zero). In case of Kepler model as it is introduced in § 4.7.5, the collinearity equations are involved in the adjustment as they are described in equations 91. The unknown parameters are nine for this model; the position vector (X, Y, Z), the velocity vector (u_x, u_y, u_z) and the rotation angles (ω, φ, κ). The Jacobian matrix, **J**, is the matrix of the partial derivatives of each equation with respect to each unknown parameter.

$$\mathbf{J} = \begin{bmatrix} \frac{\partial F_1}{\partial X} & \frac{\partial F_1}{\partial Y} & \frac{\partial F_1}{\partial Z} & \frac{\partial F_1}{\partial u_x} & \frac{\partial F_1}{\partial u_y} & \frac{\partial F_1}{\partial u_z} & \frac{\partial F_1}{\partial \omega} & \frac{\partial F_1}{\partial \varphi} & \frac{\partial F_1}{\partial \kappa} \\ \frac{\partial F_2}{\partial X} & \frac{\partial F_2}{\partial Y} & \frac{\partial F_2}{\partial Z} & \frac{\partial F_2}{\partial u_x} & \frac{\partial F_2}{\partial u_y} & \frac{\partial F_2}{\partial u_z} & \frac{\partial F_2}{\partial \omega} & \frac{\partial F_2}{\partial \varphi} & \frac{\partial F_2}{\partial \kappa} \end{bmatrix} \qquad \text{Eq. 69}$$

Furthermore, let the vector **f** be the vector of the residuals. It is the difference between the observations and the equations calculated using the initial values.

$$\mathbf{f} = \begin{bmatrix} l_1 - F_1(X_o, Y_o, Z_o, u_x, u_y, u_z, \omega, \phi, \kappa) \\ l_2 - F_2(X_o, Y_o, Z_o, u_x, u_y, u_z, \omega, \phi, \kappa) \end{bmatrix} \qquad \text{Eq. 70}$$

Thus the form of the equations in matrix notations is:

$$\mathbf{v} + \mathbf{J} \cdot \Delta\mathbf{X} = \mathbf{f} \qquad \text{Eq. 71}$$

where $\Delta\mathbf{X}$ is the adjustment values of unknown parameters **X.** The solution of $\Delta\mathbf{X}$ is:

$$\Delta \mathbf{X} = \mathbf{N}^{-1} \cdot \mathbf{t} \qquad \text{Eq. 72}$$

where

$$\mathbf{N} = \mathbf{J}^{\mathbf{T}} \cdot \mathbf{W} \cdot \mathbf{J} \qquad \text{Eq. 73}$$

and it is called the normal equations coefficient matrix (or simply normal equation matrix), and

$$\mathbf{t} = \mathbf{J}^{\mathbf{T}} \cdot \mathbf{W} \cdot \mathbf{f} \qquad \text{Eq. 74}$$

which is called normal equations constant term vector.

2.5.3.3. Precision and Accuracy assessment

The **reference standard deviation** S_o represents the precision of the adjustment. The form of the reference standard deviation for the unweighted case is:

$$S_o = \sqrt{\frac{\mathbf{v}^{\mathbf{T}} \cdot \mathbf{v}}{r}} \qquad \text{Eq. 75}$$

and the weighted case is

$$S_o = \sqrt{\frac{\mathbf{v}^{\mathbf{T}} \cdot \mathbf{W} \cdot \mathbf{v}}{r}} \qquad \text{Eq. 76}$$

where r is the degrees of freedom.

The precision of the indirectly determined quantities is represented by the standard deviation of these parameters.

$$\mathbf{S}_x^2 = S_o^2 \cdot (\mathbf{J}^{\mathbf{T}} \cdot \mathbf{W} \cdot \mathbf{J})^{-1} = S_o^2 \mathbf{N}^{-1} = S_o^2 \cdot \mathbf{Q}_{xx} \qquad \text{Eq. 77}$$

In least square adjustment the matrix $\mathbf{Q}_{xx}$ is known as the variance-covariance matrix or simply the covariance matrix. Diagonal elements of the matrix when multiplied by S_o^2

give variances of the adjusted quantities, and the off-diagonal elements multiplied by S_o^2 yield covariances. From the equation 77 the **estimated standard deviations** S_i for any unknown parameter, having been computed from a system of the observation equations, is expressed as

$$S_i = S_o \cdot \sqrt{q_{x_i x_i}} \qquad \text{Eq. 78}$$

where $q_{x_i x_i}$ is the diagonal element (from the ith row and ith column) of the $\mathbf{Q_{xx}}$ matrix, which as noted in equation 77, is equal to $\mathbf{N^{-1}}$, the inverse of the matrix of normal equations.

Since the normal equation matrix is a symmetric, its inverse is also a symmetric matrix, and thus the covariance matrix is a symmetric matrix.

When additional terms are added to polynomials, generally the resulting equation will force better fits on any given data set. (Wolf et al., 1997). However, caution should be given when doing this since the resulting transformation parameters may not be statistically significant. For this reason the statistical validity of the parameters should be checked.

The adjusted parameters divided by standard deviations represent a t statistic with n degrees of freedom. If a parameter is to be judged as statistically different from zero, and thus significant, the computed t value (the test statistic) must be greater than $t_{a/2,n}$. The test statistic is

$$t = \frac{|\, parameter \,|}{S} \qquad \text{Eq. 79}$$

The Root Mean Square Error (RMSE) of check or height points is a representation of the accuracy of the adjustment (model) or the accuracy of Digital Elevation Model (DEM), respectively and it is based in the following equation:

$$RMSE = \sqrt{\frac{\sum e_i^2}{n}} \qquad \text{Eq. 80}$$

where, n is the number of check or height points and

e_i is the difference of the calculated coordinates of points against their reference coordinates.

2.5.4. Unreliability of the least square estimator- Multicollinearity

It is known that the least square estimator is not a precise estimator when near linear dependencies between some columns of the design matrix (**J**) exist (Grob, 2003). Usually one refers to such a case as an incidence of multicollinearity, but often without accurately specifying these terms.

What makes multicollinearity a particular problem is the behaviour of the inverse of the matrix ($\mathbf{J}^T\mathbf{J}$). If multicollinearity is present then small relative changes in the matrix ($\mathbf{J}^T\mathbf{J}$) will produce large changes in the matrix $(\mathbf{J}^T\mathbf{J})^{-1}$. The difference in the inverse of $\mathbf{J}^T\mathbf{J}$ is not caused by some inaccuracy in computing the inverse. **Moreover at least some main diagonal elements will be quite large which means that some elements of the least squares estimator will have a large variance and thus the estimate is unreliable.** Consequently, the corresponding t-statistic is typically very low (eq. 80) which leads to an unreliable procedure of statistical significant of the parameters. Moreover, due to the large values of the matrix $(\mathbf{J}^T\mathbf{J})^{-1}$, the least square estimator reacts very sensitively to small changes in data.

A further characteristic feature of the multicollinearity is that usually some of the elements of the least squares estimator are highly correlated. Then the corresponding elements of the parameter may be considered as weakly identifiable.

Based on the above considerations it is natural to identify multicollinearity with the condition of a matrix. A non-singular matrix is called ill-conditioned if small relative changes in can produce large relative changes. As a measure of the degree of ill-condition one can use a **condition number *cn*(N)** as it is defined in equation 81.

$$cn(\mathbf{N}) = \sqrt{\frac{\lambda_{\max}(\mathbf{N})}{\lambda_{\min}(\mathbf{N})}} \qquad \text{Eq. 81}$$

where λ_{max}, λ_{min} represent the maximum and the minimum eigenvalues of the matrix N. If $cn(\mathbf{N})=1$, then the matrix is called perfectly conditioned. The greater the $cn(\mathbf{N})$, the more ill-condition of N.

Various methods are often used to overcome the multicollinearity and compute the exterior orientation parameters. In this thesis two of them are used.

The first one is an alternative estimator which is called **General Ridge Estimator** (§2.5.5). The General Ridge Estimator although a bias estimator is very important in the evaluation of the single image sensor model discussed in chapter 4. It provides better internal precision of the solution where it is possible to use the statistical t-test with reliability as the correlation between the parameters is reduced to minimum (§ 4.7.1.1).

Also in §4.8 it is shown that also the prediction of the exterior oreination parameters is improved. Generally, in sensor modelling a great effort is done in order to find more precise values of the exterior orientation without being interested to predict the real values (accuracy). However in case where the navigation data are provided accurately or it is important to find the parameters as accurately as possible, an estimator which can not handle efficiently the multicollinearity problem should not be the first choice. In this case an estimator such as GRE is possible to improve the accuracy of the position

vector as it is found in § 4.8. On the other hand the use of only the proper estimator is not enough. A modified sensor model is possible to improve the accuracy of the exterior orientation parameters as it is found in the evaluation of the along track sensor model where the accuracy of the velocity vector is improved very much (Table 68).

In the second method the line elements and the angle elements are solved separately in an iterative procedure. This procedure is not rigorous in theory and the orientation precision and iterative time depends on the accuracy of the initial values (Guo et al., 2002). It is used in two very important cases in sensor development:

- To define the General Ridge Estimator parameters.
- To establish the accuracy limits in the evaluation process of orbit determination propagation methods (§ 5.4.1).

2.5.5. General ridge estimator (GRE)

General Ridge Estimator (GRE for short) was presented in 1970 as a bias estimator for nonorthogonal problems. It is based on the James-Stein estimator and the basic idea is to reduce the variance by shrinking the estimator so the mean square error can be reduced. In the field of Satellite Photogrammetry a few attempts were made in the past to solve the SPOT sensor model using the Ridge Estimator by itself or in combination with other estimators (Guo et al., 2002; Tao et al., 2004). In this thesis, as it has already been mentioned, GRE is used mainly in the evaluation of the single image sensor model, in order to provide better statistical results.

The form of GRE for the weighted case is:

$$\Delta \mathbf{X} = (\mathbf{J}^T \cdot \mathbf{W} \cdot \mathbf{J} + \mathbf{k} \cdot \mathbf{I})^{-1} \cdot \mathbf{J}^T \cdot \mathbf{W} \cdot \mathbf{f} \qquad \text{Eq. 82}$$

where $\mathbf{k}$ ($\mathbf{k}>0$) represents the general ridge vector. If $\mathbf{k}=0$ the resulting estimator is the Least Squares estimator. The dimension of this vector is equal to the number of the unknown parameters, while $\mathbf{I}$ is an identity matrix with relevant dimensions. The reason

why GRE estimator can yield better estimates than the ordinary least square estimator is motivated from the fact that the matrix $\mathbf{J}^T \cdot \mathbf{W} \cdot \mathbf{J}$ is stabilized when the positive vector $\mathbf{k}$ is added to each of its main diagonal elements (Grob, 2003). This stabilisation is understood in the sense that small relative changes in matrix $\mathbf{J}^T \cdot \mathbf{W} \cdot \mathbf{J} + \mathbf{k} \cdot \mathbf{I}$ should involve also small relative changes in the inverse $(\mathbf{J}^T \cdot \mathbf{W} \cdot \mathbf{J} + \mathbf{k} \cdot \mathbf{I})^{-1}$. This can be envisaged by noting that with increasing $\mathbf{k}$ the ridge of the matrix $\mathbf{J}^T \cdot \mathbf{W} \cdot \mathbf{J} + \mathbf{k} \cdot \mathbf{I}$ is raised, so that $\mathbf{J}^T \cdot \mathbf{W} \cdot \mathbf{J} + \mathbf{k} \cdot \mathbf{I}$ resembles more and more a diagonal matrix, which has an optimal condition. The condition can of course not to be the only aspect when using the ridge estimator, since with increasing $\mathbf{k}$ the bias of the estimator grows as well.

Hence the ultimate goal is to find some $\mathbf{k}$ which is large enough to reduce the variance compared to the ordinary least squares estimator, but which is small enough to produce some acceptable low bias. Different values for $\mathbf{k}$ are proposed in the literature (Grob, 2003, Guo et al., 2002). In this thesis an evaluation process is took place in § 4.8 in order to define the most appropriate General Ridge estimator for the data used. It is based in the assumption that the appropriate $\mathbf{k}$ should give an uncorrelated solution as possible. For this reason is defined compared to standard deviation of the position vector of the solution where the line and the angle elements are solved separately. Also, in § 4.8 a comparison table of the predicted values of the position vector when LSE and GRE are used is introduced. In that table the improvement of GRE prediction is shown.

The process for computing exterior orientation parameters by GRE can be divided into several steps:

Step 1: Computation of the initial values of the exterior orientation parameters.
Step 2: Computation of the estimate of the exterior orientation parameters using Least Squares estimator.
Step 3: Computation of General Ridge estimator parameters **(k).**
Step 4: Computation of the estimate of exterior orientation parameters by GRE.

Step 5: Justification if this value is precise enough. If it is true the values of exterior orientation parameters here are the last results. Otherwise computation will go on processing iteratively by entering step 2 until the parameters are accurate enough.

If a closer look is taken in the formulation of GRE it appears to be a weighted estimator in a classical way of thinking. However in that case the weights usually represent the physical relation between the parameters while in case of GRE the only reason for the existence of **k** parameter is to reduce the effect of the multicollinearity giving a more stable solution.

Finally the Ridge Estimator represents the stochastic part of the model. It improves the internal accuracy of the solution as it is shown in chapter 4 and can be used, generally in combination with rigorous or non rigorous sensor models.

CHAPTER3.

REVIEW OF EXISTING MODELS

In this chapter, the fundamental rigorous models that have already been introduced in literature are reviewed. The first stereo images from SPOT-1, soon after its launch on 22 February 1986, with a pixel size of 10m, was the challenge for the photogrammetry scientists, to describe, as accurately as possible, the SPOT-1 sensor model. It was obvious, that the sensor model should be a reformation of the frame camera model, where the kinematic characteristics of the pushbroom scanner were taken into account, in order to use this model in analytical stereoplotters. It was a few years before the digital photogrammetric workstations appeared.

This review is divided in three parts. The first part refers to general sensor models while the second part concentrates on general along track sensor models. In the third part a summary of the findings of this review are presented along with a comparison table of the SPOT models and finally a justification for this research is introduced.

3.1. General sensor models

All general sensor models that are reviewed in this chapter were developed for SPOT images. These models are summarized and reviewed in a chronological way.

3.1.1. Dowman-Gugan model (1987, 1988)

3.1.1.1. Model description

This model was developed in University College London and it was introduced in D.J. Gugan's PhD thesis (1987). It is the first attempt to connect the exterior orientation parameters of satellite images using the geometry of its orbit.

At first the following important factors are mentioned:

- The orientation of SPOT data should be carried out in a geocentric coordinate system in order to avoid distortions caused by earth curvature and map projection and to facilitate integration with sources of metadata information that may be available (Gugan, 1987).
- The SPOT panchromatic image is recorded over a 9 seconds period. Over this period the image geometry is kinematic.

The development of the model was done in two stages. In the first one, which is very important, because it is evaluated in this thesis as the most complicated model, the physical relation between the exterior orientation parameters of the framelets was clearly understood. The relationship among consecutive framelets is characterized by the dynamic orientation parameters which are modelled with low order polynomials as a function of the sampling time (§ 2.3.4). An intensive effort was made to define the polynomial's order. Starting with second order polynomials, the exterior orientation parameters of each line were calculated, regarding the exterior orientation of the middle line, as follows, using the notation of equations 6 and 7:

$$
\begin{aligned}
X_c(t) &= X_o + a_1 t + b_1 t^2 \\
Y_c(t) &= Y_o + a_2 t + b_2 t^2 \\
Z_c(t) &= Z_o + a_3 t + b_3 t^2 \\
\omega_c(t) &= \omega_o + a_4 t + b_4 t^2 \\
\phi_c(t) &= \phi_o + a_5 t + b_5 t^2 \\
\kappa_c(t) &= \kappa_o + a_6 t + b_6 t^2
\end{aligned}
\qquad \text{Eq. 83}
$$

This model was named as a conventional space resection by the authors and it was modified to an orbital model resection in the next stage.

These equations with 18 parameters to be determined do not provide a practical set of parameters, because in a linear array, unlike frame images, certain parameters are highly correlated with one another, leading to a very unstable solution reflecting to the one dimensional nature of linear array.

In general, these movements cause different effect on aerial photographs, in linear array a small change in ω_c in indistinguishable from a small change in Y_c (Figure 27). Similarly, small changes in φ_c and X_c, respectively, can not be differentiated. It is therefore, necessary to eliminate either ω_c or Y_c and either φ_c or X_c, after which the following equations are obtained with 14 unknown parameters for each image (Gugan, 1987):

$$
\begin{aligned}
X_c(t) &= X_o + a_1 t + b_1 t^2 \\
Y_c(t) &= Y_o + a_2 t + b_2 t^2 \\
Z_c(t) &= Z_o + a_3 t + b_3 t^2 \\
\omega_c(t) &= \omega_o \\
\phi_c(t) &= \phi_o \\
\kappa_c(t) &= \kappa_o + a_6 t + b_6 t^2
\end{aligned}
\qquad \text{Eq. 84}
$$

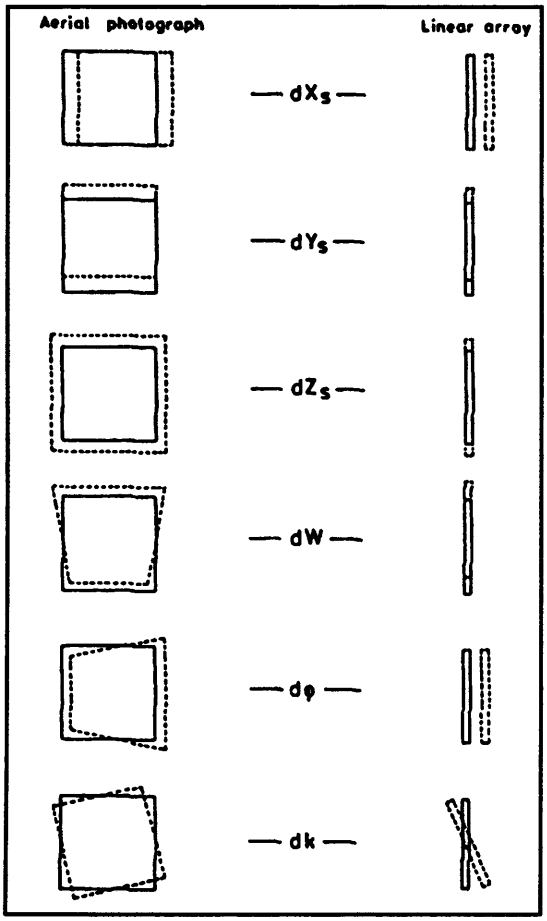

Figure 27. The effect of small changes in parameters for aerial photography and linear array (Gugan, 1987)

In the next stage the orbital sensor model is introduced as follows:

- The satellite is moving along a well defined orbit path and is always pointing towards the centre of the earth. The exterior orientation of the imagery can therefore be modelled by consideration of the orbital parameters, as they are introduced in § 2.4.5
- It is assumed that two of the six parameters have very little effect on the image geometry. These are the semi-major axis (a) of the orbit ellipse and the argument of the perigee due to the very low orbit eccentricity.
- The two parameters affected by these motions, are the true anomaly (v) and the ascending node (Ω) and are modelled by linear angular changes with time as follows (using notation of §2.4.5.):

$$v = v_o + v_1 x$$
$$\Omega = \Omega_o + \Omega_1 x \qquad \text{Eq. 85}$$

The rates of change of v and Ω can be calculated from the orbit period and the Earth rotation rate. Using this method the unknown exterior orientation parameters are four (v_o, Ω_o, i, a) thus just 2 GCPs are needed to solve the model. However, due to orbit perturbations, the sensor is unlikely to be pointing precisely towards the centre of the earth. The space resection orientation is therefore extended to allow additional sensor attitude rotations and the unknown parameters are seven. Finally, a further extension allows linear angular rates of change with time (drift rates) to be included in the additional attitude rotation matrix increasing the number of unknowns to 10, for each image.

In this research, as it was mentioned before, the conventional model is used in the evaluation process of the single image sensor model modification in chapter 4.

3.1.1.2. Model Accuracy

As a part of the Preliminary Evaluation Programme for SPOT (PEPS) the area around Aix-en-Provence, southern France had been evaluated from stereo model accuracy and image interpretation, where three SPOT level 1A images were acquired.

Ten photogrammetrically or geodetically derived GCPs were used for image orientation and 20 check points measured from 1:25000-scale map sheets were used to check the model. An additional 42 spot heights were taken from the 1:25000-scale maps to check heights. Control and check points were well distributed over the whole model. A selection of results using the 7 parameter model is given in table 8:

Number of GCPs used for the orientation	10	6
RMS Plan Accuracy (20 check points)(m)	17.7	17.7
RMS Height Accuracy (62 check points, B/H=.73)(m)	5.4	5.9
RMS Height Accuracy (53 check points, B/H=.32)(m)	8.0	

Table 8. Accuracy of Dowman and Gugan model (7 parameters) with Aix-en-Provence test site (Gugan, 1987)

A second stereopair of SPOT images over UK was also used to check the accuracy. A large number of GCPs with accuracy of 1m in X, Y and Z were provided by the Ordnance Survey. Ten GCPs used for the orientation and 17 check points were used to assess accuracy. A selection of results using the 7 and 10 parameter models is given in table 9:

Number of parameters	7	10
RMS Plan Accuracy (m)	8.8	8.7
RMS Height Accuracy (m)	10.2	7.4

Table 9. Accuracy of Dowman and Gugan model (7 and 10 parameters model) with UK test site (Gugan, 1987)

The results indicate that the high frequency rates of change of attitude can be used to improve the accuracy of the model but, more importantly, the accuracy improvement can be obtained by the use of high quality ground control data.

3.1.2. Konecny et al. model (1987)

3.1.2.1. Model description

This model was developed in the Institute of Photogrammetry and Engineering Surveys, University of Hannover (Konency et al., 1987). The method was implemented and tested on analytical photogrammetric instruments. Also the bundle adjustment program BINGO was modified using this model to handle line scanner geometry.

As it has already been mentioned, the exterior orientation of each line is given by six parameters. In case of satellite photography, the parameters of neighbouring lines are highly correlated when the sensor is on a platform of a high altitude satellite with a near-circular orbit. It is assumed that the sensor is moving uniformly without acceleration during the acquisition time of an image. As a first approximation the orientation angles are regarded as constant. If the above assumptions are adopted in the model it is clear that the model does not fit the reality.

In reality, the elliptical form of the orbit and the accelerations caused by manoeuvring action together with movements due to the nonuniform gravity field of the Earth caused the platform not to move in a defined orbit, and the angles ω, φ and κ could not to remain constant (Konency et al., 1987).

A satellite moves very gently in its orbit and additionally the terrain heights are small compared with the flight attitude. Because of the six orientation parameters of the perspective projection are highly correlated with each other the orbit refinements may exclude nonlinear changes in ω, φ and κ are allowed. The angular changes are functions of time. They may be expressed as additional parameters which change the image geometry. As a result except for the six exterior orientation parameters that represents the uniform motion, eight additional parameters were added which represent the most likely distortions. Thus, these eight additional parameters are the difference between the approximated uniform movement and the reality. The total unknown orientation

parameters are 14 for each image, although redundant additional parameters are automatically removed.

3.1.2.2. Implementation

The model was tested using a SPOT stereo pair taken over the South France. Ground control point had been taken from 1:25000-scale maps and 18 GCPs were used to stabilize the geometry in this case, because over 50 percent of the model was covered by water. The adjustment with BINGO gave the following results:

- Six parameters of exterior orientation (X,Y,Z) of the centre point of the image and ω, φ and κ.
- The values of the additional parameters representing the difference between the approximated uniform movement and the reality; redundant parameters are automatically removed.
- The correlation of the additional parameters.
- Three-dimensional coordinates of object points.
- Variances and covariances of the unknowns
- The variance components of the observations to check the stochastic model.

Using the BINGO program the implementation of the model in SPOT stereopair gave the accuracy results as introduced in table 10.

As it has already been mentioned BINGO automatically selects the additional parameters. In any case three or four parameters were selected. As a result the total unknown parameters are nine or ten for each image.

Number of GCPs used for the orientation	18	34
Number of check points used	68	52
RMSE X (m)	10.9	11.3
RMSE Y (m)	13.7	13.8
RMSE Z (m)	6.5	6.2

Table 10. Accuracy of Konecny model (Konecny et al., 1987)

3.1.3. Kratky model (1989)

3.1.3.1. Model description

This rigorous model was developed at the Canada Centre of Mapping. It was assumed that it is a universal model even in a digital environment. The model was developed in a three-dimensional coordinate system as the author mentioned that 'The three dimensional character of the photogrammetric formulation allows consideration, in the rigorous way, all physical aspect of the satellite orbiting and the earth imaging, together with geometric conditions of the time dependent intersection of corresponding imaging rays in the model space' (Kratky, 1989)

Also before the model is described the following assumption should be mentioned as they are very important in sensor model development:

- Time is the only independent variable.
- Earth rotation effect is taken into consideration.
- Coordinates along the flight path have the same scale.

As for the model itself, the total number of unknown parameters of the solution for a stereopair is 28 and they are defined in the following way:

- 12 standard orientation parameters are represented by the reference positions (X,Y,Z) of SPOT projection centres and by the reference attitude (κ, φ, ω) of sensors, all corresponding to the centre of the images.
- 12 additional parameters are linear and quadratic rates of change for attitude elements as modelled by polynomials dependent on time.
- 4 additional parameters as self calibration parameters, in order to compensate for the lack of information on the photogrammetric calibration of HRV sensors.

The attitude model can be simplified by disregarding the quadratic terms of attitude change, when judged appropriate. In this instance, the number of unknowns is reduced

by six, down to the total of 22. Also constraints are enforced in order to keep projection centres moving strictly along appropriate elliptical orbital elements.

3.1.3.2. Model Accuracy

The evaluation process was done using three different test sites: Ottawa, Sherbrooke (Canada) and Grenoble (France). The results of the first two test sites are represented here as the third test site guides us to the same conclusions.

The Ottawa test site had a very poor base to height ratio of 0.4. The accuracy results are introduced in table 11:

Number of unknown parameters	26	20	22
Number of GCPs used for the orientation	6	6	5
Number of check points used	65	65	65
RMSE E (m)	4.8	4.9	4.6
RMSE N (m)	6.0	6.3	5.3
RMSE H (m)	12.9	12.2	8.4

Table 11. Accuracy of Kratky model with the Ottawa test site (Kratky, 1989)

The Sherbrooke test site had a base to height ratio of .61. The accuracy results are introduced in table 12:

Number of GCPs	16	9	7	5
Number of check points used	237	244	246	248
RMSE E (m)	4.9	5.2	5.3	5.6
RMSE N (m)	5.1	5.8	6.1	5.3
RMSE H (m)	7.3	7.9	7.9	7.5

Table 12. Accuracy of Kratky model with the Sherbrooke test site (Kratky, 1989)

From the above test sites results it seems that the 22 parameters model appears to be optimal and is highly recommended as a standard approach and just five GCPs well distributed in the image are needed to give a good solution.

3.1.4. Westin model (1990)

3.1.4.1. Model description

This is the second attempt after the Dowman and Gugan model to connect the exterior orientation parameters of satellite images with the geometry of its orbit and is based also, on orbital elements computation. The modelling approach is the following:

- A simplified orbital model is used. It is assumed that, during the timespan of one scene, the orbit can with sufficient accuracy be approximated by a circular orbit. The orbital radius is allowed to vary with time to account for the elliptic form of the orbit. The radial shape of the orbit is determined by fitting the third order polynomials to the orbital radius derived from the ephemeris. The shape is considered fixed, except for the constant term. The set of the orbital elements to be estimated are reduced to four instead of six.
- The satellite attitude also needs to be estimated. As the attitude angular velocities are measured on board, relative attitude angles can be calculated by integration. It is assumed that these measurements are accurate enough, leaving only the constant terms to be estimated.
- The model exterior orientation parameters that need to be adjusted are the following seven:

  i, inclination

  Ω, right ascension of the ascending node

  to, time at the ascending node

  ro, orbital radius at t=to

  ω, roll

  φ, pitch

κ, yaw

Also, in this paper, additional points regarding the model coordinate systems are introduced as follows:

- The SPOT ephemeris data is given in Earth-centred, Earth fixed system using the International ellipsoid 1980. The ephemeris has to be transformed to the Earth centred inertial coordinate system before it can be used in the orbital parameters calculations.
- The most important difference from the ordinary collinearity equations in aerial photogrammetry is that the sensor x-coordinate is always zero, and all the parameters on the right side of the equations are functions of time.

3.1.4.2. Model Accuracy

Two tests were designed to investigate the potential accuracy of the model. The first test evaluates the accuracy of the scene relatively to maps, using maps for collecting control points. The second evaluate the accuracy in a scene relative to a rectified reference scene from which image chips were collected and used as a control in the adjustment. However, in this review only the results from the first evaluation are introduced because all others are not comparable to the results of the other models.

This test was done on one image (not in a stereopair). 84 well-defined GCPs were measured from 1:10000-scale maps. Using all GCPs in the adjustment resulted in the following reference standard deviations:

S_x= 2.9m
S_y= 2.7m
S_d= 4.0m

This model was extended for a sequence of SPOT scenes (§ 3.2.1).

3.1.5. O'Neill-Dowman model (1991)

This model was implemented under the aegis of the Alvey MMI-137 Real Time 2.5D Vision project at University College London. The camera model was designed to provide an accurate method of transforming SPOT imagery from image space to object space and visa versa, using the minimum amount of ground control to orient the model. Furthermore the model works accurately with both single SPOT-1 stereo pairs and strips (O'Neill et al., 1991).

The three basic design considerations for this model are:

- To use all available auxiliary information in order to reduce the number of ground control points which have to be used to set up the model.
- Functional simplicity. The use of simple, easily understood algorithms where ever possible to achieve the desired results. In spite of using this approach the model is quite complex. This is because the satellite telemetry data is of a poor quality, which means that complex relaxation and orbit reconstruction are required to achieve a tolerably accurate model.
- A modular code structure. This facilitates experimentation with the camera model.

The stereo model is set up in the following two stage process:

- Setting up a relative model using the SPOT-1 header.
- Orienting the relative model to an absolute coordinate system using a small number, typically 3 ground control points.

3.1.5.1. Setting up a relative model using the SPOT header.

In the model the following items are used from the header file of SPOT header file.

- The scene centre time
- The nominal size of a pixel on the ground

- The satellite position vector
- The satellite velocity vector
- The UT time data
- The attitude data
- The absolute time when each item of attitude data was acquired.
- The nominal look angles for the first and last sensors in the SPOT pushbroom sensor array.

Using the above information a relative orientation of SPOT is established using vector theory. It is definitely a new way of finding the orientation of the satellite sensor where the accuracy is depending directly to the provided header data.

3.1.5.2. Model Accuracy

Tests indicated that the method is robust and gives results comparable to other methods of orienting SPOT data. The notable feature of the method is that a good relative model can be formed without any control points and that there is little improvement when more than 3 points are used and that the accuracy is independent of strip length.

The results with OEEPE data from S. France are given in tables 13 and 14. From the results, it is obvious that the two GCPs are not enough to give acceptance model accuracy, especially when SPOT-1 for relative orientation establishment. However if three GCPs are used the accuracy is comparable with the accuracy of other models where more unknown parameters are used.

Number of GCPs	2	2	3	3
Number of Check Points	102	93	94	93
RMS Plan Accuracy (m)	31.8	21.6	13.8	13.5
RMS Height Accuracy (m)	12.1	11.4	10.2	10.5

Table 13. Accuracy of O'Neill and Dowman model with OEEPE strip A (O'Neill and Dowman., 1991)

Number of GCPs	2	4	3	3
Number of Check Points	130	130	130	120
RMS Plan Accuracy (m)	21.8	15.3	16.1	15.5
RMS Height Accuracy (m)	14.8	8.6	10.9	7.9

Table 14. Accuracy of O'Neill and Dowman model with OEEPE strip B (O'Neill and Dowman, 1991)

3.1.6. General sensor model summary

Table 15, is a comparison table of the accuracy achieved of the general models that are introduced in §3.3.1-3.3.5. These models could be compared, because SPOT data were used in the evaluation process of all models. However, the reference data used were not of the same accuracy which could affect the accuracy of the solution, as it was shown in the Gugan and Dowman model evaluation (§3.1.1.2 tables 8 and 9).

The total number of the unknown parameters for a stereopair can vary from 14 to 26. It is obvious to think that more parameters will lead to better accuracy which is not proven from the results (Kratky model). It seems that the accuracy is not improved due to the correlation between the unknown parameters. However, in all models horizontal accuracy close to one pixel is achieved, while the accuracy in height is better than 12.2 meters in the worst case.

Two models (Gugan-Dowman, Westin) are based in orbital elements trying to represent the satellite notion during the image acquisition. However, because of the short time interval a simplified model is used, in both cases. On the other hand in Konecky, Kratky and O'Neill models, the motion of the satellite is simulated using polynomials where their order is fixed in advance or is chosen automatically during the solution from statistical tests.

Model	Unknowns Per stereopair	GCPS	ICP	Check Points Accuracy (RMS) in meters		
Gugan-Dowman (conventional)	28	-	-	-	-	-
Gugan-Dowman (orbital)	14	10	17	8.8 (plan)		10.2 (h)
Gugan-Dowman (orbital)	20	10	17	8.7 (plan)		7.4 (h)
Konecny	18 or 20	18	68	10.9(E)	13.7(N)	6.5 (h)
Konecny	18 or 20	34	52	11.3(E)	13.8(N)	6.2 (h)
Kratky	20	6	65	4.9(E)	6.3(N)	12.2 (h)
Kratky	22	5	65	4.6(E)	5.3(N)	8.4 (h)
Kratky	26	6	65	4.8(E)	6.0(N)	12.2 (h)
Westin (one image test)	18	84	-	4 (plan GCPs standard deviation)		
O'Neill-Dowman	-	4	130	15.3 (plan)		8.6 (h)

Table 15. Comparison of general model accuracy

The conventional space resection as was developed by Gugan and Dowman (§3.1.1) is used in this thesis along with other models. The test procedure is explained in detail in §4.5. A modified model called Kepler model is adopted as the most appropriate for the description of the satellite motion during the acquisition time of a single pushbroom image. From this modified model, two different versions are developed. The first one is based on the state vector while the other one is on orbital elements (§4.9). Finally, the model based on the state vector is adopted after the stability check that is described in chapter 4.

3.2. Along track stereo models

Specific along track stereo models will be introduced. The first one was developed by Westin (Westin, 1991). Although, it was developed for along track SPOT1 images with or without overlap, it is a very interesting initial approach of the whole problem (§ 3.2.1). Mainly, after the first MOMS mission the first along track stereo sensor models where introduced. The models will be summarized and reviewed in a chronological way.

3.2.1. Westin (1991)

3.2.1.1. Model description

This model is an extension of the single scene model of SPOT images that Westin introduced in 1990 (§ 3.1.4). The single scene model is established with in total seven unknown parameters for the exterior orientation, where three of them represent a simplified satellite orbit (i, Ω, r_o) , three of them represent the rotation angles (ω, φ, κ) and the last one, t_o , represents the time at the ascending node.

To be able to extend this theory to a multi-scene solution, it is necessary to regard the four orbital parameters as corrections to the different sets of estimated values of each scene, rather than the actual orbital parameters. Start values of the simplified orbital model parameters are estimated from the ephemeris of each scene and hence each scene will give rise to different set of estimated orbital parameters. By using the same corrections to all scenes, the extended image is kept rigid and the orbital parameters for the whole pass are kept to three.

For the attitude parameters and the time of the ascending node a more complicated model is chosen. These four parameters are different for each scene. The reason for this is to make possible to obtain a solution in the cases when there is a gap in the sequence

of scenes. The reason for including the time parameter in the scene vector is similar. For scene gap is necessary to allow for a slightly different correction to the time parameter.

In the least square adjustment weights for the common unknown parameters are chosen and they are depended on whether the scenes are overlapped or separated by a scene gap. In the case of overlapped cases the weights are set infinitely high. In this way the parameters are forced to be identical to the previous scene. An adjustment of the sequence of scenes without gaps will thus give the identical results to the obtained using an adjustment model with only the seven parameters included. When the scenes are separated by a gap, the weights will be finite. For the attitude parameters, the magnitudes of the weights will depend on the gap size, while the time parameter weight will be independent of the gap size. When the scenes are separated by the data gap, there is an unknown drift in the attitude between the scenes and the weights then to be related to the expected drift. Empirical variogram models for the attitudes of SPOT 1 are computed. (Westin , 1991).

As the variogram is the variance of attitude increments as a function of time interval, the weight is given directly by the inverse of the variogram, evaluated for the time interval of the data gap.

3.2.1.2. Model Accuracy

The accuracy of this model was investigated using two SPOT scenes which were separated by a gap of four missing scenes corresponding to 210km on the ground, or 31 seconds in time.

Two GCPs were collected in the second scene to be used in the adjustment. No GCPs was used in the first scene. The geometry of the scenes after rectification was evaluated by the use of a large number of checkpoints, 84 in the first and 43 in the second. The three dimensional coordinates of the checkpoints were considered error free. Given the adjusted model and the three dimensional coordinate of the check points; it was possible to compute the expected image coordinates of each checkpoint. By identifying the

checkpoints in the image, their real image coordinates were obtained and hence the error as the difference between real and the expected. The resulting errors of the checkpoints are given in table 16.

Image	1	2
Number of GCPs	0	2
Number of Check Points	84	43
RMS in x direction(m)	8.9	4.7
RMS in y direction(m)	6.6	4.0

Table 16. Accuracy of Westin extended model for strip of two SPOT images (Westin, 1991)

The accuracy of the second image where two GCPs were measured is almost two times better than the first image where no GCPs were measured. However, in both images the accuracy is very good having in mind that only two GCPs were measured for both images.

In this thesis, the along track sensor model has some common points with Westin extended model approach. The common points are that the orbit representation is treated universally for all images, and the attitude variations are treated for each image independently. However, in this thesis, the orbit representation is based in the state vector approach and the attitude variations are calculated from GCPs, although it is possible to calculate them using tie points, in the future

3.2.2. Ebner at al. (1992)

This model is a simulation study for the MOMS-02. The model is based on the extended collinearity equations. The exterior orientation parameters are estimated only for so-called orientation images (OI), which are introduced at certain time intervals. Between the OI, the parameters of each individual image line are expressed as a function (e.g. polynomials) of the parameters of the neighbouring orientation images. A variety of

different parameter models for the reconstruction of the exterior orientation were applied. The goal of each approach is the minimization of the interpolation error using as few parameters as possible.
The camera geometry, the reconstruction of the exterior orientation and the introduction of the offset and drift parameters are described briefly in the following:

3.2.2.1. Interior Orientation

The three lenses of the MOMS-02 stereo module provide a threefold along track stereo scanning with different ground resolution. The focal length of the nadir lens is 660 mm; the forward and backward looking lenses are inclined with respect to Nadir lens and have a focal length of 237.2 mm. Self- calibration using additional parameters for the correction of systematic image errors can be applied as usual.

3.2.2.2. Exterior orientation

For each inclined lens additional 6 parameters was introduced to rigorously model the displacement Δx, Δy, Δz of the projections centres and the rotations $\Delta\varphi$, $\Delta\omega$, $\Delta\kappa$ of the image coordinate system of the nadir lens. Thus the camera geometry described by 21 parameters:2x9 parameters (Δx, Δy, Δz, $\Delta\varphi$,$\Delta\omega$,$\Delta\kappa$, x_o, y_o , c) and 3 parameters for the nadir image (x_o, y_o , c).

Extended collinearity equations are derived from the general approach and are the following:

$$x = x_0 - c\frac{R_{11}(X-X_0)+R_{21}(Y-Y_0)+R_{31}(Z-Z_0)-(M_{11}\Delta x+M_{21}\Delta y+M_{31}\Delta z)}{R_{13}(X-X_0)+R_{23}(Y-Y_0)+R_{33}(Z-Z_0)-(M_{13}\Delta x+M_{23}\Delta y+M_{33}\Delta z)}$$
$$y = y_0 - c\frac{R_{12}(X-X_0)+R_{22}(Y-Y_0)+R_{32}(Z-Z_0)-(M_{12}\Delta x+M_{22}\Delta y+M_{32}\Delta z)}{R_{13}(X-X_0)+R_{23}(Y-Y_0)+R_{33}(Z-Z_0)-(M_{13}\Delta x+M_{23}\Delta y+M_{33}\Delta z)} \quad \text{Eq. 86}$$

In case of the nadir image ($\Delta x=0$, $\Delta y=0$, $\Delta z=0$, M=I). For the orientation parameters of each line third, order polynomials are used.

3.2.2.3. Offset and drift parameters

In case of MOMS-02, the following additional information is available:

- position and attitude data from the onboard Inertial Navigation system (INS)
- position data from the Tracking Data Relay Satellite System(TDRSS)
- position data from sophisticated orbit model

In this case the different systematic errors of the position and attitude data are modelled through additional unknown parameters. Twelve additional parameters, namely an offset and drift parameters have to be estimated during the bundle adjustment.

As a simulation study the results are not introduced. The accuracy of this model using real data will be represented in §3.2.4.

3.2.3. Kornus and Lehner model, (1999)

This model was focused on the MOMS-02 sensor. Attention was given to the interior orientation of the model where an amount of parameters were added in order to represent as accurate as possible the complex inner geometry of MOMS sensor.

3.2.3.1. Interior Orientation

Five parameters were established for accurate representation of the sensor geometry:

- two displacements
- one rotation of the CCD-array in the image plane k
- one deviation of the focal length
- one parameters modelling the sensor curvature

All parameters were fed into the bundle adjustment with low weights allowing for self-calibration.

3.2.3.2. Exterior orientation

The exterior orientation is estimated only in lines using a certain time intervals as was introduced in the previous paper, while between these lines the exterior orientation is modelled by a third order polynomials function. The attitude and the position information of the navigation data are treated as uncorrelated observations. Systematic errors in these data like biases and linear drifts are treated as additional unknowns and are estimated simultaneously with the other unknowns in the adjustment.

3.2.3.3. Model Accuracy

For the model evaluation 9 image scenes of orbit T083C were composed in a strip approximately 415 km long, covering part of Southern Germany and Austria. The image quality of the nadir channel is adversely affected (strong defocusing effect).

For the German part of the strip (covering 5 images) the GCPs and Check Points are transformed of the geodetic to geocentric. The estimated standard deviations of the coordinates are 2.5m in all directions.

For the entire strip 8 orientation images (OI) were employed. The distance between the OI was set to 3330 image lines, corresponding to 8.2 seconds flight time, which proved to be sufficient to model the temporal course of the exterior orientation parameters.

A subset of the results is introduced in table 17, using a data set of 148 GCPs which are measured stereoscopically in the 3-ray GCPs. The results are in UTM. From these 7 or 4 points are selected as GCPs while all others are used as check points. The following combinations of tests were done:

1: 7 GCP in 3-ray area

2: 4 GCP in 3-ray area

a: Position and attitude data

b: Position only, no attitude data

c: No navigation data at all

Case	1a	1b	1c	2a	2b	2c
E_E (m)	7.7	7.7	8.2	7.8	7.9	11.6
E_N(m)	7.2	7.2	7.6	7.0	7.1	10.1
E_H(m)	10.8	10.9	11.1	10.8	12.5	62.3

Table 17. Accuracy of Kornus model with MOMS data

From the table the following conclusions could be extracted:

- No difference is visible between case 1a and 2a, demonstrating that the number of GCPs does not affect the accuracy of photogrammetric point determination if precise navigation data are available.
- If only position data is used (case b) the influence of the number of GCPs increases. Seven GCPs are sufficient to establish such stable geometric conditions and the attitude observation do not improve the results and can be completely neglected.
- Even if no navigation data are available at all, seven GCPs give comparable accuracy to the previous cases. Here the strength of the along track 3-line stereoscopic images is visible, which enables the rigorous reconstruction of spatial objects exclusively by photogrammetric methods and GCPs.

3.2.4. Ebner and et al. model (1999)

3.2.4.1. Model description

In this paper an enhanced model for MOMS is introduced. Referring to the Ebner model (§ 3.2.1), although it is clearly understood that this approach reduces the number of the

orientation parameters to a reasonable amount, its inherent disadvantage is that the estimated position parameters are not associated with the physical model of the spacecraft trajectory.

To overcome this drawback, the bundle adjustment algorithm is supplemented by a rigorous dynamical modelling of the spacecraft motion to take orbital constraints into account. The camera position parameters which have been estimated at certain time intervals are now expressed by the six parameters of the epoch state vector and additional force model parameter.

Compared to the orientation point approach, the orbital constrains approach has essential advantages, which can be summarized as follows:

- Full utilization of the information content of the tracking data in a statistically consistent way.
- A reduced number of unknown parameters
- Accuracy improvements for the photogrammetric results as well as the epoch state vector.

3.2.4.2. Model accuracy

Four images #15-#18 were selected covering an approximately 37x430 km wide area in Northern Australia. Seventy-seven points were measured by Melbourne University using differential GPS. Finally 64 points were used in various combinations as GCPs or check points.
Only the conclusions from the results are introduced here, mainly, because the authors assumed that the planimetric accuracy potential of the images is not verified, since the GCPs and the check points could not be identified in the imagery with the required accuracy.
The conclusions are the following:

- The attitude data does not improve the accuracy.

- The accuracy improved slightly if 1000 tie points is used instead of 100.
- Height accuracy of up to 4.1m is obtained, corresponding to 0.3 of the ground pixel size of the oblique looking channels.

3.2.5. Fritsch and Stallmann model (2000)

3.2.5.1. Model description

This paper is based on an extension of a SPOT model developed by V. Kratky. The geometric solution combines the principle of rigorous photogrammetric bundle formulation with additional constraints derived from known relations assuming an elliptic orbit. The attitude parameters are modelled by a simple polynomial model being linear or quadratic. Ephemeris data are not necessary but are optional. The parameters of the interior orientation are determined by self calibration.
The sensor position is derived from known nominal orbital relations, while the attitude variations are modelled by a simple polynomial model (linear or quadratic). For self-calibration two additional parameters are added. The focal length and the principal point correction. The exterior orientation and the additional parameters of the sensor are determined in a general formulation of the least-square adjustment. The ephemeris data can be used to approximate or reset some of the unknown parameters.

The principal assumptions in this paper are the following:

- The satellite is moving along a well defined close to circular elliptic orbit.
- In along track mode the sensor is always pointing to the centre of the earth.
- The images are taken with a pushbroom scanner sensor using a constant time interval.
- A single image consists of a fixed number of consecutive scan lines.
- Each line has each own time depended position and attitude parameters.
- Not all the six parameters of the exterior orientation need to be reconstructed, but these parameters are highly correlated for neighbouring lines.

- The very narrow field of view results in nearly parallel imaging rays. This causes in a high correlation between the projection centre coordinates and the sensor view angle.
- For compensation, additional constraints of the usage or the usage of orbital position and attitude are required.

3.2.5.2. Model accuracy

For this evaluation T08C5 and T08FE were available which were taken in stereo mode D. The processing level was level 1A. The ground control points were measured in topographic maps of scale 1:25000 and 1:50000 with an accuracy of approx. 5m respectively 10m.

Several versions were calculated using a short (S) orbital segment (scenes 27 and 28) and a long (L) orbital segments (scenes 27-30), using linear (L) or quadratic (Q) attitude model. The results are introduced in table 18.

Significant differences between the versions did not exist. However, as expected, the use of quadratic attitude model gave slightly better results than the linear model. The accuracy derived from the check points was 11-14m in planimetric and 13m in height.

Orbit	Model	GCP	CHP	RMSx(m)	RMSy(m)	RMSz(m)
S	L	9	35	14.5	12.7	12.2
S	Q	9	35	11.8	13.5	13.1
L	L	10	24	11.1	13.6	13.4
L	Q	10	24	11.2	11.4	13.7
L	L	15	20	10.4	14.1	13.0
L	Q	15	20	10.1	10.5	13.8

Table 18. Accuracy of Fritsch and Stallmann model with MOMS data (Fritsch and Stallmann, 2000)

3.2.6. Poli model (2004)

3.2.6.1. Model description

This model has been developed in the Institute of Geodesy and Photogrammetry at ETH Zurich. It is a general rigorous sensor model and has already been applied to satellite and airborne sensors. Moreover it was applied to along-track stereo capability and to multi-lens sensors (i.e. SPOT-5/HRS, ASTER, MOMS-02, MISR), too. In this case the Ebner model is modified.

The photogrammetric collinearity equations describe the perspective geometry in each image line. The sensor position and attitude are modelled with piecewise 2nd order polynomial functions depending on time. The platform trajectory is divided into segments according to the number and distribution of available Ground Control Points (GCPs) and Tie Points (TPs) and for each segment the sensor position and attitude are modelled by 2nd order polynomials. At the points of conjunction between adjacent segments constraints on the zero, first and second order continuity are imposed on the trajectory functions. Additional pseudo-observations can fix some or all parameters to suitable values. The sensor model includes also a self-calibration, which is required for the correction of the systematic errors due to principal point displacement (*dx*, *dy*), focal length variation (*dc*), radial symmetric (*k1*, *k2*) and decentering lens distortion (*p1*, *p2*), scale variation in CCD line direction (*sy*) and the CCD line rotation in the focal plane (θ).

In case of satellite imagery, the available ephemeris (usually sensor position and velocity at fixed intervals) are used to generate the approximate values for the parameters modelling the sensor external orientation (position and attitude). The required geometric parameters (focal length(s), viewing angles, number and size of CCD elements in each array) are usually available from the imagery provider or from literature. The reference frame used in the adjustment is the fixed Earth Centered Cartesian system, also called ECR.

3.2.6.2. Model accuracy

Although this model was evaluated using a variety of satellite and airborne data, only the results from the SPOT5- HRS test under HRS-SAP Initiative will be introduced. An HRS stereopair over Bavaria and Austria was used for the evaluation process. The available ephemeris (sensor position and velocity) were used to generate the approximate values for the parameters modelling the sensor external orientation (position and attitude) in the fixed Earth-centred geocentric Cartesian system. From the available 41 object points, a group of them was used as GCPs and the remaining as check points. The best results in terms of RMSE in the check points were obtained by modelling the external orientation with two 2^{nd} order polynomials and with self-calibration. The self-calibration parameters that influenced mostly the model were *k1*, *k2*, *p2* and *sy* for both lenses. The other self-calibration parameters could not be estimated due to the high correlation with the tie points coordinates and external orientation parameters. By changing the number of GCPs and check points, the RMSE were always less than 1 pixel. The results of this test are summarized in table 19.

Number of GCPs and Check points	RMSE east (m)	RMSE north (m)	RMSE height (m)
8+31	3.68	6.52	4.75
16+25	3.46	6.22	3.75
41+0	3.24	5.52	3.68

Table 19. Accuracy of Poli model with HRS data (Poli, 2004)

3.2.7. MOMS along track sensor model summary

Along track stereo models are developed mainly for MOMS data (§3.2.2- §3.2.5) except Westin model which is summarized in §3.2.1 and Poli model which is more general model. MOMS sensor in reality is not a permanent spaceborne instrument (§2.2.3) with

a lot of functional problems when it was on board in MIR space station. These along track models have a great number of parameters for the representation of the exterior orientation as the orbit and the spacecrafts themselves where the MOMS was on board, were not developed as a remote sensing satellite. Moreover additional parameters are used for detailed description of inner orientation MOMS complexity.

The exterior orientation parameters are estimated only for the so-called orientation images (OI), which are introduced at certain time intervals. Between the OI, the parameters of each individual image line are expressed as a function (e.g. polynomials) of the parameters of the neighbouring orientation images.

In all these models the concept is to describe the motion of the spacecraft where MOMS was on board. Only one case (Ebner, 1999) an attempt was done to improve the model and describe as accurately as possible the orbit of the vehicle.

3.3. Literature summary

A summary of the findings is introduced, along with a justification of what can be done in this research as a new approach of modelling the along track stereo geometry.

The development of a satellite sensor model, as it has already been mentioned from almost all the researchers, has the following differences and in a way, disadvantages compared to the classical frame camera model:

- The satellite model is kinematic because the acquisition interval of one image is not instantaneous.
- Each image line has its own orientation parameters. However the parameters of neighbouring lines are highly correlated when the sensor is on a platform of a high altitude satellite on a sun-synchronous orbit.
- The along track field of view is very narrow, giving an unstable solution if the model is not developed properly.

On the other hand the satellite moves very gently in its orbit under the influence mainly of the gravity field. It is worth trying to model the satellite motion using orbit determination methods which are combined with collinearity equations in order to use the image coordinates as observation in the solution. As it has already been mentioned in the introduction this is the way of reaching the sensor modelling development in this thesis. The effort is to model the forces that act on the satellite and not the results (satellite motion) of them.

A few attempts have already been done in order to take into account this opportunity. These are the Gugan and Dowman orbital model and the Westin model where some of the orbital elements are used in the solution (§3.1.1, 3.1.4). As can be seen from the comparison table (table 15), these models are accurate enough, having the fewer unknown parameters. It seems that this way of developing the sensor model is very effective. The use of navigation data is extensive as initial values or even as additional parameters improve and stabilize the solution.

However, all the above models use classical orbital elements to define the satellite position on orbit. It is believed in this research, that instead of the orbital elements the state vector should be used for the following reasons:

- The state vector is used in modern orbit determination procedures.
- The state vectors are provided in the navigation data.
- Some classical orbital elements in polar close to circular orbits are highly correlated.

An extensive test is done in §4.9 in order to examine the stability of the solution using the two alternatives (state vector or orbital elements)

In the reviewed models the satellite images in case of the exterior orientation are treated as follows:

- Each line of the satellite image is an individual image with its own exterior orientation parameters (one dimensional) where the relationship among

sampling lines or segments are modelled with low order polynomials as a function of the sampling time.

- The exterior orientation parameters are estimated only for so-called orientation images (OI), which are introduced at certain time intervals. Between the OI, the parameters of each individual image line are expressed as function (e.g. polynomials) of the parameters of the neighbouring orientation images.

From the comparison table (table 15) it is obvious that the developed models with the best accuracy have at about 20-22 unknown parameters for the stereopair. Thus, a small number of GCPs are needed to achieve an accurate solution.

Some very important issues are arising from this review, which are the objectives of this thesis:

- In all the along track stereo models the determination of the orbit is not taken into account in a way to find common exterior orientation parameters for all images or express some parameters regarding others (except of the Westin model where a simplified orbit model is used).

- If the model is developed with the above modification, all the along track images could be oriented simultaneously, giving a more stable solution. Moreover, the simultaneous solution extends the narrow field of view of each satellite image, because, all along track images are treated as one iconic image, with field of view equal to the angle between the first and the last image.

- The order of the polynomials of the attitude data it seems to be in some models important factor for the accuracy of model. This is an issue that should be examined, in depth.

- In some models self-calibration is applied. This should be examined, having in mind the correlation between the unknown parameters. When this procedure could be used without affecting the stability of the solution?

- Finally the use of navigation data in order to stabilise the solution or moreover to solve the model without using any GCPs should be examined. In the models review, navigation data mainly used as initial values of the solution or to establish the relative orientation.

Further comments on the reviewed sensor models and a comparison with the developed model is given in § 6.3.5.

CHAPTER 4.

GENERIC SENSOR MODEL FOR A SINGLE IMAGE

4.1. Introduction

In this chapter the acquisition geometry of the pushbroom scanner is examined and a generic rigorous sensor model for a single image is developed. The generic rigorous along track stereo model is based on this.

In the first part of this chapter, the development of the modified general sensor model is carried out step by step in §4.7. In § 4.9 two different versions of the generic rigorous model is introduced. In the first one the exterior orientation parameters are the state vector while in the second one the orbital elements are involved in the exterior orientation. Extensive tests are done in order to understand the behaviour of each version. From the results the conclusion is that the solution where the orbital elements are computed is not stable. For this reason, mainly, the state vector sensor model is adopted. This model is modified in order to follow the along track acquisition geometry. Finally, in §4.8 the general ridge estimator value is estimated which is best fit the data provided (§2.5.5) which is used in the evaluation process.

4.2. General considerations

The meaning of the term 'rigorous' as it is given in this thesis, is introduced. **In a rigorous model each parameter should express, in advance, an identifiable physical or geometric quantity**. As an example, the frame camera model is a rigorous sensor model, where the exterior orientation parameters represent the position of the principal point and the rotation from the ground to the image coordinate system. On the other hand, mainly for satellite images, there are models (rational polynomials function, affine models, etc.) where a simulation of the real world is carried out using a large number of parameters in order to improve the accuracy of the model. There is no physical meaning

given in these parameters, as it has already been mentioned (§1.2, § 3.3). Moreover, some of the rigorous models which are introduced in chapter 3 are not totally rigorous, because the satellite motion is simulated using polynomials, where their order is determined during the solution according to the expected accuracy or from statistics, without understanding the physical representation of them.

As it was mentioned (§ 1.1.) the pushbroom model is a kinematic model. **What makes this model kinematic and how this model could be described rigorously?**

This model is kinematic because the image is not acquired instantaneously. The scanning effect on the ground is due to the motion of the satellite (§ 2.2.1.). A single image consists of a number of framelets which are independent one-dimensional images with their own exterior orientation parameters; perspective projection is maintained perpendicular to the direction of flight. Thus, **in a rigorous sensor model the satellite motion in space should be described** as accurately as possible. In other words, a rigorous sensor model **should describe the state of the satellite** during the acquisition time of the image or images (§ 2.4.4.). Six parameters are enough to establish the state of the satellite at an epoch (time stamp), which are the state vector associated with position and velocity vectors or the orbital elements ((§ 2.4.4, 2.4.5).

Hence, the simplest sensor model should have nine unknown exterior orientation parameters, where the six of them represent the state vector or the orbital elements of the perspective center and the other three the rotations angles from the geocentric coordinate system to the framelet coordinate system.

4.3. Adopted points from the literature for the along track images.

From the literature the following general points are adopted. Some of them are effective, also, in case of along track stereo sensor model in the next chapter:

- The satellite is moving along a well defined, smooth, close to circular elliptical orbit.

- The images are acquired with a pushbroom scanner using a constant time interval. As a result the coordinates along the flight path have the same scale.
- The satellite sensor model is a kinematic model. A single image consists of a number of framelets. The relationship among framelets is characterized by the kinematic orientation parameters which are modelled with low order polynomials as a function of the sampling time.
- It is assumed a stationary world and the moving camera.
- The sensor array is approximately perpendicular to the direction of motion.
- Attention must still be paid to the solution stability that may occur from the over-parameterization of the model.
- The orientation satellite images should be carried out in a geocentric coordinate system in order to avoid distortions caused by earth curvature and map projection and to facilitate integration with sources of metadata information that may be available.
- During the satellite's flight a perspective projection is maintained across track. On the other hand a curvilinear projection is maintained along the flight direction.

4.4. Fundamental point in the sensor modelling development

In this section the fundamental point in the sensor modelling research is introduced.

If a thorough examination is taken, to the form of the second order polynomials (e.g. $X_c(t) = X_o + a_1 t + b_1 t^2$), it is clearly understood that because the results should be in meters, the units of the coefficient a_1 should be in meters/sec and the b_1 units should be in meters/sec^2. **Generally, this definitely means that the first order coefficient represents the velocity of the satellite on the reference axis and in the same way the second order represents the acceleration on the same axis.** For the same reason, the first and the second order coefficients in the rotation angles polynomials, represent the angular velocity and the angular acceleration, accordingly.

As a conclusion, using the notation of equation 6 the $X_c(t), Y_c(t), Z_c(t)$ should be at least, first order polynomials, representing the position and the velocity of the base point (state vector) while the polynomials $\omega_c(t), \varphi_c(t), \kappa_c(t)$ at least, constant (eq. 7). In §4.7 a thorough test is done in order to find the most appropriate rigorous sensor model for the representation of a single satellite image geometry.

4.5. Single image model development

The development procedure of one satellite image sensor model is carried out, step by step, from the simplest to the most complex sensor model which is the Gugan and Dowman model in §4.7. This direction of development from the simplest to most complex model is chosen for the following reasons:

- From step to step the accuracy improvement is defined.
- The correlation between the exterior orientation parameters and the necessity of use them is better understood and controlled.

The simplest model that can be found in image orientation modelling is the frame camera model. Although, it is definitely sure, that this model is totally inappropriate for satellite images from pushbroom sensors, it is tested in this initial step in order to have a feeling of the imprecision caused, when this model is used in pushbroom satellite images. Moreover, the correlation matrix and the standard deviation of the unknown parameters are calculated, using the least squares and the general ridge estimator techniques for comparison. This information is useful, having in mind that the frame model is the simplest model where the correlation between the unknown parameters is expected to be the minimum. Finally, starting from the frame camera model it is known how much the precision of the pushbroom models should be improved.

In the second step the velocity vector is added in the model which means that the first order coefficients in the positions polynomials are added as was described in §4.4. It is the simplest model for the pushbroom sensor as has already been mentioned (§4.4). If this model is adopted, it is assumed that the velocity and the rotations of the satellite

during the acquisition time of one image are constant. From now on, this model is referred as **velocity vector model**. The total number of exterior orientation parameters is nine for each image. A detailed introduction of this model along with the accuracy results are found in § 4.7.2.

In the third step the angular velocities are added in the previous model. In this model first order polynomials are used for each orientation parameter. The total number of exterior orientation parameters is twelve for each image. A detailed introduction of this model along with the accuracy results are found in § 4.7.3. From now on this model is referred as **angular velocity vector model**.

In the fourth step, **the Gugan and Dowman (§3.1.1) conventional space resection model** is used as the most complex of the models that are evaluated in this test. The total number of exterior orientation parameters is fourteen for each image. A detailed introduction of this model along with the accuracy results are found in § 4.7.4.

In the final step the **Kepler model for a single image** that is the adopted model in this thesis as the most appropriate for single image orientation, is introduced. **The basic idea of this model is that the motion of the satellite during the acquisition time of one image is a Keplerian motion. The rotation angles during the acquisition time of one image remain constant.** The number of unknown parameters is nine for each image as in the velocity vector model. A detailed introduction of this model along with the accuracy results are found in § 4.7.5.

In § 4.7.6., a comparison table of the precision results for the position vector is provided giving the opportunity to understand the advantages and disadvantages of each method. Finally the proposed model is chosen, along with the main research assumptions which are going to extent in the along track stereo sensor model (§ 4.10).

In § 4.9 two different versions of the generic rigorous model are introduced. In the first one, the state vector represents the exterior orientation parameters while in the second the orbital elements do. After extensive tests the state vector sensor model is adopted.

4.6. Data sets-Reference data

4.6.1. Data sets

For the single image model evaluation two along track stereo data sets are used. These data sets are the following:

- An ASTER data set that covers the Vegoritis area in Northern Greece which is a test site for the Centre for Observation and Monitoring of Earthquake and Tectonics (COMET).
- A SPOT5 HRS data set that covers an area located around Aix-en-Provence in SE France which is provided under the SPOT Assessment Project (SAP) set up by CNES and ISPRS (Baudoin et al., 2003).

Detailed information about these data sets are given in § 6.2

4.6.2. Reference data

4.6.2.1. Aster reference data

The ground control points were located on 1:5000 maps which were produced by Hellenic Military Geographical Service (HMGS). The maps were produced from aerial photographs with a scale of 1:12000-1:15000 using analytical photogrammetric instruments and then scanned at a 300dpi resolution. They were then georeferenced in EGSA-87 Greek Geodetic System. The planimetric accuracy of these maps is about 2 meters while the height accuracy is better than 4m. A total of 20 Reference Points were measured in ASTER images having a very good distribution all over the images, and all of them are used as Ground Control Points.

4.6.2.2. HRS reference data

The grounds control points were originally provided by IGN for the OEEPE test of SPOT data and were mainly extracted from 1:25000 maps. The geodetic coordinates are given in the French NTF system, where the reference ellipsoid is Clarke 1880. The Lambert III projection is used. A total of 33 Reference Points were measured in HRS

images having a very good distribution all over the HRS images, and all of them are used as Ground Control Points. Mainly the GCPs which are used in Gugan PhD thesis (Gugan, 1987) are used in this thesis, too.

4.6.3. Coordinate Systems used during the development

4.6.3.1. Image space coordinate system

The framelet coordinate system that is established for all images is described in §2.3.3. From both data sets the base framelet as it is determined in §2.3.5., is the middle pixel of the center line of each image.

4.6.3.2 Reference coordinate system.

In this research, an inertial coordinate system should be used, in order to meet the principal assumption of Keplerian motion as it is described in §2.4.3.

The GCPs for both data sets are provided in a geodetic coordinate system. The transformation in inertial geodetic system should be done in two steps; first a transformation in a geocentric system and then in an inertial system (§2.4.1).

For the transformation from a geodetic system to a geocentric system the geoid undulation for the coordinates should be given, because the heights that provided are orthometric heights so it is necessary to transform them, in ellipsoidal heights (§ 2.4.1.6). However, the area of the data sets the geodetic undulation is not known and the EGM96 is used that is based on a spherical harmonic expansion of the disturbing potential to degree and order 360.

Finally, for the transformation from the geocentric to inertial coordinate system the acquisition time of the base line should be known very accurately as it is needed for accurate transition from the CTS to CIS as it was described in §2.4.1.4.

4.7. Implementation of the models

In this evaluation process mainly the physical meaning and the contribution of each parameter in the exterior orientation of the pushbroom scanner is examined in depth along with statistical criterions. These criterions are the following (§2.5.3.3):

- Reference standard deviation of the solution (S_o)
- Standard deviation of unknown parameters
- Correlation matrix of the unknown parameters
- t-parameter of the unknowns

It is assumed that if the reference standard deviation of the solution is better **than a pixel is accepted as precise enough** for this evaluation of one image sensor model. **The unknown parameters should be as uncorrelated as possible and the t-parameter of each unknown parameter should fulfill the t-test with the 95% confidence level (§2.5.3.3).**

Only in the frame camera, the accuracy of unknown parameters using the Least Squares Estimator (LSE) and the general ridge estimator are compared. For all other tests only the accuracy of unknown parameters using the General Ridge Estimator (GRE) is presented. Also, similar results or results with similar meaning are not displayed.

4.7.1. Frame camera model accuracy

The frame camera model is the simplest rigorous model for the representation of acquisition geometry of a static image. Although, this model is not appropriate for pushbroom images, it is involved in this test in order to have a feeling of the error caused if a static model like the frame model is implemented in a pushbroom sensor. The classic camera model is based in the collinearity equations:

$$x - x_o = -c\frac{m_{11}(X - X_o) + m_{12}(Y - Y_o) + m_{13}(Z - Z_o)}{m_{31}(X - X_o) + m_{32}(Y - Y_o) + m_{33}(Z - Z_o)}$$
$$y - y_o = -c\frac{m_{21}(X - X_o) + m_{22}(Y - Y_o) + m_{23}(Z - Z_o)}{m_{31}(X - X_o) + m_{32}(Y - Y_o) + m_{33}(Z - Z_o)} \quad \text{Eq. 87}$$

where

c is the focal length

x_o, y_o is the offset from the fiducial-based origin to a perspective center origin.

X, Y, Z are the ground coordinates of a point

X_o, Y_o, Z_o are the ground coordinates of the perspective center

and,

$$M = \begin{bmatrix} m_{11} & m_{12} & m_{13} \\ m_{21} & m_{22} & m_{23} \\ m_{31} & m_{32} & m_{33} \end{bmatrix} =$$
$$= \begin{bmatrix} \cos\phi\cos k & \cos\omega sink + \sin\omega\sin\phi\cos k & \sin\omega\sin k - \cos\omega\sin\phi\cos k \\ -\cos\phi\sin k & \cos\omega\cos k - \sin\omega\sin\phi\sin k & \sin\omega\cos k + \cos\omega\sin\phi\sin k \\ \sin\phi & -\sin\omega\cos\phi & \cos\omega\cos\phi \end{bmatrix} \quad \text{Eq. 88}$$

M is a 3x3 rotation axis which brings the ground coordinate system parallel to the framelet coordinate system as a function of time

ω is the rotation along X-axis

φ is the rotation along Y-axis

κ is the rotation along Z-axis

x,y are the image coordinates of the corresponding point.

4.7.1.1. HRS

The frame model is solved for HRS1 and HRS2 using ground control points. The reference standard deviation of the solution and standard deviation of the unknown

parameters using the least squares estimator (LSE) and the general ridge estimator (GRE) are given in table 20.

	HRS-1		HRS-2	
S_o(pixel)	3.928		2.618	
	Standard deviation of the unknown parameters		Standard deviation of the unknown parameters	
	LSE	GRE	LSE	GRE
X_o(m)	9315.106	88.048	5219.176	67.775
Y_o(m)	8080.140	31.659	5346.205	18.899
Z_o(m)	8591.252	45.645	6312.037	82.115
ω(rad)	0.0124727	0.0000501	0.00923426	0.0000395
φ(rad)	0.0140128	0.0000828	0.00928307	0.0000891
κ(rad)	0.0084091	0.0003153	0.00710821	0.0002108

Table 20. Reference standard deviation and standard deviation of the unknown parameters for HRS images using the frame model

The following comments are extracted from this table:

- The reference standard deviation of both images is not as accurate as expected from a rigorous model, because a static model is used.
- The precision should be improved only four pixels (or about three pixels because it is not possible to eliminate it into zero) the addition of more parameters should be done very carefully and gently.
- The standard deviation of the unknown parameters using general ridge estimator is much better than the standard deviation where of the least squares estimator.

Finally, for the HRS evaluation test using the frame model, the correlation matrices of the HRS-1 image are given using the least square estimator(LSE) (table 21) and the general ridge estimator(GRE) are given (table 22).

	X_o	Y_o	Z_o	ω	φ	κ
X_o	1.00	0.08	**-0.99**	-0.20	1.00	0.23
Y_o	0.08	1.00	-0.24	-0.99	0.10	0.99
Z_o	**-0.99**	-0.24	1.00	0.36	-0.99	-0.39
ω	-0.20	**-0.99**	0.36	1.00	-0.22	-1.00
φ	**1.00**	0.10	**-0.99**	-0.22	1.00	0.25
κ	0.23	**0.99**	-0.39	-1.00	0.25	1.00

Table 21. Correlation matrix of HRS-1 in frame camera model using LSE

	X_o	Y_o	Z_o	ω	φ	κ
X_o	1.00	0.00	-0.02	0.03	0.90	0.00
Y_o	0.00	1.00	0.00	-0.94	-0.04	0.10
Z_o	-0.02	0.00	1.00	0.18	-0.43	-0.02
ω	0.03	**-0.94**	0.18	1.00	-0.01	-0.09
φ	**0.90**	-0.04	**-0.43**	-0.01	1.00	0.07
κ	0.00	0.10	-0.02	-0.09	0.07	1.00

Table 22. Correlation matrix HRS-1 in frame camera model using GRE

First of all, these tables lead to the conclusion that the general ridge estimator provides a less correlated and more representative solution of the exterior orientation parameters. From now on, only the general ridge estimator will be used in the evaluation process of a single image sensor model.

Another important comment which comes out from the table 22, is that the correlation (§3.1.1) between X_o coordinate and φ rotation along with the Y_o coordinate and ω rotation is found here, even in this case where the frame camera model is used.

4.7.1.2. Aster

The frame model is also implemented in the ASTER NADIR and BACK images. The reference standard deviations of the solution (S_o) and of the unknown parameters using the general ridge estimator are given in table 23.

The comments here are almost identical with the HRS evaluation results regarding the reference standard deviation of the solution. It is definitely obvious that the addition of more parameters should be done very carefully and gently, as it has already been mentioned (§4.7.1.1).

The only additional comment that should be made is that the standard deviation of the unknown parameters of the nadir image is better than the standard deviation of the unknown parameters of the back image. Attention is paid in the following tests if this is a general conclusion and finally the nadir image geometry gives more accurate results

(which it is expected). The correlation matrixes have the same pattern as the correlation matrices of HRS solution and for this reason they are not introduced, here.

	Nadir image	Back image
S_0(pixel)	4.349	4.474
	Standard deviation of the unknown parameters	
X_0(m)	95.086	96.396
Y_0(m)	56.789	20.732
Z_0(m)	26.808	119.879
ω(rad)	0.0000861	0.0001189
φ(rad)	0.0001238	0.0001234
κ(rad)	0.0007984	0.0008324

Table 23. Reference standard deviation and standard deviation of the unknown parameters for ASTER images using the frame camera model and General Ridge Estimator

4.7.2. Velocity vector model.

The velocity vector is added to the previous model, which means that the first order coefficients in the positions polynomials in the equation 6 are added as it was described in §4.5. It is the simplest model for the pushbroom sensor as it has already been mentioned (§4.4, §4.5). **If this model is adopted, it is assumed that the velocity and the rotations of the satellite during the acquisition time of one image are constant.** The total number of exterior orientation parameters is nine for each image; three for the position, three for the velocity and three for the attitude. A revised formulation of the modified collinearity equations (equation 5) follows:

$$0 = -c\frac{m_{11}(X-(X_o+u_xt))+m_{12}(Y-(Y_o+u_yt))+m_{13}(Z-(Z_o+u_zt))}{m_{31}(X-(X_o+u_xt))+m_{32}(Y-(Y_o+u_yt))+m_{33}(Z-(Z_o+u_zt))}$$
$$y = -c\frac{m_{21}(X-(X_o+u_xt))+m_{22}(Y-(Y_o+u_yt))+m_{23}(Z-(Z_o+u_zt))}{m_{31}(X-(X_o+u_xt))+m_{32}(Y-(Y_o+u_yt))+m_{33}(Z-(Z_o+u_zt))}$$

Eq. 89

where

c is the focal length

t is the corresponding time of the framelet containing a point on the image (eq. 8)

X,Y,Z are the ground coordinates of a point

X_o, Y_o, Z_o are the ground coordinates of the perspective center of the base framelet

u_x, u_y, u_z represent the velocity vector of the perspective center of the base framelet

M is a 3x3 rotation axis which brings the ground coordinate system parallel to the framelet coordinate system as a function of time (same as the frame camera model, equation 88)

x,y are the image coordinates of the corresponding point.

4.7.2.1. HRS

The reference standard deviation of the solution (S_o) and the standard deviation of the unknown parameters for HRS images using the general ridge estimator along with the t-parameter estimation are given in table 24 and the correlation matrix of HRS-1 image in table 25. The t-value for HRS in this test is 2.00315 (66 observation and 9 unknowns).

	HRS-1		HRS-2	
S_o(pixel)	0.956		0.874	
	Standard deviation of the unknown parameters	t-parameter	Standard deviation of the unknown parameters	t-parameter
X_o(m)	26.098	188793.23	32.984	164866.886
u_x(m/sec)	0.577	9227.563	0.861	6349.526
Y_o(m)	8.629	62024.882	7.561	52203.196
u_y(m/sec)	0.330	4473.569	0.398	3788.551
Z_o(m)	27.774	187175.113	22.451	209619.936
u_z(m/sec)	0.623	8362.761	0.829	6402.966
ω(rad)	0.0000119	12226.006	0.0000239	2360.944
φ(rad)	0.0000301	12079.112	0.0000278	42613.019
κ(rad)	0.0000792	1178.326	0.0000755	3504.26

Table 24. Reference standard deviation and standard deviation of the unknown parameters for HRS images using the velocity vector model

The following comments are extracted from this table:

- The reference standard deviation of the solution of both images is improved from the value of the previous model and it is inside the expected boundaries as it is better than a pixel (§4.7).
- The standard deviation of the unknown parameters is better than the previous model.
- All the unknown parameters pass the t-test as their t-parameter value is much larger than the t-value.
- All the unknown parameters are almost uncorrelated except in case of, X_o coordinate and φ rotation along with the Y_o coordinate and ω rotation, as it is found also in the frame camera model (§4.7.1).

	X_o	u_x	Y_o	u_y	Z_o	u_z	ω	φ	κ
X_o	1.00	0.00	0.00	0.01	-0.05	0.00	0.00	0.93	0.00
u_x	0.00	1.00	0.00	0.00	0.00	0.02	0.00	0.00	-0.07
Y_o	0.00	0.00	1.00	0.00	-0.01	0.00	-0.86	-0.02	0.05
u_y	0.01	0.00	0.00	1.00	0.02	0.01	0.01	0.00	0.01
Z_o	-0.05	0.00	-0.01	0.02	1.00	-0.01	0.46	-0.41	-0.03
u_z	0.00	0.02	0.00	0.01	-0.01	1.00	0.00	0.00	0.03
ω	0.00	0.00	**-0.86**	0.01	**0.46**	0.00	1.00	-0.15	-0.04
φ	**0.93**	0.00	-0.02	0.00	**-0.41**	0.00	-0.15	1.00	0.06
κ	0.00	-0.07	0.05	0.01	-0.03	0.03	-0.04	0.06	1.00

Table 25. Correlation matrix of HRS-1 image using the velocity vector model

4.7.2.2. ASTER

The reference standard deviation of the solution and the standard deviation of the unknown parameters for ASTER images using the general ridge estimator along with the t-parameter estimation are given in table 26. The t-value for HRS in this test is 2.040 (40 observation and 9 unknowns)

The following comments are extracted from this table:

- The reference standard deviation of the solution of both images are improved from the value of the previous model and are inside the expected boundaries which is better than a pixel (§4.7). However the reference standard deviation of the nadir image is almost two times better than the back image.
- Moreover the standard deviation of the unknown parameters of the nadir image is better than the standard deviation of the unknown parameters of the back image.
- All the unknown parameters pass the t-test as their t-parameter value is much larger than the t-value for this test.

The correlation matrices give the same conclusion as the HRS correlation matrices and for this reason they do not introduced.

	Nadir		Back	
S_o(pixel)	.466		.706	
	Standard deviation of the unknown parameters	t-parameter	Standard deviation of the unknown parameters	t-parameter
X_o(m)	15.939	312178.301	21.093	249345.572
u_x(m/sec)	0.270	18937.206	.679	7632.107
Y_o(m)	9.613	215844.032	9.050	228142.637
u_y(m/sec)	0.083	1897.496	0.166	1023.383
Z_o(m)	14.214	322170.407	19.862	213307.041
u_z(m/sec)	0.196	28896.869	0.617	9155.513
ω(rad)	0.0000213	27055.212	0.0000637	19239.892
φ(rad)	0.0000209	34567.692	0.0000159	74827.279
κ(rad)	0.0000149	3442.099	0.0000250	4251.639

Table 26. Reference standard deviation, standard deviation of the unknown parameters and t-parameter for ASTER images using the velocity vector model

4.7.3. Angular velocities vector model

In the third step the angular velocities are added in the previous model. Thus, in this model first order polynomials are used for each orientation parameter. The total number of exterior orientation parameters is twelve for each image; three for the position, three

for the velocity and six for the rotation angles. **If this model is adopted, it is assumed that the velocity and the angular velocities of the satellite during the acquisition time of one image are constant.** In the revised collinearity equation as it is described for the previous model (Equation 89) only the rotation angles are modified. Using the formulation of the equation 8 the rotation angles of a framelet are expressed as follows:

$$\begin{aligned} \omega_c(t) &= \omega_o + \omega_1(t) \\ \phi_c(t) &= \phi_o + \phi_1(t) \\ \kappa_c(t) &= \kappa_o + \kappa_1(t) \end{aligned} \qquad \text{Eq. 90}$$

where

t is the corresponded time of the framelet containing a point on the image (eq. 8)

ω_o, φ_o, κ_o are the rotation angles of the perspective center of the base framelet

ω_1 ,φ_1,κ_1 represent the angular velocity vector of the perspective center of the base framelet

4.7.3.1. HRS

The reference standard deviation of the solution (S_0) where the angular velocity model is used and the standard deviation of the unknown parameters for HRS images using the general ridge estimator along with the t-parameter estimation are given in table 27 and the correlation matrix of HRS-1 image in table 28. The t-value for HRS in this test is 2.006 (66 observation and 12 unknowns).

The following comments are extracted from tables 27 and 28, compared to the previous results:

- The reference standard deviation of the solution of both images are inside the expected boundaries which is better than a pixel (§4.7). However, the reference standard deviation of this model is almost identical with the reference standard deviation of the previous model.
- The standard deviation of the unknown parameters is slightly improved.

- However **not all the unknown parameters pass the t-test**. In HRS2 solution κ_1 parameter does not pass the t-test. Also, the κ_1 in HRS1 solution is close to this value along with the ω_1 in HRS2 solution.
- The velocity t-parameters in the velocity vector model have larger values, in almost all cases, than the corresponding values in the angular velocity model. This means that the statistical significance of the velocities in this model is reduced.
- The correlation between the unknown parameters is increased. Except of the correlations (§3.1.1) between X_o coordinate and φ_o rotation along with the Y_o coordinate and ω_o rotation is found again in this evaluation, there is slight correlation between the ω_o and φ_o (-0.24) , κ_o and φ_1(0.42), κ_1 and φ_1(0.59) and κ_o and κ_1 (0.30).

	HRS-1		HRS-2	
S_o(pixel)	.946		.875	
	Standard deviation of the unknown parameters	t-parameter	Standard deviation of the unknown parameters	t-parameter
X_o(m)	25.926	190665.337	30.509	178302.378
u_x(m/sec)	0.183	1499.800	0.581	5609.247
Y_o(m)	5.013	106106.468	7.487	54435.829
u_y(m/sec)	0.341	5697.216	0.489	3785.702
Z_o(m)	28.415	182746.835	21.170	222068.565
u_z(m/sec)	0.734	4134.451	0.229	1561.336
ω_o(rad)	0.0000086	16631.805	0.0000241	2647.341
ω_1(rad/sec)	0.0000028	322.784	0.0000067	9.310
φ_o(rad)	0.0000301	12717.147	0.0000259	45971.701
φ_1(rad/sec)	0.0000035	1768.423	0.0000028	2388.108
κ_o(rad)	0.0000865	1090.964	0.0000827	3276.610
κ_1(rad/sec)	0.0000734	7.227	0.0000473	1.612

Table 27. Reference standard deviation, standard deviation of the unknown parameters and t-parameter for HRS images using the angular velocity model

	X_o	u_x	Y_o	u_y	Z_o	u_z	ω_o	ω_1	φ_o	φ_1	κ_o	κ_1
X_o	1.00	0.00	0.00	0.00	-0.05	0.00	0.00	0.04	0.91	0.01	0.00	0.00
u_x	0.00	1.00	0.00	0.00	0.00	0.00	0.00	0.00	0.00	0.05	0.00	0.00
Y_o	0.00	0.00	1.00	0.00	0.00	0.00	-0.70	0.01	-0.01	0.00	0.03	0.00
u_y	0.00	0.00	0.00	1.00	0.00	0.00	0.00	**-0.14**	0.00	-0.01	0.00	0.00
Z_o	-0.05	0.00	0.00	0.00	1.00	0.00	0.64	0.10	-0.43	0.04	-0.02	0.00
u_z	0.00	0.00	0.00	0.00	0.00	1.00	0.00	0.05	0.00	-0.09	0.00	0.00
ω_o	0.00	0.00	**-0.70**	0.00	**0.64**	0.00	1.00	0.06	-0.24	0.04	-0.02	0.02
ω_1	0.04	0.00	0.01	-0.14	0.10	0.05	0.06	1.00	0.00	0.05	0.05	0.06
φ_o	**0.91**	0.00	-0.01	0.00	**-0.43**	0.00	**-0.24**	0.00	1.00	0.03	0.07	0.04
φ_1	0.01	0.05	0.00	-0.01	0.04	-0.09	0.04	0.05	0.03	1.00	0.42	0.59
κ_o	0.00	0.00	0.03	0.00	-0.02	0.00	-0.02	0.05	0.07	**0.42**	1.00	0.30
κ_1	0.00	0.00	0.00	0.00	0.00	0.00	0.02	0.06	0.04	**0.59**	**0.30**	1.00

Table 28. Correlation matrix HRS-1 solution using the angular velocity model

4.7.3.2. ASTER

The angular velocity model is also tested in ASTER data. The reference standard deviation of the solution (S_o) and the standard deviation of the unknown parameters for ASTER images using the general ridge estimator along with the t-parameter estimation are given in table 29. The t-value for HRS in this test is 2.048 (40 observation and 12 unknowns).

The following comments are extracted from this table, compared to the previous results:

- The reference standard deviation of the solution of both images are worse compared to the velocity vector model results although it is inside the expected boundaries which is better than a pixel (§4.7).
- The standard deviation of the unknown parameters is about the same with the values of previous model.
- However as in case of HRS images **not all the unknown parameters pass the t-test**. The t-test value is 2.048. In Nadir and back solution, κ_1 parameter does not pass the t-test.
- The velocity t-parameters in the velocity vector model do not have larger values, than the corresponding values in the angular velocity model. This means that the statistical significance of the velocities in this model is increased. This

conclusion is exactly opposite of the HRS images and it is not taken into consideration.

	Nadir		Back	
S_o(pixel)	0.498		.828	
	Standard deviation of the unknown parameters	t-parameter	Standard deviation of the unknown parameters	t-parameter
X_o(m)	13.790	360537.486	23.193	226559.586
u_x(m/sec)	0.113	47342.303	0.849	5457.959
Y_o(m)	8.450	245621.715	16.579	124696.213
u_y(m/sec)	0.027	4097.650	0.322	3131.243
Z_o(m)	16.776	273194.312	18.578	229401.047
u_z(m/sec)	0.784	7358.877	0.542	9961.872
ω_o(rad)	0.0000217	26227.565	0.0000595	19363.335
ω_1(rad/sec)	0.0000018	14.708	0.0000052	70.391
φ_o(rad)	0.0000203	35258.343	0.0000224	52368.126
φ_1(rad/sec)	0.0000014	255.379	0.0000019	658.634
κ_o(rad)	0.0000224	2150.202	0.0003318	2987.759
κ_1(rad/sec)	0.0000428	0.825	0.0000409	0.181

Table 29. Reference standard deviation, standard deviation of the unknown parameters and t-parameter for ASTER images using the angular velocity model

The correlation matrices give the same conclusion as the HRS ones and for this reason they are not introduced.

4.7.4. Gugan and Dowman model

Gugan and Dowman conventional space resection model is developed and evaluated here in the same way as it is introduced by the authors in § 3.1.1. In few words, in this model the relationship among consecutive framelets is characterized by the dynamic orientation parameters which are modelled with low order polynomials as a function of the sampling time. The order of the polynomials is defined as: second order for the position (X,Y,Z), constant for the rotations omega(ω) and phi(φ) and second order for the rotation kappa(κ) (Eq. 84)

4.7.4.1. HRS

The reference standard deviation of the solution (S_o) where the angular velocity model is used and the standard deviation of the unknown parameters for HRS images using the general ridge estimator along with the t-parameter estimation are given in table 30 and the correlation matrix of HRS-1 image in table 31. The t-value for HRS in this test is 2.008 (66 observation and 14 unknowns).

	HRS-1		HRS-2	
S_o(pixel)	0.899		0.810	
	Standard deviation of the unknown parameters	t-parameter	Standard deviation of the unknown parameters	t-parameter
X_o(m)	29.928	164969.515	12.543	433279.299
u_x(m/sec)	1.214	4373.682	0.999	5405.036
a_x(m/ses^2)	0.070	771.721	0.189	770.083
Y_o(m)	11.079	48074.406	6.779	58315.153
u_y(m/sec)	0.472	3155.577	0.395	3821.515
a_y(m/ses^2)	0.052	408.640	0.008	173.803
Z_o(m)	21.395	242823.984	19.345	243669.119
u_z(m/sec)	0.581	9057.040	0.684	7789.931
a_z(m/ses^2)	0.133	840.472	0.0674	798.521
ω_o(rad)	0.0000140	10166.676	0.0000209	2548.039
φ_o(rad)	0.0000329	11398.204	0.0000210	56076.963
κ_o(rad)	0.0000966	978.105	0.0000114	2286.300
κ_1(rad/sec)	0.0000511	1.236	0.0000391	0.538
κ_2(rad/ses^2)	0.0000432	5.193	0.0000614	3.940

Table 30. Reference standard deviation, standard deviation of the unknown parameters and t-parameter for HRS images using the Gugan and Dowman model

The following comments are extracted from this table, compared to the previous results:

- The reference standard deviation of the solution of both images are improved from the value of the previous model and it is inside the expected boundaries which is better than a pixel (§4.7). The reference standard deviation is slightly improved compared to the angular velocity vector.
- The standard deviation of the unknown parameters is also slightly improved.

- However **not all the unknown parameters pass the t-test**. In both HRS-1 images the κ_1 parameter does not pass the t-test. Also, the κ_2 parameter again for both HRS images is close to this value.
- The correlation between the unknown parameters is slightly increased but it is not as large as the angular velocity model. Except of the correlations (§3.1.1) between X_o coordinate and φ_o rotation along with the Y_o coordinate and ω_o rotation is found again in this evaluation, there is correlation between κ_o and κ_2 (-0.62).

	X_o	u_x	a_x	Y_o	u_y	a_y	Z_o	u_z	a_z	ω_o	φ_o	κ_o	κ_1	κ_2
X_o	1.00	0.00	0.00	0.00	0.01	0.00	-0.05	0.00	0.00	0.01	0.96	0.00	0.00	0.00
u_x	0.00	1.00	0.00	0.00	0.00	0.00	0.00	0.03	0.00	0.00	-0.01	-0.09	-0.22	-0.08
a_x	0.00	0.00	1.00	0.00	0.00	0.00	0.00	0.00	0.00	0.00	0.00	0.00	-0.01	-0.01
Y_o	0.00	0.00	0.00	1.00	0.00	0.00	-0.01	0.00	0.00	-0.94	-0.02	0.05	0.00	0.00
u_y	0.01	0.00	0.00	0.00	1.00	0.00	0.02	0.01	0.00	0.00	0.01	0.01	0.01	0.00
a_y	0.00	0.00	0.00	0.00	0.00	1.00	0.00	0.00	0.00	0.00	0.00	0.00	0.00	0.00
Z_o	-0.05	0.00	0.00	-0.01	0.02	0.00	1.00	0.00	0.00	0.30	-0.31	-0.02	0.00	0.00
u_z	0.00	0.03	0.00	0.00	0.01	0.00	0.00	1.00	0.00	0.00	0.00	0.01	0.03	0.01
a_z	0.00	0.00	0.00	0.00	0.00	0.00	0.00	0.00	1.00	0.00	0.00	0.00	0.01	0.00
ω_o	0.01	0.00	0.00	**-0.94**	0.00	0.00	**0.30**	0.00	0.00	1.00	-0.05	-0.05	0.00	0.00
φ_o	**0.96**	-0.01	0.00	-0.02	0.01	0.00	**-0.31**	0.00	0.00	-0.05	1.00	0.04	0.02	0.00
κ_o	0.00	-0.09	0.00	0.05	0.01	0.00	-0.02	0.01	0.00	-0.05	0.04	1.00	0.18	**-0.62**
κ_1	0.00	-0.22	-0.01	0.00	0.01	0.00	0.00	0.03	0.01	0.00	0.02	0.18	1.00	-0.19
κ_2	0.00	-0.08	-0.01	0.00	0.00	0.00	0.00	0.01	0.00	0.00	0.00	**-0.62**	-0.19	1.00

Table 31. Correlation matrix HRS-1 solution using Gugan-Dowman model

4.7.4.2. ASTER

The Gugan and Dowman model is also evaluated also tested in ASTER data. The reference standard deviation of the solution (S_o) and the standard deviation of the unknown parameters for ASTER images using the general ridge estimator along with the t-parameter estimation are given in table 32. The t-value for HRS in this test is 2.056 (40observation and 14 unknowns).

- The reference standard deviation of the solution of both images is better especially for the back image where the reference standard deviation of the nadir image is reached. The precision for both images are two time better than the expected boundaries (§4.7).
- The standard deviation of the unknown parameters is about the same with the values of previous model.
- However **not all the unknown parameters pass the t-test**. In Nadir solution, κ_1 and κ_2 parameter does not pass the t-test. Also, the same parameters in back solution is close to this value.
- The velocity t-parameters in the velocity vector model have smaller values, in almost all cases, than the corresponding values in the angular velocity model. This means that the statistical significance of the velocities in this model is reduced.

	NADIR		BACK	
S_o(pixel)	.465		.462	
	Standard deviation of the unknown parameters	t-parameter	Standard deviation of the unknown parameters	t-parameter
X_o(m)	14.865	344472.798	14.271	368192.99
u_x(m/sec)	0.302	16722.393	0.487	10263.805
a_x(m/ses^2)	0.001	25720.048	0.055	1192.898
Y_o(m)	9.534	217883.809	6.668	310247.922
u_y(m/sec)	0.049	2446.927	0.065	1577.58
a_y(m/ses^2)	0.001	26461.019	0.034	728.864
Z_o(m)	4.761	962262.205	19.318	220396.321
u_z(m/sec)	0.422	13598.660	0.366	15494.018
a_z(m/ses^2)	0.038	825.774	0.025	585.281
ω_o(rad)	0.0000160	35917.354	0.0000579	20140.493
φ_o(rad)	0.0000171	41935.831	0.0000131	89514.946
κ_o(rad)	0.0000762	6360.932	0.0002582	3893.114
κ_1(rad/sec)	0.0000899	1.797	0.0000612	6.679
κ_2(rad/ses^2)	0.0000258	1.506	0.0000321	4.649

Table 32. Reference standard deviation, standard deviation of the unknown parameters and t-parameter for ASTER images using the Gugan and Dowman model

4.7.5. Kepler model

In this final step the **Kepler model** is introduced. It is the adopted model in this thesis as the most appropriate for single image orientation. The basic idea of this model is that the motion of the satellite during the acquisition time of a single image is a Keplerian motion. On the other hand, the rotation angles during the acquisition time of one image remain constant. The number of unknown parameters is nine for each image.

The formulation of this model is based on the modified collinearity equations (equation 6) where the position functions $(X_c(t), Y_c(t), Z_c(t))$ of the image are determined as follows, using equations 18; based on the general law of accelerated motion

$$X_c(t) = X_o + u_x \cdot t - \frac{GM \cdot X_o \cdot t^2}{2 \cdot (X_o^2 + Y_o^2 + Z_o^2)^{3/2}}$$

$$Y_c(t) = Y_o + u_y \cdot t - \frac{GM \cdot Y_o \cdot t^2}{2 \cdot (X_o^2 + Y_o^2 + Z_o^2)^{3/2}} \qquad \text{Eq. 91}$$

$$Z_c(t) = Z_o + u_z \cdot t - \frac{GM \cdot Z_o \cdot t^2}{2 \cdot (X_o^2 + Y_o^2 + Z_o^2)^{3/2}}$$

where

(X_o, Y_o, Z_o) is the position vector of the perspective center of the base framelet

(u_x, u_y, u_z) is the velocity vector of the perspective center of the base framelet

t is the acquisition time is it calculated for equation 8, and

GM is the Earth gravitational parameter with value of $398600{,}4415 km^3 / s^2$

4.7.5.1. HRS

The reference standard deviation of the solution (S_o) where the Kepler model is used and the standard deviation of the unknown parameters for HRS images using the

general ridge estimator along with the t-parameter estimation are given in table 33 and the correlation matrix of HRS-1 image in table 34. The t-value for HRS in this test is 2.00315 (66 observation and 9 unknowns).

The following comments are extracted from this table, compared to the previous results:

- The reference standard deviation of the solution of both images is worse than the value of the previous model. However it is inside the expected boundaries which is better than a pixel (§4.7). The reference standard deviation is slightly improved compared to the velocity and angular velocity vector models for HRS1 image while is worse for HRS2 image.
- The standard deviation of the unknown parameters is slightly improved.
- However **all the unknown parameters pass the t-test**.
- The correlation between the unknown parameters are minimum, where the correlations between X_o coordinate and φ rotation along with the Y_o coordinate and ω rotation is found again in this evaluation, as in the frame camera and velocity vector models.

	HRS-1		HRS-2	
S_o(pixel)	0.935		0.889	
	Standard deviation of the unknown parameters	t-parameter	Standard deviation of the unknown parameters	t-parameter
X_o(m)	28.534	172692.361	19.985	245808.487
u_x(m/sec)	0.568	9385.076	0.647	9204.952
Y_o(m)	8.939	59860.322	7.644	69545.974
u_y(m/sec)	0.437	3382.338	0.445	3266.632
Z_o(m)	18.781	276784.286	27.657	187050.918
u_z(m/sec)	1.271	4099.912	0.816	5866.626
ω(rad)	0.0000115	12612.241	0.0001236	426.088
φ(rad)	0.0000311	11671.19	0.0000928	12739.975
κ(rad)	0.0000776	1203.136	0.0001377	1895.379

Table 33. Reference standard deviation, standard deviation of the unknown parameters and t-parameter for HRS images using the Kepler model

	X_o	u_x	Y_o	u_y	Z_o	u_z	ω	φ	κ
X_o	1.00	0.00	0.00	0.01	-0.04	0.00	0.01	0.97	0.00
u_x	0.00	1.00	0.00	0.00	0.00	0.04	0.00	0.00	-0.07
Y_o	0.00	0.00	1.00	0.00	-0.01	0.00	-0.92	-0.02	0.05
u_y	0.01	0.00	0.00	1.00	0.01	0.02	0.00	0.00	0.01
Z_o	-0.04	0.00	-0.01	0.01	1.00	-0.01	0.32	-0.27	-0.02
u_z	0.00	0.04	0.00	0.02	-0.01	1.00	0.00	0.00	0.06
ω	0.01	0.00	-0.92	0.00	0.32	0.00	1.00	-0.05	-0.04
φ	0.97	0.00	-0.02	0.00	-0.27	0.00	-0.05	1.00	0.05
κ	0.00	-0.07	0.05	0.01	-0.02	0.06	-0.04	0.05	1.00

Table 34. Correlation matrix HRS-1 solution using Kepler model

4.7.5.2. ASTER

The Kepler model is also evaluated using ASTER image. The reference standard deviation of the solution (S_o) and the standard deviation of the unknown parameters for ASTER images using the general ridge estimator along with the t-parameter estimation are given in table 35. The t-value for HRS in this test is 2.040 (40 observation and 9 unknowns).

	Nadir		Back	
S_o(pixel)	0.498		0.474	
	Standard deviation of the unknown parameters	t-parameter	Standard deviation of the unknown parameters	t-parameter
X_o(m)	15.745	316145.771	14.261	350360.074
u_x(m/sec)	0.630	8048.134	0.370	14658.636
Y_o(m)	10.173	203815.329	11.232	183014.890
u_y(m/sec)	0.009	14380.351	0.110	2481.238
Z_o(m)	8.877	515773.765	11.498	393550.479
u_z(m/sec)	0.061	92799.838	0.418	12905.238
ω(rad)	0.0000187	30489.443	0.0000716	16424.022
φ(rad)	0.0000188	38493.149	0.0000196	60123.328
κ(rad)	0.0001751	2761.949	0.0001889	5365.016

Table 35. Reference standard deviation, standard deviation of the unknown parameters for ASTER images using Kepler model

- The reference standard deviation of the solution is better especially for the back image where the reference standard deviation of the nadir image is reached. The precision for both images are two time better than the expected boundaries (§4.7).
- The standard deviation of the unknown parameters is about the same with the values of previous model.
- **All the unknown parameters pass the t-test.**

4.7.6. Model comparison

In table 36 the number of unknown parameters for each model is summarized. Also in tables 37 and 38 the reference standard deviation of the solution (S_o) are showed and the standard deviation of the unknown parameters for all tests of HRS and ASTER images, respectively.

Method	Number of unknowns
Frame	6
Velocity	9
Angular	12
Gugan	14
Kepler	9

Table 36. Number of unknowns parameters for each single image model

The following general comments could be done here:

- All the pushbroom models from the velocity vector model to the Kepler model the reference standard deviation is in the expected limits which one pixel.
- However the reference standard deviation of the Gugan and Kepler models gives overall better results especially for ASTER back image.
- The standard deviation of the unknown parameters is better in Gugan-Dowman and Kepler models.
- Some parameters of the Gugan-Dowman and angular models do not pass the t-test.
- Finally, the correlation in Gugan-Dowman and angular models are increased.

Method	HRS-1				HRS-2			
	S_o (pixels)	Standard deviation of the unknown parameters			S_o (pixels)	Standard deviation of the unknown parameters		
		X_o(m)	Y_o(m)	Z_o(m)		X_o(m)	Y_o(m)	Z_o(m)
Frame	3.928	88.048	31.659	45.645	2.618	62.775	18.889	82.115
Velocity	0.956	26.098	8.629	27.774	0.874	32.984	7.561	22.451
Angular	0.946	25.926	5.013	28.415	0.875	30.509	7.487	21.170
Gugan	0.899	29.928	11.079	21.395	0.810	12.543	6.779	19.345
Kepler	0.935	28.534	8.939	18.781	0.889	19.985	7.644	27.657

Table 37. Reference standard deviation, standard deviation of the unknown parameters for HRS images using all models

Method	NADIR				BACK			
	S_o (pixels)	Standard deviation of the unknown parameters			S_o (pixels)	Standard deviation of the unknown parameters		
		X_o(m)	Y_o(m)	Z_o(m)		X_o(m)	Y_o(m)	Z_o(m)
Frame	4.349	95.086	56.789	26.808	4.475	96.396	20.732	119.879
Velocity	0.466	15.939	9.613	14.214	0.706	21.093	9.050	19.862
Angular	0.498	13.790	8.450	16.776	0.828	23.193	16.579	18.578
Gugan	0.465	14.865	9.534	4.761	0.462	14.271	6.668	19.318
Kepler	0.498	15.745	10.173	8.877	0.474	14.261	11.232	11.498

Table 38. Reference standard deviation, standard deviation of the unknown parameters for ASTER images using all models

On the other hand, important general conclusions could be extracted from these results:

- The precision in Y-axis is almost two times better than the precision of other axes in all cases.
- The standard deviation of the unknown parameters of the ASTER nadir image is better than the standard deviation of the unknown parameters of the back image especially on the Z-direction.
- The reference standard deviation of ASTER images is almost two times better than the reference standard deviation of HRS images. It seems that the more accurate reference data that are in the case of ASTER data (1:5000 scale maps) instead of the 1:25000 scale maps that are used for HRS data. It seems that precision depends on the combination of sensor and GCPs.

Having in mind the above conclusions and the fact that Kepler model has five less unknown parameters that the Gugan and Dowman model while its solution is more precise and less correlated than the solution of Gugan-Dowman model it is chosen as the most appropriate model for the description of a single pushbroom image.

4.8. General Ridge estimator definition-Problems

The general ridge estimator is a vector with the same dimension as the number of unknown parameters (§ 2.5.5). It has already been mentioned that different values are proposed in the literature for the general ridge estimator (Grob, 2003, Guo et al., 2002). The ultimate goal is to find some **k** which is large enough to reduce the variance compared to the ordinary least squares estimator, but which is small enough to produce some acceptable low bias (§ 2.5.5). The point is to find an uncorrelated solution if possible.

Thus, in this thesis its value is defined compared to standard deviation of the position vector of the solution where the line and the angle elements are solved separately. The position vector is used only as there is a serious incompatibility in the velocity vector accuracy which is discussed later. These tests are done for all the methods that are introduced in §4.7 (except of frame camera model) while in table 39 are shown the standard deviations of the position and velocity vectors for HRS and ASTER data of Kepler model solution. In this process all the available reference points are used as Ground Control Points in both data sets. On the other hand in table 40 the results of the standard deviation of the position vector are introduced for HRS1 image using various formulas starting for the proposed ones in the literature. The vector $\hat{\mathbf{a}}$ which appears in table 40 is defined as follows:

$$\hat{\mathbf{a}} = \hat{\mathbf{X}} \cdot \mathbf{Q} \qquad \text{Eq. 92}$$

where $\mathbf{Q}$ is the eigenvector matrix of $\mathbf{J}^{\mathrm{T}} \cdot \mathbf{W} \cdot \mathbf{J}$,

and $\hat{\mathbf{X}}$ is vector computed by Least Square estimator.

	HRS-1	HRS-2	ASTER-NADIR	ASTER-BACK
POSITION X (m)	27.518	16.152	11.375	14.717
POSITION Y (m)	10.416	8.825	8.932	8.436
POSITION Z (m)	15.309	25.555	8.696	8.872

Table 39. Standard deviation of the position vector in a solution method where the line elements and the angle elements are solved separately

If the values of tables 39 and 40 are compared it seems that the most appropriate estimator is the $\frac{\sqrt{S_o}}{\hat{\mathbf{a}}}$ which gives almost the same results as the standard deviation of the position vector of the solution where the line and the angle elements are solved separately.

Ridge estimator	**Standard deviation of the position vector**		
	X (m)	**Y (m)**	**Z (m)**
$(n-r)\frac{S_o^2}{\hat{\mathbf{a}}^2}$ (Grob,2002)	16637.147	3050.551	6456.511
$\frac{S_o^2}{\hat{\mathbf{a}}^2}$ (Guo et al., 2002)	17233.528	3344.531	6654.208
$\frac{S_o^2}{\hat{\mathbf{a}}}$	2041.063	639.313	846.875
$\frac{S_o}{\hat{\mathbf{a}}^2}$	15277.535	2998.205	5915.572
$\frac{S_o}{\hat{\mathbf{a}}}$	160.886	64.724	79.417
$(n-r)\frac{S_o}{\hat{\mathbf{a}}}$	23.103	7.281	22.387
$r\frac{S_o}{\hat{\mathbf{a}}}$	79.489	21.063	37.192
$\frac{\sqrt{S_o}}{\hat{\mathbf{a}}}$	28.534	8.939	18.781
$r\frac{\sqrt{S_o}}{\hat{\mathbf{a}}}$	13.507	5.423	10.555

Table 40. Standard deviation of the position vector using various values of general ridge estimator (HRS1 image).

In table 41 the results of the standard deviation of the position vector are introduced for HRS2 image using only the formulas that give results close to the standard deviation of the position vector of the solution where the line and the angle elements are solved separately. In Table 42 the same results are given for ASTER NADIR and BACK images respectively. In all cases it is shown that the same estimator seems to be the most appropriate. This estimator value is used in the evaluation process in § 4.7. Generally, the general ridge estimator is very useful during the evaluation process of the single image sensor model.

Ridge estimator	**Standard deviation of the position vector**		
	X (m)	**Y (m)**	**Z (m)**
$(n-r)\frac{S_o}{\hat{\mathbf{a}}}$	20.003	6.149	22.445
$r\frac{S_o}{\hat{\mathbf{a}}}$	45.136	16.716	60.306
$\frac{\sqrt{S_o}}{\hat{\mathbf{a}}}$	19.985	7.644	27.657
$r\frac{\sqrt{S_o}}{\hat{\mathbf{a}}}$	12.509	4.658	18.316

Table 41. Standard deviation of the position vector using various values of general ridge estimator (HRS2 image).

Ridge estimator	**Standard deviation of the position vector**					
	NADIR			**BACK**		
	X (m)	**Y (m)**	**Z (m)**	**X (m)**	**Y (m)**	**Z (m)**
$(n-r)\frac{S_o}{\hat{\mathbf{a}}}$	34.058	6.190	13.289	23.849	14.315	20.613
$r\frac{S_o}{\hat{\mathbf{a}}}$	43.096	16.579	41.369	42.627	16.343	26.254
$\frac{\sqrt{S_o}}{\hat{\mathbf{a}}}$	15.745	10.173	8.877	14.261	11.232	11.498
$r\frac{\sqrt{S_o}}{\hat{\mathbf{a}}}$	10.728	4.067	6.066	6.106	6.706	9.218

Table 42. Standard deviation of the position vector using various values of general ridge estimator for ASTER images

In table 43 the difference between the predicted values of the position vector by Least Squares and General Ridge estimator and the high accurate values derived from the navigation data are shown for HRS-1 image. **It seems that with exactly the same conditions (model, GCPs) the prediction of the exterior orientation parameters is improved when General Ridge is used in the solution.** In this table the proposed General Ridge parameter is used.

Exterior orientation parameter	LSE	GRE
X (m)	-31194.730	-14829.261
Y (m)	287.592	862.920
Z (m)	12859.483	65.321

Table 43. Difference of predicted values of the position vector by LSE and GRE and the high accurate navigation data (Kepler model for single images) for HRS-1 image

However the General Ridge estimator is a bias estimator and it seems that in case of a single image solution there is a drawback which is not found in case of an along track sequence. From table 68 the standard deviation of the velocity vector of the solution where the line and the angle elements are solved separately it is shown that the velocity vector is not calculated precisely while the results with ridge estimator show exactly the opposite. On the other hand when the along track sensor model is solved using the same method (line and angle elements are solved separately) it is shown that the velocity vector is calculated precisely. The above is mentioned in order to strengthen the point that in the single image solution the general ridge estimator fails to represent the precision of the velocity vector. In case of the rotation angles the general ridge estimator gives almost the same precision as the solution where the line and the angular elements are solved separately.

It seems that generally by using the ridge square estimator it is possible to improve the solution and give more precise and accurate results than the least square estimator. However the geometry of the single image sensor model does not help to

give the reliability that it is needed. This drawback is overcome from the along track sensor model as it will shown in chapter 5 and 6.

4.9. State vector model vs. orbital elements model

The adopted Kepler model as a rigorous generic model for a single image has as unknown parameters the state vector and the rotation angles of the perspective center of the base framelet. As, it is mention in §2.4.4 the state of the satellite it is possible to describe using the state vector or the orbital elements.

At this point the orbital elements version of the Kepler model is developed and evaluated. The development of orbital elements models is based in equations 21.

In this evaluation process except of the statistical criteria that are used in the evaluation process of the previous models an additional test is done in order to check the stability of orbital elements model solution compared to the solution of state vector model. During this test the base framelet is not constant and it is changed along the track with the step of 25 framelets. If there is a dispersion of the unknown exterior orientation parameters along the track it seems that the solution is not stable.

4.9.1. Orbital elements model accuracy

The reference standard deviation of the solution (S_o), the standard deviation of the unknown parameters and the t-test values for HRS-1 and ASTER nadir image are introduced in table 44. Also the correlation matrix of HRS-1 is introduced in table 45 and for ASTER nadir in table 46.

The following comments are extracted:

- The reference standard deviation of HRS-1 image is slightly worse than the value of the same image in the Kepler state vector model evaluation (0.935). One the other hand the difference of the reference standard deviation of ASTER

nadir image is three times worse than the corresponding reference standard deviation of Kepler state vector model and it is not inside the expected boundaries.

- Only the standard deviation of the rotation angles could be compared. In both images the standard deviation of these values using the Kepler state vector model is at least ten times better than the ones of the orbital elements model.
- All the unknown parameters passed the t-test although except of semi major axis value all the others are small.
- The correlation between the unknown parameters is very high as it is shown in the correlation matrixes. Especially in ASTER nadir image there is high correlation (positive or negative) between almost all the orbital elements except of the semi major axis. Also there is correlation between the orbital elements and the rotations.

	HRS-1		ASTER nadir	
S_o(pixel)	0.970		1.451	
	Standard deviation of the unknown parameters	t-parameter	Standard deviation of the unknown parameters	t-parameter
α(m)	65.206	114766.840	43.252	165576.473
Ω(rad)	0.0003717	13999.689	0.0011683	5260.639
ω(rad)	0.0120612	224.501	0.0153873	53.114
v(rad)	0.0122478	481.255	0.0154741	103.128
i(rad)	0.0003003	5850.785	0.0112743	1542.384
e	0.0002899	141.278	0.0089164	14.733
ω(rad)	0.0034218	82.432	0.0042386	62.203
φ(rad)	0.0028038	118.364	0.0023879	312.045
κ(rad)	0.0010950	1059.621	0.0029706	3.547

Table 44. Reference standard deviation, standard deviation of the unknown parameters and t-parameter for HRS-1 and ASTER nadir images using orbital elements model.

To summarize the above comments it is obvious that the high correlation between the parameters is responsible of the inaccuracy of the model especially of in ASTER case which also caused small t-values. The obvious reason for this high correlation is the close to circular orbit. In near circular orbit some of the classical orbital elements are correlated as it is mention in §2.4.5.2. However another reason for the imprecision in

general, could be the attempt of describing the orbit (shape and orientation) which has a period of almost 101 minutes using information (image) covering only 10 seconds of this orbit. This statement it is seems that is true from the following test.

	a	Ω	ω	v	e	i	ω	φ	κ
a	1.00	0.00	0.00	0.00	0.00	0.03	-0.01	0.00	-0.01
Ω	0.00	1.00	-0.01	0.02	-0.02	-0.03	0.23	-0.66	0.23
ω	0.00	-0.01	1.00	-1.00	0.01	0.83	0.34	0.16	0.35
v	0.00	0.02	**-1.00**	1.00	-0.01	-0.85	-0.37	-0.18	-0.38
e	0.00	-0.02	0.01	-0.01	1.00	0.00	0.19	-0.59	0.19
i	0.03	-0.03	**0.83**	**-0.85**	0.00	1.00	0.77	0.38	0.77
ω	-0.01	0.23	0.34	-0.37	0.19	**0.77**	1.00	0.15	1.00
φ	0.00	**-0.66**	0.16	-0.18	**-0.59**	0.38	0.15	1.00	0.14
κ	-0.01	0.23	0.35	-0.38	0.19	**0.77**	1.00	0.14	1.00

Table 45. Correlation matrix for HRS-1 image where orbital elements model is used

	a	Ω	ω	v	e	i	ω	φ	κ
a	1.00	0.00	0.00	0.00	0.00	0.00	0.00	-0.01	0.00
Ω	0.00	1.00	-0.84	0.85	-0.94	0.87	0.51	0.14	0.47
ω	0.00	**-0.84**	1.00	-1.00	0.95	-1.00	-0.03	-0.32	0.02
v	0.00	**0.85**	**-1.00**	1.00	-0.95	1.00	0.04	0.30	-0.01
e	0.00	**-0.94**	**0.95**	**-0.95**	1.00	-0.96	-0.19	-0.26	-0.14
i	0.00	**0.87**	**-1.00**	**1.00**	**-0.96**	1.00	0.09	0.30	0.04
ω	0.00	**0.51**	-0.03	0.04	-0.19	0.09	1.00	-0.25	0.98
φ	-0.01	0.14	-0.32	0.30	-0.26	0.30	-0.25	1.00	-0.30
κ	0.00	0.47	0.02	-0.01	-0.14	0.04	**0.98**	-0.30	1.00

Table 46. Correlation matrix for ASTER nadir image where orbital elements model is used

4.9.2. Dispersion of orbital elements solution

In ASTER nadir image the base framelet is changed along the track. In figure 28 the dispersion of the semi major axis is introduced. From this scatter plot along with the values of the correlation matrixes a very important conclusion is extracted.

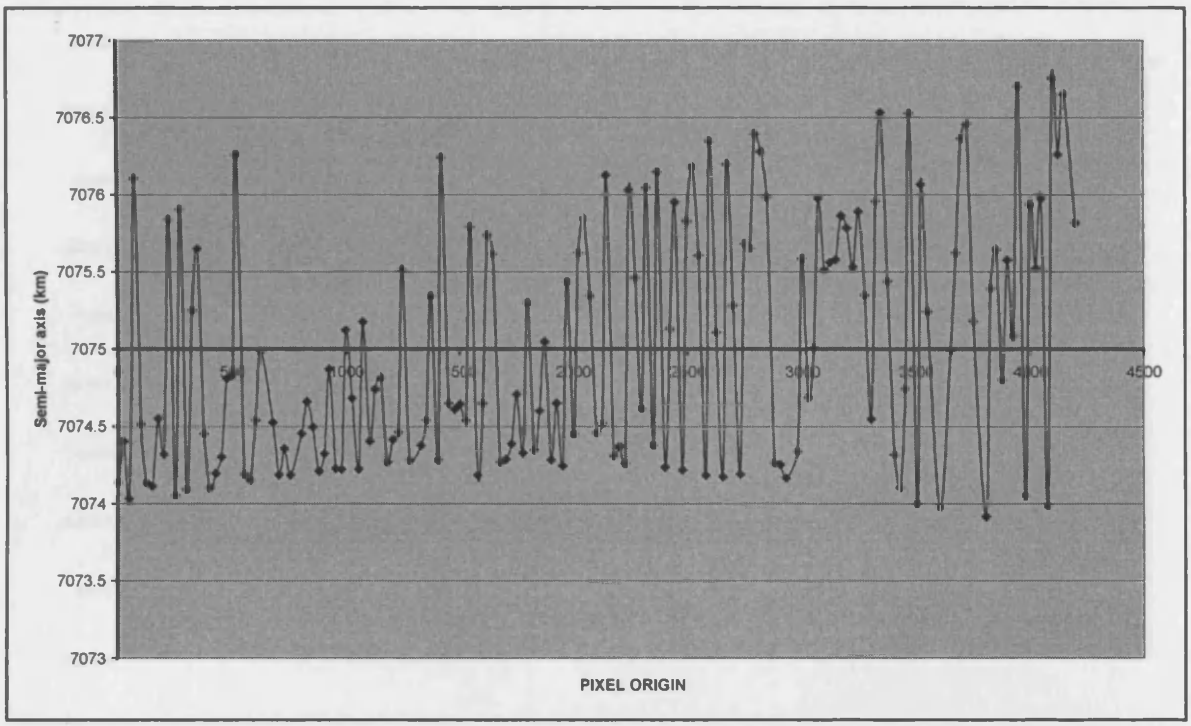

Figure 28. Semi major axis dispersion in km during ASTER nadir image acquisition

From the correlation matrix the semi major axis is uncorrelated with all other orbital elements. If the only reason for the inaccuracy of the Kepler orbital elements model is the high correlation of the orbital elements the semi major axis should be constant at least during the acquisition of the image. However on the scatter plot the values of the semi major axis are from 7073.8 km to 7076.8 km during 10 second acquisition time. This means that the provided information (GCPs on 10sec image) is not enough to calculate precisely a quantity which is valid for 101 minutes. After all and in case of the non-singular orbital elements the semi major axis is also presented. It is believed that even in this case is going to have the same problem. However, in a future work the above statement should be checked along with the improvement of the solution if the orbital elements model is implemented in an along track images.

On the other hand, the same test is done to the Kepler state vector model. As an example the scatter plot of the position and the velocity along X axis are introduced in figures 29 and 30, respectively. In order to have the same scale with figure 28 the scatter plots are shown are for the first 400 lines.

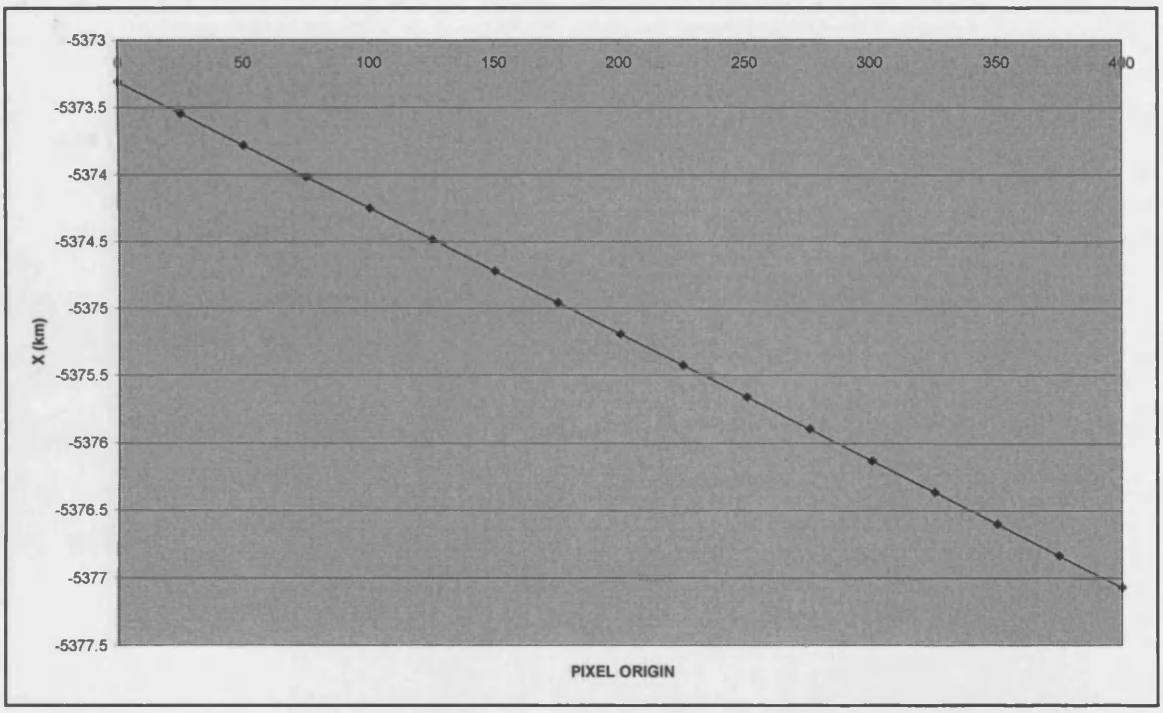

Figure 29. Scatter plot of the position of the perspective centre along X axis in km for the first 400 lines (in order to have the same scale as the previous figure) during ASTER nadir image acquisition

The scatter plots of the others unknown parameters have the same pattern. This is exactly the expected behaviour of the model where the positions and velocities are changed smoothly without peaks.

The conclusion is that the Kepler orbital elements solution is not stable for the following reasons:

- The high correlation of the classical orbital elements as the orbit of the remote sensing is near circular.
- the attempt of describing the orbit (shape and orientation) which has a period of almost 101 minutes using information (image) covering only 10 seconds of this orbit.

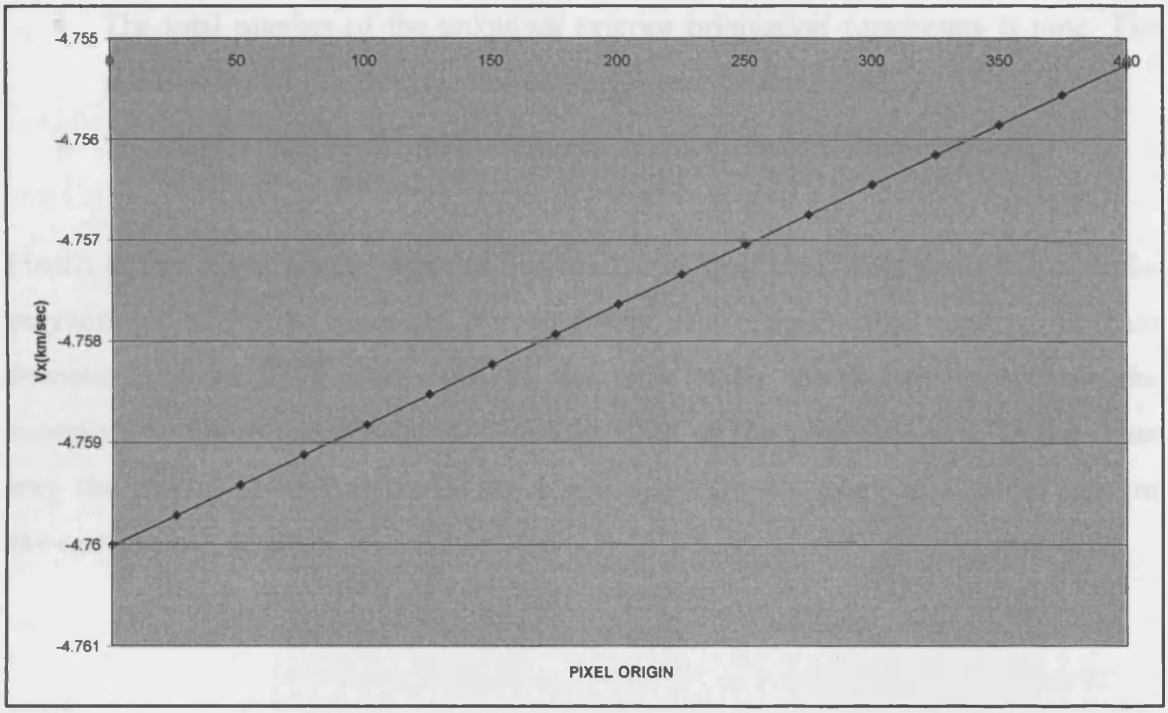

Figure 30. Scatter plot of the velocity of the perspective centre along X axis in km/sec for the first 400 lines (in order to refer to the same picture area as the previous figure) during ASTER nadir image acquisition

As it has already been mentioned future work should be done in order to check the stability of along track images solution using non-singular elements or in along track sequence.

4.10. Adopted generic rigorous sensor model for a pushbroom image

The following conclusions come out from this chapter in relation to adopted model of a single pushbroom satellite image:

- The satellite motion during the acquisition time of **one** image is a Keplerian motion. The adopted model is based in Kepler's problem.
- The **attitudes** (ω,φ and k rotations) of the satellite are remaining **constant** during the acquisition time of one image.

- The total number of the unknown exterior orientation parameters is nine. The position vector (3), the velocity vector (3) and the rotations (3).
- The Kepler (classical) orbital elements model gives an unstable solution.

Finally the most important statement that need to be mentioned here again is that in the polynomials which are represent the movement of the perspective point of the base framelet($X_c(t), Y_c(t), Z_c(t), \omega_c(t), \varphi_c(t), \kappa_c(t)$) **the first order coefficient represents the velocity (or the angular velocity) of the satellite on the reference axis. In the same way the second order represents the acceleration (or the angular acceleration) on the same axis.**

CHAPTER 5.

ALONG TRACK STEREO SENSOR MODELS

5.1. Introduction

It has already been mentioned in the very beginning of this thesis that the aim is to develop a generic rigorous sensor model for high resolution optical satellite sensors, with along track stereoscopic capabilities, where it is possible to orientate directly and simultaneously all the along track stereo images . The concept is to establish the orbit of the satellite platform during the acquisition time of all images, trying to find common exterior orientation parameters for all images directly or indirectly. Thus, the number of unknown parameters is reduced which guide us to a less correlated solution. Moreover, the simultaneous solution extends the narrow field of view of each satellite image because all along track images are treated as one iconic image, with the field of view equal to the angle between the first and the last image, thus giving a more stable solution.

In the previous chapter the first elementary steps were done. A kinematic rigorous model is adopted based in the assumption that the motion of the satellite is a Keplerian motion during the acquisition time of a single pushbroom image (§ 4.7.5).

In this chapter various versions of the along track stereo sensor model are introduced. These models are a combination of the photogrammetry equations (collinearity equations) with astrodynamics (various orbit determination-propagation methods). The procedures where these methods are combined together in a sensor model are explained in detail.

In the second part of this chapter an accuracy assessment is presented for the different orbit determination-propagation methods used in along track model. In this process the extracted values of the models are compared with the navigation data of SPOT 5 which

are included in the metadata file of HRS images which has an accuracy better than one meter (DORIS POINTS, §2.2.5.3.2), thus it is assumed that they represent the true values of the unknown exterior orientation parameters. The final step is to find if the time interval at which the assumption that the motion of the satellite is a Keplerian motion is larger than the acquisition time interval of HRS images.

5.2. Description of the generic rigorous along track sensor model

The generic rigorous along track stereo sensor model is an extension of the adopted single image model. The fundamental assumptions of this model are followed. Most of them have already been introduced in the single image model description, but it is repeated here in order to emphasize their importance and also for the reader convenience.

- The satellite is moving along a well defined, smooth, close to circular elliptical orbit.
- The images are acquired with a pushbroom scanner using a constant time interval. As a result the coordinates along the flight path have the same scale.
- The satellite sensor model is a kinematic model. A single image consists of a number of framelets.
- The sensor array is approximately perpendicular to the direction of motion.
- The orientation satellite images should be carried out in a geocentric coordinate system in order to avoid distortions caused by earth curvature and map projection and to facilitate integration with sources of metadata information that may be available.
- **The satellite motion during the acquisition time of along track stereo images is a keplerian motion.** In combination with the previous assumption an inertial coordinate system is used.
- The **attitudes** (ω,φ and k rotations) of the satellite are remaining **constant** during the acquisition time of **each** image.

At a first glance, the main extension from the single image assumption is that the Keplerian motion of the satellite is maintained from the first to the last image acquisition that reduces the number of unknown parameters. As an example in case of two along track images, where the Kepler method is used (§5.3.1), the total number of unknown parameters for both images is 12:

- The position vector (3) of the first image,
- the velocity vector (3) of the first image
- and the rotations (6) of both images.

The generic along track sensor model is very flexible as it could be transformed in various versions depending on the used orbit determination-propagation method (§5.3), where the assumption that the motion of a satellite is a Keplerian motion is always under use. Moreover, it is possible to apply more complicated orbit determination models if the accuracy of the solution does not fulfil the requirements.

The introduction of the various versions of along track stereo model is followed. The first one based on the Kepler problem (orbit propagation) which can be used in more than two along track images. The second is based on Gauss-Lambert method which can be used only for two along track images like SPOT-HRS and TERRA-ASTER. Finally the Herrick-Gibbs method is combined with the Gauss-Lambert method which can be used in case of more than two along track images. **These variations of the model emphasize its flexibility.**

5.3. Description of different versions of the along track model

5.3.1. Kepler model

This version of the model is based on the Kepler problem (§2.4.8.2.4). In the simplest case of two along track stereo images the number of unknown parameters is twelve in total. **The state vector of the base framelet of the first image represents six of these**

unknown parameters. The state vector of the base framelet of the second image is related to the state vector of the base framelet of the first image by the Kepler equation (equation 18) thus is not an unknown in the solution. **The other six unknown parameters are the rotation angles of the two images;** three rotations for each image as it is assumed that the rotations remain constant during the acquisition of each image (§5.2). If these images are treated individually the number of unknown parameters are nine for each one (§ 4.7.5), which means eighteen unknown parameters in total, thus the number of unknown parameters is reduced by six. Moreover, as it is shown later, the precision of the velocity vector is also improved (§6.3.1.1). The reason for this improvement is that the along track images are treated as one iconic image and thus the field of view is increased giving more stable geometry.

The formulation of the Kepler model of two images case is described in detail by following equations.

For the first image the modified collinearity equations are defined as follows:

$$0 = -c\frac{m_{11}^1(t)(X - X_c(t)) + m_{12}^1(t)(Y - Y_c(t)) + m_{13}^1(t)(Z - Z_c(t))}{m_{31}^1(t)(X - X_c(t)) + m_{32}^1(t)(Y - Y_c(t)) + m_{33}^1(t)(Z - Z_c(t))}$$

Eq. 93

$$y - y_o = -c\frac{m_{21}^1(t)(X - X_c(t)) + m_{22}^1(t)(Y - Y_c(t)) + m_{23}^1(t)(Z - Z_c(t))}{m_{31}^1(t)(X - X_c(t)) + m_{32}^1(t)(Y - Y_c(t)) + m_{33}^1(t)(Z - Z_c(t))}$$

where $X_c(t)$, $Y_c(t)$, $Z_c(t)$ are the ground coordinates of the base framelet perspective center as a function of time which are defined as follows:

$$X_c(t) = X_o + u_x \cdot t - \frac{GM \cdot X_o \cdot t^2}{2 \cdot (X_o^2 + Y_o^2 + Z_o^2)^{3/2}}$$

$$Y_c(t) = Y_o + u_y \cdot t - \frac{GM \cdot Y_o \cdot t^2}{2 \cdot (X_o^2 + Y_o^2 + Z_o^2)^{3/2}} \qquad \text{Eq. 94}$$

$$Z_c(t) = Z_o + u_z \cdot t - \frac{GM \cdot Z_o \cdot t^2}{2 \cdot (X_o^2 + Y_o^2 + Z_o^2)^{3/2}}$$

For the second image the modified collinearity equations are:

$$0 = -c \frac{m_{11}^2(t)(X - X_c(t)) + m_{12}^2(t)(Y - Y_c(t)) + m_{13}^2(t)(Z - Z_c(t))}{m_{31}^2(t)(X - X_c(t)) + m_{32}^2(t)(Y - Y_c(t)) + m_{33}^2(t)(Z - Z_c(t))}$$

Eq. 95

$$y - y_o = -c \frac{m_{21}^2(t)(X - X_c(t)) + m_{22}^2(t)(Y - Y_c(t)) + m_{23}^2(t)(Z - Z_c(t))}{m_{31}^2(t)(X - X_c(t)) + m_{32}^2(t)(Y - Y_c(t)) + m_{33}^2(t)(Z - Z_c(t))}$$

where

$$X_c(t) = X_o + u_x \cdot (t + dt) - \frac{GM \cdot X_o \cdot (t + dt)^2}{2 \cdot (X_o^2 + Y_o^2 + Z_o^2)^{3/2}}$$

$$Y_c(t) = Y_o + u_y \cdot (t + dt) - \frac{GM \cdot Y_o \cdot (t + dt)^2}{2 \cdot (X_o^2 + Y_o^2 + Z_o^2)^{3/2}} \qquad \text{Eq. 96}$$

$$Z_c(t) = Z_o + u_z \cdot (t + dt) - \frac{GM \cdot Z_o \cdot (t + dt)^2}{2 \cdot (X_o^2 + Y_o^2 + Z_o^2)^{3/2}}$$

and

c is the focal length

t is the acquisition time a framelet which is defined in terms of each image coordinates and it calculated from equation 8

dt is the time interval between the acquisition of the base framelet of each image.

(X_o, Y_o, Z_o) is the position vector of the perspective center of the base framelet of the first image

(u_x, u_y, u_z) is the velocity vector of the perspective center of the base framelet of the first image

(X,Y,Z) are the ground coordinates of a point

$m_{11}^1, m_{12}^1, .., m_{33}^1$ are the rotation matrix components of the first image base framelet (equation 88) and

$m_{11}^2, m_{12}^2, .., m_{33}^2$ are the rotation matrix components of the second image base framelet (equation 88) and

GM is the Earth gravitational parameter with value of $398600{,}4415 km^3 / s^2$

In case of more than two along track images this model is modified as follows: The state vector of the base framelet of the first image is unknown in the solution, as in case of two along images. **The state vector of the base framelet of the all other images is related to the state vector of the base framelet of the first image by the Kepler equation (equation 18) thus is not unknown in the solution. For each image three unknown parameters are added representing its rotation angles.** Thus, in case of N along track stereo images the total number of unknown parameters is:

6	+	3	*	N	Eq. 97
(state vector of first image)		(rotation angles of each image)		(number of images)	

If these images are treated individually the number of unknown parameters are nine for each one (§ 4.7.5). In table 47 the number of unknown parameters is presented if Kepler model is used in case of two to five along track images.

It is obvious that **the number of unknown parameters is reduced dramatically as the number of images is increased compared to the method where all images are**

solved individually (Table 65). Except of the first image where the state vector of its base framelet and the corresponding rotation angles are unknowns parameters in the solution, for the other images only three unknown parameters are added representing their rotations angles.

Number of images	Number of unknown parameters
2	12
3	15
4	18
5	21

Table 47. Number of unknown parameters of Kepler model from 2 to 5 along track images.

In the Kepler model, all along track images are treated as one iconic image where its coordinates are found if the acquisition time interval of the corresponding image from the first image is added (in general case of more than two images) on the framelet coordinates of each image(equation 8). In other words, **in Kepler model the transition factor from the first image to the others is their acquisition time interval**.

5.3.2. Lambert-Gauss model

This version of the model is based in the Gauss-Lambert problem (§2.4.8.3). **It can be used by itself only in case of two along track stereo images**. The number of unknown parameters is twelve in total as in the Kepler model. In the case of more than two images is used in combination with the Herrick-Gibbs method (§2.4.8.4.). **The position vectors of the base framelet of both images represent six of the unknown exterior orientation parameters**. The velocity vector of the base framelet of each images are related to position vectors by the Gauss-Lambert method thus are not unknowns in the

solution. **The other six unknown parameters are the rotation angles of the two images as they are described in Kepler model solution (§5.3.1).** The number of unknown parameters is also reduced by six, compared to the solution where the two images are solved individually.

For the first image the modified collinearity equations are defined as follows:

$$0 = -c\frac{m_{11}^1(t)(X - X_c^1(t)) + m_{12}^1(t)(Y - Y_c^1(t)) + m_{13}^1(t)(Z - Z_c^1(t))}{m_{31}^1(t)(X - X_c^1(t)) + m_{32}^1(t)(Y - Y_c^1(t) + m_{33}^1(t)(Z - Z_c^1(t))}$$

Eq. 98

$$y - y_o = -c\frac{m_{21}^1(t)(X - X_c^1(t)) + m_{22}^1(t)(Y - Y_c^1(t)) + m_{23}^1(t)(Z - Z_c^1(t))}{m_{31}^1(t)(X - X_c^1(t)) + m_{32}^1(t)(Y - Y_c^1(t)) + m_{33}^1(t)(Z - Z_c^1(t))}$$

where $X_c^1(t), Y_c^1(t), Z_c^1(t)$ are the ground coordinates of the base framelet perspective center of the first image as a function of time which are defined as follows:

$$X_c^1(t) = X_1 + u_{1x}\cdot t - \frac{1}{2}a_{1x}\cdot t^2 = X_1 + \frac{X_2 - f\cdot X_1}{g}\cdot t - \frac{GM\cdot X_1\cdot t^2}{2\cdot(X_1^2 + Y_1^2 + Z_1^2)^{3/2}}$$

$$Y_c^1(t) = Y_1 + u_{1y}\cdot t - \frac{1}{2}a_{1y}\cdot t^2 = Y_1 + \frac{Y_2 - f\cdot Y_1}{g}\cdot t - \frac{GM\cdot Y_1\cdot t^2}{2\cdot(X_1^2 + Y_1^2 + Z_1^2)^{3/2}} \qquad \text{Eq. 99}$$

$$Z_c^1(t) = Z_1 + u_{1z}\cdot t - \frac{1}{2}a_{1z}\cdot t^2 = Z_1 + \frac{Z_2 - f\cdot Z_1}{g}\cdot t - \frac{GM\cdot Z_1\cdot t^2}{2\cdot(X_1^2 + Y_1^2 + Z_1^2)^{3/2}}$$

For the second image the modified collinearity equations are:

$$0 = -c\frac{m_{11}^2(t)(X - X_c^2(t)) + m_{12}^2(t)(Y - Y_c^2(t)) + m_{13}^2(t)(Z - Z_c^2(t))}{m_{31}^2(t)(X - X_c^2(t)) + m_{32}^2(t)(Y - Y_c^2(t) + m_{33}^2(t)(Z - Z_c^2(t))}$$

Eq. 100

$$y - y_o = -c\frac{m_{21}^2(t)(X - X_c^2(t)) + m_{22}^2(t)(Y - Y_c^2(t)) + m_{23}^2(t)(Z - Z_c^2(t))}{m_{31}^2(t)(X - X_c^2(t)) + m_{32}^2(t)(Y - Y_c^2(t)) + m_{33}^2(t)(Z - Z_c^2(t))}$$

where $X_c^2(t), Y_c^2(t), Z_c^2(t)$ are the ground coordinates of the framelet perspective center of the second image as a function of time which are defined as follows:

$$X_c^2(t) = X_2 + u_{2x} \cdot t - \frac{1}{2}a_{2x} \cdot t^2 = X_2 + \frac{\dot{g} \cdot X_2 - X_1}{g} \cdot t - \frac{GM \cdot X_2 \cdot t^2}{2 \cdot (X_2^2 + Y_2^2 + Z_2^2)^{3/2}}$$

$$Y_c^2(t) = Y_2 + u_{2y} \cdot t - \frac{1}{2}a_{2y} \cdot t^2 = Y_2 + \frac{\dot{g} \cdot Y_2 - Y_1}{g} \cdot t - \frac{GM \cdot Y_2 \cdot t^2}{2 \cdot (X_2^2 + Y_2^2 + Z_2^2)^{3/2}} \quad \text{Eq. 101}$$

$$Z_c^2(t) = Z_2 + u_{2z} \cdot t - \frac{1}{2}a_{2z} \cdot t^2 = Z_2 + \frac{\dot{g} \cdot Z_2 - Z_1}{g} \cdot t - \frac{GM \cdot Z_2 \cdot t^2}{2 \cdot (X_2^2 + Y_2^2 + Z_2^2)^{3/2}}$$

c	is the focal length
t	is the acquisition time a framelet which is defined in terms of image coordinates and it calculated from equation 8
(X_1, Y_1, Z_1)	is the position vector of the perspective center of the base framelet of the first image
(X_2, Y_2, Z_2)	is the position vector of the perspective center of the base framelet of the second image

(u_{1x}, u_{1y}, u_{1z}) is the velocity vector of the perspective center of the base framelet of the first image

(u_{2x}, u_{2y}, u_{2z}) is the velocity vector of the perspective center of the base framelet of the second image

(a_{1x}, a_{1y}, a_{1z}) is the acceleration vector of the perspective center of the base framelet of the first image

(a_{2x}, a_{2y}, a_{2z}) is the acceleration vector of the perspective center of the base framelet of the second image

(X, Y, Z) are the ground coordinates of a point

$m_{11}^1, m_{12}^1, .., m_{33}^1$ are the rotation matrix components of the base framelet of first image (equation 88) and

$m_{11}^2, m_{12}^2, .., m_{33}^2$ are the rotation matrix components of the base framelet of the second image (equation 88)

$f, g, \dot{f}, \dot{g}$ are the transition functions as they are defined in § 2.4.8.2.2. and

GM is the Earth gravitational parameter with value of $398600{,}4415 km^3 / s^2$

In Gauss-Lambert model, both along track images are also treated as one iconic image. However, it is assumed that the framelet coordinates are calculated from the corresponding base framelet of each image. In other words, **this model divides the iconic image in two segments with their own perspective centers which are related to each other by Gauss-Lambert equations (§ 2.4.8.3.2).**

5.3.3 Combined Gauss-Lambert and Herrick-Gibbs model

It has already been mentioned that Gauss-Lambert model can be used by itself only in case of two along track stereo images (§ 5.3.2.). For more than two along track images Gauss-Lambert model can be used in combination with the Herrick-Gibbs method (§2.4.8.4).

In case of a triplet (ALOS PRISM) the combined model are developed in the following way: **The position vectors of the perspective centers of the base framelet of each image are unknowns in the solution (nine unknown parameters). Using Herrick-Gibbs method the velocity vector of perspective centers of the base framelet of the middle along track image is calculated.** On the other hand using the Lambert-Gauss model the velocity vectors of the two edge images are also calculated. As a result, the velocity vectors of all images are not unknowns in the solution. The rotation angles of each image are also unknown parameters in the solution (nine unknown parameters). **Thus, in case of three along track images the number of unknown parameters is eighteen in total, which are the position vector and the rotation angles of each image.** The number of unknown parameters is reduced by nine, compared to the solution where the three images are solved individually (table 65).

For the edge images the modified collinearity equation is introduced in equations 98-101. For the middle image the modified collinearity equations are as follows:

$$0 = -c\frac{m_{11}^{M}(t)(X - X_c^{M}(t)) + m_{12}^{M}(t)(Y - Y_c^{M}(t)) + m_{13}^{M}(t)(Z - Z_c^{M}(t))}{m_{31}^{M}(t)(X - X_c^{M}(t)) + m_{32}^{M}(t)(Y - Y_c^{M}(t) + m_{33}^{M}(t)(Z - Z_c^{M}(t))}$$

Eq. 102

$$y - y_o = -c\frac{m_{21}^{M}(t)(X - X_c^{2}(t)) + m_{22}^{M}(t)(Y - Y_c^{M}(t)) + m_{23}^{M}(t)(Z - Z_c^{M}(t))}{m_{31}^{M}(t)(X - X_c^{M}(t)) + m_{32}^{M}(t)(Y - Y_c^{M}(t)) + m_{33}^{M}(t)(Z - Z_c^{M}(t))}$$

where

$$X_c^{M}(t) = X_M + u_{Mx}\cdot t - \frac{1}{2}a_{2x}\cdot t^2 = X_M + u_{Mx}\cdot t - \frac{GM\cdot X_M\cdot t^2}{2\cdot(X_M^2 + Y_M^2 + Z_M^2)^{3/2}}$$

$$Y_c^{M}(t) = Y_M + u_{My}\cdot t - \frac{1}{2}a_{2x}\cdot t^2 = Y_M + u_{My}\cdot t - \frac{GM\cdot Y_M\cdot t^2}{2\cdot(X_M^2 + Y_M^2 + Z_M^2)^{3/2}}$$

Eq. 103

$$Z_c^M(t) = Z_M + u_{Mz} \cdot t - \frac{1}{2} a_{2x} \cdot t^2 = Z_M + u_{Mz} \cdot t - \frac{GM \cdot Z_M \cdot t^2}{2 \cdot (X_M^2 + Y_M^2 + Z_M^2)^{3/2}}$$

and

$$\vec{u}_M = -dt_{2M}\left(\frac{1}{dt_{M1} \cdot Dt_{31}} + \frac{GM}{12 \cdot r_1^3}\right)\vec{r}_1 + (dt_{2M} - dt_{M1}) \cdot \left(\frac{1}{dt_{M1} \cdot dt_{2M}} + \frac{GM}{12 \cdot r_M^3}\right)\vec{r}_M + dt_{M1}\left(\frac{1}{dt_{2M} \cdot dt_{21}} + \frac{GM}{12 \cdot r_2^3}\right)\vec{r}_2$$

Eq. 104

where

c	is the focal length
t	is the acquisition time a framelet which is defined in terms of image coordinates and it calculated from equation 7
$\vec{r}_1, \vec{r}_M, \vec{r}_2$	are the position vectors of first, middle and third image respectively
(X_M, Y_M, Z_M)	is the position vector of the perspective center of the base framelet of the middle image
$\vec{u}_M =$ (u_{Mx}, u_{My}, u_{Mz})	is the velocity vector of the perspective center of the base framelet of the middle image
(X, Y, Z)	are the ground coordinates of a point
$m_{11}^M, m_{12}^M, ..., m_{33}^M$	is the rotation matrix components of the base framelet of the second image and
GM	is the Earth gravitational parameter with value of $398600{,}4415 km^3/s^2$

This combined method could be extended in the case of more than three along track images as follows: **The position vectors of the perspective centers of the base framelet of each along track images are unknowns in the solution. Using Herrick-**

Gibbs method the velocity vectors of perspective centers of the base framelet of the intermediate along track images are calculated. On the other hand using the Lambert-Gauss model the velocity vectors of the two edge images are also calculated. Thus, the velocity vectors of all images are not unknowns in the solution. The rotation angles of each image are also unknown parameters in the solution. In case of N along track stereo images the total number of unknown parameters is:

$$(3 + 3) * N \quad \text{Eq. 105}$$

(position vector of each image) (rotation angles of each image) (number of images)

In table 48 the number of unknown parameters is presented if this combined model is used in case of three to five along track images.

Number of images	Number of unknown parameters
3	18
4	24
5	30

Table 48. Number of unknown parameters in Gauss-Lambert in combination with Herrick-Gibbs model from two to five along track images.

In this combined model, all along track images are also treated as one iconic image. However it is assumed that the framelet coordinates are calculated from the corresponding base framelet of each image. In other words, **this model divides the iconic image in a number of segments which are as many as the along track images where the perspective centers of the base framelet of the edge images are related to each other by Gauss-Lambert equations while the perspective centers of the base framelet of intermediate images are related to the images by Herrick-Gibbs equations.**

5.4. Accuracy assessment of orbit models

5.4.1. Accuracy evaluation strategy

An accuracy assessment of the different orbit determination-propagation methods used in along track model is made. This evaluation process takes place in an inertial space and only in the initial tests in a geocentric coordinate system (in order to understand the importance of the inertial space in the Keplerian motion). As it has already been mentioned in the introduction of this chapter the extracted values of the models are compared with the navigation data of SPOT 5 which are included in the metadata file of HRS images with accuracy better than one meter (DORIS POINTS, §2.2.5.3.2), thus it is assumed that they represent the true values of the unknown exterior orientation parameters. The navigation data which are used in this evaluation is the position and velocity vectors of the satellite measured by the DORIS system every 30 seconds with respect to ITRF90 (International Reference Frame 1990) which is almost identical to WGS84 coordinate system. These data is interpolated in order to find the state vectors of the base framelets of each image and then it is transformed to an inertial coordinate system.

A critical factor in this assessment is to define the accuracy limits of the position and velocity vector components regarding the characteristics of the images used (SPOT5-HRS). In this thesis its value is defined compared to standard deviation of the position vector of the solution where the line and the angle elements are solved separately (§ 2.5.4). In this process the standard deviation of the position vector of HRS images is calculated (table 39). The standard deviation of the velocity vector is not calculated in single image solution and it is assumed that the velocity in each direction should have a precision of about 1 meter per second. The standard deviation values are multiplied by 3 in order to represent a confidence interval of 99% and the accepted values are shown in table (table 49).

The values of this solution method (line and angle elements solved separately) are decided to be the more representative in this assessment because the strong correlation effect between the position vector and the rotation angles is eliminated, thus these values give an almost independent uncertainty of the position and the velocity vectors from the effect of other parameters.

It should be mentioned here that although the position accuracy is larger that the pixel size of the HRS images on the ground it is accepted as being accurate. In this process the pixel size is not a representative value. The reason is that the pushbroom model is a kinematic model where the position vector is involved in the model, interact with other parameters (e.g. velocity) in the final solution thus its accuracy is not directly comparable to the accuracy of a static and fixed value as it is the pixel size. Pixel size is used to compare the standard deviation of the solution (precession of the solution) and of RMSE of check or height points.

	Confidence interval
POSITION X (m)	75
POSITION Y (m)	30
POSITION Z (m)	45
VELOCITY u_x (m/sec)	3
VELOCITY u_y (m/sec)	3
VELOCITY u_z (m/sec)	3

Table 49. Precision limits of the position and velocity vectors for SPOT5-HRS images.

5.4.2. Position and velocity vector calculations of the centre framelet

The position and velocity vector at the centre line of each image are interpolated from the position and velocity vectors of DORIS system which are given every 30 seconds. In the interpolation process, instead of Lagrange interpolation as suggested in the SPOT SATELLITE GEOMETRY HANDBOOK, (SPOT, 2002), third order polynomials are used. The achieved accuracy (RMSE) of the interpolation process is determined to be

better than one centimetre for the position vector and better than one millimetre per second for the velocity. The determined values for the HRS images are given in table 50.

The next step is to transform the state vector in an inertial coordinate system in order to meet the fundamental assumption of the keplerian motion (§2.4.4). The procedure is described in (§2.4.1.4) and the transformed state vectors of the centre framelets of each HRS image are in table 51.

	HRS1	**HRS2**
POSITION X (m)	4968288.039	5441070.518
POSITION Y (m)	534776.203	398899.474
POSITION Z (m)	5181805.082	4697760.247
VELOCITY u_x (m/sec)	5416.469	4889.934
VELOCITY u_y (m/sec)	-1423.242	-1537.696
VELOCITY u_z (m/sec)	-5033.787	-5518.345

Table 50. State vectors of base (center) framelet of HRS images in WGS84 as it is calculated from the metadata file

	HRS1	**HRS2**
POSITION X (m)	-3179513.689	-3355182.388
POSITION Y (m)	3854041.934	4301223.017
POSITION Z (m)	5182473.251	4698462.750
VELOCITY u_x (m/sec)	-2074.628	-1754.937
VELOCITY u_y (m/sec)	5073.740	4674.771
VELOCITY u_z (m/sec)	-5033.379	-5518.004

Table 51. State vectors of base (center) framelet of HRS images from the previous table in Inertial Coordinate system.

5.4.3. Kepler model

For the Kepler model evaluation it is assumed that the true value of state vector at the perspective center of the base framelet of the HRS1 image is known (from the previous paragraph). Then, using Kepler equation the state vectors of the perspective center of the base framelet of the HRS2 image is calculated. Finally this value is compared with the true value of HRS2 image (table 51) in order to find the accuracy of the Kepler model transformation in case of HRS images

It has already been mentioned (§2.4.8.2.1.) in the developed Keplerian model, that the satellite motion is simulated during the acquisition time of the images without solving the Keplerian equation, itself. In other words the equation 15 contribution in the model is only with its physical effect, as only the state vectors at the perspective center of base framelet of the first image is computed and not the state vectors of the base framelets of the rest images. This approach is adopted because the model is simpler than the one where the exterior orientation parameters and the state vector of the base framelets of all images are computed. **It is needed, for this accuracy test to use another procedure where the Kepler's problem is solved. This method is the Universal Value solution for Kepler problem (§2.4.8.2.4.).** The state vector of the HRS2 base framelet is calculated in an inertial coordinate system. The results are in table 52.

	Calculated state vector of HRS2	**Difference from the true values**
POSITION X (m)	-3355156.642	25.746
POSITION Y (m)	4301190.774	-32.243
POSITION Z (m)	4698479.731	16.981
VELOCITY u_x (m/sec)	-1754.390	0.546
VELOCITY u_y (m/sec)	4674.086	-0.685
VELOCITY u_z (m/sec)	-5517.606	0.398

Table 52. Kepler model accuracy for HRS2 state vector in Inertial Coordinate system.

The state vector of the HRS2 base framelet is also calculated in WGS84 coordinate system, which is a geocentric (not inertial) coordinate system. The accuracy results are in table 53.

First of all, the importance of the inertial space is obvious. Comparing tables 52 and 53 the accuracy of HRS2 state vector is much better in an inertial space than in WGS84 coordinate system which is much worse than the defined accuracy limits (table 53).

Compared to critical values the HRS2 accuracy difference is slightly worse in Y direction while is much better in the other two directions. Thus it is an essential model for the orbit simulation of SPOT 5 orbit during the acquisition time of HRS images.

	Calculated HRS2	**Difference from the true values**
POSITION X (m)	5441812.095	741.577
POSITION Y (m)	402096.869	3197.395
POSITION Z (m)	4697778.388	18.141
VELOCITY u_x (m/sec)	4096.369	16.434
VELOCITY u_y (m/sec)	-1469.151	68.545
VELOCITY u_z (m/sec)	-5517.896	0.448

Table 53. Kepler model accuracy for HRS2 state vector in WGS84 coordinate system

5.4.4. Gauss-Lambert model

For the Gauss-Lambert model evaluation it is assumed that the true value of the position vectors of the perspective centers of the base framelet of both HRS images are known (§5.3.2). Then, using Gauss-Lambert equation the velocity vectors of the perspective centers of the base framelet of both HRS images are calculated. These values are compared with the true value of HRS images in order to understand how accurate the velocity vectors are found by Gauss-Lambert method. The computed values and the accuracy of the velocity vectors are in tables 54 and 55. The velocity vectors of the

perspective center of the base framelet of both HRS images are calculated in WGS84 coordinate system, which is a geocentric (not inertial) coordinate system. The accuracy results are in table 56 and 57.

	Calculated HRS1	**Difference from the true values**
VELOCITY u_x (m/sec)	-2074.909	-0.281
VELOCITY u_y (m/sec)	5074.092	0.352
VELOCITY u_z (m/sec)	-5033.565	-0.186

Table 54. Gauss model accuracy for HRS1 velocity vector in Inertial Coordinate system.

	Calculated HRS2	**Difference from the true values**
VELOCITY u_x (m/sec)	-1754.671	0.266
VELOCITY u_y (m/sec)	4674.438	-0.333
VELOCITY u_z (m/sec)	-5517.790	0.214

Table 55. Gauss model accuracy for HRS2 velocity vector in Inertial Coordinate system.

	Calculated HRS1	**Difference from the true values**
VELOCITY u_x (m/sec)	5408.394	-8.074
VELOCITY u_y (m/sec)	-1458.169	-34.927
VELOCITY u_z (m/sec)	-5033.959	-0.172

Table 56. Gauss model accuracy for HRS1 velocity vector in WGS84

	Calculated HRS2	Difference from the true values
VELOCITY u_x (m/sec)	4898.249	8.315
VELOCITY u_y (m/sec)	-1503.927	33.768
VELOCITY u_z (m/sec)	-5518.143	0.201

Table 57. Gauss model accuracy for HRS2 velocity vector in WGS84.

It is shown as in case of Kepler model accuracy, the importance of the inertial space. Comparing tables 54 and 55 with tables 56 and 57 the accuracy of the velocity vectors is much better in an inertial space than in WGS84 coordinate system. Moreover, the accuracy in WGS84 coordinate system is much worse than the defined accuracy limits (table 49). This is the final test in WGS84 coordinate system as it is definitely sure that it is not the appropriate coordinate system for the model implementation.

Compared to critical values the velocity vectors accuracy is inside the accuracy limits. Although it is not directly comparable the achieved accuracy of the velocity vectors in Gauss-Lambert model is better than the accuracy of Kepler model, while the number of unknown parameters is the same. It seems that the number of position vectors involved in the model has an important role in the accuracy. This statement come over from the finding that in Kepler model only one position vector is involved in the solution instead of the two position vectors in Gauss-Lambert model.

Finally, the Gauss-Lambert model is an essential model for the orbit simulation of SPOT 5 orbit during the acquisition time of HRS images.

5.4.5. Herrick-Gibbs model

For the accuracy evaluation of Herrick-Gibbs model a third position vector is needed (§5.3.3). For this reason, it is assumed that in the sequence of two along track HRS

images an imaginary-nadir image is added. From the metadata file the time acquisition of this image is found assuming that it was acquired at the middle of the time interval between the HRS images and then its state vector is calculated (table 58)

	Middle point WGS84	**Middle point inertial**
POSITION X (m)	5210714.529	-3271012.416
POSITION Y (m)	468149.894	4082205.470
POSITION Z (m)	4945336.722	4946022.826
VELOCITY u_x (m/sec)	5159.159	-1916.939
VELOCITY u_y (m/sec)	-1483.001	4879.734
VELOCITY u_z (m/sec)	-5281.984	-5281.609

Table 58. State vectors of base (center) framelet of the imaginary-nadir image (HRS) in WGS84 as it is calculated from the metadata file and the transformed state vector in inertial coordinate system

For the Herrick-Gibbs model evaluation it is assumed that the true value of the position vectors of the perspective centers of the base framelet of both HRS images and the nadir image are known. Then, using Herrick-Gibbs equation the velocity vector of perspective center of the base framelet of the nadir image is calculated. These values are compared with the true value of nadir image velocity in order to understand how accurate the velocity vector of the middle image is found by Herrick-Gibbs method. The computed values and the accuracy of the velocity vector are in tables 59.

	Calculated middle point	**Difference from the true values**
VELOCITY u_x (m/sec)	-1916.927	0.012
VELOCITY u_y (m/sec)	4879.722	-0.012
VELOCITY u_z (m/sec)	-5281.625	-0.016

Table 59. Herrick-Gibbs model accuracy for the imaginary-nadir velocity vector in inertial coordinate system

On the other hand in order to be able to compare the accuracy of all model used in this evaluation process for this imaginary nadir image the following calculations are done:

- The state vector of the imaginary-nadir image is found by Kepler method from the HRS1 state vector (table 60).
- The velocity vectors of HRS1 and of the imaginary-nadir image are found by Gauss-Lambert method using the position vector of HRS1 and nadir image (table 61).

	Calculated HRS2	**Difference from the true values**
POSITION X (m)	-3271012.416	6.845
POSITION Y (m)	4082205.470	-8.474
POSITION Z (m)	4946022.826	3.629
VELOCITY u_x (m/sec)	-1916.939	0.293
VELOCITY u_y (m/sec)	4879.734	-0.363
VELOCITY u_z (m/sec)	-5281.609	0.168

Table 60. Kepler model accuracy for the imaginary-nadir state vector in inertial coordinate system

	Calculated middle point	**Difference from the true values**
VELOCITY u_x (m/sec)	-1916.795	0.144
VELOCITY u_y (m/sec)	4879.555	-0.179
VELOCITY u_z (m/sec)	-5281.518	0.091

Table 61. Gauss model accuracy for the imaginary-nadir velocity vector in inertial coordinate system

Compared to the critical values the velocity vectors accuracy using Herrick-Gibbs model is very good and definitely inside the accuracy limits. Although it is not directly comparable the achieved accuracy of the velocity vector is better than the accuracy of the previous models. It seems that the combination of three position vectors in the model instead of one position and one velocity vector (Kepler model) or two position vectors(Gauss-Lambert model) provides better accuracy. Keeping in mind the statement of the previous paragraph **it seems that for the same orbit period the increase of the position vectors guide to an improvement of the accuracy of the model.**

Finally, the Herrick-Gibbs model is definitely an essential model for the orbit simulation of SPOT 5 orbit during the acquisition time of HRS images.

5.5. Validity of Kepler motion statement

The above accuracy tests show that the achieved accuracy of all models for HRS images is in acceptable limits. In other words, the above model could be used in case of along track stereo images with acquisition time interval of about 90 seconds.

Going one step further the question that arises now is: **Which is the validity time duration of the assumption that the satellite motion during the acquisition time of along track stereo images is a keplerian motion?** This question could be answered again by using all the metadata information of HRS images. If the navigation information of both HRS images is integrated together the state vectors of the satellite motion is known for 420 seconds with 30 seconds interval. The adopted scenario of the validation process for each model follows:

- Kepler model: The first given state vector of the navigation data is known. Using Kepler equation the state vectors for 420 seconds with 30 seconds interval are computed. These computed vectors are computed with the given values from the navigation data and the accuracy difference is presented in table 62.

- Gauss-Lambert model: The first given position vector is known. The second position vector which is needed in this model is changing from the second to last given position vector where the velocity vectors are calculated in each case. These computed vectors are computed with the given values from the navigation data and the accuracy difference is presented in table 63.
- Herrick-Gibbs model: The first and the last given position vectors are known. The third position vector which is needed in this model is changing from the second to the penultimate given position vector where the velocity vector is calculated in each case. These computed vectors are computed with the given values from the navigation data and the accuracy difference is presented in table 64.

5.5.1. Kepler model accuracy

From table 62 the conclusion is **that Kepler model could be used with acceptable accuracy for orbit period of about 90 seconds (as it is the time interval between the HRS images) for satellites-sensors of same characteristics as SPOT5-HRS combination.**

Time (sec)	dX (m)	dY (m)	dZ (m)	du_x (m/sec)	du_y (m/sec)	du_y (m/sec)
30	4.176	-4.334	-2.019	0.278	-0.290	-0.129
60	16.592	-17.395	-7.367	0.549	-0.581	-0.222
90	37.005	-39.171	-14.996	0.810	-0.870	-0.281
120	65.130	-69.573	-23.897	1.062	-1.156	-0.306
150	100.643	-108.443	-33.100	1.302	-1.435	-0.302
180	143.185	-155.555	-41.689	1.530	-1.705	-0.267
210	192.361	-210.621	-48.807	1.745	-1.964	-0.204
240	247.749	-273.295	-53.656	1.945	-2.212	-0.115
270	308.904	-343.182	-55.509	2.129	-2.445	-0.004
300	375.363	-419.838	-53.709	2.298	-2.663	0.128
330	446.643	-502.779	-47.675	2.450	-2.865	0.277
360	522.257	-591.493	-36.903	2.587	-3.048	0.443
390	601.585	-685.394	-21.083	2.706	-3.213	0.621
420	684.357	-783.985	0.328	2.809	-3.358	0.809

Table 62. Kepler model accuracy using the navigation data provided with HRS images (420 seconds time interval)

On the other hand the following additional comments should be done:

- The inaccuracy of the position components in X and Y direction is increasing proportional to the time interval.
- The inaccuracy of the velocity components in X and Y direction is increasing proportional to the time interval, too.
- However, the inaccuracy of the position and the velocity components in Z direction shows a different behavior (Figure 31), which is simulated with second order curve.

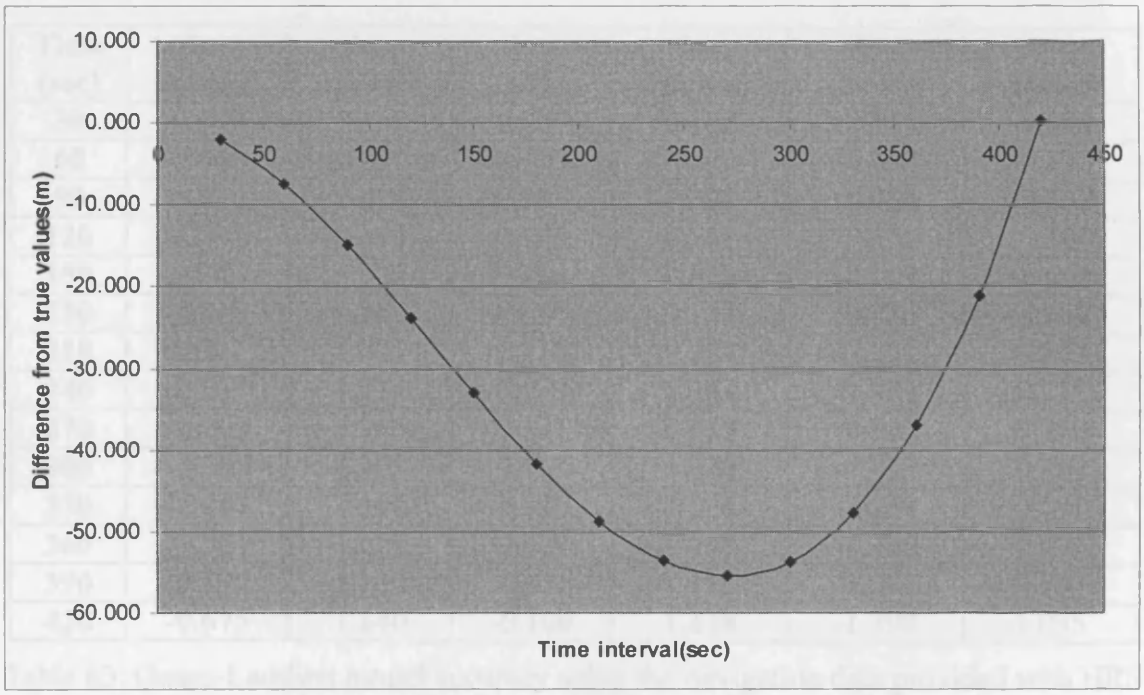

Figure 31. Difference from the true value of the position component in Z direction (second order curve) using Kepler model

With the provided orbit information the cause of this behaviour could not be identified. For the first site, there are two possible reasons:

- Perturbations of the orbit of the specific satellite which can not be modelled without additional information.
- The model itself.

As another two validation processes are following attention should be taken in the behaviour of the corresponding parameters.

5.5.2. Gauss-Lambert model

From table 63, the most important comment is **that Gauss-Lambert model could be used with acceptable accuracy for orbit period of about 420 seconds for satellites-sensors of same characteristics as SPOT5-HRS combination. Perhaps, this model could be used for larger periods of time which can not be defined here as the duration of the data provided is only 420 seconds.**

Time (sec)	du_{1x} (m/sec)	du_{1y} (m/sec)	du_{1z} (m/sec)	du_{2x} (m/sec)	du_{2y} (m/sec)	du_{2z} (m/sec)
30	0.799	0.140	0.071	0.142	-0.151	-0.058
60	0.660	0.290	0.123	0.272	-0.292	-0.098
90	0.525	0.436	0.165	0.398	-0.434	-0.112
120	0.394	0.580	0.196	0.518	-0.575	-0.100
150	0.266	0.723	0.214	0.629	-0.709	-0.068
180	0.142	0.863	0.221	0.731	-0.835	-0.013
210	0.023	1.001	0.216	0.822	-0.952	0.062
240	-0.093	1.135	0.199	0.902	-1.059	0.158
270	-0.203	1.265	0.171	0.969	-1.152	0.270
300	-0.308	1.391	0.133	1.026	-1.233	0.399
330	-0.408	1.512	0.086	1.068	-1.299	0.541
360	-0.503	1.627	0.029	1.098	-1.348	0.696
390	-0.592	1.737	-0.036	1.115	-1.383	0.861
420	-0.675	1.840	-0.109	1.118	-1.398	1.035

Table 63. Gauss-Lambert model accuracy using the navigation data provided with HRS images (420 seconds time interval)

On the other hand the following comments should be done:

- The inaccuracy of the velocity component of HRS1 in X direction shows a different behavior (Figure 32) which is simulated with a simple line.
- The inaccuracy of the velocity component of HRS2 images in X direction is increasing proportional to the time interval.
- The inaccuracy of the velocity component of HRS1 and HRS2 images in Y is increasing proportional to the time interval.

- The inaccuracy of the velocity component of HRS1 and HRS2 images in Z direction shows the same behavior as in figure 31 (Kepler model)

Although the behavior of the velocity component of HRS1 in X direction shows a slightly different behavior, generally the accuracy deference of the velocity vector in Kepler model and the Gauss-Lambert model gives the same trends. It will be examined as a whole in the next paragraph during the validation test of Herrick-Gibbs model.

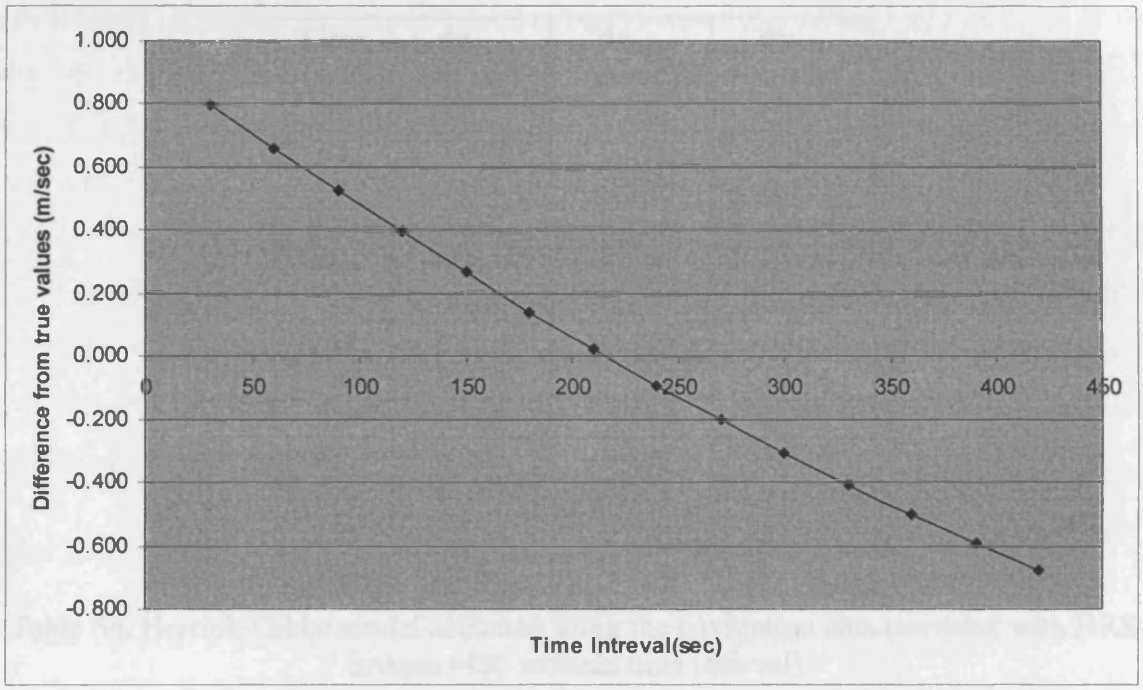

Figure 32. Difference from the true value of the velocity component in X direction using Gauss-Lambert model

5.5.3. Herrick-Gibbs model

From table 64 it is obvious **that Herrick-Gibbs model could be used with acceptable accuracy for orbit period of about 420 seconds for satellites-sensors of same characteristics as SPOT5-HRS combination. Perhaps, this model could be used for larger periods of time which can not be defined here as the duration of the data provided is only 420 seconds.**

On the other hand the following comments should be done:

- The inaccuracy of the velocity component in X and Y direction have the same behavior as the velocity component in Z direction in previous models (second order curve trend).
- The inaccuracy of the position and the velocity components in Z direction shows a different behavior (third order curve trend)

Time (sec)	du_{Mx} (m/sec)	du_{My} (m/sec)	du_{Mz} (m/sec)
30	0.053	-0.081	-0.009
60	0.098	-0.150	-0.018
90	0.136	-0.208	-0.023
120	0.167	-0.256	-0.025
150	0.189	-0.292	-0.025
180	0.206	-0.317	-0.020
210	0.214	-0.330	-0.012
240	0.212	-0.332	-0.001
270	0.202	-0.319	0.010
300	0.183	-0.292	0.021
330	0.153	-0.248	0.027
360	0.115	-0.186	0.030
390	0.062	-0.104	0.021

Table 64. Herrick-Gibbs model accuracy using the navigation data provided with HRS images (420 seconds time interval)

In both the Gauss-Lambert and Herrick-Gibbs model the accuracy difference are inside the limits. The variation of the behavior of the accuracy difference of the velocity vectors in each model guide us to the say that it depends on the model. However, because there is also a variation (improvement) in the accuracy of each model it is obvious that the orbit is simulated better in the more accurate models. As a result, the reason caused these variations in the accuracy difference could not be defined easily. Further work should be done here using more images of the same or different sensor with the essential navigation data in order to understand what is going on.

5.5.4. Important comment in validation procedure

This procedure started in trying to find the validity duration of the assumption that satellite motion during the time of along track stereo images is a Keplerian motion. **In fact it is found that the validity duration of this assumption depends on the method used in the model.** As an example Kepler model provides accurate results for about 90 seconds. On the other hand, Gauss-Lambert model which is based to the same assumption (keplerian motion) provides accurate results for at least 420 seconds using the same number (but different type) of unknown parameters. Finally, Herrick-Gibbs model which is based again to the same assumption provides better accuracy than the previous model in the duration of the navigation data given (420 seconds) and it seems that is capable to provide accurate results for more than this period of time. It seems that the important factor in the accuracy improvement is the number of position parameters in the model. **It seems that the increase of the position vectors in the solution does not only increase the accuracy of the model as it is mentioned in § 5.4.5, but also the validity duration of this model.**

5.6. Summary

In this chapter a generic model for along track stereo images are introduced in various versions, in depth. The fundamental assumptions of all versions are the same. For each version different orbit determination-propagation methods are used. The first one based on the Kepler problem (orbit propagation) which can be used in more than two along track images. The second one is based on Gauss-Lambert method which can be used only for two along track images like SPOT-HRS and TERRA-ASTER. The final one is based on Herrick-Gibbs method which is combined with the Gauss-Lambert method in order to be used in case of more than two along track images.

In table 65, the number of unknown exterior orientation parameters for each version is given in case of 2 to 5 along track images. For comparison reasons the number of unknown parameters if the images are solved individually are also given in the same table.

In table 66, the accuracy of unknown parameter for the imaginary-nadir HRS image are provided as it is possible to compare the accuracy of all model used in this evaluation process.

Number of images	Number of unknown parameters solving each image individually	Number of unknown parameters using Kepler model	Number of unknown parameters using Gauss-Lambert model	Number of unknown parameters using combined method
2	18	12	12	-
3	27	15	-	18
4	36	18	-	24
5	45	21	-	30

Table 65. Number of unknown parameters for all in case of 2 to 5 along track images.

	Accuracy of unknown parameters using Kepler model	Accuracy of unknown parameters using Gauss-Lambert model	Accuracy of unknown parameters using combined method
POSITION X (m)	6.845	-	-
POSITION Y (m)	-8.474	-	-
POSITION Z (m)	3.629	-	-
VELOCITY u_x (m/sec)	0.293	0.144	0.012
VELOCITY u_y (m/sec)	-0.363	-0.179	-0.012
VELOCITY u_z (m/sec)	0.168	0.091	-0.016

Table 66. Along track models accuracy for the imaginary-nadir velocity vector in inertial coordinate system

From the evaluation of Kepler method (§5.5.1) the following points should be mentioned:

- It is less accurate than Gauss-Lambert method in case of two along track images while the number of unknown parameters is the same.
- It has a clear advantage in case of more than two along track images where less unknown parameters are needed for the solution although it is again less accurate than the combined Gauss-Lambert and Herrick-Gibbs model.
- Finally, the validity of the model is dramatically smaller that the others and it is assumed to about 90 seconds for images having the same characteristics as SPOT5-HRS. **It is just accepted for HRS images.**

From the evaluation of Gauss-Lambert method (§5.5.2) the following points should be mentioned:

- The accuracy of Gauss-Lambert method is better than the accuracy of Kepler method while the number of unknown parameters is the same.
- It can not be used by itself in more than two along track images.
- Finally the validity of this method is at least 420 seconds for images having the same characteristics as SPOT5-HRS.

From the evaluation of Herrick-Gibbs (§5.5.3) the following point should be mentioned:

- The accuracy of Herrick-Gibbs method is better than the accuracy of all the other methods
- In can be used in combination with Gauss-Lambert method in order to solve more than two along track images. However the number of the unknown parameters are larger than the case of Kepler model
- Finally the validity of this method is at least 420 seconds for images having the same characteristics as SPOT5-HRS.

It is possible to develop a more complicated model which could be a combination of the developed versions. As an example assuming that there is a sequence of ten along track images. The first and the last could be solved using the Gauss- Lambert model (12 unknowns-2 position vectors and rotation angles) while the 4, 7 are solved with the combined model (12 additional unknowns-2 position vectors and rotation angles) and

finally all other images with Kepler model (18 unknowns- only the rotation angles of six images). The total number of unknown parameters is 42 for ten images with accuracy inside the defined limits. If only Kepler model is used the total number of the unknown parameters is 36 where the accuracy of the transformation is not acceptable while if only the combined solution is used which provides acceptable accuracy the total number of unknown parameters is 60. **It is obvious from this example that the developed model in general is very flexible and the developed method can be combined creatively in order to improve the accuracy and simultaneously to reduce the number of unknown parameters.**

In this chapter **the generic rigorous along track model is introduced and the most importantly the accuracy of each version of this model is examined using the HRS high accurate navigation data, before they are used in the specific along track model.** In chapter 6 the model is evaluated using HRS and ASTER data and also it is compared with the single image sensor model.

CHAPTER 6.

EVALUATION OF THE ALONG TRACK STEREO SENSOR MODELS

6.1 Introduction

In this chapter the evaluation process of the along track stereo sensor model is presented which covers precision and accuracy issues. In this process SPOT5-HRS images are used along with ASTER-NVIR images (§6.2). A comparison is made between single image sensor model and the various versions of the along track sensor model (§6.3).

At first the along track model is solved indirectly using GCPs. It has already been mentioned that the along track sensor model has less unknown parameters than the case where the along track images are solved separately. However the solution of along track sensor model gives more accurate results than the solution where the along track images are solved as single images (table 73). Moreover, the imprecision of the velocity vector (§4.8) is overcome (table 68). Secondly, an attempt is done to solve the along track sensor model directly using the navigation data provided with the SPOT5-HRS images (§6.4).

It was mentioned in the introduction of the thesis that an effort is made in order to solve the model with less constraints as possible included tie points. The reason is to understand how the model itself simulates the acquisition process of along track stereo images.

6.2. Data sets- Reference data

For the along track sensor model evaluation three along track stereo data sets are used. These data sets are the following:

- Two ASTER data set that cover the Vegoritis and Grevena area in Northern Greece (Figure 33) which is a test site for the Centre for Observation and Monitoring of Earthquake and Tectonics (COMET).
- A SPOT5 HRS data set that covers an area located around Aix-en-Provence in SE France which is provided under the SPOT Assessment Project (SAP) set up by CNES and ISPRS (Figure 34) (Baudoin et al., 2004).

6.2.1. Detailed description of ASTER data sets

Two TERRA-ASTER data sets is used to evaluate the along track model. They were acquired on 8 Oct 2001 on the same orbit, covering high mountainous areas around Vegoritis Lake and Grevena Town in Northern West Greece. The difference in height within the images is about 1000m and the slopes in some areas are very large.

The data sets are Level 1A. The ASTER Level-1A data consists of the image data, the radiometric coefficients, the geometric coefficients and other auxiliary data, without applying the coefficients to the image data. Level-1A is the most appropriate data to use for photogrammetric applications, because the geometry and the pixel values are the same as when they are acquired.

ASTER images are distributed in HDF (Hierarchical Data Format) format. It is a free library and platform independent data format for the storage and exchange of scientific data. The advantage of using this format is that important information regarding the acquisition geometry of the images which is included in the same file. The acquisition time for the nadir (for 13 lines along the image) and back image (for 16 lines along the image) is given (Dowman and Michalis, 2003). The position, velocity and attitude vectors are also provided for the same lines. In this model using the observation time values the time interval between the nadir and back image was calculated. For both data sets this value is 49.12314 seconds. It is assumed that this value was calculated very accurately and it is used as a known parameter in the model. However, all other

information, (position, velocity and attitude vector), are used as initial values in the model as they are not as accurate as is needed (table 1).

Figure 33. Location map of study area (for Philips's Concise World Atlas, 1998)

6.2.2. Detailed description of HRS data sets

The test area is located around Aix-en-Provence in SE France and covers IGN map sheet 3244 (Figure 34). The images are acquired on 14 August 2002. The data was made available to the CEOS WGCV Terrain Mapping WG by permission of UCL and IGN. A number of tests have been carried out over this site on different types of data.

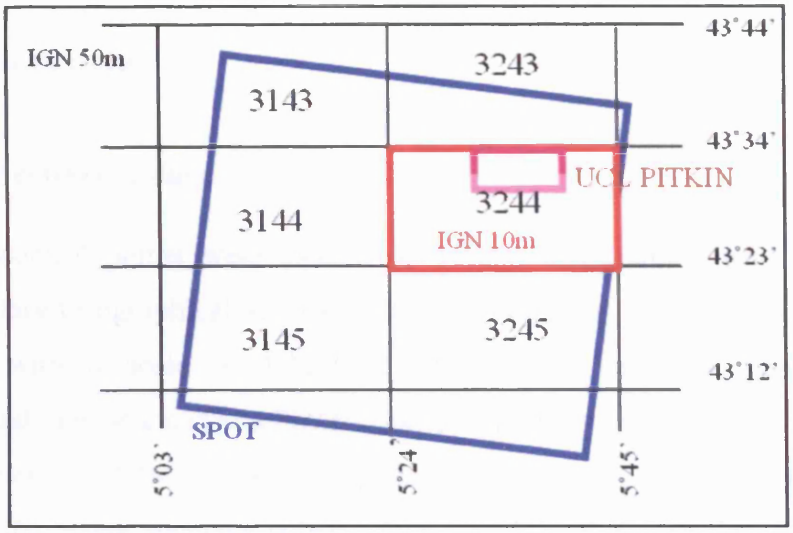

Figure 34. SPOT5-HRS test site

The SPOT 5 HRS Level 1A product is delivered in DIMAP format which is the standard format for SPOT 5 products. According to the DIMAP specification the images are in tiff format while the metadata file is in XML format. The structure of XML SPOT 5 metadata format is introduced in DIMAP Dictionary version 1.1 - Edition 01 September 2003 - SPOT Scene profile (SPOT, 2003).

The following information from the metadata file could be used to solve the sensor model directly:

- Position and velocity vectors of the satellite measured by the DORIS system every 30 seconds with respect to ITRF90 (International Reference Frame 1990).
- Absolute attitude data measured by the on-board star tracking unit for about seven times per second with respect to the local orbital coordinate frame.
- The look direction table for all pixels of the array.
- The scene centre time and the sampling time.

The time interval between the images is calculated from the metadata. It is 91.67486 seconds.

6.2.3. Reference data

6.2.3.1. Aster reference data

The ground control points were located on 1:5000 maps which were produced by Hellenic Military Geographical Service (HMGS). The maps were produced from aerial photographs with a scale of 1:12000-1:15000 using analytical photogrammetric instruments and then scanned at a 300dpi resolution. They were then geo referenced in EGSA-87 Greek Geodetic System. The planimetric accuracy of these maps is about 2 meters while the height accuracy is better than 4m. A total of 20 points were measured for the Vegoritis test site and 12 for Grevena test site having a very good distribution all over the images. For the Vegoritis test site 8 of them are used as Ground Control Points (GCP) while the other 12 as Check Points (§ 6.3.2.1-2). In § 6.3.2.3 all points from both test sites are used as Ground Control Points to evaluate the precision of the model.

For vertical control a Digital Terrain Model with 30m pixel size was used. The DEM was also provided by the Hellenic Military Geographical Service (HMGS). The vertical accuracy is better than fifteen meters.

6.2.3.2. HRS reference data

The grounds control points were originally provided by IGN for the OEEPE test of SPOT data and were mainly extracted from 1:25000 maps. The geodetic coordinates are given in the French NTF system, where the reference ellipsoid is Clarke 1880. The Lambert III projection is used. A total of 33 reference points were measured in HRS images having a very good distribution all over the whole HRS images. Twelve of them are used as Ground Control Points in this evaluation process while the rest 21 are used as Check Points.

The following DEMs are available:

Source	UCL Pitkin	IGN	IGN
Grid	30m	50m	10m
RMSE	±1.3m	5-2.5m	1m
Source	Aerial	Aerial	Aerial
Extent (km)	12.4 x 6.9	61 x 63	30.6 x 21.7

Table 67. Reference DEM for HRS test site

6.3. Solution without use of navigation data

6.3.1. HRS-data

HRS evaluation without using any navigation data is the most extended of all the others. In this evaluation only Kepler model for along track images (§ 5.3.1) and Gauss-Lambert model (§ 5.3.2) is tested. The combined model of Gauss-Lambert and Herrick-Gibbs is not tested as more than two images are needed which are not existed in case of HRS. For comparison reasons, in order to understand the improvement in the solution when specific along track sensor models are used, the results when the HRS images are solved separately are also introduced. As it has already been mentioned twelve points are used as GCPs and twenty one as Check points. The distribution of these points is shown in figure 35. It is shown in §6.3.3 that just 6 GCPs are enough to solve accurately enough the along track models.

The following tables are presented for each model:

- Reference Standard Deviation of the solution and of the unknown velocity vector parameters when HRS1 image is solved as a single image and in along track sequence by Kepler model when line and angular elements are solved separately in order to understand the improvement in the geometry when along track model is used (Only in along track Kepler model).
- Standard deviation of the solution and of the unknown parameters using Ridge Estimator when HRS1 image is solved as a single image and in along track sequence.

- Difference of the Coordinates (reference-calculated) in an Inertial space for the Ground Control and Check Points when HRS images solved independently and in an along track sequence.
- RMSE in Inertial Coordinate System of Ground Control Points and Check Points when HRS images solved independently and in an along track sequence.

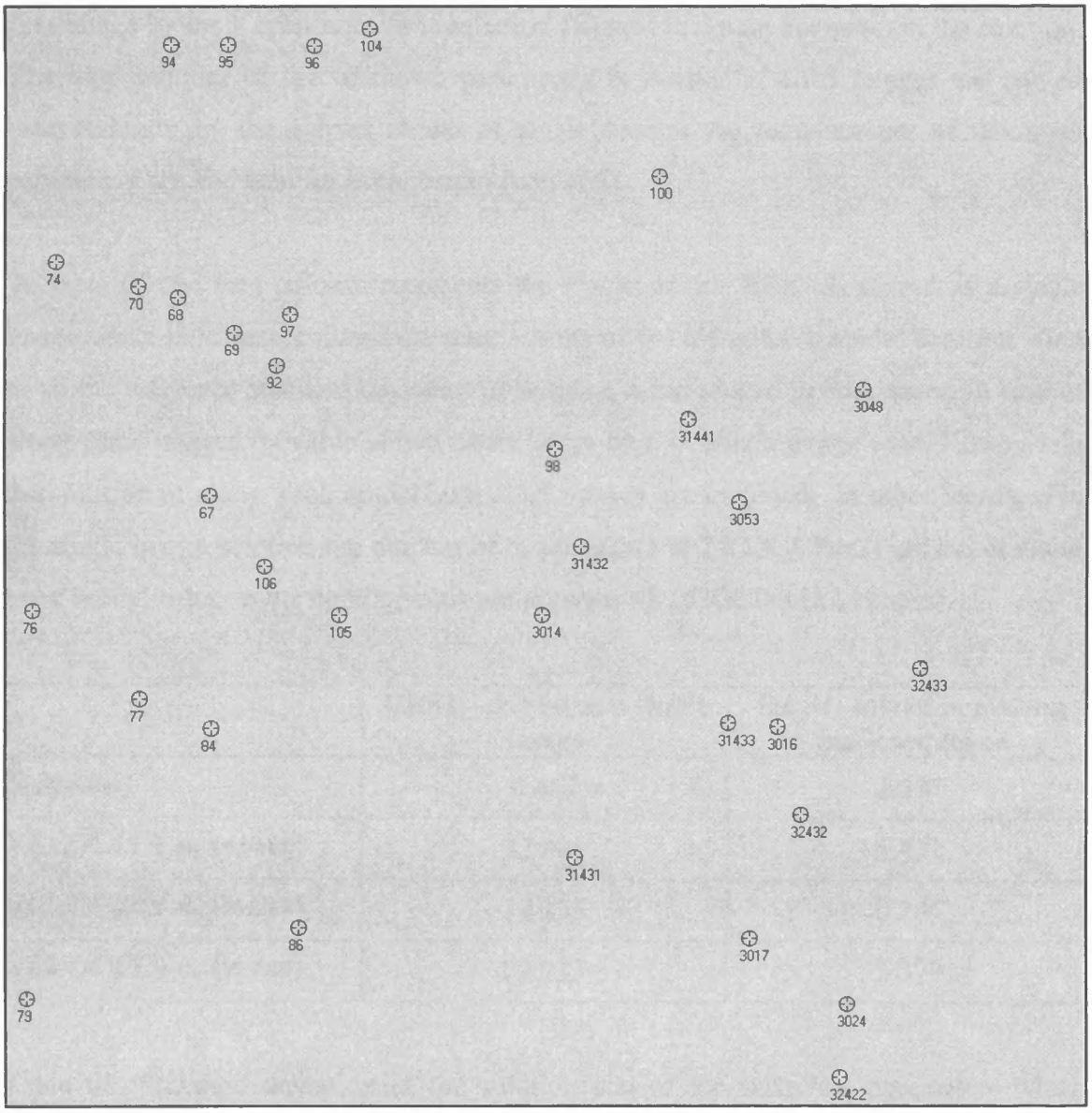

Figure 35. Distribution of Reference Points on HRS images.

6.3.1.1. Kepler model

The Kepler model for along track images is evaluated. This model is introduced in § 5.3.1. The unknown parameters for this model are the state vector of the base framelet of the HRS1 image and the rotation angles of both HRS images. The state vector of the base framelet of the HRS2 image is related to the state vector of the base framelet of the first image by the Kepler equation (equation 18) thus is not an unknown in the solution. The total number of the unknown parameters is twelve. If HRS images are solved independently by the Kepler model of single images the total number of unknown parameters are eighteen for both images (table 65).

In table 68 the first column represents the results where HRS1 is solved as a single image while in second column the same results of the along track model solution. First of all the reference standard deviation of solution is introduced in both cases. In case of along track images its value is two times larger than in single image case. However in the solution of along track model both HRS images are involved. In other words, if in the single image solution the number of observations is 24(12GCPsx2) in case of along track model solution the number of observations is 48 (12GCPsx2x2 images).

	HRS1 – solved as a single image	**HRS1- solved in a along track sequence**
S_0 (pixels)	0.658	1.337
VELOCITY u_x (m/sec)	32.804	1.421
VELOCITY u_y (m/sec)	14.235	0.204
VELOCITY u_z (m/sec)	72.733	1.379

Table 68. Standard deviation of the solution and of the unknown parameters when HRS1 image is solved as a single image and in along track sequence by Kepler model (line and angle elements are solved separately)

Hence, **the most important comment of the above table is that in along track solution the precision of the velocity vector is increased dramatically (standard**

deviation is decreased) compared to the single image solution. It is one of the advantages of the along track sensor model and great attention is taken in order to confirm this statement to the following tests.

In table 69 the results of the solution (single and along track) is introduced when the ridge estimator involved in the solution. In case of along track model solution it seems that the incompatibility of the false estimation of the velocity vector precision is overcome.

	HRS1 – solved as a single image	**HRS1- solved in a along track sequence by Kepler model**
S_0 (pixels)	0.721	1.444
POSITION X (m)	26.474	54.851
POSITION Y (m)	20.329	24.962
POSITION Z (m)	28.699	69.276
VELOCITY u_x (m/sec)	1.101	1.426
VELOCITY u_y (m/sec)	0.705	1.104
VELOCITY u_z (m/sec)	1.259	1.829

Table 69. Standard deviation of the solution and of the unknown parameters using Ridge Estimator when HRS images are solved as a single images and in along track sequence by Kepler model

In tables 70 and 71 the difference of the Coordinates (reference-calculated) in an Inertial space for the twelve Ground Control Points and RMSE when HRS images solved independently and in an along track sequence is introduced, respectively. In the case where the HRS images are solved separately the number of unknown parameters is 18 and they used to intersect the Check Points in order to estimate the accuracy. Moreover as it is mentioned during the description of Kepler model (§5.3.1) is not possible to calculate the state vector of HRS2 image (of the second image), thus in the comparison tables only the HRS1 image state vector is compared. The RMSE values are almost the same in X and Y direction while in Y direction the single image solution gives slightly better value.

	HRS–solved as a single images			HRS-solved in a along track sequence		
	dX(m)	dY(m)	dZ(m)	dX(m)	dY(m)	dZ(m)
67	-2.923	-2.356	6.945	-3.361	-1.893	5.666
68	-12.738	0.543	8.957	-12.544	4.289	8.364
70	-1.508	-0.856	4.961	-1.547	-0.9124	5.218
74	13.480	1.352	-16.786	12.914	-7.983	-14.611
84	1.175	-0.776	0.82	0.611	-6.994	1.039
86	-1.459	1.201	-1.313	-0.601	-1.545	0.125
3014	4.730	-5.969	0.09	5.326	5.502	-2.554
3016	2.759	7.664	1.009	2.938	9.828	-1.221
31431	0.596	4.178	-3.1	1.887	13.123	-3.941
31432	-2.760	3.980	-0.391	-2.3	15.026	-2.601
32432	-2.615	-8.984	2.498	-2.92	-12.235	5.266
32433	1.257	0.018	-3.692	-0.397	-16.210	-0.738

Table 70. Difference of the Coordinates (reference-calculated) in an Inertial space for the Ground Control Points when HRS images solved independently and in an along track sequence by Kepler model

	HRS images – solved as a single images	HRS images solved in a along track sequence
RMSE X (m)	5.808	5.723
RMSE Y (m)	4.271	9.465
RMSE Z (m)	6.244	5.791

Table 71. RMSE in Inertial Coordinate System of Ground Control Points when HRS images solved independently and in an along track sequence by Kepler model

In tables 72 and 73 the difference of the Coordinates (reference-calculated) in an Inertial space for the twenty-one Check Points and RMSE when HRS images solved independently and in an along track sequence is introduced, respectively. Here the conclusion is opposite. **The along track sensor model solution gives better results in the three direction and especially in Y direction where the improvement is about two times.** Moreover the most interesting point where in the images this improvement occurs. If compare table 72 (or better figures 36, 37 and 38 which the coordinate difference of the check points are represented). **The larger improvements are at the edges of the images** (check points 79, 94, 95, 96, 104, 3024). **It seems that the along**

track sensor model overall represents better the images acquisition geometry than the single image solution. Just to remind that both models are based in Kepler equation.

	HRS images – solved as a single images			HRS1- solved in a along track sequence by Kepler model		
	dX(m)	**dY(m)**	**dZ(m)**	**dX(m)**	**dY(m)**	**dZ(m)**
69	-15.125	-26.8639	13.713	-14.779	-19.3922	12.167
76	17.443	27.5768	-7.206	14.808	1.1423	-3.358
77	9.2	14.2776	0.98	7.839	0.4125	2.711
79	16.059	44.3594	-16.984	13.813	3.4884	-7.395
92	-7.973	-10.9727	8.358	-7.565	-1.4983	6.318
94	-13.654	-18.8243	-8.444	-11.396	-6.989	-6.692
95	-12.343	-25.0994	-13.321	-9.858	-9.0159	-12.211
96	-14.875	-31.9314	-7.361	-12.169	-11.7721	-6.665
97	-8.189	-2.6604	2.089	-7.485	8.9886	0.13
98	14.359	8.2866	-6.471	14.918	20.7934	-8.437
100	6.07	7.8823	-27.155	7.243	15.9789	-24.117
104	-23.658	-25.4598	1.667	-20.737	-3.7279	2.789
105	8.21	-2.9101	1.442	8.433	4.0644	-0.882
106	5.223	-14.2529	4.112	5.088	-10.7988	2.015
3017	2.641	10.0715	-4.993	3.332	10.8548	-1.485
3024	-7.622	14.979	3.267	-7.388	8.7232	9.258
3048	14.391	4.9335	-17.537	13.446	-7.6234	-13.873
3053	10.52	-18.7354	-15.993	10.447	-15.89	-16.904
31433	-0.74	-20.738	5.178	-0.413	-16.0746	3.432
31441	13.207	2.8983	-18.481	13.189	7.5366	-17.313
32422	-9.796	-1.9819	-6.274	-8.83	-6.3033	0.207

Table 72. Difference of the Coordinates (reference-calculated) in an Inertial space for the Check Points when HRS images solved independently and in an along track sequence by Kepler model

	HRS images – solved as a single images	**HRS images solved in a along track sequence**
RMSE X (m)	12.183	11.101
RMSE Y (m)	19.419	10.769
RMSE Z (m)	11.368	9.863

Table 73. RMSE in Inertial Coordinate System of Check Points when HRS images solved independently and in an along track sequence by Kepler model

6.3.1.2. Gauss-Lambert model

The Gauss-Lambert model for along track images is evaluated. This model is introduced in § 5.3.2. It can be used by itself only in case of two along track stereo images. The number of unknown parameters is twelve in total as in the Kepler model. In the case of more than two images is used in combination with the Herrick-Gibbs method (§2.4.8.4.). The position vectors of the base framelet of both images represent six of the unknown exterior orientation parameters. The velocity vector of the base framelet of each images are related to position vectors by the Gauss-Lambert method thus are not unknowns in the solution. The other six unknown parameters are the rotation angles of the two images as in Kepler model solution.

In table 74 the results of the solution (single and along track) is introduced when the ridge estimator involved in the solution. Compared these results with the results of the Kepler model solution (table 69) it seems that in Gauss-Lambert model the precision is improved in Y direction while is worse in the other two, although reference standard deviation is almost the same. As in case of the Kepler model the value of reference standard deviation of along track images is two times larger than in single image case (the reason is explained in Kepler model evaluation).

	HRS – solved as a single images		**HRS- solved in a along track sequence by Kepler model**
S_0 (pixels)	0.721	0.703	1.459
POSITION X_1 (m)	26.474		71.647
POSITION Y_1 (m)	20.329		11.942
POSITION Z_1 (m)	28.699		84.389
POSITION X_2 (m)	20.174		69.998
POSITION Y_2 (m)	5.486		15.289
POSITION Z_2 (m)	28.391		69.359

Table 74. Standard deviation of the solution and of the unknown parameters using Ridge Estimator when HRS1 image is solved as a single image (Kepler model) and in along track sequence by Gauss-Lambert model

In tables 75 and 76 the difference of the Coordinates (reference-calculated) in an Inertial space for the Ground Control Points and RMSE when in an along track sequence is introduced by Gauss-Lambert model. Compare these values with the RMSE of Kepler along track model solution and the solution where the images are solved separately it gives almost the same values as the Kepler along track solution.

	dX(m)	dY(m)	dZ(m)
67	-2.863	-1.1934	6.711
68	-12.876	4.0917	7.9
70	-1.914	-1.4109	4.709
74	12.42	-9.151	-15.213
84	1.246	-5.8075	2.114
86	-0.723	-1.189	-0.415
3014	5.821	6.1829	-2.104
3016	2.372	9.586	-0.436
31431	1.731	11.6938	-4.251
31432	-1.762	16.3123	-2.551
32432	-2.944	-13.9166	4.468
32433	-0.502	-15.2029	-0.909

Table 75. Difference of the Coordinates (reference-calculated) in an Inertial space for the Ground Control Points when HRS images are in an along track sequence by Gauss-Lambert model.

RMSE X (m)	5.690
RMSE Y (m)	9.650
RMSE Z (m)	5.886

Table 76. RMSE in Inertial Coordinate System of Ground Control Points when HRS images solved independently and in an along track sequence by Gauss-Lambert model

In tables 77 and 78 the difference from the calculated values in an Inertial Coordinate system for the Check Points and RMSE when HRS images solved in an along track sequence by Gauss-Lambert model is introduced. The conclusions are almost identical as in the Kepler evaluation model. **The along track sensor model solution by Gauss-Lambert model gives better results in the three direction. The larger improvement**

is also at the edges of the images having about the same behaviour as the Kepler model for along track images.

	dX(m)	dY(m)	dZ(m)
69	-14.916	-19.115	11.926
76	15.723	2.798	-1.834
77	8.634	1.951	3.93
79	13.681	7.481	-8.569
92	-7.529	-0.916	6.248
94	-13.793	-8.805	-11.274
95	-12.208	-10.021	-17.012
96	-14.41	-11.501	-11.903
97	-7.705	9.555	-0.516
98	15.381	22.685	-8.978
100	6.821	21.104	-29.171
104	-23.05	-2.613	-3.162
105	9.044	4.779	0.111
106	5.636	-9.966	3.235
3017	2.795	7.476	-3.194
3024	-8.684	3.741	6.867
3048	13.772	-2.327	-16.184
3053	10.708	-13.302	-17.334
31433	-0.593	-16.333	3.886
31441	13.904	10.614	-19.083
32422	-10.857	-12.512	-2.973

Table 77. Difference of the Coordinates (reference-calculated) in an Inertial space for the Check when HRS images are in an along track sequence by Gauss-Lambert model.

RMSE X (m)	11.995
RMSE Y (m)	11.365
RMSE Z (m)	11.530

Table 78. RMSE in Inertial Coordinate System of Check Points when HRS images solved independently and in an along track sequence by Gauss-Lambert model

6.3.1.3 Summary of the along track models evaluation of HRS data without use of navigation data

In §6.3.1.1 and in §6.3.1.2 the along track sensor model in two versions (Kepler and Gauss-Lambert) is evaluated along with the solution where the HRS images are solved separately for a comparison reasons.

The initial comments for these tests are the following:

- **In along track solution the precision of the velocity vector is increased dramatically compared to the single image solution.**
- The RMSE of the Ground Control points are slightly better in case of separately solved images.
- **The along track sensor model overall represents better the images geometry** as the RMSE of the check points is much better than the case where the images are solved separately. **The larger improvements are at the edges of the images**. In figures 36, 37, 38 the differences along track of the Coordinates (reference-calculated) in an inertial space of the Check Points are shown (Along track models solution along with single image solution).
- Finally, the Kepler and Gauss-Lambert model give generally almost identical accuracy. This conclusion comes out from the RMSE of the Ground Control and Check Points are compared. However, from figures 36,37,38 it seems that the orbit simulations is slightly different where Kepler model in many cases gives better accuracy (points 94,95,96). This conclusion is a little surprising this conclusion as it is expected for Gauss-Lambert model to be more accurate than the Kepler model (§5.6).

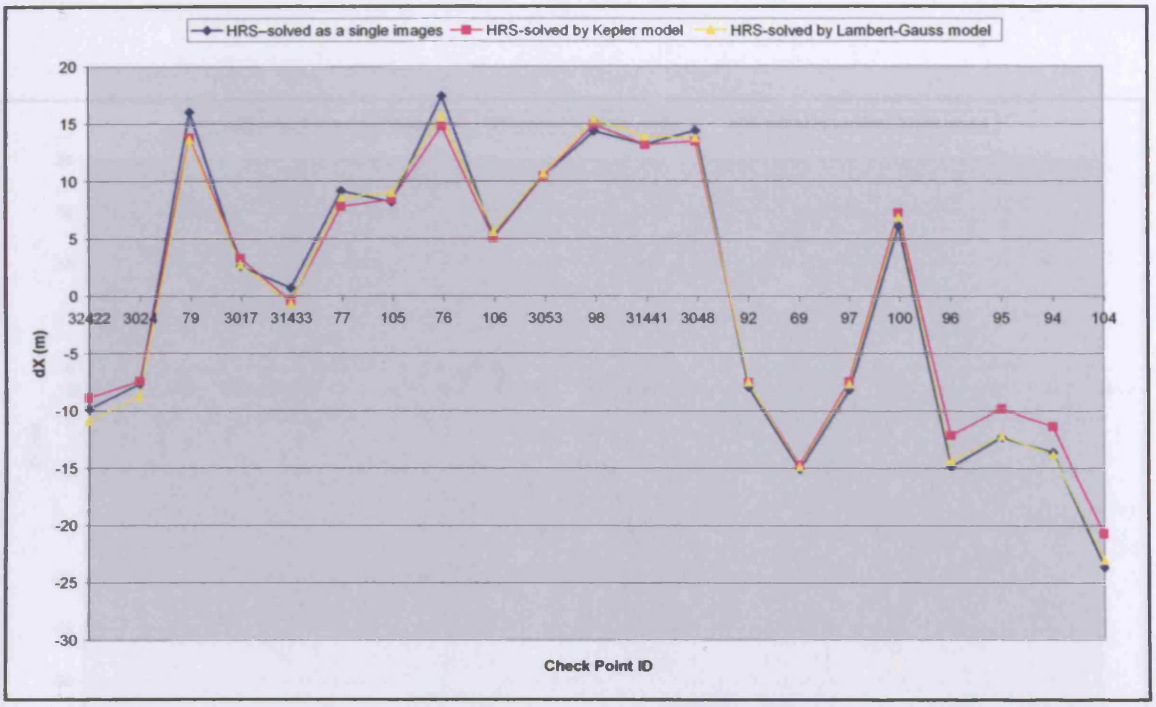

Figure 36. Along track X-coordinate difference of the calculated values in the solution of along track and single models

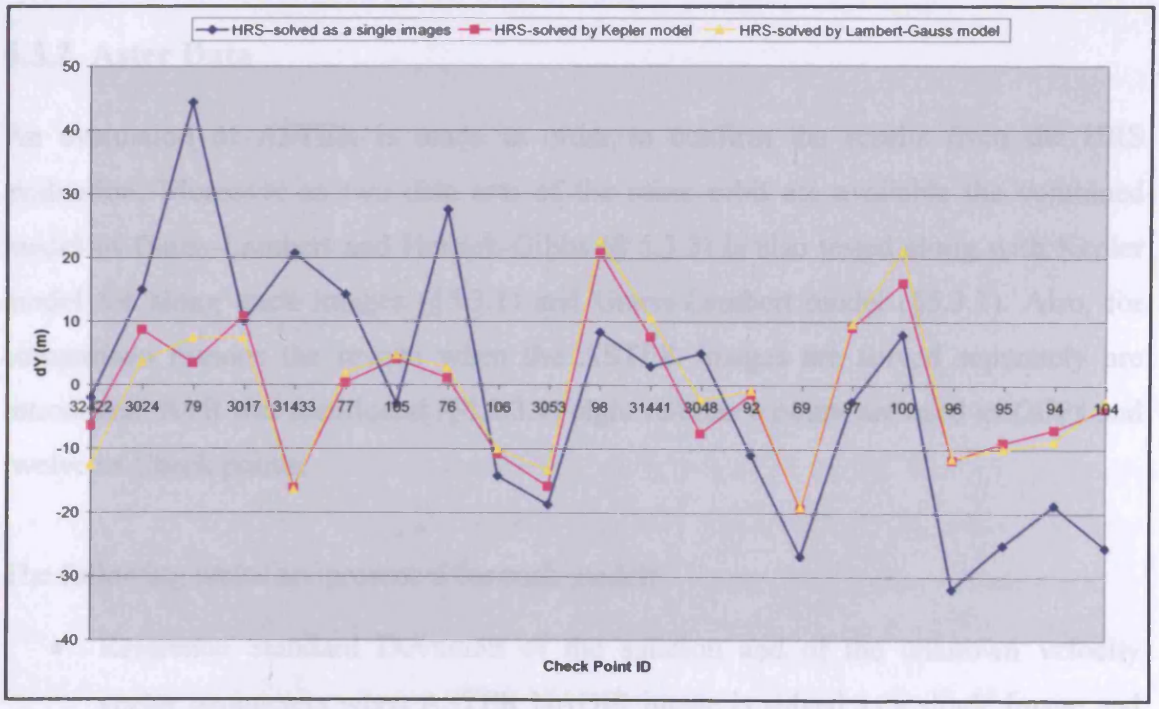

Figure 37. Along track Y-coordinate difference of the calculated values in the solution of along track and single models

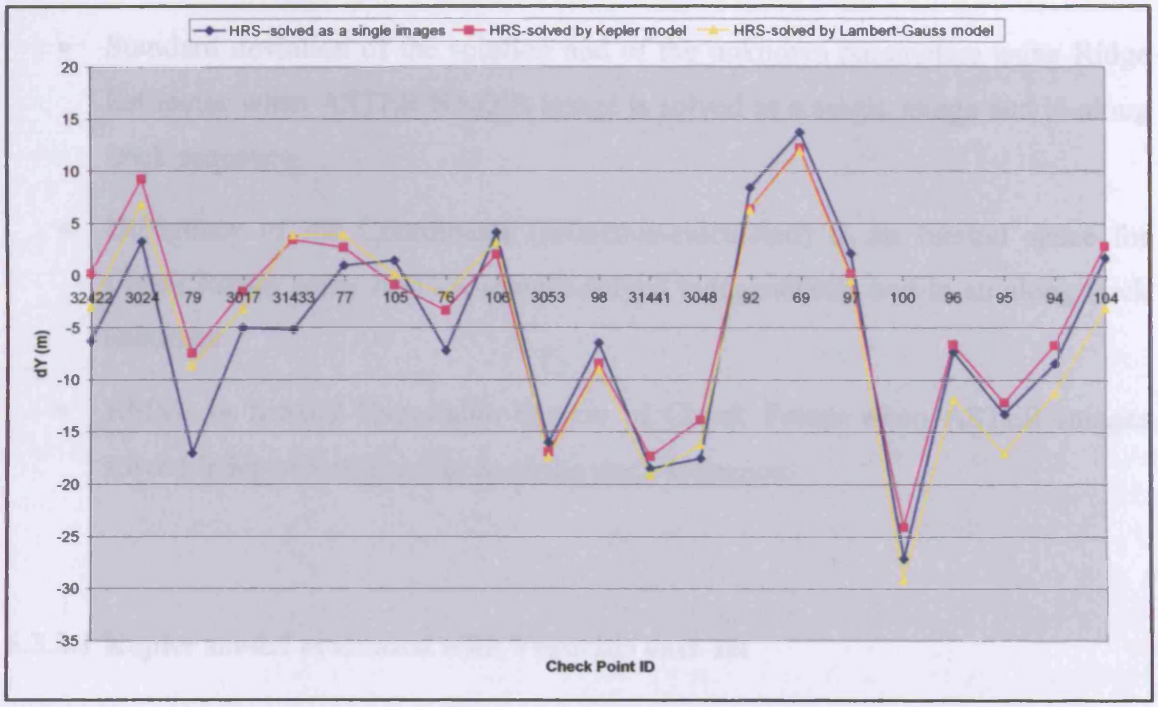

Figure 38.Along track Z-coordinate difference of the calculated values in the solution of along track and single models

6.3.2. Aster Data

An evaluation of ASTER is made in order to confirm the results from the HRS evaluation. Moreover as two data sets of the same orbit are available the combined model of Gauss-Lambert and Herrick-Gibbs (§ 5.3.3) is also tested along with Kepler model for along track images (§5.3.1) and Gauss-Lambert model (§5.3.2). Also, for comparison reasons the results when the ASTER images are solved separately are introduced. As it was mentioned (§6.2.3.1) eight reference points are used as GCPs and twelve as Check points.

The following tables are presented for each model:

- Reference Standard Deviation of the solution and of the unknown velocity vector parameters when ASTER NADIR image is solved as a single image and in along track sequence by Kepler model when line and angular elements are

solved separately in order to understand the improvement in the geometry when along track model is used (only for Kepler model)

- Standard deviation of the solution and of the unknown parameters using Ridge Estimator when ASTER NADIR image is solved as a single image and in along track sequence.
- Difference of the Coordinates (reference-calculated) in an Inertial space for Check Points when ASTER images solved independently and in an along track sequence.
- RMSE in Inertial Coordinate System of Check Points when ASTER images solved independently and in an along track sequence.

6.3.2.1 Kepler model evaluated with Vegoritis data set

The Kepler model for along track images is evaluated. This model is introduced in § 5.3.1. The unknown parameters for this model are the state vector of the base framelet of the ASTER-NADIR image and the rotation angles of both ASTER images. The state vector of the base framelet of the ASTER-BACK image is related to the state vector of the base framelet of the first image by the Kepler equation (equation 18) thus is not an unknown in the solution. The total number of the unknown parameters is twelve. If ASTER images are solved separately by the Kepler model of single images the total number of unknown parameters are eighteen for both images (table 65).

In table 79 the first column represents the results where ASTER-NADIR is solved as a single image while in second column the same results are given in the along track model solution. First of all the reference standard deviation of solution is introduced in both cases. In case of along track images its value is four times larger than in single image case. As it has already been mentioned the solution of the along track in the solution of along track model both ASTER images are involved. However, as in case of HRS images the reference standard deviation of the along track sequence is expected at about

two times larger, not four. It seems that the nadir image alone provides more precise solution.

	ASTER NADIR– solved as a single image	ASTER NADIR- solved in a along track sequence by Kepler model
S_0 (pixels)	0.324	1.534
VELOCITY u_x (m/sec)	74.921	8.138
VELOCITY u_y (m/sec)	40.724	2.640
VELOCITY u_z (m/sec)	67.895	4.868

Table 79. Standard deviation of the solution and of the unknown parameters when ASTER-NADIR image is solved as a single image and in along track sequence by Kepler model (line and angle elements are solved separately)

From the above table, also in case of ASTER images **is found that in along track solution the precision of the velocity vector is increased dramatically (standard deviation is decreased) compared to the single image solution.**

In table 80 the results of the solution (single and along track) is introduced when the ridge estimator involved in the solution.

	ASTER – solved as a single images	ASTER- solved in a along track sequence by Kepler model
S_0 (pixels)	.500	1.568
POSITION X (m)	6.434	58.262
POSITION Y (m)	20.604	48.667
POSITION Z (m)	4.985	74.654
VELOCITY u_x (m/sec)	0.906	2.359
VELOCITY u_y (m/sec)	0.178	0.698
VELOCITY u_z (m/sec)	0.999	1.514

Table 80. Standard deviation of the solution and of the unknown parameters using Ridge Estimator when ASTER images are solved as single images and in along track sequence by Kepler model

In the case of along track model solution it seems that the incompatibility of the false estimation of the velocity vector precision is overcome (§4.8).

In tables 81 the RMSE when HRS images solved independently and in an along track sequence is introduced. The conclusions are the same as in HRS case. **The along track sensor model solution gives better results in the three direction and especially in Y direction where the improvement is about two times**

	ASTER– solved as a single images	**ASTER- solved in a along track sequence**
RMSE X (m)	12.587	13.521
RMSE Y (m)	24.291	11.345
RMSE Z (m)	15.525	13.800

Table 81. RMSE in Inertial Coordinate System of Check Points when ASTER images solved independently and in an along track sequence by Kepler model

6.3.2.2 Gauss-Lambert model evaluated with Vegoritis data set

The Gauss-Lambert model for along track images is evaluated. This model is introduced in § 5.3.2. It can be used by itself only in case of two along track stereo images. The number of unknown parameters is twelve in total as in the Kepler model. In the case of more than two images is used in combination with the Herrick-Gibbs method (§2.4.8.4.). The position vectors of the base framelet of both images represent six of the unknown exterior orientation parameters. The velocity vector of the base framelet of each images are related to position vectors by the Gauss-Lambert method thus are not unknowns in the solution. The other six unknown parameters are the rotation angles of the two images as in Kepler model solution.

In table 82 the results of the solution (single and along track) is introduced when the ridge estimator involved in the solution. Compared these results with the results of the Kepler model solution (table 80) it seems that in Gauss-Lambert model the precision is

improved in Y direction while is worse in the other two, although as a total it seems that are the same, as in case of HRS images.

	ASTER – solved as a single images		ASTER- solved in a along track sequence
S_0 (pixels)	0.324	0.521	1.612
POSITION X_1 (m)	6.434		70.312
POSITION Y_1 (m)	20.604		20.794
POSITION Z_1 (m)	4.985		73.436
POSITION X_2 (m)	33.996		76.123
POSITION Y_2 (m)	28.243		28.384
POSITION Z_2 (m)	28.841		69.532

Table 82.Standard deviation of the solution and of the unknown parameters using Ridge Estimator when ASTER images are solved as single images (Kepler model) and in along track sequence by Gauss-Lambert model

In table 83 the RMSE when ASTER images solved in an along track sequence by Gauss-Lambert model is introduced. The conclusions are almost identical as in the Kepler evaluation model. **The along track sensor model solution by Gauss-Lambert model gives better results in the three direction.**

RMSE X (m)	12.481
RMSE Y (m)	12.336
RMSE Z (m)	12.613

Table 83. RMSE in Inertial Coordinate System of Ground Control Points when ASTER images in an along track sequence by Gauss-Lambert model

6.3.2.3. Herrick-Gibbs model evaluated with Vegoritis and Grevena data sets

As two ASTER data sets of the same orbit are available the combined model of Gauss-Lambert and Herrick-Gibbs (§ 5.3.3) is also tested along with Kepler model for along track images (§5.3.1). The time interval between the first and the last image is 57.17611

seconds. As the data sets do not intersect to each other only the reference standard deviation and the standard deviation of the velocity vector is calculated. As it shown in table 84 the standard deviation for both models are almost the same and moreover the accuracy of the velocity vector is increased more compared to table 79, where two images are involved in the solution.

S_0 (pixels) solved by Kepler model	1.443
S_0 (pixels) solved by Herrick-Gibbs model	1.483
VELOCITY u_x (m/sec)	5.873
VELOCITY u_y (m/sec)	1.666
VELOCITY u_z (m/sec)	3.006

Table 84. Standard deviation of the solution and of the unknown parameters when two ASTER data is solved as along track sequence by Kepler model and Herrick-Gibbs model (line and angle elements are solved separately)

6.3.3. Solve HRS-data with a few GCPs

An additional test is made trying to solve the along track Kepler model using as few GCPs as possible. Theoretically, the number of unknown parameters in this model for two along track images is 12 in total. Thus 3 GCPs are enough to have a solution. In table 85 the RMSE of the same 21 Check Points which are used in the previous HRS test where 12 GCPs are used (in order to have a direct comparison) in each direction is presented in the following cases:

- Three GCPs used which are 68,86,3016.
- Four GCPs used which are 68,86,3016,31432.
- Six GCPs used which are 68,84,86,3016,3432,32433.

If table 85 is compared with table 76 the conclusions are:

- The along track model with just four GCPs has almost the same accuracy as single image solution with 12 GCPs. It is should be mentioned here that if the

HRS images are solved separately the number of unknown parameters is 18; thus with 4 GCPs there is no solution.

- The along track model using 6 GCPs reaches the accuracy of along track model with 12 GCPs.

	Along track Kepler model using 3 GCPs	**Along track Kepler model using 4 GCPs**	**Along track Kepler model using 6 GCPs**
S_0(pixels)	-	1.418	1.492
RMSE X (m)	13.268	12.569	12.207
RMSE Y (m)	26.357	19.930	13.782
RMSE Z (m)	16.372	13.338	12.579

Table 85. Along track sensor model accuracy with different number of GCPs used

6.3.4. Summary of the along track models without use of navigation data

The along track sensor model in three versions is evaluated using Ground Control Points. For each version different orbit determination-propagation methods are used. The first one based on the Kepler problem (orbit propagation) which can be used in more than two along track images is tested using HRS and two ASTER data sets. The second one is based on Gauss-Lambert method which can be used only for two along track images and it is tested using HRS and ASTER Vegoritis data sets. The final one is based on Herrick-Gibbs method which is combined with the Gauss-Lambert method in order to be used in case of more than two along track images and it is tested using two ASTER data sets. Also for comparison, if it is needed, the data sets are solved as separate (not in along track sequence) images.

The conclusions of all the above tests are summarized as follows:

- **In the along track solution the precision of the velocity vector is increased dramatically compared to the single image solution.**

- **The along track sensor model overall is better represent the image acquisition geometry. The larger improvements are at the edges of the images** as found in case of HRS images.
- **The number of GCPs needed in order to have accepted accuracy is definitely less in case of the along track model than in case where the images are solved separately. For HRS images which cover an area of 120km by 60 km it seems that 6 well distributed GCPs are enough.**
- The Kepler and Gauss-Lambert model give generally almost identical accuracy. This conclusion comes out if the RMSE of the Ground Control and Check Points are compared.
- The solution of four along track images (two ASTER data sets) gives better accuracy than the two images solution. It is believed that this conclusion leads to the hypothesis that if many images are involved in the solution, the accuracy is improved.

6.3.5. Comparison of single and along track Kepler model with existing models

Table 86 is a comparison table of the Kepler model in single and along track versions with existing models. The coordinates of the Check points which are calculated by the Kepler model (both versions) are transformed from inertial space to a Geodetic Coordinate System (Lambert III- IGN) in order to be directly comparable to the results of the other models.

In the evaluation of the Gugan-Dowman model (Aix-en-Provence test site), of the Konency model and of the Kepler model in both versions the Ground Control are of the same accuracy (from 1:25000 maps). Moreover in the first and the last one, some of the control points are the same. In the evaluation of the Gugan-Dowman model (UK test site) and Poli model the accuracy of the control points is +/-1 meter. Also in the Poli model self calibration is involved in the adjustment. The SPOT HRV images are half the width of those used in this evaluation HRS images. Finally, for the Bavaria test site (Poli model) the distribution of the GCPs is not over the whole image while in the

Kepler model the reference points have a good distribution in the whole images. After these comments the following points could be mentioned:

- It is obvious once again that improved accuracy of the solution can be obtained by the use of high quality ground control data. It can be assumed that when the two different test sites of Gugan-Dowman model are compared the accuracy of the Kepler model can be improved when more accurate control points are used.
- Compared with the results for Aix-en-Provence test of Gugan-Dowman and the Kepler along track model it is obvious that with Kepler model better accuracy is achieved, having in mind that the HRS covers a two times larger area that HRV images with less unknown parameters.
- Compared to the results of HRS images evaluation (Kepler and Poli model), the accuracy of the Kepler model could be improved when self calibration is involved in the model.

Model	Unknowns Per stereopair	Number of GCPS	Number of ICPs	Check Points Accuracy (RMS) in meters		
				E	N	h
Gugan-Dowman (Aix-en-Provence)	14	10	62	17.7		5.4
Gugan-Dowman (UK)	14	10	17	8.8		10.2
Gugan-Dowman (UK)	20	10	17	8.7		7.4
Konecny	18 or 20	18	68	10.9	13.7	6.5
Konecny	18 or 20	34	52	11.3	13.8	6.2
Poli	-	8	31	3.7	6.5	4.7
Kepler single	18	12	21	18.9	14.3	9.6
Kepler Along track	12	12	21	10.5	12.8	7.8

Table 86. Comparison of single and along track Kepler model with reviewed models from the literature

Thus, in the future self calibration should be used in Kepler model. Also, the Kepler model should be tested in test sites with more accurate reference data.

6.4. HRS data-Solution with use of navigation data

6.4.1. Introduction

In SPOT satellite geometry Handbook (SPOT, 2002) the series of elementary transformation are described trying to calculate the viewing angles at each pixel in the SPOT-HRS array. As it is presented in SPOT satellite geometry Handbook (SPOT, 2002): "A "*viewing geometry model*" consists in establishing a relation between any pixel (l,p) of the level 1A image and the relative point (λ,φ) on a terrestrial reference system. In this relation, the altitude h of the point on the ground is supposed to be known". However the most important point is that this relation between pixels and the ground (Terrestrial Coordinate System) is not based in the collinearity equations (Photogrammetry) as it is shown in the following paragraphs. For this relation even the focal length of the lens is not needed to be known. Thus, all the data provided with the images focuses on solving the specific geometry problem. In order to establish a generic photogrammetric solution, additional information should be known, as explained in §6.4.4. As in this thesis a generic along track model is developed a modified model is proposed where these unknown quantities are calculated using Ground Control Points.

6.4.2. Calculations of Position and velocity vectors

The way the position and velocity vectors are calculated from the metadata information is in § 5.4.2.

6.4.3. Calculation of rotation angles

The formulation that is introduced here is totally different than the formulation proposed in SPOT Geometry handbook because as it has already been mentioned different method is used to solve the problem of exterior orientation.

Going back in §2.3.4 the rotation matrix M is a 3x3 matrix **which brings the ground coordinate system parallel to the framelet coordinate system.** The formulation of the rotation matrix is described in equation 88, as one of the fundamental assumption of the along track sensor model is that the rotation angles during the acquisition time of a single pushbroom image is constant. In the procedure of the rotation angles calculation the following points are taken into consideration:

The transformation from Ground coordinate system to framelet coordinate system is done in three steps (*It is assumed that the origin of the navigation system is the perspective center of the image*).

- The first step is to calculate the rotations angles from the Ground coordinate system to the Orbital coordinate system (§ 6.4.3.1)
- The second step is to calculate the rotation angles from Orbital coordinate system to Navigation coordinate system. (§ 6.4.3.2)
- and the third step is to calculate the rotation angles from the Navigation coordinate system to the Framelet coordinate system. (§ 6.4.3.3)

6.4.3.1. Calculation of the rotations angles from the Ground coordinate system to the Orbital coordinate system.

The Orbital Coordinate system (O_2, X_2, Y_2, Z_2) is defined in § 2.3.3. As a reminder the origin is the spacecraft center of mass O_2, with the Z_2 axis pointing from the Earth center of mass to the spacecraft center of mass. The X_2 axis is the normalized cross product of the instantaneous velocity vector with Z_2 axis. Y_2 is the third unitary vector of the system. The X_2, Y_2, Z_2 axis are calculated by the equations 2.

The rotation angles from Orbital Coordinate system to Ground coordinate system is defined as follows (SPOT, 2002):

$$M_{ORB} = \begin{bmatrix} (X_2)_X & (Y_2)_X & (Z_2)_X \\ (X_2)_Y & (Y_2)_Y & (Z_2)_Y \\ (X_2)_Z & (Y_2)_Z & (Z_2)z \end{bmatrix} \qquad \text{Eq. 106}$$

where

X_2 represent the pitch axis

Y_2 represent the roll axis

Z_2 represent the yaw axis

The rotation matrix which brings the Ground coordinate system to the Orbital coordinate system is the transpose of the M_{ORB}

$$M_{ORB}^{T} = \begin{bmatrix} (X_2)_X & (X_2)_Y & (X_2)_Z \\ (Y_2)_X & (Y_2)_Y & (Y_2)_Z \\ (Z_2)_X & (Z_2)_Y & (Z_2)z \end{bmatrix} \qquad \text{Eq. 107}$$

The rotation angles are calculated for equations 88 and 107 as follows:

$$\varphi_{ORB} = \arcsin((Z_2)_X)$$

$$\omega_{ORB} = arcsin\left(-\frac{(Z_2)_Y}{\cos\varphi_{ORB}}\right) \qquad \text{Eq. 108}$$

$$\kappa_{ORB} = arcsin\left(-\frac{(Y_2)_X}{\cos\varphi_{ORB}}\right)$$

6.4.3.2. Calculation of the rotations angles from Orbital coordinate system to Navigation coordinate system.

The Navigation Reference Coordinate System (O_1,X_1,Y_1,Z_1) is also defined in § 2.3.3 . As a reminder the Navigation Reference Coordinate System is the body-fixed system used for spacecraft attitude determination and control. The coordinate axes are defined by the AOCS (Attitude and Orbit Control System) which attempts to keep the navigation reference frame aligned with the Orbital Coordinate System so that the optical axis of instrument without mirror deviation is always pointing towards the center of the Earth.

On SPOT, no distinction is made between the barycentre of instruments O_1 of the Navigation Reference Coordinate System and the spacecraft center of mass O_2 of the Orbital Coordinate System (O_1=O_2) (SPOT,2002).

The rotation angles (attitudes) from Navigation to Orbital coordinate system are measured with on board instruments. The accuracy of the direct location mainly depends on the accuracy of the attitude measurements. The star tracking unit (ULS) on-board SPOT5 allows measuring absolute attitude values. Precision of ULS system will allow an absolute location better than 50 meters on ground (SPOT, 2002).

For historical reasons, attitude values (rotation speed or absolute angle) are not expressed within the Navigation Reference Coordinate System (O_1,X_1,Y_1,Z_1) but within its inverted system (O_1,X_1',Y_1',Z_1').

$$\begin{aligned} \vec{X}_1' &= -\vec{X}_1 \\ \vec{Y}_1' &= -\vec{Y}_1 \\ \vec{Z}_1' &= \vec{Z}_1 \end{aligned} \qquad \text{Eq. 109}$$

The sign of roll and pitch values (rotation speed or absolute angle) found in auxiliary data will therefore be multiplied by (-1) except the yaw values which will be left unchanged.
This change of sign will appear within the formula computing the look direction here after.

Attitude variations being small and because of the presence of many samples within the scene, only a linear interpolation is performed to get the attitude values [$a_p(t)$,$a_r(t)$,$a_y(t)$] at the look time t matching the line l of the image (SPOT, 2002)

$$a_p(t) = a_p(t_i) + \left(a_p(t_{i+1}) - a_p(t_i)\right) \times \frac{t - t_i}{t_{i+1} - t_i}$$

$$a_r(t) = a_r(t_i) + \left(a_r(t_{i+1}) - a_r(t_i)\right) \times \frac{t - t_i}{t_{i+1} - t_i} \qquad \text{Eq. 110}$$

$$a_y(t) = a_y(t_i) + \left(a_y(t_{i+1}) - a_y(t_i)\right) \times \frac{t - t_i}{t_{i+1} - t_i}$$

where

i	is the index of valid attitude measurement whose time is just before t ($t_i \le t \le t_{i+1}$)
$a_p(t)$	is the rotation angle around the pitch axis at time t
$a_r(t)$	is the rotation angle around the roll axis at time t
$a_y(t)$	is the rotation angle around the yaw axis at time t
$a_p(t_i)$	is the rotation angle around the pitch axis at time t_i found in auxiliary data
$a_r(t_i)$	is the rotation angle around the roll axis at time t_i found in auxiliary data
$a_y(t_i)$	is the rotation angle around the yaw axis at time t_i found in auxiliary data

Assuming that the attitudes in the specific epoch are computed using equations 110 and 111 and found:

a_p	is the rotation angle around the pitch axis at time t_o
a_r	is the rotation angle around the roll axis at time t_o
a_y	is the rotation angle around the yaw axis at time t_o

Then the rotation angles from the Ground to Navigation coordinate system are given as follows:

$$\begin{aligned} \omega_{NAV} &= \omega_{ORB} - a_p \\ \varphi_{NAV} &= \varphi_{ORB} - a_r \\ \kappa_{NAV} &= \kappa_{ORB} - a_y \end{aligned} \qquad \text{Eq. 111}$$

The minus signs in equations 111 are because the rotations angles from Orbital coordinate system to Navigation coordinate system is needed while the given rotation angles are from the Navigation to the Orbital coordinate system.

6.4.3.3. Calculation of the rotations angles from the Navigation coordinate system to the Framelet coordinate system.

For any line l of a level 1A scene, pixel of a particular column q has been acquired by a unique CCD. The look direction matching this CCD is defined by the two angles ψ_X (along the track) and ψ_Y (across the track) expressed within the (O_1,X_1,Y_1,Z_1) Navigation Reference Coordinate System (Figure 14). For SPOT5, look angles are given for every detector in auxiliary data. In this transformation, it is assumed that the perspective center of the image is identical with the navigation coordinate system origin (which is not true finally as it is shown in §6.4.4.)

If for the perspective center of the image these angles are ψ_X and ψ_Y. The rotation angles from the Ground to the sensor coordinate system is

$$\begin{aligned} \omega_{CCD} &= \omega_{NAV} - \psi_X \\ \varphi_{CCD} &= \varphi_{NAV} - \psi_Y \\ \kappa_{CCD} &= \kappa_{NAV} \end{aligned} \qquad \text{Eq. 112}$$

The minus signs in equations 112 are because the rotations angles from CCD coordinate system to Navigation coordinate system is needed while the given rotation angles are from the Navigation to the CCD coordinate system.

The final transformation is a simple rotation counter-clockwise to the Z axis because in the Navigation coordinate system and thus in the CCD coordinate the Y axis is along the track while in the Framelet coordinate system the X axis is along the track.

$$\begin{aligned} \omega_{FRE} &= \omega_{CCD} \\ \varphi_{FRE} &= \varphi_{CCD} \\ \kappa_{FRE} &= \kappa_{CCD} - 90° \end{aligned} \qquad \text{Eq. 113}$$

6.4.3.4. Questions arise from the above procedure.

In the previous paragraphs the rotation angles from the Ground to the Framelet coordinate system are calculated using the metadata information of SPOT-HRS. The exterior orientation parameters (the state vector and the rotations angles) are calculated from the Orbital or the Navigation origin point which is assumed to be identical with the perspective center of each image. (These coordinate systems have the same origin as it was mentioned in § 6.4.3.2). The critical questions are the following:

Is this origin point the perspective center of each image? If it is not, is the offset of perspective center to the Navigation data origin known? If it is not known, it is not possible to calculate accurately the state vector and the rotation angles as they are referred to different origin than the perspective center. If the above information is not known, how should a rigorous model based in Photogrammetry be modified in order to take into consideration the above situation? Which is alternative method that is used in SPOT-HRS direct orientation process that gives so accurate results?

All the above questions are answered in § 6.4.4 using the metadata information of HRS images.

6.4.4. HRS metadata incompatibility to a direct photogrammetric solution

6.4.4.1. HRS Position and Velocity Vector origin

In the metadata file of the HRS images the position and velocity vectors of DORIS system are given every 30 seconds. For both images at the same epoch the same position and the velocity vectors are given. Thus the position and the velocity vectors are not measured from the perspective center of each image. **This means that there is a displacement for the perspective center of each image, which is not known.**

6.4.4.2. Across track look directions of the pixels.

It has already been mentioned that for any line of a level 1A scene, look angles are given for every detector in auxiliary data.

The across track values (PsiY) for each detector are imported in a file (HRS1 image). The scatter plot in figure 39 represents how the PsiY is changing along the sensor line. It is assumed that the origin is the middle pixel (6001 pixel) trying to represent the perspective geometry.

The look angles across the track are changing linearly from -0.07146 rad (-4.094°) to 0.07103 rad (4.069°) while the value for middle (6001) detector is -6.7895000000e-05. The basic statistics of the above angles are in the table 87.

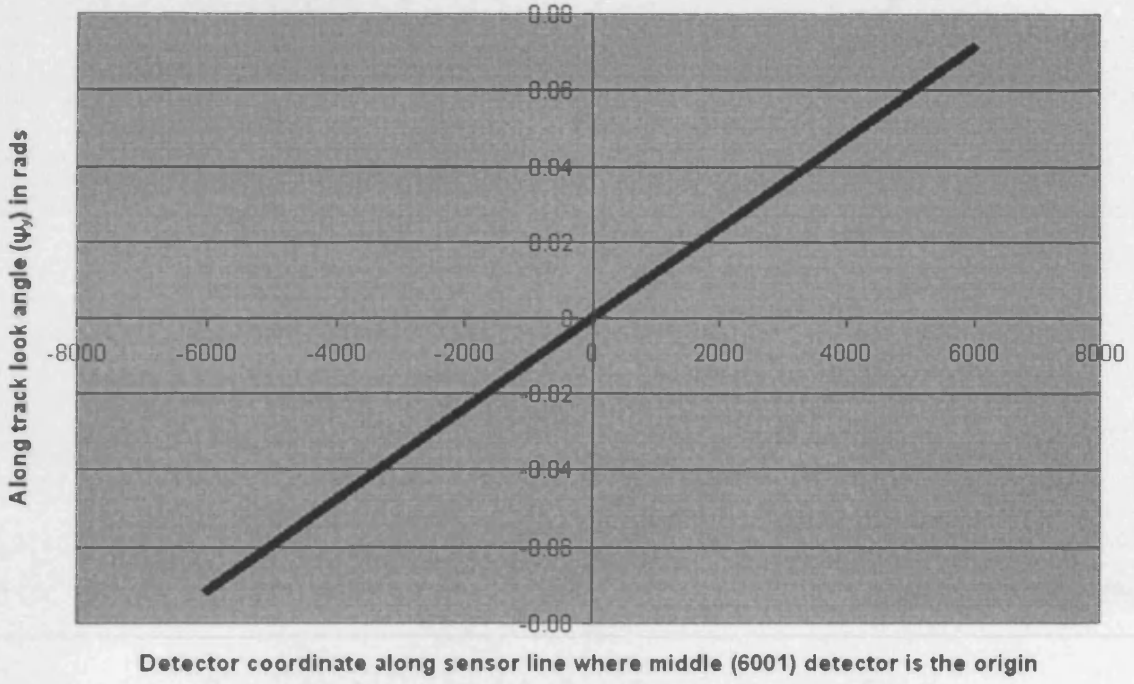

Figure 39. Change of across track look angles along the sensor line

Minimum (rad)	-0.07146
Maximum(rad)	0.07103
Median(rad)	-6.78950e-05
Mean(rad)	-7.50205e-05
Standard deviation(rad)	0.041268024

Table 87. Statistics of across look angles

Trying to explain the above scatter plot the most possible measurement frame is represented in figure 40 (the dimensions are not in correct aspect ratio). In this figure the paper plane is the Oyz plane of a coordinate system. This system is defined by the

sensor line and the direction of the origin of measurements to the middle pixel. The flight direction (x-axis) is towards paper plane. As the look angle value of the middle point is -6.7895000000e-5 and starting from negative to positive values the direction of the origin of measurements and the middle pixel is almost perpendicular to sensor line. The look angle of pixel 1 is the angle α which has negative value. In the same way

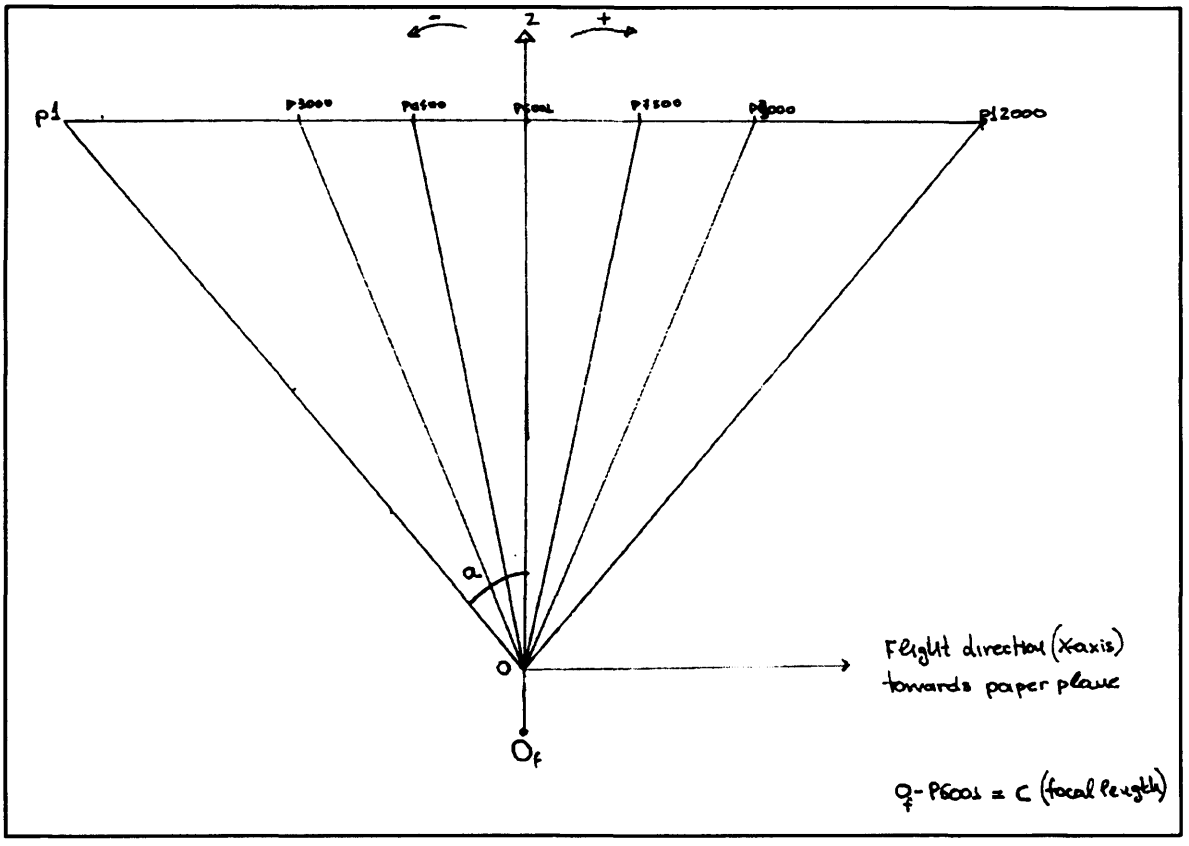

Figure 40. Across-track look angles measurement frame

the look angles of all the pixels can be defined. As the angle α and the distance p1 to p6001 are known the dimension O P_{6001} could be calculated as follows:

$$OP_{6001} = \frac{P_1 P_{6001}}{\tan a} \qquad \text{Eq. 114}$$

If the above value is calculated it is found that the O P_{6001} is 544.8501 mm. As the focal length is 580mm it is obvious that the look angles are not measured from the perspective center. If the same distance is calculated from each pixel and found the

same it seems that the Navigation Coordinate system is parallel to the previous defined coordinate system. Unfortunately, these values are changed slightly along the sensor line (close to middle pixel are not possible to calculate it as tan is going to zero) (Figure 41, 42). Similar results are achieved from the look angles calculations of HRS2 image.

From the above calculation it seems that the Navigation system is not parallel to the above system which is defined by the sensor line and the direction of the origin of measurements to the middle pixel; thus to the Framelet coordinate system (from the defined system the Framelet coordinate system is parallel. There is only an offset between these systems).

On the other hand it is explain here the reason why the look angles are defined for each pixel. It is tried to avoid of using the framelet coordinate system as additional measurements should be done (offset and rotation angles) from the navigation system which is not very easy to calculate directly. As a result the focal length could not be used in direct orientation of the sensor.

Moreover in Leica Photogrammetric Suite which was used to produce DEMs from HRS images a discrepancy was mentioned while it was produced very accurate DEMs using wrong principal distance. It was supposed that the reason for this is one of the following (Dowman and Michalis. 2004):

- The principal distance is used as an initial value in a self calibration process where the correct principal distance is computed, although it is very difficult to do this without GCPs
- The principal distance is not used. A direct transformation is computed between the object space coordinate system and the image coordinate system as it is defined in the specifications of this model.

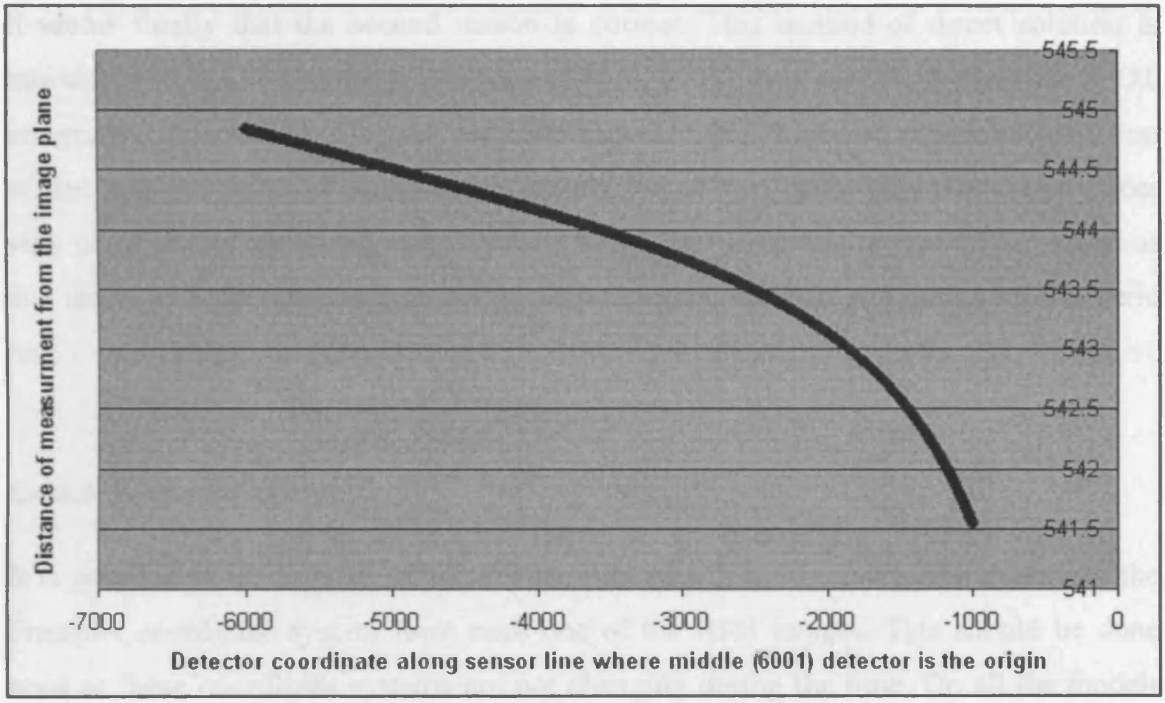

Figure 41. Distance from measurement origin to image plane as it is calculated form pixel 1 to 5000 of HRS 1 image

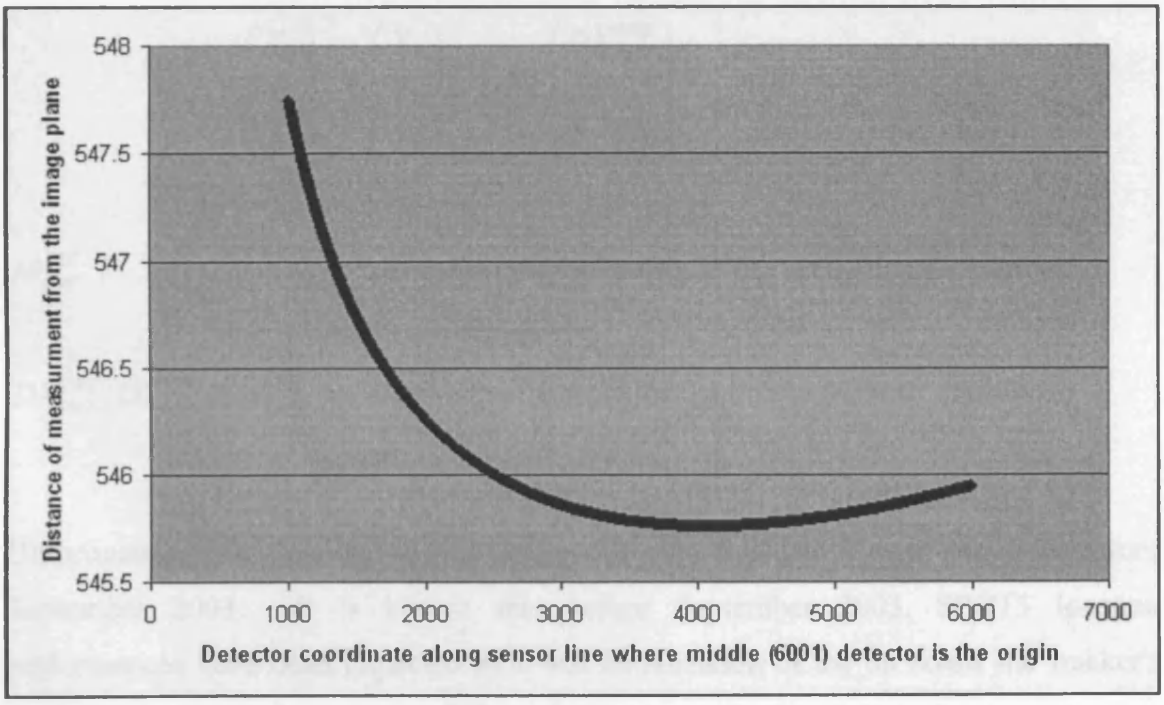

Figure 42. Distance from measurement origin to image plane as it is calculated form pixel 7000 to 12000 of HRS 1 image

It seems finally that the second reason is correct. This method of direct solution is introduced in SPOT geometry handbook (SPOT, 2002). It is specific method for SPOT images and it is solved using the metadata provided. It is based on the simple equation of line and the height is found as an intersection of two lines. This method produces very good results (Dowman and Michalis, 2004). However it is beyond of the scope of this thesis as it does not represent a photogrammetric solution and moreover a generic one.

6.4.4.3. Proposed model

It is possible to involve the offset and the rotations from the navigation system to the Framelet coordinate system form each one of the HRS images. This should be done once as these coordinate systems are not changing during the time. On all the models are developed until now the Ground coordinates of the perspective center of the base framelet (X_o, Y_o, Z_o) should be reformed as follows:

$$\begin{pmatrix} X_o \\ Y_o \\ Y_o \end{pmatrix} -> \begin{pmatrix} X_o \\ Y_o \\ Y_o \end{pmatrix} + M_{NAV}^{FRE} \begin{pmatrix} DX_{NAV}^{FRE} \\ DY_{NAV}^{FRE} \\ DZ_{NAV}^{FRE} \end{pmatrix} \qquad \text{Eq. 115}$$

M_{NAV}^{FRE} represents the rotation matrix from Navigation to framelet coordinate system and

$DX_{NAV}^{FRE}, DY_{NAV}^{FRE}, DZ_{NAV}^{FRE}$ the offset from the from Navigation to framelet coordinate system

Unfortunately the data set which given for this evaluation was acquired before September 2003. It is known that before September 2003, SPOT5 location performances have been impacted by a bad initialization of the on board star tracker's relativist compensation process. This problem causes the location performance to vary with satellite position, indeed both with latitude and time (Bouillon and Gigord, 2004; Bouillon, 2004 personal communication). It is corrected by a modification to the metadata file. Also the formulation is given to correct the metadata information before

September 2003. However this formulation is based in Viewing Geometry Model as it is defined in SPOT geometry handbook (SPOT, 2002) which is incompatible with the model developed in this thesis. Thus in order to solve the above problem new data sets are needed which should be acquired after September 2003 in an area where more accurate reference points are provided to calculate as accurate as possible the offset and the rotations angles calculations from Navigation Coordinate System to Framelet coordinate system. This calibration should be done once as the relation between these coordinates systems does not change upon the time.

CHAPTER 7.

CONCLUSIONS

7.1. PhD outline

In this thesis a new generic rigorous sensor model for along track stereo optical satellite sensors is proposed. The main and fundamental point during the development of the along track model is to benefit from the same orbit acquisition, in order to orientate simultaneously all the along track stereo images. The obvious reason is to reduce the number of unknown parameters which generally are high correlated (§3.3). Moreover, the simultaneous solution extends the narrow field of view of each satellite image because all along track images are treated as one iconic image, with the field of view equal to the angle between the first and the last image.

Starting from the definition of the model the meaning of the term 'rigorous' as it is used in this thesis, is given. **In a rigorous model each parameter should express, in advance, an identifiable physical or geometric quantity**. Thus, great effort is made trying to define the essential forces which are involved in the acquisition of the pushbroom images, according to the needed accuracy and the data provided.

The pushbroom model is a kinematic model. The scanning effect on the ground is due to the motion of the satellite (§ 2.2.1.). A single image consists of a number of framelets which are independent one-dimensional images with their own exterior orientation parameters; perspective projection is maintained perpendicular to the direction of flight. Thus, **in a rigorous sensor model the satellite motion in space should be described** as accurate as possible. In other words, a rigorous sensor model **should describe the state of the satellite** during the acquisition time of the image or images (§ 2.4.4.). Six parameters are enough to established the state of the satellite at an epoch (time stamp), which are the state vector associated with position and velocity vectors or the orbital elements (§ 2.4.4, 2.4.5).

On the other hand the model should be a generic model capable to be used in as many as possible along track satellite images. Thus, it is based on the collinearity equations which represent a generic and rigorous equation relating the image space with the ground space. However, for the simulation of the acquisition geometry of pushbroom images the collinearity equations are modified and are combined with orbit determination-propagation methods.

The fundamental assumptions is that Keplerian motion is maintained along the acquisition time of the along track images. Different versions of the model are developed based on different orbit determination-propagation methods. The first one based on the Kepler problem (orbit propagation) which can be used in more than two along track images. The second one is based on Gauss-Lambert method which can be used only for two along track images like SPOT-HRS and TERRA-ASTER. The final one is based on Herrick-Gibbs method which is combined with the Gauss-Lambert method in order to be used in case of more than two along track images.

The above statement covers the functional part of the model (§2.5.2). For the stochastic part of the model two alternatives to the Least Squares Estimator is used in this thesis. It is known that the least square estimator is not a precise estimator when near linear dependencies between some columns of the design matrix exist (§2.5.4). Usually one refers to such a case as an incidence of collinearity or multicollinearity. A further characteristic feature of the collinearity is that usually some of the elements of the least squares estimator are highly correlated. Then the corresponding elements of the parameter may be considered as weakly identifiable.

In this thesis two methods are used to overcome the correlation and compute the exterior orientation parameters. The first one is an alternative estimator which is called the **General Ridge Estimator** (§2.5.5). In the second method the line elements and the angle elements are solved separately in an iterative procedure. This procedure is not rigorous in theory and the orientation precision and iteration time depends on the

accuracy of the initial values. This method is not really involved in the solution of the sensor models. Besides, it is used in two very important cases in sensor development:

- To define the General Ridge Estimator parameters (§ 4.8)
- To establish the accuracy limits in the evaluation process of orbit determination propagation methods (§ 5.4.1)

Moreover, as it is very important to understand how the image acquisition process is described by the developed model; tie points are not used in any phase of model solution.

Thus, in this research each model is solved by estimator without weights, only using Ground Control Points (if needed). It is most important to understand how good the image acquisition process is described by the developed model instead of trying to find the best available solution.

7.2. PhD review

The research is done in steps. The first elementary step is to define a sensor model for a single image (chapter 4). The adopted model based on the following assumptions (§4.10):

- The satellite motion during the acquisition time of **one** image is a Keplerian motion. The adopted model is based in Kepler's problem.
- The **attitudes** (ω,φ and k rotations) of the satellite are remaining **constant** during the acquisition time of one image.

The total number of the unknown exterior orientation parameters is nine. The position vector (3), the velocity vector (3) and the rotations (3). Also a model based on the Kepler (classical) orbital elements model is developed which however gives an unstable solution in a single image solution (§4.9)

The second step is the development of the along track sensor model in various versions based on different the orbit determination propagation methods. The accuracy and of

time validity of them is evaluated using the high accurate SPOT5 navigation data. The conclusions for each model in this evaluation follow (§5.6):

From the evaluation of Kepler method (§5.4.3) the conclusions are:

- It is less accurate than Gauss-Lambert method in case of two along track images while the number of unknown parameters is the same.
- It has a clear advantage in case of more than two along track images where less unknown parameters are needed for the solution although it is again less accurate than the combined Gauss-Lambert and Herrick-Gibbs model.
- Finally, the validity of the model is dramatically smaller than the others and it is assumed to be about 90 seconds for images having the same characteristics as SPOT5-HRS. **It is just acceptable for HRS images.**

From the evaluation of Gauss-Lambert method (§5.4.4) the following points should be made:

- The accuracy of Gauss-Lambert method is better than the accuracy of Kepler method while the number of unknown parameters is the same.
- It cannot be used by itself for more than two along track images.
- Finally the validity of this method is at least 420 seconds for images having the same characteristics as SPOT5-HRS.

From the evaluation of Herrick-Gibbs (§5.4.5) the following point should be made:

- The accuracy of Herrick-Gibbs method is better than the accuracy of all the other methods.
- In can be used in combination with Gauss-Lambert method in order to solve more than two along track images. However the number of the unknown parameters is larger than the case of Kepler model.
- Finally the validity of this method is at least 420 seconds for images having the same characteristics as SPOT5-HRS.

In the next step the three versions of along track sensor model are evaluated using SPOT5-HRS and ASTER data sets. The conclusions of all the above tests are summarized as follows:

- **In the along track solution the precision is increased dramatically compared to the single image solution.**
- **The along track sensor model is a better representation of the image acquisition geometry. The larger improvements are at the edges of the images** as found in case of HRS images.
- **The number of GCPs needed in order to have accepted accuracy is definitely less in case of the along track model than in case where the images are solved separately. For HRS images which cover an area of 120km by 60 km it seems that 6 well distributed GCPs are enough.**
- The Kepler and Gauss-Lambert model give generally almost identical accuracy. This conclusion comes out if the RMSE of the Ground Control and Check Points are compared.
- The solution of four along track images (two ASTER data sets) gives better accuracy than the two images solution. It is believed that this conclusion leads to the hypothesis that if many images are involved in the solution, the accuracy is improved.

Unfortunately it was not possible to solve directly for the SPOT-HRS images using the generic model developed in this thesis. The metadata is designed to determine the orientation using a specific direct orientation method (SPOT, 2002). Thus, some important information needed to establish a direct photogrammetric solution is missing. This information is the offsets and the rotation angles from the navigation coordinate system to the framelet coordinate system.

As in this thesis a generic along track model is developed (and definitely not only for SPOT data) a modified model is proposed where the unknown quantities are calculated using Ground Control Points. In order to solve the above problem new data sets are needed which should be acquired after September 2003 (§ 6.4.4.3) in an area where more accurate reference points are provided to calculate as accurate as possible the

offset and the rotations angles calculations from Navigation Coordinate System to Framelet coordinate system. This calibration should be done once as the relation between these coordinates systems does not change upon the time.

The above along track model represents a general model which can be used in other sensors which have along track sensor capabilities. Moreover it is possible for it to be used in an along track sequence of images (no stereo). If images of any sensor are acquired on the same orbit the model can be used to determine the orientation. Thus sequences of SPOT5-HRG or IKONOS data could be solved by this model. The only restriction is, because this model is based on collinearity equations, the inner orientation of the sensor should be known. Finally, the single model based on Kepler equation could be used in any pushbroom sensor with the same restriction.

This is the first time that a rigorous along stereo sensor model is developed in this way, where the collinearity equations are used directly with orbit determination-propagation methods. It is proven that using this combination, the accuracy, precision and stability of the solution is improved compared to the single image models. It is a simple model from a user point of view, as little information should be known in advance, and the effort of the user is only to measure the reference points (if needed). Tie points or weights on the estimator are not used in order to investigate the behaviour of the model itself during the acquisition of the along track images. It is understood from the tests that described in chapters 4,5,6 and 7 that the developed model can simulate effectively the satellite orbit during the acquisition of the along track images.

7.3. Further work

The most important work that should be done is the in-flight calibration of SPOT5-HRS. New data which is acquired after September 2003 should be used. The next step is the self-calibration process as it was mentioned in § 3.3.

In depth investigation should be carried out to reduce the number of unknown attitude parameters. One way is to find a relative relation between the rotation angles of the images as Westin found (§ 3.2.1).

General Ridge Estimator should be tested in another data sets in order to be sure that the internal accuracy of the solution is improved in general. It is found that it is more appropriate than the Least Squares Estimator in solving a pushbroom sensor model.

Another very important step is to test the model on the forthcoming ALOS-PRISM high resolution three line scanner. It is believed that the stability of the solution is increased with the three line geometry (§6.3.2.3) and it should be possible to prove this statement with the evaluation of ALOS-PRISM.

The sensor model which is based on the orbital elements (rather than state vectors) is not tested in along track sequence. It is necessary to evaluate this model with more than one image in order to have a better understanding of the stability of this model.

Finally, the model should be linked with DEM generation software. It is a field where the use of a good sensor model is critical.

REFERENCES

Abrams M., Hook S., Ramachardan B., 2002. ASTER User Handbook, Version 2.

Airault S, Gigord P, Cunin L, Breton E, Bouillon A, Gachet, Bernard M, 2003. Reference3D location performance review and prospects. ISPRS workshop on High Resolution mapping from space 2003, Hanover. Proceedings on CDROM.

Bate R., Mueller D.,White J., 1971. Fundamentals of Astrodynamics. Dover.

Baudoin A., Schroeder M., Valorge C., Bernard M., Rudowski V., 2004. HRS-SAP initiative: A scientific assessment of the High Resolution Stereoscopic instrument on board of SPOT 5 by ISPRS investigators. The International Archives of the Photogrammetry, Remote Sensing and Spatial Information Sciences, Vol. XXXV, Part B1, Commission I, Istanbul, pp. 372-378.

Bouillon A., Gigord P., 2004. SPOT5 HRS location Performance tuning and monitoring pinciples. The International Archives of the Photogrammetry, Remote Sensing and Spatial Information Sciences, Vol. XXXV, Part B1, Commission I, Istanbul, pp. 379-384.

Chen T., Shibasaki R., Tsuno K., 2004. Triplet-Matching for DEM generation with PRISM,ALOS. The International Archives of the Photogrammetry, Remote Sensing and Spatial Information Sciences, Vol. XXXV, Part B1, Commission III, Istanbul. Proceedings on CDROM

Dowman I.J., (Ed.).1991. Test of Triangulation of SPOT data. OEEPE Publication, 26, 206pp.

Dowman I.J., Dolloff J.,2000. An evaluation of rational functions for photogrammetric restitution. International Archives of Photogrammetry and Remote Sensing, Vol. XXXIII, Part B3, Commission I, Amsterdam. pp 254-266.

Dowman I.J., Michalis P.,2003. Generic Rigorous model for along track stereo satellite sensors. ISPRS workshop on High resolution mapping from Space 2003, Hanover 2003. Proceedings on CDROM

Dowman I.J., Michalis P., 2004. A rigorous model and DEM generation for SPOT5-HRS. The International Archives of the Photogrammetry, Remote Sensing and Spatial Information Sciences, Vol. XXXV, Part B1, Commission I, Istanbul. pp 410-415.

Ebner H., Kornus W., Ohlhof T. and Putz E., 1999. Orientation of MOMS-02/D2 and MOMS-2P/PRIRODA imagery. ISPRS Journal of Photogrammetry and Remote Sensing 54, pp. 332-341.

Ebner H., Kornus W. and Ohlhof T., 1992. A simulation study on point determination for the MOMS-02/D2 space project using an extended functional model. International Archives of Photogrammetry and Remote Sensing, Vol. XXIX, Part B4, Washington DC. pp. 458-464.

ERSDAC (Earth Remote Sensing Data Analysis Center), 2001. ASTER User's Guide, Part I, General, Ver. 3.1.

Fraser C.,2000. High-Resolution satellite imagery: A review of metric aspect. International Archives of Photogrammetry and Remote Sensing, Vol. XXXIII, Part B7, Commission III, Amsterdam. pp 452-459.

Fritsch D. and Stallmann D., 2000. Rigorous photogrammetric processing of high resolution satellite imagery. International Archives of Photogrammetry and Remote Sensing, Vol. XXXIII, Part B1, Amsterdam. pp. 313-321.

Grob J., 2003. Linear Regression. Springer.

Guo, H.T., Zhang, B. M., Gui Q.M., 2002. Application of generalized ridge estimation in computing the exterior orientation elements of satellite linear array scanner imagery. The International Archives of the Photogrammetry, Remote Sensing and Spatial Information Sciences, Vol. XXXIV, Part 2, Xi'an,China, pp. 153-156.

Gugan D.J.,1987. Practical aspects of topographic mapping from SPOT imagery. Photogrammetric Record, 12(69), pp. 349-355.

Gugan D.J., 1987. Topographic Mapping from SPOT Imagery. PhD thesis submitted to University of London. pp253.

Gugan D.J. and Dowman I.J., 1988. Topographic mapping from SPOT imagery. Photogrammetric Engineering and Remote Sensing, Vol 54, No 10, October 1988, pp. 1409-1414.

Gugan D.J. and Dowman I.J.,1988. Accuracy and completeness of topographic mapping from SPOT imagery. Photogrammetric Record, 12(72), pp. 787-796.

Hirano A., Welch R., Lang H.,2003. Mapping from ASTER stereo image data: DEM validation and accuracy assessment. ISPRS Journal of Photogrammetry and Remote sensing , 57, pp. 356-370.

Konecny G., Lohmann P., Engel H. and Kruck E.,1987. Evaluation of SPOT imagery on analytical Photogrammetric instrument. Photogrammetric Engineering and Remote Sensing, Vol 53, No 9, September 1987, pp. 1223-1230.

Kornus W. and Lehner M, 1999. Photogrammetric point determination and DEM generation using MOMS-02/PRIRODA three-line scanner. ISPRS workshop on Sensor and mapping from space, Hanover.

Kornus W., Lehner M. and Schroeder M.,1999. Geometric inflight calibration by block adjustment using MOMS-02P imagery of three intersecting stereo-strips. ISPRS workshop on Sensor and mapping from space, Hanover.

Kratky V., 1989. Rigorous photogrammetric processing of SPOT images at CCM Canada. ISPRS Journal of Photogrammetry and Remote Sensing ,44, pp. 53-71.

Leica , 2003. Leica Photogrammetry Suite- User Guide.

McGlone J.C., 2004. Manual of Photogrammetry. ASPRS.

Mikhail E, Bethel J and McGlone J C., 2001. Introduction to Modern photogrammetry. Wiley.

Montenbruck O. and Gill E., 2001. Satellite Orbits. Spinger.

Newcomb S., 1960. A Compendium of Spherical Astronomy. Reprinted edition. Dover Publications.

O'Neill M. and Dowman I.,1991. A new camera model for the orientation of the SPOT data and its application to the OEEPE test of triangulation of SPOT data. OEEPE Publication, 26, pp. 153-163.

Osawa Y.,2004. Optical and microwave sensors on Japanese mapping satellite ALOS. The International Archives of the Photogrammetry, Remote Sensing and Spatial Information Sciences, Vol. XXXV, Part B1, Commission I, pp. 309-312, Istanbul.

Poli D.,2004. Orientation of satellite and airborne imagery from multi-line pushbroom sensors with a rigorous sensor model. The International Archives of the Photogrammetry, Remote Sensing and Spatial Information Sciences, Vol. XXXV, Part B1, Commission I, pp. 130-135, Istanbul.

Poli D., Li Z., Gruen A., 2004. Spot5 / HRS stereo images orientation and automatic DSM orientation. The International Archives of the Photogrammetry, Remote Sensing and Spatial Information Sciences, Vol. XXXV, Part B1, Commission I, pp. 421-432, Istanbul.

Seeber G, 1993. Satellite Geodesy. Walter de Gruyter.

Seige P., Reinartz P., Schroeder M., 1999. More than three years experiment with the MOMS-2P camera onboard the MIR-space station. ISPRS workshop on Sensor and mapping from space, Hanover.

SPOT IMAGE, 2002. Spot Satellite Geometry Handbook, S-NT-73-12-SI , Edition 1, Rev. 0, Toulouse.

SPOT IMAGE, 2003. DIMAP Dictionary version 1.1- SPOT Scene profile - Edition01.

Tadono T., Shimada M., Watanade M., Hashimoto T., Iwata T., 2004. Calibration and Validation of Prism Onboard ALOS. The International Archives of the Photogrammetry, Remote Sensing and Spatial Information Sciences, Vol. XXXV, Part B1, Commission I, pp. 13-18, Istanbul .

Tokanaga M., Hara S., Ishikawa S., Murai S, 1994. DEM Generation using JERS1 OPS Stereo Data, Asian Conference on Remote Sensing. Available at http://www.gisdevelopment.net/aars/acrs/1994/ts6/ts6008.shtml (last visited January 2005).

Tao W., Yong-sheng Z., Yan Z., 2004. Combined Ridge-Stein estimator in exterior orientation for linear pushbroom imagery. The International Archives of the Photogrammetry, Remote Sensing and Spatial Information Sciences, Vol. XXXV, Part B1, Commission IV, Istanbul.

Valorge C., 2003. 3D Restitution and rendering through high resolution imagery: State of the art and new challenges, ISPRS workshop on High Resolution mapping from space, Hanover.

Verger F., Sourbes-Verger I., Ghirardi R., 2003. The Cambridge Encyclopedia of Space, Cambridge University Press.

Westin T.,1990. Precision rectification of SPOT imagery, Photogrammetric Engineering and Remote Sensing, Vol 56, No 2, pp. 247-253.

Westin T.,1991. Empirical models for attitude variability of the SPOT 1 satellite, Photogrammetric Record, 13(78), pp. 917-922.

Westin T.,1991. Pass Processing and extrapolation of SPOT image geometry, Photogrammetric Record, 13(78), pp. 923-929.

Wolf P., Ghilani C., 1997. Adjustment computations. Statistics and Least squares in surveying and GIS, Wiley.

Vallado D, 2001. Fundamentals of Astrodynamics and Applications, second edition, The Space Technology Library.